Title

Novel Distinct Roles for Intestinal/Macrophage COX-2 and Apolipoprotein Mimetic Peptides in the Development and Treatment of Inflammatory Bowel Diseases

Author

Meriwether, David

Publication Date

2018

Peer reviewed|Thesis/dissertation

UNIVERSITY OF CALIFORNIA

Los Angeles

Novel Distinct Roles for Intestinal/Macrophage Cyclooxygenase 2 and Apolipoprotein Mimetic Peptides in the Development and Treatment of Inflammatory Bowel Diseases

A dissertation submitted in partial satisfaction of the

requirements for the degree Doctor of Philosophy

in Molecular and Medical Pharmacology

by

David Meriwether

2018

ABSTRACT OF THE DISSERTATION

Novel Distinct Roles for Intestinal/Macrophage COX-2 and Apolipoprotein Mimetic Peptides in the Development and Treatment of Inflammatory Bowel Diseases

by

David Meriwether

Doctor of Philosophy in Molecular and Medical Pharmacology

University of California, Los Angeles, 2018

Professor Srinivasa T. Reddy, Chair

Cyclooxygenase 2 (COX2) has been associated with the development of inflammatory bowel disease (IBD), but the nature of this association has remained unclear. I demonstrate that mice that lack COX2 lose tolerance to pathogen associated molecular patterns. Thus, challenge with dietary cholate—an environmental trigger that I show impairs intestinal barrier function—induces severe intestinal inflammation in COX2 knock-out mice. COX2 knock-out within the myeloid compartment is sufficient to drive disease upon cholate challenge, while also altering upon disease the balance between pro-inflammatory and inflammation resolving mediators towards a pro-inflammatory phenotype. ApoA-I mimetic peptides including 4F have been investigated as potential anti-inflammatory therapies. I show that 4F targets the small intestine, where it is transported into the intestinal lumen in a cholesterol-dependent manner. In turn, 4F can increase trans-intestinal cholesterol efflux, a secondary cholesterol efflux pathways whose modulation is of therapeutic import. 4F therapy abrogates disease in the

myeloid COX2 knock-out and cholate model of IBD, while rescuing the elevated levels of pro-inflammatory mediators in macrophages, intestinal tissue, and plasma. 4F can directly clear lipid pro-inflammatory mediators from tissue and plasma, strongly suggesting a causative role for changes in the levels of these mediator in both the protective mechanism of 4F and the pathogenic mechanism of COX2-mediated IBD. Further investigation into the protective mechanism of 4F identified a novel trans-intestinal lipid transport clearance pathway for inflammatory mediators, which pathway may be involved in 4F's protective mechanism. These findings are vivid examples of the synergy that can result from simultaneously investigating both pathogenic and protective mechanisms in genetic mouse models of disease.

The dissertation of David Meriwether is approved.

Samson A. Chow

Harvey R. Herschman

Daniel L. Kaufman

Martin G. Martin

Srinivasa T. Reddy, Committee Chair

University of California, Los Angeles

2018

To my mother, Jean Serafin Meriwether (January 29, 1947 – May 28, 2017),

and to my daughter, Dahlia Jean (October 27, 2017 -).

TABLE OF CONTENTS

LIST OF TABLES

List of Figures

ACKNOWLEDGEMENTS

Chapter 2 was previously published as: Meriwether, D., D. Sulaiman, A. Wagner, V. Grijalva, I. Kaji, K. J. Williams, L. Yu, S. Fogelman, C. Volpe, S. J. Bensinger, G. M. Anantharamaiah, I. Shechter, A. M. Fogelman, and S. T. Reddy. 2016. Transintestinal transport of the anti-inflammatory drug 4F and the modulation of transintestinal cholesterol efflux. *J Lipid Res* **57**: 1175-1193.

For this work, I would like to acknowledge Sulaiman for Ussing chambers; Wagner for RCT; Grijalva for mice; Williams for GCMS; Kaji for Ussing chambers; Fogelman S for editing; Volpe for work with mice; Bensinger for advice; Anantharamaiah for peptides; Shechter for guidance; Fogelman AM for guidance. Reddy ST was the principal investigator for this work.

Chapter 3 is in preparation as: Meriwether, D. Sulaiman, D. Volpe, C. Grijalva, V. O'Connor, E. Borreh, N. Jedian, V. Trost, H. Martin, MG. Fogelman, AM. Reddy, ST COX2 dependent dysregulation of inflammatory signaling is rescued by apoA-I mimetic therapy in mouse models of IBD.

For this work, I would like to acknowledge Sulaiman for Ussing chambers, Volpe for mice, Grijalva for mice and cell culture, O'Connor for mass spec, Borreh for mass spec, Jedian for mass spec, Trost for mice, Martin for guidance, Fogelman for guidance. Reddy ST was principal investigator for this work.

The **Appendix** was previously published as: Meriwether, D., S. Imaizumi, V. Grijalva, G. Hough, L. Vakili, G. M. Anantharamaiah, R. Farias-Eisner, M. Navab, A. M. Fogelman, S. T. Reddy, and I. Shechter. 2011. Enhancement by LDL of transfer of L-4F and oxidized lipids to HDL in C57BL/6J mice and human plasma. *J Lipid Res* **52**: 1795-1809.

For this work, I would like to acknowledge Imaizumi for mass spec, Grijalva for mice, Hough for FPLC, Vakili for lipoproteins, Anantharamaiah for peptides, Farias-Eisner for guidance, Navab for mice, Fogelman for guidance. Both Reddy ST and Shechter I were co-principal investigators for this work.

Overall, I would like to acknowledge my funding sources: NIH Grants P02 HL-30568, HL-71776, F31 DK108592; Network Grant from the Leducq Foundation; and Castera, Laubisch and M.K. Grey Funds at UCLA.

Last but most important, I wouldn't have made it here without the support of my family and friends, as well as my mentors at UCLA: my father, David Meriwether Jr; my brother, Steven Meriwether; my fiancé and mother of my child, Olive Tang; and my close friends Alan Wagner, Justin Kirvan, Byron Stead, Rick Rever, Tom Rapier, and Carolyn Hong. And at UCLA, to all the members of my thesis committee, and particularly to Martin Martin, Sam Chow, and especially Srinu Reddy—friends and advisors who have encouraged and supported me throughout the course of my scientific journey so far. Thank you all.

Vita

Education:

Harvard University	BA	1997	Philosophy
UCLA	MA	2005	Philosophy
UCLA	PhD, expected	2018	Molecular and Medical Pharmacology

Positions/Employment, Memberships and Honors

1995-1997	Harvard University, Department of Chemistry, teaching assistant
1999-2007	Dean's Del Almo University Fellowship, UCLA
2001	Research mentorship fellowship, UCLA
2000-2007	Teaching Assistant, Department of Philosophy, UCLA
2009-2012	Staff Research Associate, Department of Medicine, Division of Cardiology, UCLA
2012-present	Graduate student researcher, Molecular and Medical Pharmacology, UCLA
2015-2017	NIH NIDDK F31 pre-doctoral fellowship

Publications

Meriwether, D. Sulaiman, D. Volpe, C. Grijalva, V. O'Connor, E. Borreh, N. Jedian, V. Trost, H. Martin, MG. Fogelman, AM. Reddy, ST COX2 dependent dysregulation of inflammatory signaling is rescued by apoA-I mimetic therapy in mouse models of IBD. (In preparation)

Mukherjee P, Hough G, Chattopadhyay A, Navab M, Fogelman HR, **Meriwether D**, Williams K, Bensinger S, Moller T, Faull KF, Lusis AJ, Iruela-Arispe ML, Bostrom KI, Tontonoz P, Reddy ST and Fogelman AM. Transgenic tomatoes expressing the 6F peptide and ezetimibe prevent diet-induced increases of IFN-β and cholesterol 25-hydroxylase in jejunum. *Journal of Lipid Research*. 2017;58:1636-1647.

Charles-Schoeman C, **Meriwether D**, Lee YY, Shahbazian A and Reddy ST. High levels of oxidized fatty acids in HDL are associated with impaired HDL function in patients with active rheumatoid arthritis. *Clinical rheumatology*. 2017.

Meriwether D, Sulaiman D, Wagner A, Grijalva V, Kaji I, Williams KJ, Yu L, Fogelman S, Volpe C, Bensinger SJ, Anantharamaiah GM, Shechter I, Fogelman AM and Reddy ST. Transintestinal transport of the anti-inflammatory drug 4F and the modulation of transintestinal cholesterol efflux. *J Lipid Res*. 2016;57:1175-93.

Navab M, Chattopadhyay A, Hough G, **Meriwether D**, Fogelman SI, Wagner AC, Grijalva V, Su F, Anantharamaiah GM, Hwang LH, Faull KF, Reddy ST, Fogelman AM. Source and role of intestinally-derived lysophosphatidic acid in dyslipidemia and atherosclerosis. *J Lip Res* 2015 Feb 2 [Epub ahead of print]

Sharma S, Umar S, Potus F, Iorga A, Wong G, **Meriwether D**, Breuilis-Bonnet S, Mai D, Navab K, Ross D, Navab M, Provencher S, Fogelman AM, Bonnet S, Reddy ST, Eghbali M., Apolipoprotein A-I mimetic peptide 4F rescues pulmonary hypertension by inducing microRNA-193-3p. *Circulation* 2014 **130**(9): p. 776-85.

Morgantini C, **Meriwether D**, Baldi S, Venturi E, Pinnola S, Wagner AC, Fogelman AM, Ferrannini E, Natali A, Reddy ST. Hdl lipid composition is profoundly altered in patients with type 2 diabetes and atherosclerotic vascular disease. *Nutr Metab Cardiovasc Dis*. 2014;24:594-599.

Navab M, Hough G, Buga GM, Su F, Wagner AC, **Meriwether D**…Fogelman AM. Transgenic 6f tomatoes act on the small intestine to prevent systemic inflammation and dyslipidemia caused by western diet and intestinally derived lysophosphatidic acid. *J Lipid Res*. 2013;54:3403-3418.

Vigant F, Lee J, Hollman A, Tanner L, Ataman Z, Yun T, Shui G, Aguilar-Carreno H, Zhang D, **Meriwether D**…Lee B. A mechanistic paradigm for broad-spectrum antivirals that target virus-cell fusion. *PLoS Pathogens* 2013; 9(**4**): e1003297.

Chattopadhyay A, Navab M, Hough G, Gao F, **Meriwether D**…Reddy ST, Fogelman AM. A novel approach to oral apoa-i mimetic therapy. *J Lipid Res*. 2013;54:995-1010

Devarajan A, Grijalva V, Bourquard N, **Meriwether D**, Imaizumi S., Shin B, Devaskar S, Reddy ST. Macrophage PON2 regulates calcium homeostasis and cell survival under ER stress conditions and is sufficient to prevent the development of atherosclerosis in PON2-def/apoE -/- mice on a Western diet. *Mol Genet Metab* 2012 Nov;107(3):416-27

Kelesidis T, Reddy ST, Huynh D, **Meriwether D**, Fogelman AM, Navab M, Yang O. Effects of lipid-probe interactions in biochemical fluorometric methods that assess oxidative properties of HDL. *Lip Health Dis*. 2012 July 6;11:87

Su F, Grijalva V, Navab K, Ganapathy E, **Meriwether D**, Imaizumi S, Navab M, Fogelman AM, Reddy ST, Farias-Eisner R. HDL mimetics inhibit tumor development in both induced and spontaneous mouse models of colon cancer. *Mol Cancer Ther.* 2012 Mar 13 [Epub ahead of print]

Kelesidis T, Currier J S, Huynh D, **Meriwether D**, Charles-Schoeman C, Reddy ST, Fogelman AM, Navab M, Yang OO. A biochemical fluorometric method for assessing the oxidative properties of HDL. *J Lip Res*. 2011 Dec;52(12):2341-51.

Meriwether D, Imaizumi S, Grijalva V, Hough G, Vakili L, Anantharamaiah GM, Farias-Eisner R, Navab M, Fogelman AM, Reddy ST, Shechter I. Enhancement by LDL of Transfer of L-4F and Oxidized Lipids to HDL in C57Bl/6J Mice and Human Plasma. *J Lipid Res.* 2011 Oct;52(10):1795-809.

Imaizumi S, Navab M, Morgantini C, Charles-Schoeman C, Su F, Gao F, Kwon M, Ganapathy E, **Meriwether D**, Farias-Eisner R, Fogelman AM, Reddy ST. Dysfunctional high-density lipoprotein and the potential of apolipoprotein A-1 mimetic peptides to normalize the composition and function of lipoproteins. *Circ J.* 2011 Jun 24;75(7):1533-8.

Ganapathy E, Su F, **Meriwether D**, Devarajan A, Grijalva V, Gao F, Chattopadhyay A, Anantharamaiah GM, Navab M, Fogelman AM, Reddy ST, Farias-Eisner R. D-4F, an apoA-I mimetic peptide, inhibits proliferation and tumorigenicity of epithelial ovarian cancer cells by upregulating the antioxidant enzyme MnSOD. *Int J Cancer*. 2011 Mar 21. doi: 10.1002/ijc.26079.

Gao F, Vasquez SX, Su F, Roberts S, Shah N, Grijalva V, Imaizumi S, Chattopadhyay A, Ganapathy E, **Meriwether D**, Johnston B, Anantharamaiah GM, Navab M, Fogelman AM, Reddy ST, Farias-Eisner R. L-5F, an apolipoprotein A-I mimetic, inhibits tumor angiogenesis by suppressing VEGF/basic FGF signaling pathways. *Integr Biol.* 2011 Apr;3(4):479-89.

Chapter 1: Introduction

The following thesis investigation divides into 3 parts, and in a sense 3 stages. First, in both the Appendix and in Chapter 2, I investigate the intestinal targeting and clearance of the apoA-I mimetic peptide 4F. I detail a mechanism by which 4F associates with lipoproteins in the circulation, transferring oxidized free fatty acids from apoB-containing fractions of the plasma onto HDL. Interestingly, this lipoprotein-associated 4F is itself cleared very quickly from the circulation, as it is taken up by the small intestine and transported intact directly into the intestinal lumen. I observe that this trans-intestinal transport of 4F is mediated by the trans-intestinal efflux of cholesterol (TICE). I further observe that intestinal 4F can itself modulate TICE: showing that 4F can increase reverse cholesterol transport (RCT) through the TICE pathway while also demonstrating that 4F itself can directly enhance TICE. As TICE has only recently been shown to play an important role in cholesterol homeostasis in humans, it offers an enticing pharmaceutical target for the lowering of plasma total cholesterol. While it is possible to increase TICE through use of LXR agonists, these have severe side-effects including steatosis of the liver. 4F and other apoA-I mimetics have proven remarkably safe and free of toxicological side effects. I have thus identified a promising new class of TICE modulators that can also lower plasma total cholesterol.

The second stage of this investigation concerns the pathogenic mechanism of the COX2 KO and cholate model of IBD. Mice that lack total or myeloid-specific COX2 develop severe inflammation in their ileo-ceco-colic junctions when challenged with a cholate-containing chow or cholate-containing high fat (CCHF) diet. While we had previously reported the existence of this inflammatory phenotype and proposed that COX2 KO and CCHF might constitute an important new model of IBD, we had not further worked out the pathogenic mechanism behind the chronic intestinal inflammation of this model. I had set out originally to investigate this mechanism, and I had proposed an overall hypothesis and 3 aims of investigation. I had hypothesized that in the absence of COX2, CCHF damaged intestinal

epithelium and altered barrier function in a manner that resulted in the translocation of pathogen associated molecular patterns. I further hypothesized that in the absence of COX2, dysregulation of both tissue repair and inflammation resolution pathways would interact together to amplify the developing inflammation through a sort of dysregulated positive feedback loop. I moreover aimed to investigate: a) the manner in which CCHF initiates inflammation in the COX2 and CCHF model; b) the role of COX2 in intestinal epithelial tissue repair; and c) the role of COX2 in the resolution of inflammation. I address the first and third of these aims in the first part of Chapter 3, while I revisit this overall conceptual framework and address the second aim in my concluding chapter 4.

The third stage of this thesis involves the convergence of these first two lines of investigation, a convergence that takes place in the second half of Chapter 3 and continues through Chapter 4. The Appendix and Chapter 2 constitute a partial account of the PKPD of the apoA-I mimetic 4F. Through the course of this investigation, I will have learned that 4F localizes to the intestine, where it can modulate lipid transport. I will moreover have noticed that 4F can alter the transport of lipid pro-inflammatory mediators within the circulation. In the opening sections of Chapter 3, I report that CCHF alters barrier permeability and increases translocation of PAMP, but that only in the absence of COX2 is there a loss of tolerance to these inflammatory stimuli. The absence of myeloid COX2 increases the levels of pro-inflammatory cytokine mediators in LPS-activated macrophages. More strikingly, in response to CCFH it increases the levels of lipid pro-inflammatory mediators in plasma, while altering the balance of pro-inflammatory and inflammation resolving mediators in intestinal tissue.

I thus sought to determine whether 4F could protect against intestinal inflammation in the COX2 MKO and CCHF model of IBD. Strikingly, 4F largely abrogated disease. Moreover, 4F rescued the COX2 MKO dependent elevation of lipid pro-inflammatory mediators in intestinal tissue and plasma, and it appeared to do so directly by increasing the clearance of these mediators from intestinal tissue and lipoproteins. It had been an open question whether the elevations of pro-inflammatory mediators were

causes or mere correlates of disease. We now had at least partial evidence that a therapy that inhibits disease also directly counter-acts these elevations—raising the probability that changes in the levels of these pro-inflammatory mediators partially constitute both the pathogenic mechanism of disease and the protective mechanism of 4F. Thus, the payoff from the convergence of these two lines of investigation has been not only the identification of a promising new class of therapies for IBD, but also a deeper understanding of the basic biology of this disease and the protective mechanisms of these therapies—a vivid illustration of the interplay between disease biology and PKPD.

A brief note on how to approach and read this thesis. First, Chapters 2, 3, and the Appendix all constitute investigations capable of standing on their own. Chapters 2 and the Appendix have already been published, and Chapter 3 is in its last revisions prior to submission. Each of these chapters but especially Chapters 2 and 3 contain in-depth introductions that cover the background and references that I would otherwise have put forward here. Because of the existence of these additional introductions (to 4F and TICE in Chapter 2, and to COX2 and IBD in Chapter 3), I will not revisit this material in this brief introduction.

Second, while the work of the Appendix is conceptually prior to the investigation presented in Chapter 2, the Appendix is an early and somewhat misleading effort whose lasting import is best understood in light of the work of Chapter 2. When I began the work of the Appendix, we had originally assumed that 4F—which had shown itself to protective in number of animal models of atherosclerosis—acted in the plasma and at the site of atherosclerosis to improve disease. I thus was guided by the question of whether 4F could directly interact with lipoproteins in the circulation, as a way of understanding how these 4F-lipoprotein complexes might mediate disease protection in atherosclerotic vessels. However, we came to understand that it was intestinal concentration rather than plasma concentration that correlated with the efficacy of the drug. Chapter 2 was written on the cusp of, and

played a part in, that paradigm shift regarding the protective mechanism of the apoA-I mimetic class of drugs.

I offer a precis of the Appendix in Chapter 4, where I tie together the work on the PKPD of 4F at the same time that I elaborate on and further develop this opening theme regarding the synergistic convergence of my first two stages of investigation. I would thus recommend that the reader turn to the Appendix only in light of its discussion in the opening section of Chapter 4. The limitations of that early publication will by that point perhaps reflect less harshly on me, and the reader might appreciate noticing how early observations of misunderstood import can nonetheless find a place within a newer and one hopes more accurate paradigm. The world is as the world is, one might say, no matter how one wants it to be.

I thus recommend proceeding through this thesis in its current order, moving from this brief introduction directly into Chapter 2, and only visiting the Appendix when prompted during Chapter 4. In Chapter 2, I first ask the question whether circulating 4F targets the small intestine, and I develop an account of the intestinal PKPD of this drug. In Chapter 3, I introduce the COX2 and CCHF model of IBD. I partially detail its pathogenic mechanism, before investigating the potential role of 4F as translational therapy for IBD. In Chapter 4, I return to the theme of this introduction—that of a synergy between disease biology and PKPD—while developing it further and with better articulation. I offer new data while I summarize my working models regarding the PKPD of 4F, the pathogenic mechanisms of the COX2 and CHHF model of IBD, and the protective mechanisms of 4F against this disease. I detail ongoing investigations, and I point towards what I think are some of the more exciting findings and avenues of investigation associated with this thesis work.

Chapter 2: Trans-intestinal transport of the anti-inflammatory drug 4F and the modulation of TICE

Abstract

The site and mechanism of action of the apoA-I mimetic peptide 4F are incompletely understood. Trans-intestinal cholesterol efflux (TICE) is a process involved in the clearance of excess cholesterol from the body. While TICE is responsible for at least 30% of the clearance of neutral sterols from the circulation into the intestinal lumen, few pharmacological agents have been identified that modulate this pathway. We show first that circulating 4F selectively targets the small intestine (SI) and that it is predominantly transported into the intestinal lumen. This transport of 4F into the SI lumen is trans-intestinal in nature, and it is modulated by TICE. We also show that circulating 4F increases reverse cholesterol transport from macrophages as well as cholesterol efflux from lipoproteins *via* the TICE pathway. We identify the cause of this modulation of TICE either as 4F being a cholesterol acceptor with respect to enterocytes, from which 4F enhances cholesterol efflux; or as 4F being an intestinal chaperone with respect to TICE. Our results assign a novel role for 4F as a modulator of the TICE pathway and suggest that the anti-inflammatory functions of 4F may be a partial consequence of the co-dependent intestinal transport of both 4F and cholesterol.

Supplementary key words: ●atherosclerosis ●apolipoprotein A-I mimetic peptides ●cholesterol ●reverse cholesterol transport ●trans-intestinal cholesterol efflux (TICE)

Introduction

Increasing evidence, both direct and indirect, indicates that the small intestine (SI) may be an important modulator of atherosclerosis. As a result, the SI offers promising therapeutic targets for the prevention and treatment of this disease.

The small intestine is linked to atherosclerosis in at least four respects. First, intestinal inflammation in the form of inflammatory bowel disease (IBD) has been linked to an increased prevalence of early stage vascular disease in patients without the classical cardiovascular risk factors. (1-3) Second, our own recent research has established a link between aberrant levels of lipid signals in the SI and both dyslipidemia and atherosclerosis. Intestinally-derived unsaturated lysophosphatidic acids (LPAs) and eicosanoids can both induce dyslipidemia as well as systemic inflammation in LDLR-/- mice.(4, 5) Dietary LPA can also induce atherogenesis,(6) and the levels of unsaturated LPAs in the SI correlate with the extent of atherosclerosis in LDLR-/- mice fed western diet (WD).(7)

Third, the small intestine is an important source of apoAI,(8) and at least in mice approximately 30% of the steady-state plasma HDL-cholesterol pool is derived from the small intestine.(9) Moreover, while HDL can interrupt atherogenesis by preventing oxidative modification of LDL(10-13) and promoting reverse cholesterol transport (RCT) from macrophages,(14-17) both protective functions of HDL can be lost in a manner that also implicates the small intestine. During inflammation HDL proteins and lipids can become oxidatively and enzymatically modified, and HDL can lose its capacity to inhibit LDL oxidation by fatty acid hydroperoxides.(18, 19) Intestinal inflammation(3) and aberrant levels of oxidized lipids in the SI(5) can affect this aspect of HDL function. Likewise, the cholesterol efflux capacity of HDL is sensitive to oxidation. For example, the myeloperoxidase (MPO) product hypochlorous acid oxidizes HDL and impairs ABCA1-dependent cholesterol transport,(20) and MPO activity is elevated in IBD.(21)

Fourth, the intestine itself is directly involved in cholesterol efflux and, together with the luminal reabsorption of cholesterol, the modulation of overall whole body cholesterol load. It is commonly understood that HDL and other lipoproteins return excess peripheral cholesterol to the liver hepatocytes, where the lipoproteins are taken up and transported into the cells. The cholesterol is then converted or secreted into bile and thereby excreted into the intestinal lumen for either re-uptake or loss to the feces.(22, 23) However, a non-biliary pathway for cholesterol excretion—known as "trans-intestinal cholesterol efflux" (TICE)—has also been recently identified.(24-28) Surgical models involving bile diversion have established that TICE is responsible for approximately 33% of total fecal neutral sterol loss in chow fed C57BL/6J mice(29) and for approximately 20% in chow fed FVB mice.(30) Additional studies involving genetic mouse models with severely diminished biliary cholesterol secretion have further confirmed the existence of TICE while also establishing that TICE is a dynamic process that can be stimulated under conditions of biliary insufficiency. For example, Mdr2 P-glycoprotein-deficient mice (*Mdr2*-/-), which are unable to secrete cholesterol into bile, nonetheless have no decrease in fecal neutral sterol loss compared to controls.(30) Of particular relevance to this paper, mice which highly over-express human Neiman-Pick C1-like 1 (NPC1L1) in their livers ($NPC1L1^{-LiverTg112}$ mice—hereafter Tg112 mice) have < 10% of the biliary cholesterol secretion of C57BL/6J controls, but they have no decrease in fecal neutral sterol levels. As these mice also exhibit no difference in intestinal cholesterol absorption, TICE must account for the bulk of the sterol excretion into the feces in these mice.(31, 32)

Increasing cholesterol efflux through the intestine might lower LDL cholesterol directly, potentially amplifying the athero-protective effects of statins and cholesterol uptake inhibitors.(33) Targeting TICE also raises the possibility of enhancing reverse cholesterol transport itself.(28) Moreover, selectively targeting TICE would avoid the side effect of gallstones that could come from modulating RCT by increasing biliary cholesterol secretion.(34) Alternatively, targeting intestinal inflammation as well as

oxidized lipids in the small intestine hold promise as treatments for atherosclerosis, for the reasons elucidated above.

The apoAI mimetic peptide 4F is an 18 amino acid amphipathic helix 4F that has the structure Ac-D-W-F-K-A-F-Y-D-K-V-A-E-K-F-K-E-A-F-NH_2.(35) 4F synthesized from L amino acids (L-4F) and from D amino acids (D-4F) have both been used in biological studies. D-4F and L-4F were shown to have the same *in vitro* and *in vivo* properties, indicating that stereo-specificity is not essential to the activity of the peptide.(36, 37)

4F has been shown to be effective as a treatment for atherosclerosis in numerous animal models.(38, 39) 4F has also been shown to improve HDL function,(40, 41) reduce systemic inflammation,(42) reduce oxidative stress,(43) and increase the clearance of oxidized lipid species from the circulation.(44) Given these effects, and given the nature and location of atherosclerosis itself, our laboratory had long assumed that the circulation was the site of action for 4F.(45) However, when we investigated the relationships between mode of administration, plasma levels, and efficacy of the drug, we discovered that the plasma levels of 4F did not in fact determine its efficacy.(46) Both oral and subcutaneous (SQ) D-4F at doses of 4.5 and 45 mg/kg significantly improved markers of HDL function and systemic inflammation equally for a given dose, but these modes of administration achieved very different plasma levels of peptide, with SQ levels being approximately 1000x higher. Rather, the equally effective SQ and oral doses achieved equal concentrations of 4F only in the feces(46) and the small intestine.(47) This finding suggested that the intestine may be the site of action for 4F. Of note, the second study further established that both SQ and oral D-4F lowered the levels of oxidized signaling lipids in the small intestine while simultaneously improving markers of HDL function and systemic inflammation.(47)

Our prior work did not further investigate whether and in what manner circulating 4F targets the SI. This current study thus began as a mechanistic pharmacokinetic investigation into the

distribution and excretion of IV-administered and circulating 4F as regards the small intestine. We have here determined that circulating 4F selectively targets the proximal small intestine and is largely transported into the intestinal lumen in a trans-intestinal manner. We have further observed that lumen-side 4F can be taken back up into intestinal tissue, suggesting the possibility of cycling or re-circulating 4F through both lumen and tissue.

TICE also selectively targets the proximal SI,(28) and lipoproteins including VLDL and LDL(48) and possibly HDL(49) are sources of the cholesterol effluxed through the TICE pathway. We have previously shown that circulating 4F has a high affinity for HDL and other lipoproteins(44) as well as for cholesterol.(50) Thus, we next hypothesized that the trans-intestinal transport of 4F might partially depend upon the trans-intestinal efflux of cholesterol. Using the genetic Tg112 mouse model as well as *ex vivo* studies involving Ussing chambers, we have here discovered that the transport of 4F into the intestinal lumen is partially mediated by TICE.

Interestingly, when we investigated the converse—whether 4F and 4F secretory transport can themselves modulate cholesterol efflux—we observed that circulating 4F can increase RCT from macrophages as well as cholesterol efflux from lipoproteins in Tg112 mice. We further observed *ex vivo* that 4F can increase the trans-intestinal efflux of cholesterol across duodenal explants. Together, these data indicate that 4F can modulate cholesterol excretion via the TICE pathway. As such, we here report on a novel means of increasing trans-intestinal cholesterol efflux while also adding detail regarding the intestinal-specific mechanism of the anti-inflammatory and anti-atherogenic drug 4F.

Materials and Methods

ApoA-I Mimetic Peptide 4F. The amino acid sequence of 4F is Ac-DWFKAFYDKVAEKFKEAF-NH_2. 4F was synthesized from L-amino acids (L-4F) and D-amino acids (D-4F) by the solid phase peptide synthesis method previously described.(51, 52) During the peptide chain elongation the ε-amino groups of the lysines were protected by t-Butyloxycarbonyl (t-BOC). The final step for the cleavage of the peptide from the resin along with the cleavage of tBOC protecting groups was accomplished using trifluoroacetic acid with suitable scavengers. Under these conditions the N-terminal acetyl group is stable whereas all of the other t-butanol protecting groups are cleaved. For synthesizing ^{14}C-peptide, ^{14}C-acetic anhydride was used instead of acetic anhydride as previously described.(53) Peptide purity was ascertained by mass spectral analysis and analytical HPLC. L-4F, D-4F, and ^{14}C-L-4F, as well as 4F-IS (^{15}N,^{13}C-4F), were synthesized in the laboratory of G.M. Anantharamaiah at the University of Alabama.

Mice, diets, and treatments. Wild-type C57BL/6J mice were obtained from the breeding colony of the Department of Laboratory and Animal Medicine at the David Geffen School of Medicine at UCLA after having been originally purchased from Jackson Laboratories. NPC1L1$^{-LiverTg112}$ mice (Tg112 mice) were developed and supplied by the laboratory of Liqing Yu.(31) All mice were maintained on a chow diet (Ralston Purina) unless otherwise noted. Western-type diet (Harlan-Teklad TD.88137) consisted of 0.2% cholesterol and 21% total fat. For the studies involving western diet (WD), mice were fed WD for six weeks prior to the experiments. LXR agonist treatment consisted of T0901317 (Cayman 71810) suspended in a vehicle containing 1.0% carboxymethlycellulose (CMC) and 0.1% tween 80. Mice were gavaged with 25 mg/kg T0901317 once daily for a period of seven days.(32) For all experiments, approximately equal numbers of male and female mice were used. All experiments were performed

using protocols approved by the Animal Research Committee at UCLA and in conformity with the Public Health Service Policy on Humane Care and Use of Laboratory Animals.

Isolation of lipoproteins from human plasma. Healthy human donor subjects were recruited after written consent approved by the University of California at Los Angeles (UCLA) Institutional Review Board. Fasting blood was collected in heparinized tubes (Becton Dickinson) and the plasma was separated by centrifugation. Human LDL and HDL were isolated by density centrifugation and were obtained from the Atherosclerosis Research Unit Core facility. LDL was isolated between densities of 1.019 - 1.063 g/ml and HDL between densities of 1.063 - 1.21 g/ml. After isolation the lipoproteins were dialyzed to remove the added salts.(54)

Determination of radioactivity. Radioactivity was determined as DPM by scintillation counting in 10.0 ml BioSafe II scintillation fluid (RPI Corporation) on a Packard Tri-Carb Model A900TR using QuantaSmart software.

LC/MS/MS analysis. LC/MS/MS was performed using a 5500 QTRAP quadruple mass spectrometer (SCIEX) equipped with electrospray ionization source. The HPLC system utilized an Agilent 1290 series LC pump equipped with a thermostatted autosampler (Agilent Technologies). Chromatography was performed using YMC-Pack ODS-AQ column (3 µm particle, 50 × 2.0mm; YMC) with a security guard cartridge at 45^{o}C. Mobile phase A consisted of 0.1% formic acid in water, and mobile phase B consisted of 0.1% formic acid in acetonitrile. The auotosampler was set at 4^{o}C. The injection volume was 10 µl, and the flow rate was controlled at 0.2 mL/min. The gradient program was as follows: 0-12min, linear gradient from 5%-95% B; 12-14 minutes, 95% B; 14-14.5 min, linear gradient to 5% B; 14.5-20 minutes, 5% B. The data acquisitions and instrument control were accomplished using Analyst 1.6.2 software

(SCIEX). Detection was accomplished by using the multiple reaction monitoring (MRM) mode with positive ion detection; the parameter settings used were: ion spray voltage= 5500 V; curtain gas=10 (nitrogen); ion source gas 1=60; ion source gas 2=70; temperature=500^{o}C. Collision energy, declustering potential and collision cell exit potential were optimized for each compound to obtain optimum sensitivity. The transitions monitored were for mass-to-charge ratios (m/z) 578.6/103.1 and 578.6/120 for both L-4F and D-4F; and 581.8/84.2 for 4F-IS (^{15}N,^{13}C-4F). Quantification was performed relative to IS using Analyst 1.6.2.

GC-MS analysis. Derivitized sterol samples in pyridine and BSTFA + TMCS reagent were run on an Agilent 7890B/5977A with a ZB-MR1 column (Zebron 7HG-G016-11). 1µl of sample was injected in split mode. Full oven program and mass spectrometry settings are available upon request.(55) MS detector was run in SIM mode. For *in vivo* studies involving analysis of fecal neutral sterols, fecal neutral sterol mass represents the sum of cholesterol, coprostanol, and coprostanone in each sample.(56) Internal standard 5α-cholestane was detected by parental ion of 372 m/z. The trimethylsilyl forms of coprostanol, cholesterol, and coprostanone were identified by RT relative to standards as well as by parental ions 460.4, 458.4, and 458.4 m/z respectively. Quantification was by the ratio of AUC of parental ions to AUC of IS, relative to the parental ion to IS ion ratios of the appropriate standard curves. For the ex vivo study involving analysis of cholesterol alone, the internal standard stigmastanol was detected by the trimethylsilyl form at m/z = 488.4, while cholesterol was detected by the cholesterol TMS fragment at 329.4.

Sample preparation for MS analysis. For LC-MS/MS analysis of 4F in mucosal media, internal standard was added to mucosal media, and the media were injected directly into the LC-MS/MS without further sample preparation. 4F was extracted from tissue and from SI rinse using the method of Bligh and

Dyer(57) following addition of internal standard, and upon concentration the aqueous phase was injected directly into the LC-MS/MS. For GC-MS analysis of neutral sterols in feces, cage feces was dried overnight at 50˚C . Approximately 100 mg of feces was isolated, crushed into a fine powder, and weighed exactly. 50 μg of 5α-cholestane was added. Sterols were first saponified in 2 ml of ethanol, together with 200 μl of 50% (w/v) KOH, and the mixture was homogenized and heated at 65˚C for 2 hrs. 1 ml of ionized water was added, and then sterols were extracted twice into 2 ml of n-hexane.(58) 200 μl of hexane from the combined extractions was dried down, and samples were derivitized by adding 50 μl of anhydrous pyridine (Sigma, 270970) and 50 μl of BSTFA + TMCS, 99:1 (Sigma, 33155-U). For determination of fecal neutral sterols in the feces of individual mice, approximately 10-20 mg of feces was isolated from the distal colons of mice before being dried, weighed, and treated as above. For determination of cholesterol in mucosal media from the Ussing chamber experiments, 2 μg of stigmastanol was first added to 1 ml of media; the sterols were extracted using the method of Folch;(59) and samples were further treated as above.

4F distribution studies. 4F (L-4F, D-4F, or ~0.2 μCi ^{14}C-L-4F) was administered at 25 mg/kg via tail vein. At predetermined time points between 3 and 60 minutes, the animals were sacrificed and perfused, and organs were dissected. Organs were homogenized, and ^{14}C-L-4F was determined by scintillation counting, while both L-4F and D-4F were determined by LC-MS/MS.

***In vivo* 4F secretory transport studies.** In order to assess whether circulating 4F was transported into the intestinal lumen, C57BL/6J mice were IV-administered 25 mg/kg ^{14}C-L-4F (~2.0 μCi) via tail vein. After 1 or 3 hours, the animals were bled, euthanized, and perfused. The entire SI from stomach to cecum was dissected, before being sequentially rinsed three times using PBS, 0.6% taurocholate, and 1.0% triton-X 100. The rinses were collected and combined for analysis. Large intestine was dissected

and washed with PBS three times, while the contents of the gall bladder were collected via insulin syringe. Tissues were dissected and homogenized prior to analysis. Radioactivity was determined in all samples via scintillation counting. This experiment was then repeated with L-4F, with the SI wash consisting only of 3 x PBS, and analysis being performed via LC-MS/MS. High (100 mg/kg) and low-dose (25 mg/kg) secretory transport studies in C57BL/6J were performed similarly. The effect of WD on the secretory transport of 4F was studied in Tg112 mice by first feeding the animals with WD or chow for 6 weeks. 25 mg/kg ^{14}C-L-4F was injected via tail vein, and radioactivity in SI rinse was determined as above. Feces from these individual mice were collected directly from the distal colon of these mice, and levels of neutral sterols in the feces were determined by GC-MS.(56)

Bile duct ligation study. C57BL/6J mice were anesthetized with isoflourane (5% induction, 1-2% maintenance), and bile ducts were either ligated or sham-ligated. We validated our surgical technique in a pilot study by monitoring Alcian blue that had been injected directly into the gall bladder: ligated mice showed no passage of Alcian blue into the duodenum. Because of the constraints of our surgical protocol as well as our interest in observing the transport of intact peptide, we then injected 25 mg/kg L-4F (rather than ^{14}C-L-4F) via tail vein into both ligated and sham ligated mice, and after 1 hour we determined L-4F in intestinal PBS rinse using LC-MS/MS.

Lung lavage. In order to study the transport of 4F into the alveolar space, ^{14}C-L-4F was IV-administered to C57BL/6J mice at both t = 0 hrs and t = 3 hrs. At t = 4 hrs, the mice were sacrificed. The lungs and trachea of the mouse were exposed by cutting longitudinally along the sternum, being careful to avoid damaging the lungs or trachea. A needle (20G, Fisher) was introduced into the proximal portion of the trachea, parallel with the trachea. Once secured, a 3ml syringe (Fisher) filled with 1.3mL PBS was attached to the needle and the lung was flushed three times, allowing for the total volume to fill the

lung with each flush. The lavage fluid was collected and the procedure was repeated 3-4 times for a total of 5 mL/mouse.(60) ^{14}C-label was determined in the wash by scintillation counting.

Ussing chamber studies: general. Ussing chamber experiments were carried out in an EasyMount Ussing Chamber System (EM-CSYS-2-Physiologic Instruments). For all studies, duodenal explants (muscle on) from C57BL/6J mice, 8-10 weeks of age, were mounted on sliders (P2304-Physiologic Instruments). Once in the Ussing Chambers, intestinal explants were incubated at 37^{o}C. The serosal and mucosal chambers contained 4 ml Krebs-Ringer buffers that were gassed at 95% O_2, 5% CO_2 (serosal bath) and 100% O_2 (mucosal bath). The Krebs-Ringer Buffers were at pH 7.4 after initial gassing with 95% O_2, 5% CO_2; and they had the following composition: 115 mM NaCl, 25 mM $NaHCO_3^-$, 2.4 mMK_2HPO_4, 1.2 mM $CaCl_2$, 1.2 mM $MgCl_2$, 0.4 mM KH_2PO_4, with 10 mM glucose and 10 mM mannitol added in the serosal and mucosal buffers, respectively.(61) The Ussing chamber runs lasted 90 minutes and 500µl samples were taken from each chamber every 0, 30, 60, and 90 minutes. Unless otherwise noted, all mucosal chambers also contained 1x micelles, in accord with the preparation of Iqbal et al. 0.14 mM sodium cholate, 0.15 mM sodium deoxycholate, 0.17 mM phosphatidylcholine, 1.2 mM oleic acid, and 0.19 mM monopalmitoylglycerol (62) Where indicated, serosal chambers contained human LDL and HDL at 0.72 mg protein/ml and 0.174 mg protein/ml, respectively. Non-permeable 70kDa FITC-Dextran Beads (Sigma Aldrich) were utilized to determine intestinal explant integrity by observing their absence in the mucosal chamber when added into the serosal chamber from 90-100 minutes.(49)

Ussing chamber studies: 4F uptake and secretory transport. *In vivo-ex vivo* 4F secretory transport studies. 800 µg (~ 25-30 mg/kg) of D-4F or L-4F in 300 µl saline was injected via tail vain into C57BL/6J mice. After 30 minutes, the mice were sacrificed and duodenal explants were mounted in Ussing chambers as above. Serosal chambers either did or did not contain HDL + LDL, while mucosal chambers

contained 1x micelles. 4F in both tissue and mucosal media was determined by LC-MS/MS, while cholesterol in mucosal media was determined by GC-MS. The levels of 4F in mounted tissues were compared to the levels of 4F in matching pieces of duodenum that had been taken from the same mice but that had not been mounted. *Ex vivo* 4F uptake studies**.** Duodenal explants from C57BL/6J mice were mounted in Ussing chambers. 50 μg/ml of L-4F alone was added to the mucosal chambers. After 90 minutes, the explants were removed and washed 3 x in PBS. Uptake of 4F by the tissue was determined by LC-MS/MS. 50 μg/ml of ^{14}C-L-4F was added to the serosal chambers of additional explants. Again after 90 minutes, the tissue was washed 3 x and uptake of 4F by the tissue was determined by scintillation counting.

Ussing chamber studies: TICE. *In vivo-ex vivo* trans-intestinal cholesterol efflux study**.** To investigate the effect of 4F on TICE within our Ussing chamber system, C57BL/6J mice were first injected with 800 μg D-4F (~ 25-30 mg/kg) via tail vein. After 30 minutes, the animals were sacrificed and explants were mounted in Ussing chambers as above. Each 4F-loaded explant had a sham-injected control explant that was run simultaneously and under identical conditions. Serosal medias contained ^{3}H-cholesterol loaded LDL and HDL, while mucosal medias contained 1x micelles. ^{3}H-label was determined in both tissue and mucosal media by scintillation counting. *Ex vivo* trans-intestinal cholesterol efflux study**.** Duodenal explants from C57BL/6J mice were mounted in Ussing chambers as above. Serosal media contained ^{3}H-labelled LDL + HDL, prepared as below, while mucosal media contained 0.25x micelles with or without 50 μg/ml D-4F. ^{3}H-label was determined in both mucosal media and tissue after 90 minutes. For both of these studies, D-4F rather than L-4F was used, in order to sidestep the possibility of loss of peptide function due to proteolysis across the 90 minutes of the Ussing chamber incubations.

J774 Cell Culture and ^{3}H-Cholesterol Loading. J774 mouse macrophages were grown in RPMI-1640 medium supplemented with 10% FBS, 100 U/ml penicillin, and 100 μg/ml streptomycin. Cells were incubated with 5 μCi/ml ^{3}H-cholesterol (Cholesterol [7-3H(N)], ARC) and 100 μg/ml acetylated LDL for 48 hours. Prior to injection, the resulting foam cells were washed, equilibrated, harvested, and re-suspended in media without FBS. All cell suspensions were analyzed microscopically to determine the number of live cells, and radioactivity was determined as above. On average, injections consisted of $2x10^{6}$ cells and 1 μCi ^{3}H-cholesterol.

***In vivo* macrophage RCT studies in Tg112 and WT mice.** The investigation of macrophage RCT in Tg112 and WT mice was performed in accord with the Rader group protocol,(63) except that we measured cholesterol efflux into the SI lumen rather than sterol excretion into the feces.(32) At t = 0 hours, mice were injected IP with approximately 500 μl of ^{3}H-cholesterol labeled foam cell suspension. After 8 hours, the mice were sacrificed and luminal rinse was collected. The rinse was then subjected to chloroform/methanol extraction by adding 4.5 ml of chloroform:methanol (2:1, v/v) to 2 ml of the lumen PBS rinse.(32) Following centrifugation, the lower chloroform phase containing ^{3}H-cholesterol was collected, dried, and re-suspended in scintillation cocktail for determination of radioactivity. The upper aqueous phase containing ^{3}H-bile acids was added directly to scintillation cocktail for determination of label. In order to study the effect of circulating 4F on cholesterol efflux in this model, 25 mg/kg ^{14}C-L-4F was IV-administered at t = 4 hours and again at t = 7 hours. At t = 8 hrs, SI rinse was collected and ^{3}H-cholesterol was determined, and ^{14}C label was determined directly in PBS rinse. ^{14}C-L-4F and scintillation counting, rather than L-4F and LC-MS/MS, were used in this study to determine peptide levels in order to avoid the possibility of tritium contamination of the instruments.

***In vivo* cholesterol efflux studies in Tg112 and WT mice.** Human HDL and LDL were labeled by adding ethanol-suspended ^{3}H-cholesterol directly to the lipoprotein mix and then removing any precipitate by centrifugation. For each mouse, 2 μCi ^{3}H-cholesterol was combined with 0.1 mg HDL cholesterol and 0.1 mg LDL cholesterol. Labeled lipoprotein was then pre-mixed with ^{14}C-L-4F (25 mg/kg/mouse) or vehicle before injection by tail vein into both Tg112 and litter-mate control mice. At t = 3 hrs, an additional 25 mg/kg ^{14}C-L-4F or vehicle was injected into each mouse. After 4 hrs, the mice were sacrificed and processed as above. As before, ^{14}C-L-4F and scintillation counting, rather than L-4F and LC-MS/MS, were used in this study to determine peptide levels in order to avoid the possibility of tritium contamination of the instruments.

Primary enterocyte cholesterol efflux study. Primary enterocytes were extracted and loaded with ^{3}H-cholesterol following the method of Iqbal et al.(62) C57BL/6J mice were fasted overnight and then sacrificed. SI was removed by dissection. Contents from the intestinal lumen were removed, washed with 117 mM NaCl, 5.4 mM KCl, 0.96 mM NaH_2PO_4, 26.19 mM $NaHCO_3$, and 5.5 mM glucose, and then filled with 67.5 mM NaCl, 1.5 mM KCl, 0.96 mM NaH_2PO_4, 26.19 mM $NaHCO_3$, 27 mM sodium citrate, and 5.5 mM glucose (buffer A). Intestines were bathed in oxygenated saline at 37^0 C for 10 min. After discarding the buffer, the intestinal lumen was refilled with buffer A containing 1.5 mM EDTA and 0.5 mM dithiothreitol and incubated in 0.9% sodium chloride solution at 37^0 C for 10 minutes. Luminal contents were collected and centrifuged at 1,500 rpm for 5 minutes. All buffers were adjusted to pH 7.4, gassed with 95% O_2/5% CO_2 for 20 min, and maintained at 37^0 C prior to use. Enterocytes were then suspended in 1.5 ml DMEM containing approximately 1 μCi/ml ^{3}H-cholesterol and incubated at 37^0 C. Cells were gassed with 95%0_2/5%CO_2 every 15 minutes. After 1 hour, enterocytes were centrifuged and washed three times with DMEM before being incubated with vehicle, micelles, or L-4F. After 2 hours, the cells were pelleted and ^{3}H-label was determined in the supernatants by scintillation counting.

Statistical Analyses. Error is reported throughout as ± standard error of the mean (±SEM). Statistical analyses were performed by unpaired two-tailed Student's t-tests, except where experimental groups were paired with matched controls, in which cases analyses were performed by paired two-tailed t-tests. Significance was set at $p < 0.05$.

Results

4F that is introduced directly into the circulation preferentially associates with the proximal small bowel.

In order to investigate the distribution of circulating 4F, we first administered 25 mg/kg ^{14}C-L-4F to C57BL/6J mice (n = 3) via tail vein. We observed that peptide label selectively targeted the small intestine 60 minutes post-injection (**Figure 1A**). In order to determine the kinetics of 4F uptake by the intestine, we examined the accumulation of 4F label at multiple time points from 3 to 60 minutes. We observed that both the duodenum and the jejunum but not the ileum or colon showed significant uptake of label across 0 - 60 minutes ($p = 0.003$ and 0.001, respectively), with duodenal uptake peaking at 15 - 30 minutes (**Figure 1B**). Next, in order to rule out the possibility that we had observed the uptake of mere label rather than intact peptide, we IV-administered 25 mg/kg L-4F (**Figure 1C**) and D-4F (**Figure 1D**), and we determined at 15 minutes post-injection the intestinal distribution of intact peptide by LC-MS/MS. We here observed similar patterns of distribution for L-4F and D-4F at 15 minutes as for ^{14}C-L-4F at both 15 and 60 minutes, indicating that the prior apparent uptake of 4F by the duodenum and jejunum but not ileum was neither the result of proteolysis nor clearance by the jejunum. Approximately 7.5% of total injected L-4F and D-4F were present intact in the duodenum and jejunum, but the concentrations of L-4F and D-4F were significantly higher for both in the duodenum compared to the jejunum ($p = 0.001$ and 0.005, respectively), indicating that both circulating L-4F and D-4F selectively target the proximal small bowel. The concentration of D-4F in both the ileum and cecum was higher than that of L-4F likely indicating that at least some proteolysis of L-4F in the distal SI had taken place. However, both IV-administered L-4F and D-4F behaved comparably as regards distribution from the circulation to the small intestine.

Circulating 4F that associates with the small intestine is transported into the SI lumen by directly and selectively crossing the intestinal epithelium.

In the experiments described above (Figure 1), we perfused the mice but did not clear the small intestinal contents before determining the distribution pattern of 4F. We next sought to determine with what radial compartment of the small intestine—lumen, mucosa, submucosa, muscle, or serosa—4F associated. In pilot experiments, we IV-administered 25 mg/kg ^{14}C-L-4F into C57BL/6J mice; and after 1 hour, we sacrificed and perfused the animals (n = 3). We freed the lumen of chyme; we tied off and filled the SI with a lower salt buffer followed by a high salt buffer containing EDTA and DTT; and we thereby isolated enterocytes.(64) We observed that the label was largely present in the first buffer rather than in enterocyte fraction or in the remaining tissue (data not shown), suggesting that 4F had been transported into the SI lumen. We then IV-administered 25 mg/kg ^{14}C-L-4F (1.8 uCi) into C57BL/6J mice, and at the end of 1 or 3 hours (n = 3 mice/time point) mice were sacrificed and perfused. We collected and determined radioactivity in a series of rinses of the SI: PBS alone, followed by a rinse of simple taurocholate micelles (TC) in order to penetrate the mucin layer,(65, 66) followed by a rinse of 1% Triton X-100 (TX) in order to dissolve the cell membranes of the mucosa.(67) We further analyzed the remaining intestinal tissues, as well as the liver and contents of the gall bladder (**Figure 2A**). Approximately 66% of the label associating with the small intestine was present in the PBS rinse by 1 hr, with no further label added by 3 hrs. After 3 hrs, label associated with the SI rinses and SI tissue had decreased by 33% from approximately 260,000 DPM to 170,000 DPM, while label present in the cecum and contents had increased 20-fold from 4000 to 80,000 DPM—indicating that label that had been released into the lumen by 1 hour was traversing the SI to the cecum. Label was also present in the feces by 3 hrs. In addition, label was found in the liver and the contents of the gall bladder, with gall

bladder label increasing approximately 2-fold from 1 to 3 hrs. In order to confirm that the results of Figure 2A were for intact peptide and not merely peptide label, we repeated the 1 hour time point experiment described in Figure 2A using L-4F, and we determined by LC-MS/MS that approximately 5% of total injected peptide was present intact in the initial PBS rinse (**Figure 2B**).

The data of Figure 2A are consistent with 4F reaching the SI lumen both trans-intestinally and through the hepatobiliary pathway. Consistent with label loading the SI tissue from the circulation before being released directly into the lumen, label was present in both the TX rinse and in the remaining SI tissue homogenate, with this label decreasing over time. However, consistent with 4F entering the lumen through the hepatobiliary pathway, label was also present in the contents of the gall bladder. While label in the gall bladder increased during the same time window in which label in the SI lumen was decreasing—suggesting a trans-intestinal pathway for 1 hr luminal 4F—there nonetheless exist reports that some lipophilic peptides are excreted into the SI lumen through the liver and bile.(68) Thus, in order to investigate the path by which 4F enters the SI lumen, we ligated the bile ducts of C57BL/6J mice and compared the amount of intact L-4F in the luminal PBS rinse of ligated animals compared to sham-ligated controls. We first validated our surgical procedure by injecting Alcian blue into the gall bladders of both ligated and sham-ligated mice and showed that blue dye entered the duodenum only in sham-ligated animals (**Supplemental Figures 1A** and **1B**). Next, we IV-administered 25 mg/kg L-4F to both ligated and sham-ligated mice (n = 3 mice/group), sacrificed the animals after 1 hr, and determined the levels of intact L-4F in the SI rinse by LC-MS/MS. We observed no difference in 4F transport between ligated and sham-ligated mice ($p = 0.5$) (**Figure 3A**), showing that under these conditions L-4F enters the SI lumen via a trans-intestinal rather than the hepatobiliary pathway.

In the bile duct ligation experiment, the amount of 4F recovered in the SI rinse in both experimental and control animals was many-fold lower than observed previously (compare Figures 2B and 3A). During the bile duct ligation experiment, the animals were under constant isoflourane

anesthesia, which has been shown to significantly reduce gastrointestinal motility in rats.(69) It is thus possible that the anesthesia itself depressed baseline intestinal clearance of 4F in this experiment. Moreover, the bile duct ligation model excludes from the SI lumen biliary delivery of cholesterol and, importantly, bile salts—which are important modulators of the trans-intestinal efflux of cholesterol.(70) We thus sought to confirm that 4F can indeed transport from intestinal tissue into the SI lumen by IV-administering 4F in vivo before studying its clearance from duodenal explants ex vivo within a Ussing chamber—an ex vivo physiological system for detecting and quantifying the transport of ions and drugs across epithelial tissues.(61) We IV-administered 800 μg D-4F (~25-30 mg/kg) into C57BL/6J mice (n = 7). We had previously observed that the concentration of 4F associated with the duodenum achieved its maximum around 30 minutes post-injection (see Figure 1B). Thus, after 30 minutes we sacrificed the animals and mounted duodenal explants within Ussing chambers that contained bile salt-containing micelles in their mucosal media and lipoproteins in their serosal media (see Methods for micelle and lipoprotein compositions). We then sampled the mucosal media from 0 – 90 minutes and determined the levels of intact D-4F released from the explants by LC-MS/MS. We observed a steady increase in D-4F transported from duodenal epithelium into the mucosal-side media across 90 minutes—with most of the transport occurring within the first 30 minutes, and with an average of 45 ng of D-4F released from the 0.1 cm^2 of exposed epithelium by 90 minutes (**Figure 3B**). Extrapolating from the amount of 4F released from 0.1 cm^2 explants to the approximately 7 cm^2 of the entire duodenum,(71) approximately 3 μg of transportable 4F was present in the duodenal tissue at 30 minutes post-injection. We also observed that the concentration of D-4F in these explants significantly decreased by approximately 60% after the 90 minute ex vivo run ($p < 0.05$), compared to paired control tissues that had not been mounted in the Ussing chambers (**Figure 3C**). While we chose to use D-4F in this experiment in order to sidestep the possibility of proteolysis of L-4F within the mucosal media over 90 minutes, we observed comparable transport when we repeated the experiment using L-4F (data not shown).

The experiments represented in Figures 3A-C establish not only that trans-intestinal secretory transport of 4F is possible (Figures 3B-C), but also that at least under some conditions, all circulating 4F that ends up present in the intestinal lumen arrives via a trans-intestinal rather than hepatobiliary pathway (Figure 3A). We last sought to determine whether 4F selectively targets intestinal epithelium, or whether 4F crosses any large epithelial barrier. We thus again IV-administered 25 mg/kg ^{14}C-L-4F to C57BL/6J mice (n = 6). After 1 hr, we sacrificed the animals and lavaged the lungs with PBS in order to assess trans-alveolar secretory transport via scintillation counting. We also determined radioactivity present in the SI rinse. In contrast to the SI rinse, we observed no label present in the lung lavage (**Figure 3D**) demonstrating comparative intestinal epithelium specificity.

Intestinal transport of circulating 4F is modulated by TICE.

We began our investigation into the mechanism of 4F intestinal secretory transport by first IV-administering low (25 mg/kg) and high (100 mg/kg) doses of L-4F to C57BL/6J mice (n = 4 and 6, respectively) and then after 1 hour determining the levels of intact peptide in the SI PBS rinse by LC-MS/MS. We observed no significant difference as regards transport of intact peptide into the lumen (p = 0.4) (**Figure 4A**). This result indicated that some aspect of the secretory transport pathway was saturable at high doses.

We observed that the concentration of 4F was highest in the proximal small bowel (see Figures 1C-D). Trans-intestinal cholesterol efflux is also greatest in the proximal small bowel.(25, 28) We had previously reported that 4F binds with high affinity to lipoproteins including VLDL and HDL(44) as well as to cholesterol alone.(50) Lipoproteins including LDL and VLDL(48) and possibly HDL(49) deliver cholesterol from the circulation to the basolateral side of small intestinal enterocytes, and TICE is itself an active and saturable pathway.(25) We thus hypothesized that the trans-intestinal secretory transport

of 4F could be modulated by TICE. Consistent with this hypothesis the 90 minute uptake of 4F from the serosal side was significantly greater than from the mucosal side of duodenal explants in a Ussing chamber (**Figure 4B**).

In order to further test this hypothesis, we required a model that would allow us to manipulate TICE while observing the effect on the secretory transport of 4F. A diet high in fat and cholesterol has been reported to increase TICE 50-100% in WT mice.(70) This effect of Western diet on TICE is enhanced several fold in NPC1L1$^{-LiverTg112}$ mice (Tg112 mice), which secrete little to no biliary cholesterol but whose levels of both cholesterol absorption and fecal neutral sterols are comparable to WT regardless of diet.(32) We thus obtained two male mice hemizygous for the NPC1L1 transgene. We bred these mice with WT C57BL/6J females: genotyping demonstrated the presence of the human NPC1L1 transgene (677 bp) together with a VLDL-specific positive control (320 bp) in half of the offspring, as predicted (**Supplemental Figure 2**). For further validation, we measured fecal neutral sterol levels by GC-MS(56) in the Tg112 offspring and found no difference compared to the levels in WT mice, consistent with prior reports (**Figure 5A**). (31, 32) We next fed both male and female Tg112 mice and littermate controls (n = 4 mice/gender/group) a western-type diet (WD) or chow for six weeks, after which we IV-administered 675 μg per mouse (~ 25 mg/kg) ^{14}C-L-4F to all mice. After 1 hour, the mice were sacrificed, and label was determined in the SI rinse by scintillation counting. Both male and female mice had significantly more 4F transport into the SI lumen on WD compared to control ($p = 0.007$ and 0.005, respectively). Interestingly, while male and female mice showed no significant difference with respect to 4F secretory transport when on chow ($p = 0.2$), male mice exhibited more such 4F transport than female mice when both were fed WD ($p = 0.008$) (**Figure 5B**). As all mice in the current experiment had been dosed at 675 μg ^{14}C-L-4F/mouse (rather than 25 mg/kg as before), this sex difference as regards 4F transport was not due to the heavier male mice receiving more total peptide. Fortuitously, this unexpected difference also allowed us to use fecal neutral sterol levels as a marker for TICE in these

two groups, in order to confirm that enhanced 4F transport correlates with enhanced TICE in this model. Were one comparing chow vs. WD fed animals alone, the relation between TICE and fecal neutral sterol levels would be confounded by the difference in the cholesterol content of the diets themselves. Thus, the fact that WD-fed animals had higher levels of fecal neutral sterols would not of itself tell us that these animals exhibited greater TICE: the difference could be the mere result of the pass-through or incomplete absorption of the cholesterol in the food. Both the male and female mice of our final comparison were on WD, however, thereby removing this particular confounding variable. We thus determined by GC-MS the fecal neutral sterol levels of the individual mice of Figure 5B. Of interest, male mice on WD had significantly higher levels of neutral sterols in their feces compared to female mice on WD ($p = 0.01$) (**Figure 5C**), independently supporting the conclusion that the levels of 4F secretory transport in this experiment correlated with the levels of TICE.

Nonetheless, WD presumably has many effects on Tg112 mice beyond increasing TICE. Even if we allow that the experiment of Figures 5B-C establishes a correlation between TICE and 4F secretory transport, it does not thereby establish causation. Recently, TICE has been studied using murine duodenal explants within a Ussing chamber system.(49) We thus turned again to the in vivo/ex vivo model of Figure 3B, in order to study the effect of TICE on the secretory transport of 4F within a simpler system. First, we established the existence of TICE ex vivo by observing the transport of ^{3}H-cholesterol across duodenal explants from C57BL/6J mice that had been mounted in our Ussing chambers (for an example of baseline TICE within the Ussing chamber system, see the control group of Figure 7A). Next, we IV-administered 800 μg D-4F (~25-30 mg/kg) to C57BL/6J mice ($n = 7$), and after 30 minutes we sacrificed the mice and mounted within Ussing chambers duodenal explants together with matched controls from the same animals. For every matched pair, the serosal media of one explant contained HDL+LDL while the media of the other explants was basic serosal media alone; and the mucosal medias for all samples contained micelles (for micelle and lipoprotein compositions, see Methods). We sampled

the mucosal media across 90 minutes and determined the concentrations of D-4F and cholesterol present in the media at 30 and 60 minutes (data not shown) as well as at 90 minutes by LC-MS/MS and GC-MS, respectively. We observed that the presence of serosal-side lipoprotein significantly enhanced the transport of both D-4F (by 171 %) and cholesterol (by 270%) from the experimental explants into the mucosal media compared to the matched controls ($p = 0.044$ and 0.047) (**Figure 5D**). This experiment was conducted pair-wise, in order to compensate for the possibility of variable loading of 4F into the duodenum. The data in Figure 5D is thus expressed as % change compared to the matched controls. However, total 4F and cholesterol averaged across all groups also increased, from approximately 80 ng (0.034 nmol) 4F and 110 ng (0.28 nmol) cholesterol to 120 ng (0.052 nmol) 4F and 260 ng (0.67 nmol) cholesterol. Of further note, the secretory transport of 4F over time mirrored that of Figure 3B: approximately linear through 30 minutes before tapering off to 90 minutes.

Our results from the above two separate models (in vivo and ex vivo) suggest that trans-intestinal secretory transport of 4F can be modulated by TICE. In both models, the degree of TICE correlates with the degree of 4F transport. And while it is possible that in either model taken by itself, the initiating cause (WD on the one hand, serosal side lipoproteins on the other) may independently increase both TICE and 4F transport, the existence of correlations between 4F transport and TICE in two separate models strongly suggests a causal connection between both processes.

IV-administered 4F increases macrophage RCT and cholesterol efflux from lipoproteins in TG112 mice.

Trans-intestinal efflux of cholesterol appears to help drive 4F transport from intestinal epithelium. 4F also binds with high affinity to lipoproteins(44) and to cholesterol.(50) These facts suggest a model in which 4F associates with cholesterol as it is taken up and transported apically by enterocytes. What of the converse: does 4F transport itself modulate cholesterol efflux? Oral D-4F can

increase macrophage RCT. (72) While 2 week treatment of 45 mg/kg/day oral D-4F only achieves plasma Cmax of approximately 500 ng/ml, the concentration of D-4F at that dose in intestinal tissue is markedly higher, with approximately 100 μg present in the SI.(5) As shown in **Figure 4D**, in duodenal explants not only is 4F taken up from the serosal media, it can be taken up from mucosal media as well. These facts suggest that the mechanism by which oral 4F increases macrophage RCT is at least partially intestinal in nature, perhaps through the upregulation of TICE. As IV-administered 4F achieves concentrations in the intestine comparable to that achieved by high dose oral D-4F (compare Figures 1C-D with Table 1(5)), we hypothesized not only that IV-administered 4F could increase macrophage RCT, but that it would do so at least in part by modulating TICE.

Temel et al. investigated macrophage RCT using the Rader protocol,(63) and they showed no difference in cholesterol excretion between Tg112 and WT mice. While intestinal cholesterol absorption was unchanged in Tg112 mice compared to controls, biliary sterol secretion was largely inhibited (> 90% reduction). Temel et al. concluded that only TICE could account for the fact that cholesterol excretion in Tg112 mice was nonetheless comparable to that in WT mice, and they thus concluded that TICE could modulate macrophage RCT. They supported this latter conclusion by repeating the macrophage RCT experiment in bile-diverted versus surgical control mice and again found no difference in luminal cholesterol excretion, further establishing that macrophage RCT can indeed follow the TICE pathway.(32) Others have called this conclusion into question, however. Of note, Njistad et al. assessed macrophage RCT using *Abcb4*-/- mice as well as in a bile duct ligation model, and they observed that in the absence of biliary cholesterol secretion macrophage RCT was mostly ablated.(73)

Because of this controversy, we first repeated the macrophage RCT experiment of Temel et al. in Tg112 vs. WT mice, with modification. In particular, we applied their protocol for studying ^{3}H-cholesterol efflux in the biliary diversion model, to the study of TICE in Tg112 mice. (63) Thus, we loaded J774 macrophages with acetylated LDL and ^{3}H-cholesterol and at time t = 0 hrs administered the

macrophages by intraperitoneal injection to both Tg112 and WT mice. At t = 8 hrs, the mice were sacrificed, the luminal contents of the entire SI were collected with a PBS rinse, and a chloroform/methanol extraction was performed. Radioactivity in the chloroform phase was determined, as a measure of ^{3}H-cholesterol; while radioactivity in the aqueous phase was also determined, as a measure of ^{3}H-bile acids (**Figure 6A**). When Temel et al. studied macrophage RCT in Tg112 mice, they measured ^{3}H-cholesterol in the feces; and they observed no difference in cholesterol efflux between Tg112 and WT mice. Consistent with this observation, we saw no difference in ^{3}H-cholesterol efflux into the lumens of Tg112 and WT mice.

We next asked whether IV-administration of L-4F could increase macrophage RCT in both Tg112 and WT mice. The timeline for this experiment was as follows: at t = 0 hrs, we administered by intraperitoneal injection ^{3}H-cholesterol loaded J774 macrophages to both Tg112 and littermate control mice; at t = 4 hrs, we IV-administered 25 mg/kg ^{14}C-L-4F or saline vehicle (n = 5 mice/group = 20 total mice); at t = 7 hrs, we IV-administered a second equal dose of ^{14}C-L-4F or saline vehicle; at t = 8 hrs, we sacrificed the animals and analyzed the luminal rinse. Of note, we observed that IV-administered 4F significantly increased ^{3}H-cholesterol efflux into the lumen in both Tg112 and WT mice (**Figure 6B**). We further detected comparable level of ^{14}C-L-4F in the lumens of both Tg112 and WT mice (**Figure 6C**).

The result of Figure 6B establishes that IV-administered 4F can increase macrophage RCT in Tg112 mice, but it does not reveal whether 4F increases cholesterol efflux as such. Indeed, we observed—consistent with the observations of Xie et al. (72)—that 4F can dose-dependently increase cholesterol efflux from J774 foam cells in vitro (**Supplemental Figure 3**). Thus, one possibility is that 4F increased labeled cholesterol efflux from the J774 cells in vivo leading to higher levels of plasma labeled cholesterol, while the increase of labeled cholesterol in the SI was due solely to this effect without any direct effect of 4F on TICE. In order to address this possibility, we repeated the experiment of Figure

6B, except that we eliminated macrophages and directly administered HDL and LDL that had been loaded with ^{3}H-cholesterol (**Figure 6D**).

In choosing to introduce the labeled cholesterol together with HDL and LDL, we sought a generous system that would give us our best chance of independently observing an effect of 4F on cholesterol efflux into the SI lumen. While there exists evidence in the literature that HDL can play the role of lipoprotein carrier for TICE,(49) there exist competing studies that have indicated that apoB containing lipoproteins are the carriers.(48) Because of this uncertainty, we combined both HDL and LDL together when we introduced labeled cholesterol directly into the circulation in the experiment of Fig 6D.

In this experiment, we once again observed that IV-administered 4F significantly increased luminal ^{3}H-cholesterol efflux in both Tg112 and WT mice, suggesting that any effect 4F might have had on the efflux of cholesterol from J774 macrophages was not the sole cause of the effect of 4F on macrophage RCT. Rather, IV-administered 4F directly increases cholesterol efflux from the circulation into the SI. Given the nature of cholesterol excretion in Tg112 mice, this result strongly suggests that IV-administered 4F can increase TICE. Of note, however, the effect of 4F on cholesterol efflux was significantly greater in WT mice compared to Tg112 mice. While we had not observed this difference in the experiment represented in Figure 6B, this result suggests that in WT mice there remains a hepatobiliary component to the effect of 4F on luminal cholesterol efflux. This possibility is consistent with the results represented in Figure 2A, in which we observed the presence of ^{14}C label within the contents of the gall bladder.

4F increases TICE through duodenal explants and can act as a cholesterol acceptor with respect to cholesterol efflux from enterocytes.

While the experiment of Figure 6D establishes that 4F modulates luminal cholesterol efflux in both Tg112 and WT mice in a macrophage-independent manner and strongly suggests that 4F can modulate TICE, it does not fully prove the latter. Cholesterol secretion into bile is severely diminished in Tg112 mice, but it is not entirely abrogated.(32) It thus remains possible that 4F increases luminal cholesterol efflux in Tg112 mice solely by modulating this residual biliary cholesterol secretion. We thus turned once again to the Ussing chamber in order to ask the question whether 4F can in fact increase TICE. As in the experiment represented in Figure 5D, we first loaded 4F into intestinal tissue in vivo by IV-administering 800 μg D-4F (~ 25-30 mg/kg) to C57BL/6J mice. After 30 minutes, we sacrificed the animals and mounted duodenal explants into Ussing chambers, together with explants from animals that had not been administered 4F. The serosal media contained HDL and LDL that had been loaded with ^{3}H-cholesterol, and we determined radioactivity in the mucosal media at 90 minutes (**Figure 7A**). We observed that the presence of 4F within the explants significantly increased the trans-intestinal efflux of labeled cholesterol while also significantly increasing the loading of ^{3}H-choleseterol into the duodenal explants.

The results reported in Figure 7A suggest two basic mechanisms. First, 4F could act within the tissue, where it could draw more serosal-side cholesterol into the tissue itself, or where it could act as an internal chaperone with respect to cholesterol efflux. Second, 4F within the tissue is transported into the mucosal media (see Figure 3B), where it would be well positioned to act as a cholesterol acceptor with respect to TICE. In order to partially test this second possibility, we stripped enterocytes from C57BL/6J mice and loaded them with ^{3}H-cholesterol. We observed that 4F dose-dependently increased cholesterol efflux from these loaded cells (**Figure 7B**). While this result is consistent with 4F acting as a cholesterol acceptor in the experiment of Figure 7A, the primary enterocytes of Figure 7B were non-polarized. This experiment thus failed to determine whether 4F could increase cholesterol efflux from apical-side rather than basolateral-side transporters. Because of this limitation, we made use of the

polarized nature of duodenal explants within our Ussing chambers, to investigate the effect of mucosal-side 4F on TICE proper. We mounted within Ussing chambers duodenal explants together with matched controls from the same animals. As in Figure 7A, we added ^{3}H-cholesterol loaded LDL+HDL to the serosal media. For each pair of explants, the mucosal medias contained either micelles together with D-4F or micelles together with vehicle alone. We observed that mucosal-side 4F significantly increased ^{3}H-cholesterol loading into the explants, while also significantly increasing the efflux of labeled cholesterol into the mucosal media itself (**Figure 7C**). Of note, when we attempted the experiment of Fig 7C in the absence of micelles, we observed neither a stable baseline TICE nor a consistent effect of 4F (data not shown). This result is in contrast to that of Figure 7B, in which 4F promoted cholesterol efflux from primary enterocytes even in the absence of micelles. These observations suggest that micelles are an important necessary condition on TICE *ex vivo*, and in this they are consistent with the necessary role of micelles for *in vivo* TICE that has been reported in the literature.(70)

Discussion

We have here observed that circulating 4F selectively targets the SI (Fig 1), where it is largely transported intact into the SI lumen (Fig 2) in a trans-intestinal process (Fig 3) that is at least partially mediated by TICE (Fig 5). In turn, the trans-intestinal secretory transport of 4F can itself modulate TICE (Figs 6-7), at least in part by acting as a cholesterol acceptor within the SI lumen (Fig 7). 4F has been shown to be effective as a treatment for atherosclerosis and other inflammatory conditions.(38, 39, 74) Although 4F has been hypothesized to increase the clearance of pro-inflammatory and oxidized lipid species from the circulation,(44) a mechanism common to 4F's efficacy in various inflammatory disease models is not yet known. Our findings may thus help illuminate a mechanism of action of 4F. Independently, we have here identified a novel modulator of TICE—a finding of potential importance regarding the basic biology and pharmacological manipulation of this cholesterol excretion pathway.

In support of our prior hypothesis that the intestine is the site of action of 4F, we have shown here that circulating 4F selectively targets the proximal small bowel (Figure 1). Moreover we have characterized the basic mechanism by which circulating 4F targets the SI.

First, while we had previously speculated that circulating 4F might reach the SI solely through the hepatobiliary pathway,(46) we have now established that 4F is trans-intestinally transported into the SI lumen (Figures 2-3). While these findings do not preclude 4F reaching the SI lumen through the bile, the kinetics of 4F within the bile appear out of phase with the kinetics of 4F transport into the SI lumen (Figure 2A). Moreover, under anesthesia at least, all 4F transport into the SI lumen is trans-intestinal (Figure 3A); and the amount of 4F transport from duodenal explants ex vivo is consistent with the trans-intestinal pathway being predominant (Figure 3B).

Second, we have established that TICE can modulate the trans-intestinal transport of 4F (Figure 5). WD enhances TICE in Tg112 mice.(32) Correlative with this effect, WD increased the trans-intestinal

transport of 4F (Figure 5B-C). We also observed that the secretory transport of 4F that had been pre-loaded into duodenal explants can itself be enhanced by serosal-side lipoproteins and their attendant TICE (Figure 5D). This result together with those of Figures 5B-C—ex vivo and in vivo models of enhanced TICE exhibiting enhanced trans-intestinal 4F transport—strongly support the conclusion that 4F transport can be modulated by TICE. Because 4F appears to associate with lipoproteins in the circulation,(44) and because TICE involves the uptake of circulating lipoproteins by the basolateral membranes of enterocytes,(24-28) it is possible that some of the increase in 4F that we observed in Tg112 mice on WD is the result of increased targeting of circulating 4F to enterocytes (Figure 5B-C). However, we also observed that the transport of 4F that had been pre-loaded into duodenal explants can itself be enhanced by serosal-side lipoproteins and their attendant TICE (Figure 5D). The results of Figure 5D indicate that at least part of the mechanism by which TICE can enhance 4F transport is intraepithelial in nature. The saturability of the 4F transport pathway (Figure 4A) further suggests that the mechanism is transcellular. It may thus seem reasonable to hypothesize that 4F, having been carried through the circulation associated with lipoproteins and having loaded into enterocytes basolaterally, co-effluxes with intracellular cholesterol through transporters on the apical membranes of enterocytes. This hypothesis is strengthened by the fact that 4F also binds cholesterol with high affinity.(50) As against this model, however, it is worth noting that while we ourselves have shown that 4F associates with lipoproteins *in vivo*, there exist some reports in the literature that 4F does not bind to the lipoprotein fraction of the plasma *in vivo*.(75) More importantly, the stoichiometry involved weighs against a simple co-efflux model. In the experiment associated with Figure 5D, approximately 0.02 nmol peptide together with approximately 0.3 nmol cholesterol were transported into the mucosal-side media, for a molar ratio of about 1 to 15. Given the size and conformation of 4F, it is unlikely that one peptide molecule associates with 15 cholesterol molecules during any single co-efflux event. However, it remains possible that peptide could co-efflux with cholesterol at a higher molar ratio, only for peptide

then present at the apical boundary of enterocytes to further enhance the efflux of cholesterol itself, perhaps through additional transporters (see Figures 7B-C).

Lipoproteins and cholesterol can be taken up by enterocytes through LDLR as well as possibly SRB1 located on their basolateral membranes, and intracellular cholesterol is effluxed through the apical membranes via abcg5/g8 as well as abcb1a/b.(49) Abcb1, also known as P-glycoprotein 1 or multidrug resistance protein 1 (MDR1), is a member of the ATP-binding cassette transporters sub-family B. Abcb1 is an ATP-dependent drug efflux pump for xenobiotic compounds with broad substrate specificity, but it can also act as a cholesterol floppase(76) and has been shown to contribute to TICE.(49) Abcb1 is thus a good candidate for the apical transporter of 4F—perhaps explaining why there exists baseline 4F transport from duodenal explants even in the absence of TICE, but why serosal-side lipoproteins nonetheless significantly increase 4F transport (Figure 5D). We are continuing to investigate the precise molecular mechanism by which 4F is taken up from the circulation and transported into the intestinal lumen by the proximal SI.

The 4F secretory transport pathway hypothesized above could account for the manner in which SQ-administered 4F lowers levels of oxidized lipids including HETEs and HODEs in intestinal tissue and enterocytes. (5, 77) 4F binds these oxidized lipids with high affinity.(50) If circulating lipoproteins target 4F for basolateral uptake by enterocytes, and if 4F is subsequently cleared apically through e.g. abcb1a/b, 4F could carry with it any intracellular lipid species it binds with high affinity. This pathway could also account for the manner in which 4F lowers levels of oxidized lipids in plasma(78) and lipoproteins.(44) Finally, orally administered 4F achieves concentrations in intestinal tissue comparable to SQ-administered 4F for a given dose. We have shown here that mucosal-side 4F can be taken up by duodenal explants (Figure 4B). If 4F taken up from the SI lumen is itself transported back into the lumen as above, this same transport pathway could also account for the manner in which oral 4F lowers levels of oxidized lipids in enterocytes.(5) We must continue to investigate, however, whether the reduction

of oxidized lipids in the SI is a direct consequence of 4F transport as hypothesized here: whether it is the result of the direct clearance of the oxidized species, or whether it is rather the result of e.g. a clearance of substrates like arachidonic acid(5) or an effect upon enzymes including PLA_2 and 12/15 LOX.

Through the employment of the TG112 mouse model (Fig 6) as well as our ex vivo Ussing chamber system (Fig 7), we have established that 4F can modulate the TICE pathway. These findings are of potential importance as regards the mechanism of 4F. While we had previously shown that 4F can increase macrophage RCT *in vivo*,(79) the precise mechanism behind this effect was unknown. The results of Figure 6B, together with those from Figs 6D and 7, indicate that 4F can affect macrophage RCT at least in part by modulating TICE. This observation raises the possibility that the common understanding of the anti-atherogenic mechanism of 4F may be incomplete. 4F can bind oxidized lipids with much higher affinity than apoAI,(50) while its capacity to stimulate cholesterol efflux from macrophages is lower than apoAI on a per molar basis (80, 81). Facts like these have led some to argue that the cholesterol efflux capacity of 4F is of secondary importance at best compared to its anti-oxidative capacity, as regards its effects upon atherosclerosis.(82) However, if 4F affects cholesterol efflux and macrophage RCT in vivo at the level of TICE rather than at the level of cholesterol efflux from macrophages themselves—as is suggested by results reported in Figures 6B and 6D—then arguments against the importance of cholesterol efflux within the mechanism of 4F based on *in vitro* studies of cholesterol efflux from macrophages may be misplaced. It is an open question in the literature whether increasing TICE alone can protect against atherosclerosis. Likewise, while our results strongly suggest that 4F can increase macrophage RCT (Fig 6B) as well as cholesterol efflux from the circulation itself (Fig 6D) in a TICE dependent manner, we do not here directly link these phenomena to the anti-atherogenic effects of 4F. However, our present findings do at least suggest that the effects of 4F on cholesterol excretion and TICE deserve a second look. We are continuing to investigate whether the modulation of TICE by 4F plays an important role in the anti-atherogenic mechanism of this peptide.

Our in vivo studies involving the effects of 4F on macrophage RCT and cholesterol efflux from the circulation involved the use of the Tg112 mouse model. While investigating macrophage RCT, Temel et al. showed that sterol secretion was undiminished compared to controls in both Tg112 as well as a biliary diversion model. They concluded that macrophage RCT could proceed via the TICE pathway and not just the hepatobiliary pathway.(32) However, in addition to the work of Nijstad et al., (73) Xie et al. showed that macrophage RCT was reduced in Tg112 mice that had been crossed to NPC1L1 knock-out mice.(83) Our results here support Temel et al. as regards cholesterol excretion in Tg112 mice during macrophage RCT. Consistent with Temel, we observed no difference in the luminal efflux of labeled bile acids and cholesterol in Tg112 mice versus controls with respect to macrophage RCT (Figure 6A). Given that biliary sterol secretion is severely compromised in Tg112 mice,(31, 32) and given that cholesterol absorption does not differ between Tg112 and WT mice,(32) our observation that both Tg112 and WT mice exhibited comparable levels of luminal cholesterol excretion in the macrophage RCT experiment of Figure 6A suggests that most of the cholesterol label that accumulated in the SI lumen in Tg112 mice was a function of TICE.

Our investigation into the effects of 4F on cholesterol efflux took the form of an increasingly narrow or circumscribed investigation into mechanism. We first established that 4F could increase macrophage RCT in Tg112 mice (Fig 6B). Next, we ruled out the possibility that this first observation was solely the result of 4F enhancing cholesterol efflux from macrophages by observing that 4F could increase cholesterol efflux directly from the circulation of Tg112 mice (Fig 6D). Finally, we zoomed into the intra-duodenal effects of 4F within our Ussing chamber system, and we observed that even here 4F could enhance TICE (Figure 7A). We then explained this final effect in terms of the role of 4F as cholesterol acceptor on the apical side of enterocytes (Figs 7B and C). These experiments leave open at least two questions, however.

First, while 4F increased cholesterol efflux into the SI lumen both from foam cells (Fig 6B) as well as from circulating lipoproteins (Fig 6D)—suggesting that the mechanism behind the results reported in Fig 6B contains the mechanism behind the results reported in Fig 6D—it is nonetheless possible that these overlapping mechanisms may differ in at least two respects. The labeled free cholesterol (FC) from foam cells (Fig 6B) most likely enters the circulation associated with HDL, where it can be readily converted to labeled cholesterol esters (CE) by the activity of LCAT.(84) Thus, some good portion of the label from foam cells (Fig 6B) will be within HDL-associated cholesterol esters. By contrast, while the labeled lipoproteins (Fig 6D) contain HDL, they also contain LDL. And while LCAT is also associated with LDL, the degree of esterification of FC to CE is lower in LDL compared to HDL.(84) Thus, the labeled cholesterol in the lipoproteins (Fig 6D) may differ from that of the labeled cholesterol in foam cells (Fig 6B) in two respects: initial distribution over LDL and not just HDL; and a higher ratio of FC/CE label compared to the label in foam cells (Fig 6B). As HDL can transfer both FC(85) and CE(86) to LDL in circulation, the distribution of label over lipoprotein classes may not be different over time between the two routes (Figs 6B and 6D). However, while little is known about the differing roles of FC and CE in TICE, it remains possible that 4F may act on the two routes of cholesterol efflux (Figs 6B and 6D) in slightly different ways.

Second, while the results reported in Figure 7B and C strongly suggest that 4F can increase TICE by acting as an apical-side cholesterol acceptor, they do not further elucidate the mechanism involved. For one, these experiments do not identify which transporters 4F may be acting upon. Second, they fail to tease apart the role that micelles appear to play in this phenomenon. As mentioned previously, when we conducted the experiments reported in Figure 7C without micelles, we observed neither consistent baseline TICE nor consistent effects of 4F (data not shown). These observations were in contrast with the experiments shown in Figure 7B, in which 4F induced cholesterol efflux from primary enterocytes even in the absence of micelles. These results suggest that micelles are an important necessary

condition on TICE within an ex vivo system, and as such they are in keeping with prior studies on TICE that identify micelles as something approaching a necessary condition on TICE both *ex vivo*(49) and *in vivo*.(70) However, we are continuing to investigate the manner in which micelles and 4F act together to promote TICE.

Of interest, few promising pharmacological modulators of TICE have been identified to date. LXR agonists including the compound T0901317 have been shown to upregulate TICE,(29) but LXR agonist treatment is accompanied by significant side effects including increased TG and LDL-C levels.(87) Studies involving intestinal-specific activation of LXR have demonstrated enhanced macrophage RCT as well as atheroprotection,(88, 89) but as yet the effects of intestinal-specific LXR activation have not been traced back to TICE. Bile acids and phospholipids in the intestinal lumen have been shown to stimulate the amount of cholesterol secreted via TICE.(90, 91) Dietary plant sterols including campesterol and sitosterol may also stimulate TICE.(92)

We have here identified a novel pharmacological modulator of TICE. 4F could thus serve as an important investigative tool for shedding light on the basic biology of this recently identified cholesterol excretion pathway. However, enhancing TICE as well as macrophage RCT may also partially account for the anti-atherogenic and anti-inflammatory effects of 4F. The details regarding the mechanism by which 4F enhances TICE, as well as the connections between TICE and atherosclerosis and other systemic inflammatory disorders, are the subjects of ongoing investigations in our laboratory.

Bibliography

1. Papa, A., S. Danese, R. Urgesi, A. Grillo, S. Guglielmo, I. Roberto, M. Bonizzi, L. Guidi, I. De Vitis, A. Santoliquido, G. Fedeli, G. Gasbarrini, and A. Gasbarrini. 2006. Early atherosclerosis in patients with inflammatory bowel disease. *Eur Rev Med Pharmacol Sci* **10**: 7-11.

2. Yarur, A. J., A. R. Deshpande, D. M. Pechman, L. Tamariz, M. T. Abreu, and D. A. Sussman. 2011. Inflammatory bowel disease is associated with an increased incidence of cardiovascular events. *Am J Gastroenterol* **106**: 741-747.

3. van Leuven, S. I., R. Hezemans, J. H. Levels, S. Snoek, P. C. Stokkers, G. K. Hovingh, J. J. Kastelein, E. S. Stroes, E. de Groot, and D. W. Hommes. 2007. Enhanced atherogenesis and altered high density lipoprotein in patients with Crohn's disease. *J Lipid Res* **48**: 2640-2646.

4. Navab, M., G. Hough, G. M. Buga, F. Su, A. C. Wagner, D. Meriwether, A. Chattopadhyay, F. Gao, V. Grijalva, J. S. Danciger, B. J. Van Lenten, E. Org, A. J. Lusis, C. Pan, G. M. Anantharamaiah, R. Farias-Eisner, S. S. Smyth, S. T. Reddy, and A. M. Fogelman. 2013. Transgenic 6F tomatoes act on the small intestine to prevent systemic inflammation and dyslipidemia caused by Western diet and intestinally derived lysophosphatidic acid. *Journal of Lipid Research* **54**: 3403-3418.

5. Navab, M., S. T. Reddy, G. M. Anantharamaiah, G. Hough, G. M. Buga, J. Danciger, and A. M. Fogelman. 2012. D-4F-mediated reduction in metabolites of arachidonic and linoleic acids in the small intestine is associated with decreased inflammation in low-density lipoprotein receptor-null mice. *Journal of Lipid Research* **53**: 437-445.

6. Navab, M., A. Chattopadhyay, G. Hough, D. Meriwether, S. I. Fogelman, A. C. Wagner, V. Grijalva, F. Su, G. M. Anantharamaiah, L. H. Hwang, K. F. Faull, S. T. Reddy, and A. M. Fogelman. 2015. Source and role of intestinally derived lysophosphatidic acid in dyslipidemia and atherosclerosis. *Journal of Lipid Research* **56**: 871-887.

7. Chattopadhyay, A., M. Navab, G. Hough, F. Gao, D. Meriwether, V. Grijalva, J. R. Springstead, M. N. Palgnachari, R. Namiri-Kalantari, F. Su, B. J. Van Lenten, A. C. Wagner, G. M. Anantharamaiah, R. Farias-Eisner, S. T. Reddy, and A. M. Fogelman. 2013. A novel approach to oral apoA-I mimetic therapy. *Journal of Lipid Research* **54**: 995-1010.

8. Brunham, L. R., and M. R. Hayden. 2015. Human genetics of HDL: Insight into particle metabolism and function. *Progress in Lipid Research* **58**: 14-25.

9. Brunham, L. R., J. K. Kruit, J. Iqbal, C. Fievet, J. M. Timmins, T. D. Pape, B. A. Coburn, N. Bissada, B. Staels, A. K. Groen, M. M. Hussain, J. S. Parks, F. Kuipers, and M. R. Hayden. 2006. Intestinal ABCA1 directly contributes to HDL biogenesis in vivo. *J Clin Invest* **116**: 1052-1062.

10. Barter, P. J., S. Nicholls, K. A. Rye, G. M. Anantharamaiah, M. Navab, and A. M. Fogelman. 2004. Antiinflammatory properties of HDL. *Circ Res* **95**: 764-772.

11. Navab, M., J. A. Berliner, G. Subbanagounder, S. Hama, A. J. Lusis, L. W. Castellani, S. Reddy, D. Shih, W. Shi, A. D. Watson, B. J. Van Lenten, D. Vora, and A. M. Fogelman. 2001. HDL and the inflammatory response induced by LDL-derived oxidized phospholipids. *Arterioscler Thromb Vasc Biol* **21**: 481-488.

12. Christison, J., A. Karjalainen, J. Brauman, F. Bygrave, and R. Stocker. 1996. Rapid reduction and removal of HDL- but not LDL-associated cholesteryl ester hydroperoxides by rat liver perfused in situ. *Biochem J* **314 (Pt 3)**: 739-742.

13. Shao, B., and J. W. Heinecke. 2009. HDL, lipid peroxidation, and atherosclerosis. *J Lipid Res* **50**: 599-601.

14. Yvan-Charvet, L., N. Wang, and A. R. Tall. 2010. Role of HDL, ABCA1, and ABCG1 transporters in cholesterol efflux and immune responses. *Arterioscler Thromb Vasc Biol* **30**: 139-143.

15. Chau, P., Y. Nakamura, C. J. Fielding, and P. E. Fielding. 2006. Mechanism of prebeta-HDL formation and activation. *Biochemistry* **45**: 3981-3987.

16. Birner-Gruenberger, R., M. Schittmayer, M. Holzer, and G. Marsche. 2014. Understanding high-density lipoprotein function in disease: recent advances in proteomics unravel the complexity of its composition and biology. *Prog Lipid Res* **56**: 36-46.

17. Tall, A. R., L. Yvan-Charvet, M. Westerterp, and A. J. Murphy. 2012. Cholesterol efflux: a novel regulator of myelopoiesis and atherogenesis. *Arterioscler Thromb Vasc Biol* **32**: 2547-2552.

18. Navab, M., S. Y. Hama, G. P. Hough, G. Subbanagounder, S. T. Reddy, and A. M. Fogelman. 2001. A cell-free assay for detecting HDL that is dysfunctional in preventing the formation of or inactivating oxidized phospholipids. *J Lipid Res* **42**: 1308-1317.

19. Navab, M., S. Y. Hama, C. J. Cooke, G. M. Anantharamaiah, M. Chaddha, L. Jin, G. Subbanagounder, K. F. Faull, S. T. Reddy, N. E. Miller, and A. M. Fogelman. 2000. Normal high density lipoprotein inhibits three steps in the formation of mildly oxidized low density lipoprotein: ste. *J Lipid Res* **41**: 1481-1494.

20. Bergt, C., S. Pennathur, X. Fu, J. Byun, K. O'Brien, T. O. McDonald, P. Singh, G. M. Anantharamaiah, A. Chait, J. Brunzell, R. L. Geary, J. F. Oram, and J. W. Heinecke. 2004. The myeloperoxidase product hypochlorous acid oxidizes HDL in the human artery wall and impairs ABCA1-dependent cholesterol transport. *Proc Natl Acad Sci U S A* **101**: 13032-13037.

21. Boughton-Smith, N. K., J. L. Wallace, and B. J. R. Whitle. 1988. Relationship between arachidonic acid metabolism, myeloperoxidase activity and leukocyte infiltration in a rat model of inflammatory bowel disease. *Agents and Actions* **25**: 115-123.

22. Tall, A. R. 2008. Cholesterol efflux pathways and other potential mechanisms involved in the athero-protective effect of high density lipoproteins. *J Intern Med* **263**: 256-273.

23. Hong, C., and P. Tontonoz. 2014. Liver X receptors in lipid metabolism: opportunities for drug discovery. *Nat Rev Drug Discov* **13**: 433-444.

24. Vrins, C. L. 2010. From blood to gut: direct secretion of cholesterol via transintestinal cholesterol efflux. *World J Gastroenterol* **16**: 5953-5957.

25. van der Velde, A. E., G. Brufau, and A. K. Groen. 2010. Transintestinal cholesterol efflux. *Curr Opin Lipidol* **21**: 167-171.

26. Temel, R. E., and J. M. Brown. 2010. A new framework for reverse cholesterol transport: non-biliary contributions to reverse cholesterol transport. *World J Gastroenterol* **16**: 5946-5952.

27. Brufau, G., A. K. Groen, and F. Kuipers. 2011. Reverse cholesterol transport revisited: contribution of biliary versus intestinal cholesterol excretion. *Arterioscler Thromb Vasc Biol* **31**: 1726-1733.

28. Temel, R. E., and J. M. Brown. 2012. Biliary and nonbiliary contributions to reverse cholesterol transport. *Curr Opin Lipidol* **23**: 85-90.

29. van der Veen, J. N., T. H. van Dijk, C. L. Vrins, H. van Meer, R. Havinga, K. Bijsterveld, U. J. Tietge, A. K. Groen, and F. Kuipers. 2009. Activation of the liver X receptor stimulates trans-intestinal excretion of plasma cholesterol. *J Biol Chem* **284**: 19211-19219.

30. Kruit, J. K., T. Plosch, R. Havinga, R. Boverhof, P. H. Groot, A. K. Groen, and F. Kuipers. 2005. Increased fecal neutral sterol loss upon liver X receptor activation is independent of biliary sterol secretion in mice. *Gastroenterology* **128**: 147-156.

31. Temel, R. E., W. Tang, Y. Ma, L. L. Rudel, M. C. Willingham, Y. A. Ioannou, J. P. Davies, L. M. Nilsson, and L. Yu. 2007. Hepatic Niemann-Pick C1-like 1 regulates biliary cholesterol concentration and is a target of ezetimibe. *J Clin Invest* **117**: 1968-1978.

32. Temel, R. E., J. K. Sawyer, L. Yu, C. Lord, C. Degirolamo, A. McDaniel, S. Marshall, N. Wang, R. Shah, L. L. Rudel, and J. M. Brown. 2010. Biliary sterol secretion is not required for macrophage reverse cholesterol transport. *Cell Metab* **12**: 96-102.

33. Morrone, D., W. S. Weintraub, P. P. Toth, M. E. Hanson, R. S. Lowe, J. Lin, A. K. Shah, and A. M. Tershakovec. 2012. Lipid-altering efficacy of ezetimibe plus statin and statin monotherapy and identification of factors associated with treatment response: A pooled analysis of over 21,000 subjects from 27 clinical trials. *Atherosclerosis* **223**: 251-261.

34. Grunhage, F., M. Acalovschi, S. Tirziu, M. Walier, T. F. Wienker, A. Ciocan, O. Mosteanu, T. Sauerbruch, and F. Lammert. 2007. Increased gallstone risk in humans conferred by common variant of hepatic ATP-binding cassette transporter for cholesterol. *Hepatology* **46**: 793-801.

35. Venkatachalapathi, Y. V., M. C. Phillips, R. M. Epand, R. F. Epand, E. M. Tytler, J. P. Segrest, and G. M. Anantharamaiah. 1993. Effect of end group blockage on the properties of a class A amphipathic helical peptide. *Proteins* **15**: 349-359.

36. Getz, G. S., G. D. Wool, and C. A. Reardon. 2009. Apoprotein A-I mimetic peptides and their potential anti-atherogenic mechanisms of action. *Curr Opin Lipidol* **20**: 171-175.

37. Van Lenten, B. J., A. C. Wagner, M. Navab, G. M. Anantharamaiah, S. Hama, S. T. Reddy, and A. M. Fogelman. 2007. Lipoprotein inflammatory properties and serum amyloid A levels but not cholesterol levels predict lesion area in cholesterol-fed rabbits. *J Lipid Res* **48**: 2344-2353.

38. Navab, M., G. M. Anantharamaiah, S. T. Reddy, and A. M. Fogelman. 2006. Apolipoprotein A-I mimetic peptides and their role in atherosclerosis prevention. *Nat Clin Pract Cardiovasc Med* **3**: 540-547.

39. Sherman, C. B., S. J. Peterson, and W. H. Frishman. 2010. Apolipoprotein A-I mimetic peptides: a potential new therapy for the prevention of atherosclerosis. *Cardiol Rev* **18**: 141-147.

40. Navab, M., G. M. Anantharamaiah, S. T. Reddy, B. J. Van Lenten, B. J. Ansell, and A. M. Fogelman. 2006. Mechanisms of Disease: proatherogenic HDL[mdash]an evolving field. *Nat Clin Pract End Met* **2**: 504-511.

41. Bloedon, L. T., R. Dunbar, D. Duffy, P. Pinell-Salles, R. Norris, B. J. DeGroot, R. Movva, M. Navab, A. M. Fogelman, and D. J. Rader. 2008. Safety, pharmacokinetics, and pharmacodynamics of oral apoA-I mimetic peptide D-4F in high-risk cardiovascular patients. *J Lipid Res* **49**: 1344-1352.

42. Navab, M., S. T. Reddy, B. J. Van Lenten, G. M. Buga, G. Hough, A. C. Wagner, and A. M. Fogelman. 2012. High-density lipoprotein and 4F peptide reduce systemic inflammation by modulating intestinal oxidized lipid metabolism: novel hypotheses and review of literature. *Arterioscler Thromb Vasc Biol* **32**: 2553-2560.

43. Rosenbaum, M. A., P. Chaudhuri, B. Abelson, B. N. Cross, and L. M. Graham. 2015. Apolipoprotein A-I mimetic peptide reverses impaired arterial healing after injury by reducing oxidative stress. *Atherosclerosis* **241**: 709-715.

44. Meriwether, D., S. Imaizumi, V. Grijalva, G. Hough, L. Vakili, G. M. Anantharamaiah, R. Farias-Eisner, M. Navab, A. M. Fogelman, S. T. Reddy, and I. Shechter. 2011. Enhancement by LDL of transfer of L-4F and oxidized lipids to HDL in C57BL/6J mice and human plasma. *J Lipid Res* **52**: 1795-1809.

45. Navab, M., I. Shechter, G. M. Anantharamaiah, S. T. Reddy, B. J. Van Lenten, and A. M. Fogelman. 2010. Structure and function of HDL mimetics. *Arterioscler Thromb Vasc Biol* **30**: 164-168.

46. Navab, M., S. T. Reddy, G. M. Anantharamaiah, S. Imaizumi, G. Hough, S. Hama, and A. M. Fogelman. 2011. Intestine may be a major site of action for the apoA-I mimetic peptide 4F whether administered subcutaneously or orally. *J Lipid Res* **52**: 1200-1210.

47. Navab, M., S. T. Reddy, G. M. Anantharamaiah, G. Hough, G. M. Buga, J. Danciger, and A. M. Fogelman. 2012. D-4F-mediated reduction in metabolites of arachidonic and linoleic acids in the small intestine is associated with decreased inflammation in low-density lipoprotein receptor-null mice. *J Lipid Res* **53**: 437-445.

48. Vrins, C. L. J., R. Ottenhoff, K. van den Oever, D. R. de Waart, J. K. Kruyt, Y. Zhao, T. J. C. van Berkel, L. M. Havekes, J. M. Aerts, M. van Eck, P. C. N. Rensen, and A. K. Groen. 2012. Trans-intestinal

cholesterol efflux is not mediated through high density lipoprotein. *Journal of Lipid Research* **53**: 2017-2023.

49. Le May, C., J. M. Berger, A. Lespine, B. Pillot, X. Prieur, E. Letessier, M. M. Hussain, X. Collet, B. Cariou, and P. Costet. 2013. Transintestinal Cholesterol Excretion Is an Active Metabolic Process Modulated by PCSK9 and Statin Involving ABCB1. *Arteriosclerosis, Thrombosis, and Vascular Biology* **33**: 1484-1493.

50. Van Lenten, B. J., A. C. Wagner, C. L. Jung, P. Ruchala, A. J. Waring, R. I. Lehrer, A. D. Watson, S. Hama, M. Navab, G. M. Anantharamaiah, and A. M. Fogelman. 2008. Anti-inflammatory apoA-I-mimetic peptides bind oxidized lipids with much higher affinity than human apoA-I. *J Lipid Res* **49**: 2302-2311.

51. Jones, M. K., G. M. Anantharamaiah, and J. P. Segrest. 1992. Computer programs to identify and classify amphipathic alpha helical domains. *J Lipid Res* **33**: 287-296.

52. Palgunachari, M. N., V. K. Mishra, S. Lund-Katz, M. C. Phillips, S. O. Adeyeye, S. Alluri, G. M. Anantharamaiah, and J. P. Segrest. 1996. Only the two end helixes of eight tandem amphipathic helical domains of human apo A-I have significant lipid affinity. Implications for HDL assembly. *Arterioscler Thromb Vasc Biol* **16**: 328-338.

53. Handattu, S. P., D. W. Garber, D. C. Horn, D. W. Hughes, B. Berno, A. D. Bain, V. K. Mishra, M. N. Palgunachari, G. Datta, G. M. Anantharamaiah, and R. M. Epand. 2007. ApoA-I mimetic peptides with differing ability to inhibit atherosclerosis also exhibit differences in their interactions with membrane bilayers. *J Biol Chem* **282**: 1980-1988.

54. Havel, R. J., H. A. Eder, and J. H. Bragdon. 1955. The distribution and chemical composition of ultracentrifugally separated lipoproteins in human serum. *J Clin Invest* **34**: 1345-1353.

55. Williams, K. J., J. P. Argus, Y. Zhu, M. Q. Wilks, B. N. Marbois, A. G. York, Y. Kidani, A. L. Pourzia, D. Akhavan, D. N. Lisiero, E. Komisopoulou, A. H. Henkin, H. Soto, B. T. Chamberlain, L. Vergnes, M. E. Jung, J. Z. Torres, L. M. Liau, H. R. Christofk, R. M. Prins, P. S. Mischel, K. Reue, T. G. Graeber, and S. J.

Bensinger. 2013. An essential requirement for the SCAP/SREBP signaling axis to protect cancer cells from lipotoxicity. *Cancer research* **73**: 2850-2862.

56. Temel, R. E., R. G. Lee, K. L. Kelley, M. A. Davis, R. Shah, J. K. Sawyer, M. D. Wilson, and L. L. Rudel. 2005. Intestinal cholesterol absorption is substantially reduced in mice deficient in both ABCA1 and ACAT2. *J Lipid Res* **46**: 2423-2431.

57. Bligh, E. G., and W. J. Dyer. 1959. A RAPID METHOD OF TOTAL LIPID EXTRACTION AND PURIFICATION. *Canadian Journal of Biochemistry and Physiology* **37**: 911-917.

58. Gerhardt, K. O., C. W. Gehrke, I. T. Rogers, M. A. Flynn, and D. J. Hentges. 1977. Gas-liquid chromatography of fecal neutral steriods. *J Chromatogr* **135**: 341-349.

59. Folch, J., M. Lees, and G. H. Sloane Stanley. 1957. A simple method for the isolation and purification of total lipides from animal tissues. *J Biol Chem* **226**: 497-509.

60. Chavez-Santoscoy, A. V., L. M. Huntimer, A. E. Ramer-Tait, M. Wannemuehler, and B. Narasimhan. 2012. Harvesting murine alveolar macrophages and evaluating cellular activation induced by polyanhydride nanoparticles. *J Vis Exp*: e3883.

61. Clarke, L. L. 2009. A guide to Ussing chamber studies of mouse intestine. *American Journal of Physiology - Gastrointestinal and Liver Physiology* **296**: G1151-G1166.

62. Iqbal, J., and M. M. Hussain. 2005. Evidence for multiple complementary pathways for efficient cholesterol absorption in mice. *J Lipid Res* **46**: 1491-1501.

63. Zhang, Y., I. Zanotti, M. P. Reilly, J. M. Glick, G. H. Rothblat, and D. J. Rader. 2003. Overexpression of apolipoprotein A-I promotes reverse transport of cholesterol from macrophages to feces in vivo. *Circulation* **108**: 661-663.

64. Garcia, Z. C., K. S. Poksay, K. Boström, D. F. Johnson, M. E. Balestra, I. Shechter, and T. L. Innerarity. 1992. Characterization of apolipoprotein B mRNA editing from rabbit intestine. *Arteriosclerosis, Thrombosis, and Vascular Biology* **12**: 172-179.

65. Wiedmann, T. S., C. Deye, and D. Kallick. 2001. Interaction of bile salt and phospholipids with bovine submaxillary mucin. *Pharm Res* **18**: 45-53.

66. Li, C. Y., C. L. Zimmerman, and T. S. Wiedmann. 1996. Diffusivity of bile salt/phospholipid aggregates in mucin. *Pharm Res* **13**: 535-541.

67. Canny, G., A. Swidsinski, and B. A. McCormick. 2006. Interactions of intestinal epithelial cells with bacteria and immune cells: methods to characterize microflora and functional consequences. *Methods Mol Biol* **341**: 17-35.

68. Pappenheimer, J. R., M. L. Karnovsky, and J. E. Maggio. 1997. Absorption and Excretion of Undegradable Peptides: Role of Lipid Solubility and Net Charge. *Journal of Pharmacology and Experimental Therapeutics* **280**: 292-300.

69. Torjman, M. C., J. I. Joseph, C. Munsick, M. Morishita, and Z. Grunwald. 2005. Effects of isoflurane on gastrointestinal motility after brief exposure in rats. *Int J Pharm* **294**: 65-71.

70. van der Velde, A. E., C. L. Vrins, K. van den Oever, I. Seemann, R. P. Oude Elferink, M. van Eck, F. Kuipers, and A. K. Groen. 2008. Regulation of direct transintestinal cholesterol excretion in mice. *Am J Physiol Gastrointest Liver Physiol* **295**: G203-G208.

71. Casteleyn, C., A. Rekecki, A. Van der Aa, P. Simoens, and W. Van den Broeck. 2010. Surface area assessment of the murine intestinal tract as a prerequisite for oral dose translation from mouse to man. *Laboratory Animals* **44**: 176-183.

72. Xie, Q., S. P. Zhao, and F. Li. 2010. D-4F, an apolipoprotein A-I mimetic peptide, promotes cholesterol efflux from macrophages via ATP-binding cassette transporter A1. *Tohoku J Exp Med* **220**: 223-228.

73. Nijstad, N., T. Gautier, F. Briand, D. J. Rader, and U. J. Tietge. 2011. Biliary sterol secretion is required for functional in vivo reverse cholesterol transport in mice. *Gastroenterology* **140**: 1043-1051.

74. Reddy, S. T., M. Navab, G. M. Anantharamaiah, and A. M. Fogelman. 2014. Apolipoprotein A-I mimetics. *Curr Opin Lipidol* **25**: 304-308.

75. Wool, G. D., T. Vaisar, C. A. Reardon, and G. S. Getz. 2009. An apoA-I mimetic peptide containing a proline residue has greater in vivo HDL binding and anti-inflammatory ability than the 4F peptide. *J Lipid Res* **50**: 1889-1900.

76. Garrigues, A., A. E. Escargueil, and S. Orlowski. 2002. The multidrug transporter, P-glycoprotein, actively mediates cholesterol redistribution in the cell membrane. *Proc Natl Acad Sci U S A* **99**: 10347-10352.

77. Dadgostar, A., S. Vazirian, K. Farah, and M. Faraz. 2014. The 4F peptide significantly decreases intestinal oxidized fatty acids (835.1). *The FASEB Journal* **28**.

78. Imaizumi, S., V. Grijalva, M. Navab, B. J. Van Lenten, A. C. Wagner, G. M. Anantharamiah, A. M. Fogelman, and S. T. Reddy. 2010. L-4F differentially alters plasma levels of oxidized fatty acids resulting in more anti-inflammatory HDL in mice. *Drug Metab Lett* **4**: 139-148.

79. Navab, M., G. M. Anantharamaiah, S. T. Reddy, S. Hama, G. Hough, V. R. Grijalva, A. C. Wagner, J. S. Frank, G. Datta, D. Garber, and A. M. Fogelman. 2004. Oral D-4F causes formation of pre-beta high-density lipoprotein and improves high-density lipoprotein-mediated cholesterol efflux and reverse cholesterol transport from macrophages in apolipoprotein E-null mice. *Circulation* **109**: 3215-3220.

80. Yancey, P. G., J. K. Bielicki, W. J. Johnson, S. Lund-Katz, M. N. Palgunachari, G. M. Anantharamaiah, J. P. Segrest, M. C. Phillips, and G. H. Rothblat. 1995. Efflux of cellular cholesterol and phospholipid to lipid-free apolipoproteins and class A amphipathic peptides. *Biochemistry* **34**: 7955-7965.

81. Tang, C., A. M. Vaughan, G. M. Anantharamaiah, and J. F. Oram. 2006. Janus kinase 2 modulates the lipid-removing but not protein-stabilizing interactions of amphipathic helices with ABCA1. *J Lipid Res* **47**: 107-114.

82. Bielicki, J. K., H. Zhang, Y. Cortez, Y. Zheng, V. Narayanaswami, A. Patel, J. Johansson, and S. Azhar. 2010. A new HDL mimetic peptide that stimulates cellular cholesterol efflux with high efficiency greatly reduces atherosclerosis in mice. *J Lipid Res* **51**: 1496-1503.

83. Xie, P., L. Jia, Y. Ma, J. Ou, H. Miao, N. Wang, F. Guo, A. Yazdanyar, X. C. Jiang, and L. Yu. 2013. Ezetimibe inhibits hepatic Niemann-Pick C1-Like 1 to facilitate macrophage reverse cholesterol transport in mice. *Arterioscler Thromb Vasc Biol* **33**: 920-925.

84. Ng, D. S. 2004. Insight into the Role of LCAT from Mouse Models. *Reviews in Endocrine and Metabolic Disorders* **5**: 311-318.

85. Lund-Katz, S., B. Hammerschlag, and M. C. Phillips. 1982. Kinetics and mechanism of free cholesterol exchange between human serum high- and low-density lipoproteins. *Biochemistry* **21**: 2964-2969.

86. Barter, P. J., H. B. Brewer, M. J. Chapman, C. H. Hennekens, D. J. Rader, and A. R. Tall. 2003. Cholesteryl Ester Transfer Protein: A Novel Target for Raising HDL and Inhibiting Atherosclerosis. *Arteriosclerosis, Thrombosis, and Vascular Biology* **23**: 160-167.

87. Briand, F., M. Tréguier, A. André, D. Grillot, M. Issandou, K. Ouguerram, and T. Sulpice. 2010. Liver X receptor activation promotes macrophage-to-feces reverse cholesterol transport in a dyslipidemic hamster model. *Journal of Lipid Research* **51**: 763-770.

88. Lo Sasso, G., S. Murzilli, L. Salvatore, I. D'Errico, M. Petruzzelli, P. Conca, Z. Y. Jiang, L. Calabresi, P. Parini, and A. Moschetta. 2010. Intestinal specific LXR activation stimulates reverse cholesterol transport and protects from atherosclerosis. *Cell Metab* **12**: 187-193.

89. Yasuda, T., D. Grillot, J. T. Billheimer, F. Briand, P. Delerive, S. Huet, and D. J. Rader. 2010. Tissue-specific liver X receptor activation promotes macrophage reverse cholesterol transport in vivo. *Arterioscler Thromb Vasc Biol* **30**: 781-786.

90. Jakulj, L., J. Besseling, E. S. Stroes, and A. K. Groen. 2013. Intestinal cholesterol secretion: future clinical implications. *Neth J Med* **71**: 459-465.

91. van der Velde, A. E., C. L. Vrins, K. van den Oever, C. Kunne, R. P. Oude Elferink, F. Kuipers, and A. K. Groen. 2007. Direct intestinal cholesterol secretion contributes significantly to total fecal neutral sterol excretion in mice. *Gastroenterology* **133**: 967-975.

92. Brufau, G., F. Kuipers, Y. Lin, E. A. Trautwein, and A. K. Groen. 2011. A reappraisal of the mechanism by which plant sterols promote neutral sterol loss in mice. *PLoS ONE* **6**: e21576.

Figure 2-1. *L-4F that is introduced directly into the circulation preferentially associates with the proximal small bowel.* (**A**) Gross tissue distribution was first determined by injecting ^{14}C-4F (25 mg/kg, 0.2 uCi) into C57BL/6J mice via the tail vein (n=3). After 60 minutes, the mice were sacrificed and perfused, tissues were dissected and homogenized, and radioactivity was determined by scintillation counting. Counts were significantly higher in the small intestine (SI) compared to the liver (*, p = 0.04). **(B)** ^{14}C-L-4F (25 mg/kg, 2 μCi) was injected via tail vein directly into the circulation of each of 15 fasted C57BL/6J mice. At various time points, the animals were sacrificed, perfused, and dissected; and radioactivity was determined (3 mice/time point). A significant increase in radioactivity between 3 and 60 minutes was observed for both the duodenum (*: p = 0.003) and the jejunum (**: p = 0.001). (**C and D**) L-4F or D-4F (25 mg/kg) was injected via tail vein into C57BL/6J mice (n=4 per peptide). After 15 minutes, the animals were sacrificed and perfused, and levels of intact peptide were determined in intestinal tissue via LC-MS/MS. Both peptides exhibited distribution patterns comparable to each other and to that at 15 min and 60 min in (B). The concentrations of intact L-4F and D4F were both significantly higher in the duodenum compared to the jejunum (*, p = 0.001 and p = 0.005, respectively). (Error is reported as standard error of the mean [SEM]).

Figure 2-2: *Small intestinal 4F is transported into the intestinal lumen.* **(A)** ^{14}C-L-4F (25mg/kg, 1.8 μCi) was introduced via tail vein into the circulation of fasted male C57BL/6J mice. After 1 or 3 hours (3 mice/time point), the animals were bled, sacrificed, perfused, and dissected. The entire small intestines were then rinsed three times with PBS, followed by three times with 0.6% taurocholate (TC) and three times with 1.0% Triton X-100 (TX). Radioactivity was determined in all of the rinses as well as in associated tissues, cecum contents, feces, and gall bladder contents (Gall bladder). **(B)** Intact L-4F present in SI PBS rinse was determined by LC-MS/MS after 1 hour following tail vein injection of L-4F (25 mg/kg) into C57BL/6J mice (n=4). (Error is reported as standard error of the mean [SEM]).

Figure 2-3: *L-4F enters the intestinal lumen by directly and selectively crossing the intestinal epithelium.* **(A)** L-4F (25mg/kg) was introduced via tail vein into C57BL/6J mice, whose bile ducts had either been ligated or sham-ligated (n=4). Intact L-4F present in the plasma and SI PBS rinse after 1 hour was quantified by LC-MS/MS. **(B and C)** C57BL/6J mice (n=7) were injected with 800 μg (~ 25-30 mg/kg) of D-4F *via* tail vein. After 30 minutes, the mice were sacrificed and duodenal explants were mounted in Ussing chambers. Serosal side media contained LDL and HDL, while mucosal side media included micelles. Mucosal side media was sampled at 3, 30, 60, and 90 minutes; and the amount of D-4F present was determined by LC-MS/MS. Peptide was observed released from the tissue into the mucosal side media across 90 minutes **(B)**. Levels of D-4F were also quantified in these duodenal explants together with matched controls from the same mice. The controls were not mounted in the Ussing chamber and provide the baseline or time zero concentration of D-4F in the tissue **(C)**. Ussing chamber mounted tissue after 90 minutes had significantly less D-4F than controls (*: $p < 0.05$). **(D)** In order to determine whether L-4F selectively crosses intestinal epithelium, the level of L-4F present in lung alveolar space was determined via lung lavage following 2 individual 25 mg/kg injections of ^{14}C-L-4F at 1 and 3 hours prior to sacrifice (n = 6). No L-4F was present in the lung lavage, in contrast with SI PBS rinse. DPM were converted to μg L-4F. (Error is reported as standard error of the mean [SEM]).

Figure 2-4: *The process of L-4F secretory transport is saturable, while in turn luminal-side L-4F can itself be taken up into the SI tissue.* **(A)** Low (25 mg/kg) and high dose (100 mg/kg) L-4F was introduced via tail vein into C57BL/6J mice (n=4 and 6 respectively). After 1 hour, the level of L-4F in the SI lumen rinse was determined by LC-MS/MS. No significant difference was found between the two doses ($p = 0.4$), indicating that the secretory transport pathway is saturable. **(B)** L-4F or ^{14}C-L-4F + L-4F was added to either the mucosal or serosal media of the Ussing chamber, and uptake by the tissue was determined by

LC-MS/MS or scintillation counting respectively (n = 7/group). Duodenal explants took up significantly more 4F from the serosal media than from the mucosal media (*: $p < 0.005$). (Error is reported as standard error of the mean [SEM]).

Figure 2-5: *The secretory transport of 4F is modulated by trans-intestinal cholesterol efflux.* **(A)** Levels of neutral sterols in the feces from Tg112 and litter-mate control mice fed a chow diet (n=8/group) were compared by GCMS. **(B)** Western diet (WD) has been shown to upregulate TICE in Tg112 mice. Male and female Tg112 mice were fed chow or a WD for six weeks (n=4 mice/gender/group), injected with 675 μg per mouse of ^{14}C-L-4F (~ 25 mg/kg) via the tail veins, and the radioactivity in the lumen washes was determined after 1 hr. WD significantly upregulated 4F transport in both male (*, $p = 0.007$) and female mice (**, $p = 0.005$). While male and female mice exhibited no significant difference on chow ($p = 0.2$), male mice had significantly higher transport of 4F into the SI lumen than female mice when both were fed a WD (***, $p = 0.008$). **(C)** Total neutral sterols were determined by GCMS in the feces of the individual mice in (B). WD significantly increased neutral sterols in the feces of both male (*, $p = 0.001$) and female mice (**, $p = 0.02$). While male and female mice exhibited no significant difference on chow, male mice had significantly more neutral sterols in their feces compared to female mice when both were fed a WD (***, $p = 0.01$). **(D)** C57BL/6J mice were injected with 800 μg (~ 25-30 mg/kg)/300 μl saline of D-4F via their tail veins (n = 7). After 30 minutes, the mice were sacrificed and duodenal tissue explants were mounted in Ussing chambers. Each mouse contributed paired explants, whose serosal side medias both did or did not contain LDL + HDL. Levels of both D-4F and cholesterol in mucosal medias were determined by LCMS/MS and GCMS, respectively. The presence of serosal side lipoproteins significantly enhanced the transport of both D-4F and cholesterol into the mucosal media (*, **: $p < 0.05$). (Error is reported as standard error of the mean [SEM]).

Figure 2-6: *Circulating L-4F increases reverse cholesterol transport from macrophages as well as cholesterol efflux from lipoproteins in Tg112 mice.* **(A)** Macrophage RCT was determined in Tg112 mice compared to littermate controls (WT). J774 cells were grown in culture and loaded with acetylated LDL that had been labeled with ^{3}H-cholesterol. Loaded macrophages were injected IP (approximately $2x10^{6}$ cells and 1 μCi per mouse) into both WT and Tg112 mice (n=4/group). After 8 hours, the mice were sacrificed, and lumen rinse was collected. Following chloroform/methanol extraction of the rinse, label was determined by scintillation counting in both the chloroform fraction (^{3}H-cholesterol) and the methanol/water fraction (^{3}H-bile acids). **(B)** We determined the effect of IV-administered L-4F on macrophage RCT. We proceeded as in (A), except that the mice were IV-administered either 25 mg/kg ^{14}C-L-4F or vehicle at both t=4 hr and t=7 hr (n=5/group). As positive control, 3 WT animals had received 1 week pre-treatment with the LXR agonist T0901317; these were otherwise treated as vehicle controls. L-4F significantly increased RCT into the intestinal lumen for both Tg112 (*, p = 0.01) and WT (**, p = 0.001) mice. LXR agonist treatment likewise increased RCT (***, p = 0.03). Data is expressed as percent of the corresponding vehicle controls. **(C)** ^{14}C label was determined in the luminal PBS rinse of both the Tg112 and WT mice from (B), and DPM were converted to μg ^{14}C-L-4F. **(D)** In order to investigate the mechanism by which 4F modulates RCT, we repeated the basic experiments of (A) and (B) except that we used HDL and LDL rather than macrophages as the cholesterol source. Human LDL and HDL was pre-labeled with ^{3}H-cholesterol. The lipoproteins were then pre-mixed with either ^{14}C-L-4F or vehicle, and 100 μg HDL cholesterol + 100 μg LDL cholesterol + 25 mg/kg ^{14}C-L-4F (or vehicle) was injected via tail vein into both Tg112 and WT mice (n = 7 mice/group). At t = 3 hr, the mice were given a second injection of either 25 mg/kg ^{14}C-L-4F or vehicle. At t = 4 hr the mice were sacrificed, and radioactivity was determined as before. ^{14}C-L-4F significantly increased cholesterol efflux into the SI lumen in both Tg112 (*, p = 0.004) and WT (**, p = 0.001) mice. The effect in Tg112 mice strongly suggests that L-4F can upregulate cholesterol efflux via the TICE pathway. In this experiment, however, L-4F also

significantly increased cholesterol efflux in WT mice compared to Tg112 mice (***, p = 0.04), suggesting that L-4F also affects cholesterol efflux through the hepatobiliary pathway in this context. (Error is reported as standard error of the mean [SEM]).

Figure 2-7: *4F increases TICE through duodenal explants and can act as a cholesterol acceptor with respect to cholesterol efflux from enterocytes.* **(A)** 800 μg D-4F (~ 25-30 mg/kg)/300 μl saline or vehicle was injected into the tail veins of C57BL/6J mice (n = 5). After 30 minutes, the mice were sacrificed and duodenal explants from the mice injected with 4F (4F-tissue) and vehicle (Control) were mounted in Ussing chambers. After 30 min *in vivo*, the explants from 4F-injected mice had been pre-loaded with 4F (see Fig. 3B). The mucosal media for both groups contained fresh micelles, while all serosal medias contained a fresh-mixed combination of human HDL and LDL that had been pre-loaded with 1 μCi/well of ^{3}H-cholesterol. The mucosal medias were sampled through 90 minutes, and total ^{3}H-cholesteral effluxed into the mucosal medias during that time was determined by scintillation counting. At the end of the experiment, ^{3}H-cholesterol level in the tissues was also determined. Pre-loading the tissue with 4F significantly increased the amount of cholesterol label in both the mucosal media and the duodenal explants (*, **; $p < 0.05$). **(B)** Primary enterocytes were stripped from the small intestine using EDTA and loaded with ^{3}H-cholesterol for 30 minutes under constant aeration. The cells were washed and media changed, and L-4F was added to the cell suspensions. Micelles alone were also added as a positive control (n = 3/group). L-4F dose dependently increased ^{3}H-cholesterol efflux from enterocytes (Control vs. 10 μg/ml: *, p = 0.001; 10 μg/ml vs 50 μg/ml: **, p = 0.0002; ***, control vs. micelles: p = 0.01). **(C)** Duodenal explants from C57BL/6J mice were mounted in Ussing chambers. Each mouse contributed two contiguous explants, whose serosal-side medias contained ^{3}H-cholesterol loaded lipoproteins (as above). For each pair, either 50 μg/ml D-4F or vehicle was added to mucosal-side media that contained micelles. Mucosal-side 4F significantly increased cholesterol loading into the explants

(**, p = 0.044) as well as cholesterol efflux into mucosal medias themselves (*, p = 0.047) compared to the paired controls. (Error is reported as standard error of the mean [SEM]).

Figure 2-1A

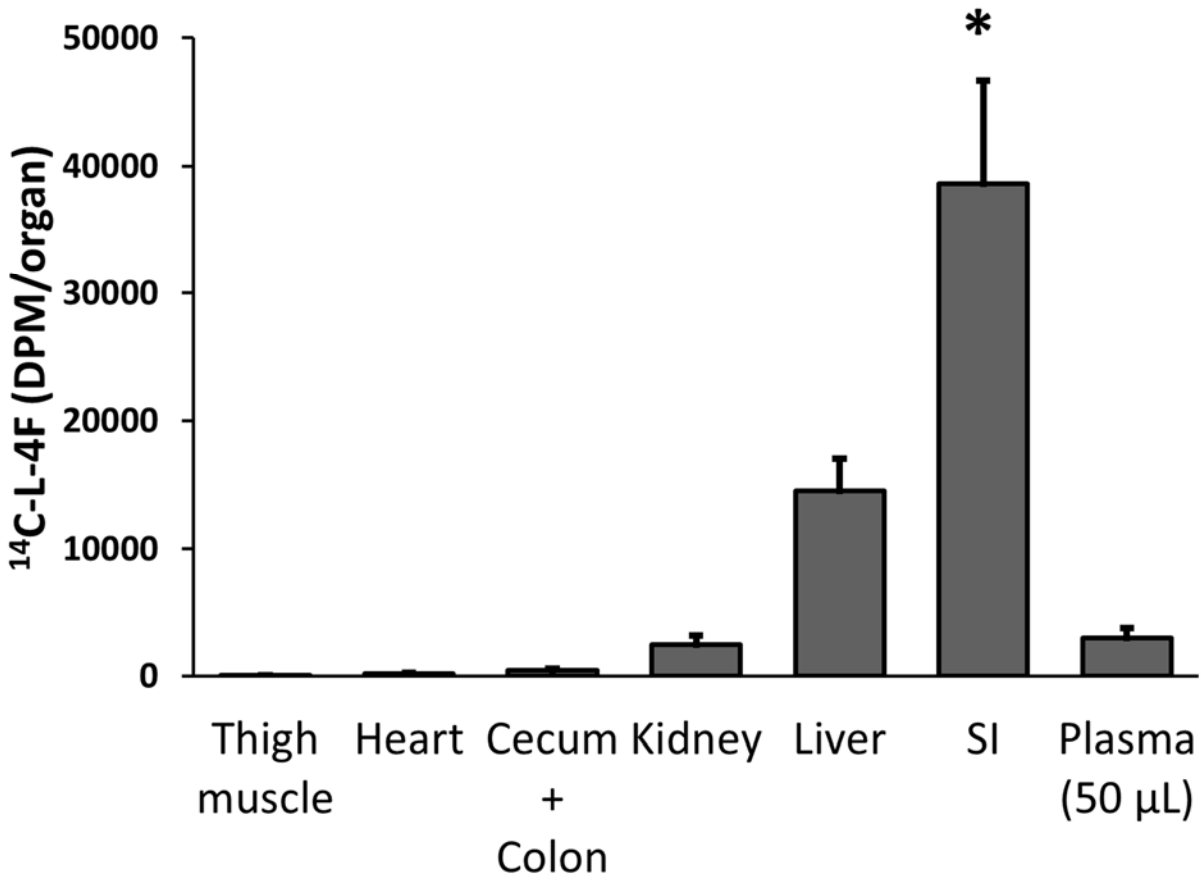
*
50000
40000
30000
20000
10000
0
^{14}C-L-4F (DPM/organ)
Thigh muscle
Heart
Cecum + Colon
Kidney
Liver
SI
Plasma (50 µL)

Figure 2-1B

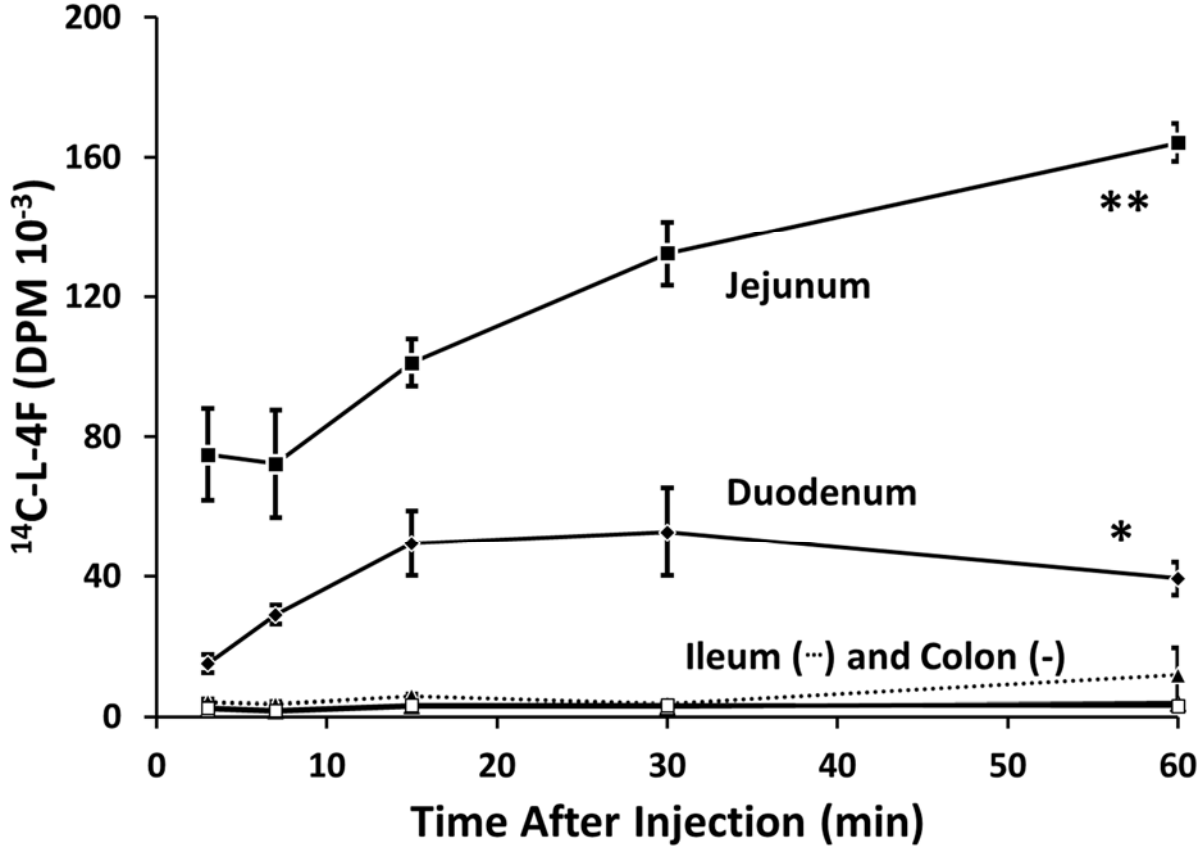
200
160
120
80
40
0
^{14}C-L-4F (DPM 10^{-3})
**
Jejunum
Duodenum
*
Ileum (···) and Colon (-)
0
10
20
30
40
50
60
Time After Injection (min)

Figure 2-1C

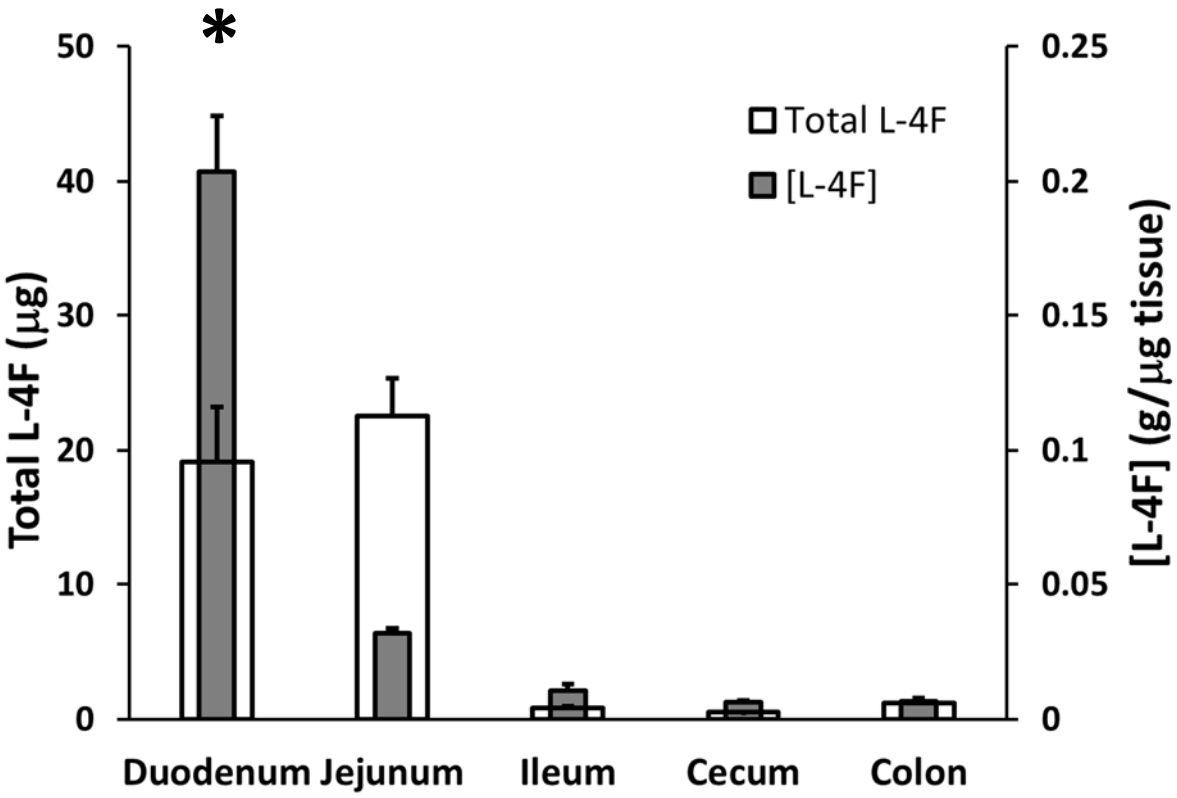
*
50
40
30
20
10
0
0.25
0.2
0.15
0.1
0.05
0
Total L-4F (µg)
[L-4F] (g/µg tissue)
Total L-4F
[L-4F]
Duodenum
Jejunum
Ileum
Cecum
Colon

Figure 1D

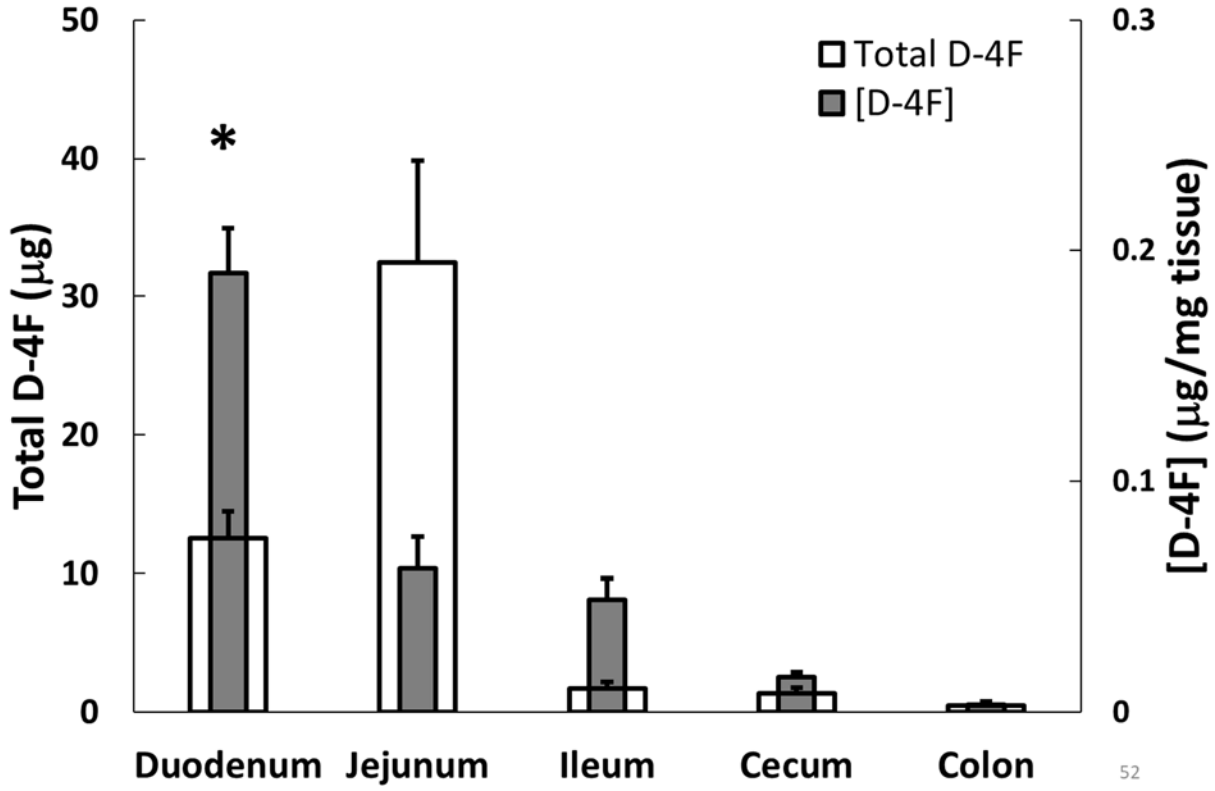
Total D-4F
[D-4F]
Total D-4F (μg)
[D-4F] (μg/mg tissue)
50
40
30
20
10
0
0.3
0.2
0.1
0
*
Duodenum
Jejunum
Ileum
Cecum
Colon
52

Figure 2A

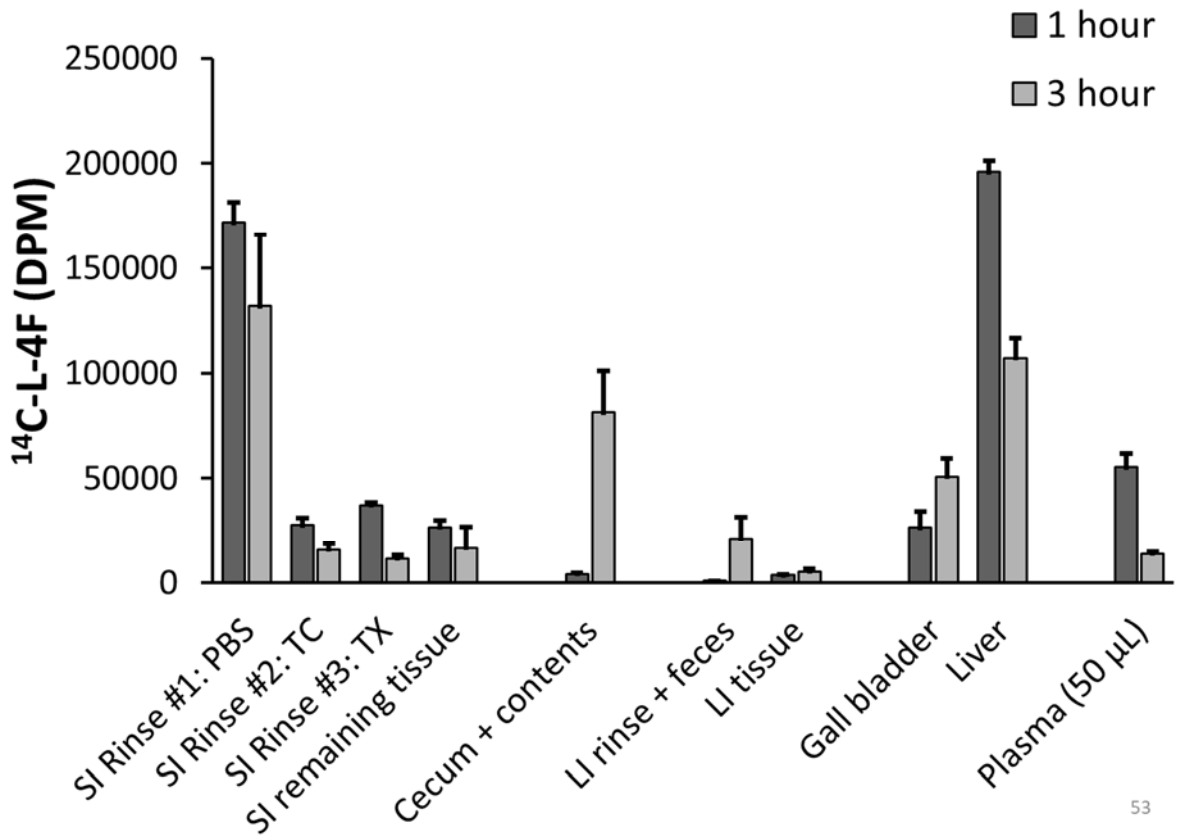
1 hour
3 hour
250000
200000
150000
100000
50000
0
^{14}C-L-4F (DPM)
SI Rinse #1: PBS
SI Rinse #2: TC
SI Rinse #3: TX
SI remaining tissue
Cecum + contents
LI rinse + feces
LI tissue
Gall bladder
Liver
Plasma (50 µL)
53

Figure 2B

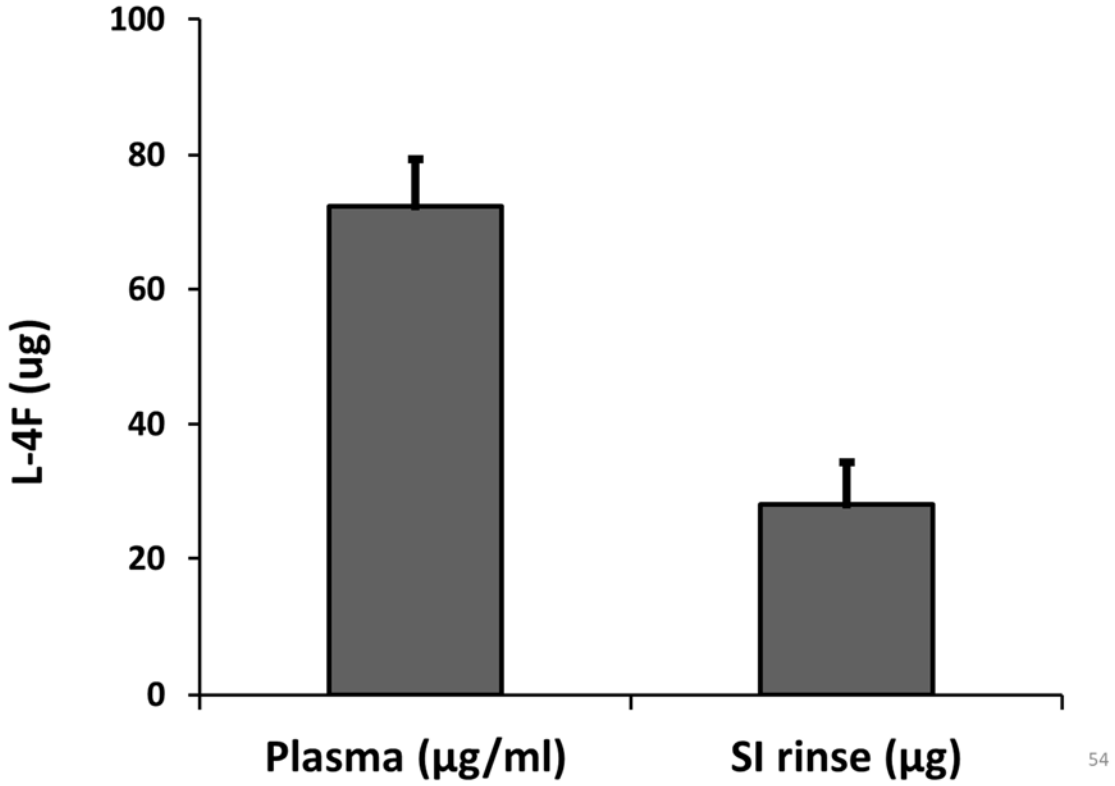

Figure 3A

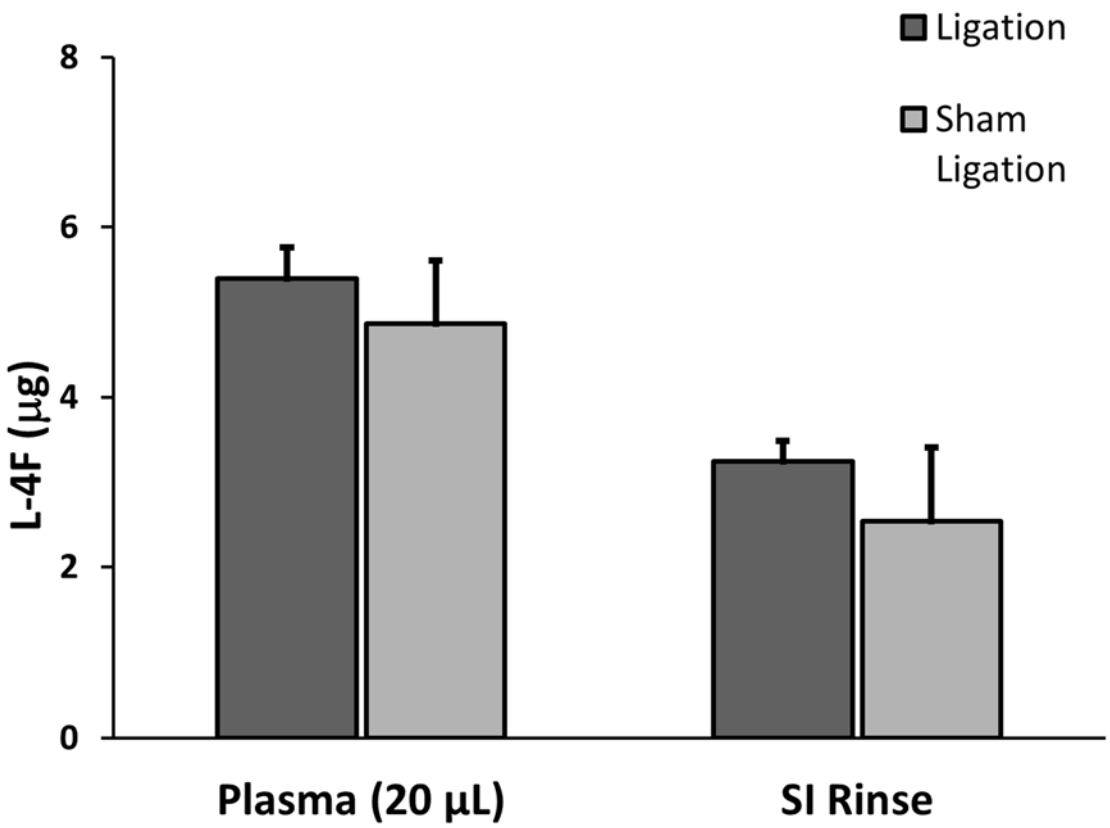

Figure 3B

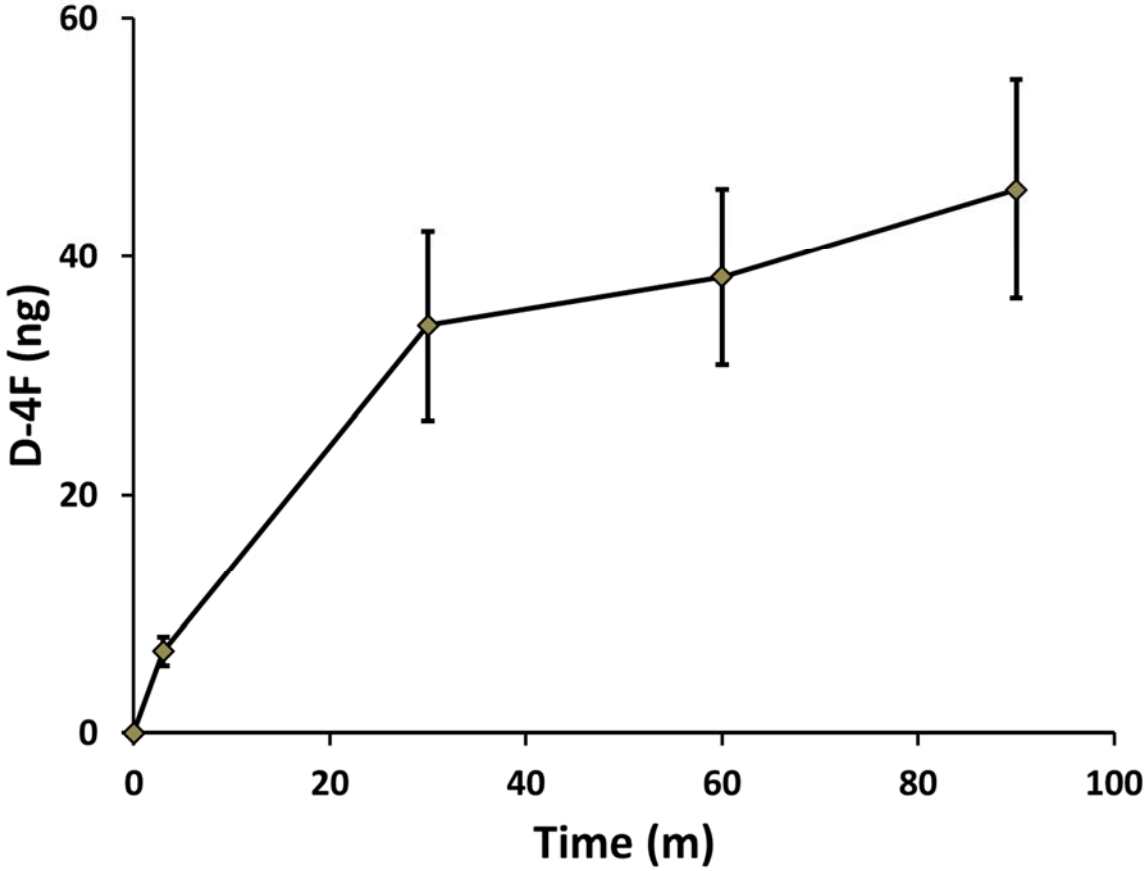

Figure 3C

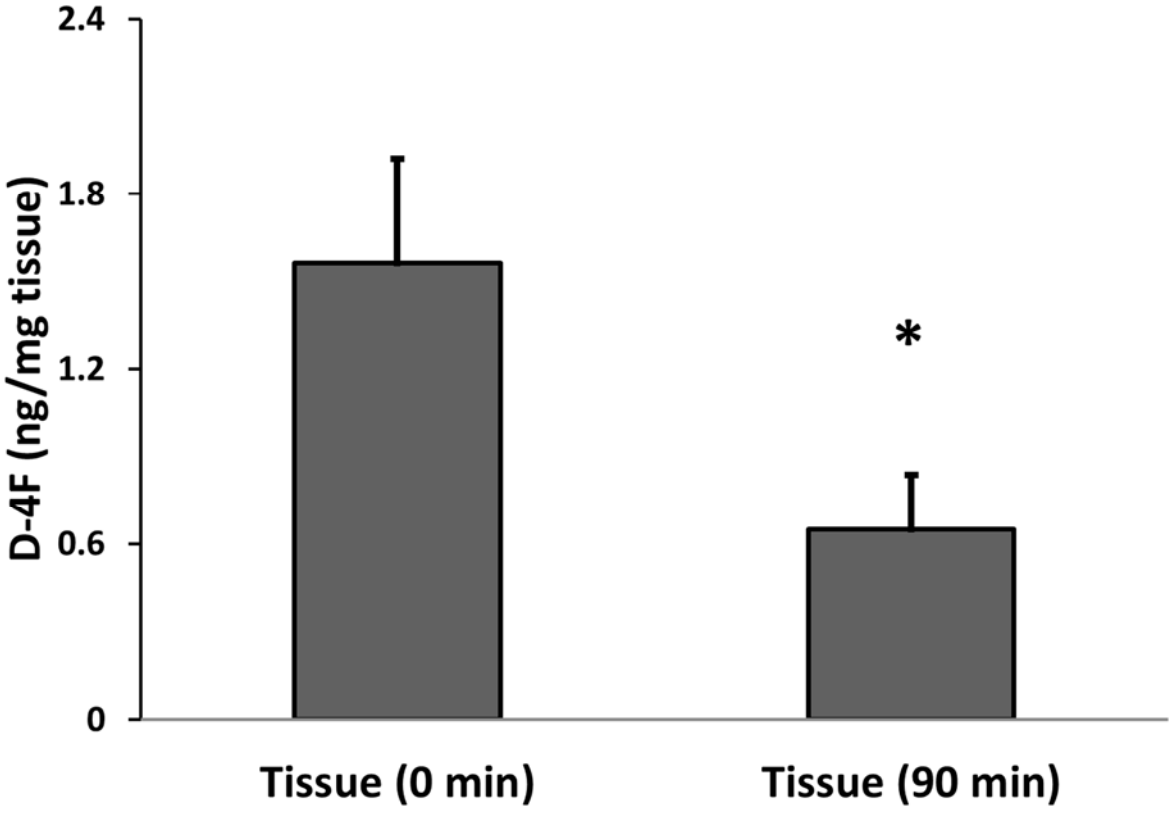

Figure 3D

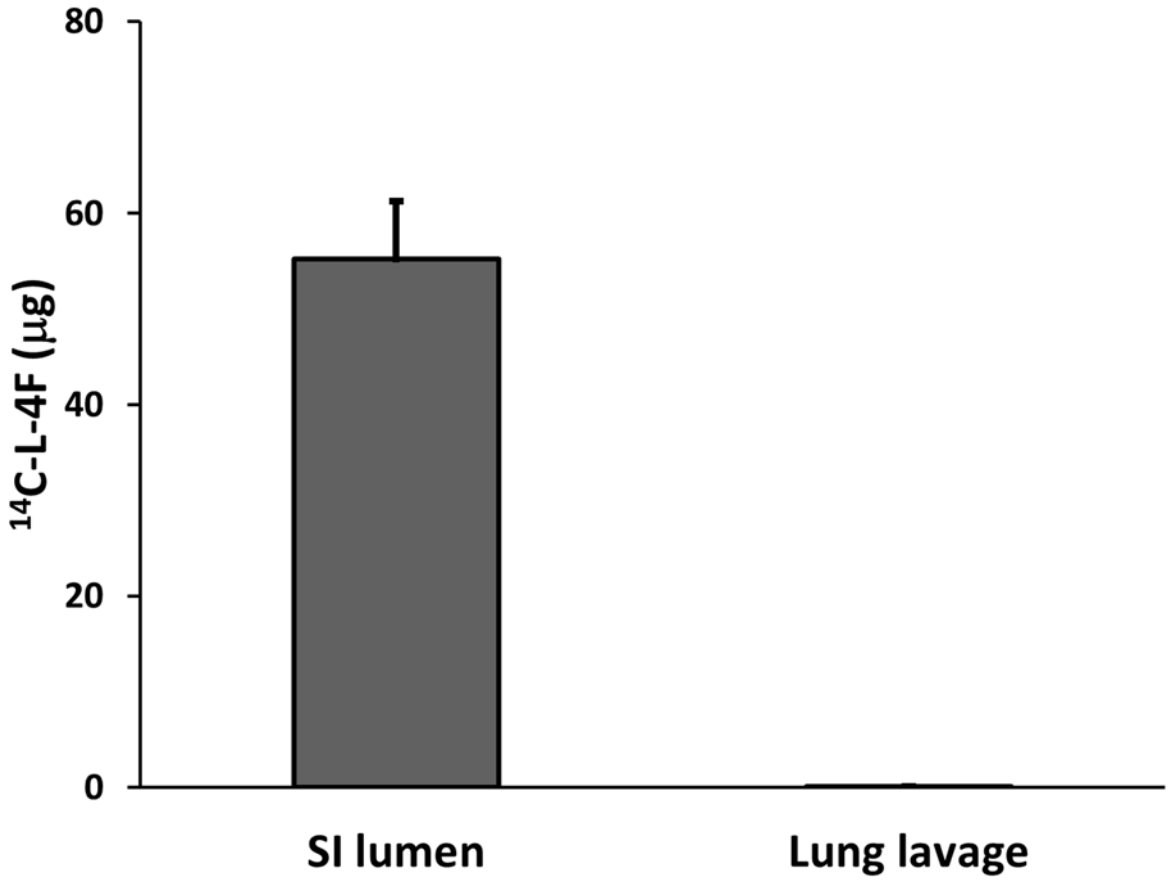

Figure 4A

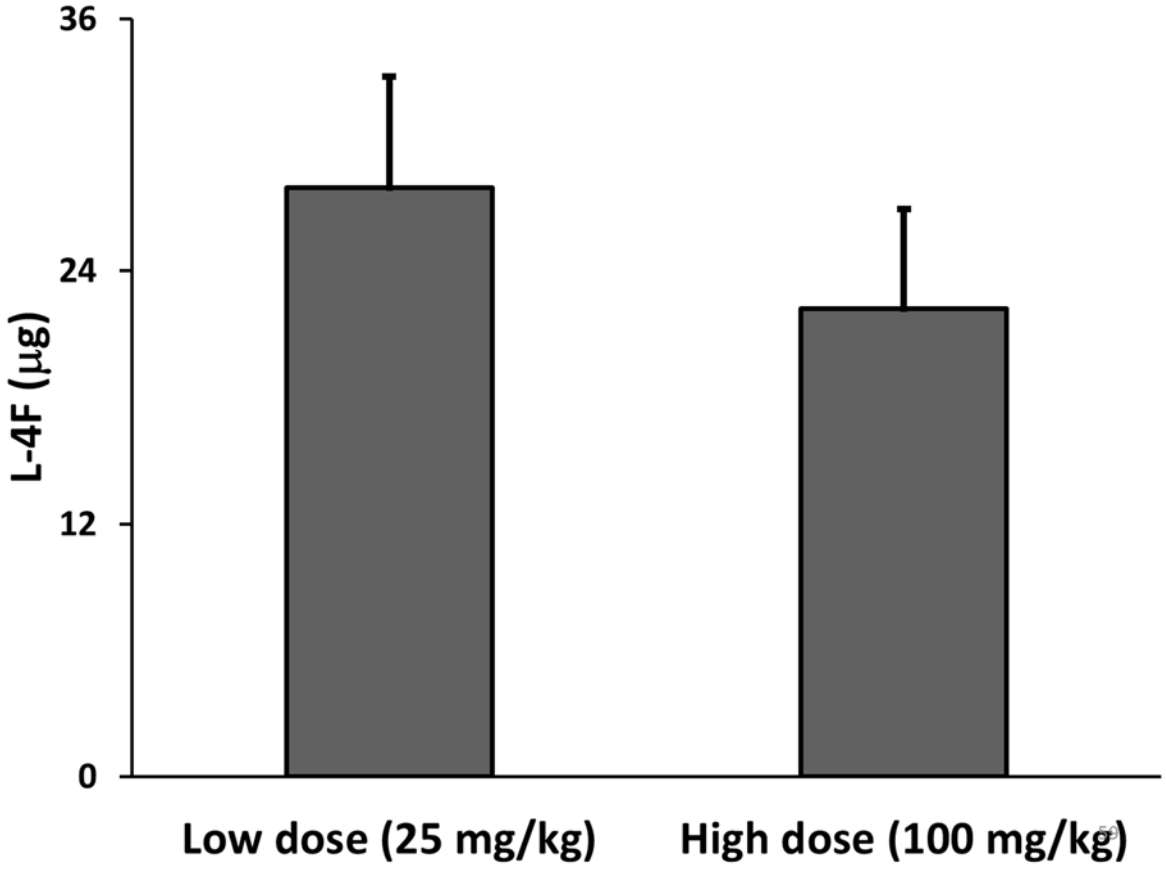

Figure 4B

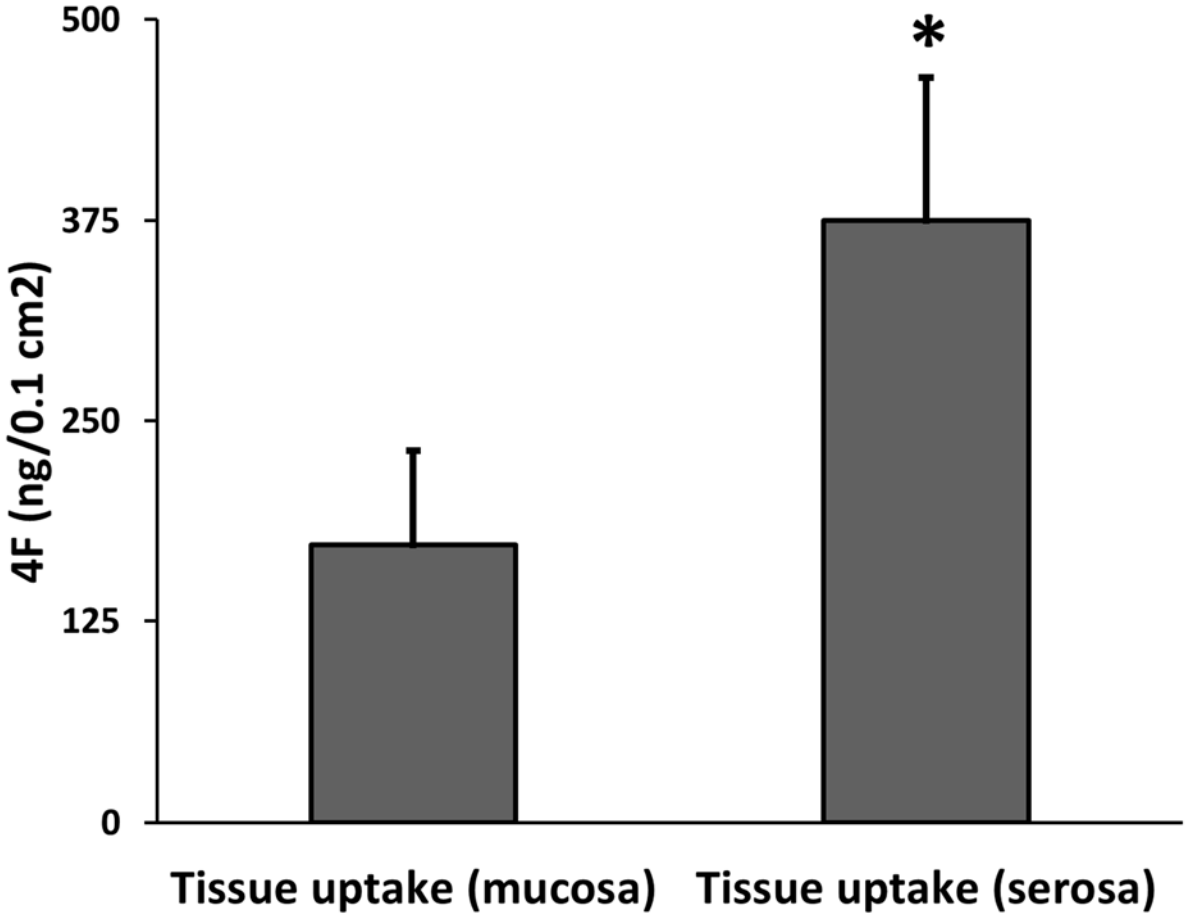
500
375
250
125
0
4F (ng/0.1 cm2)
*
Tissue uptake (mucosa)
Tissue uptake (serosa)

Figure 5A

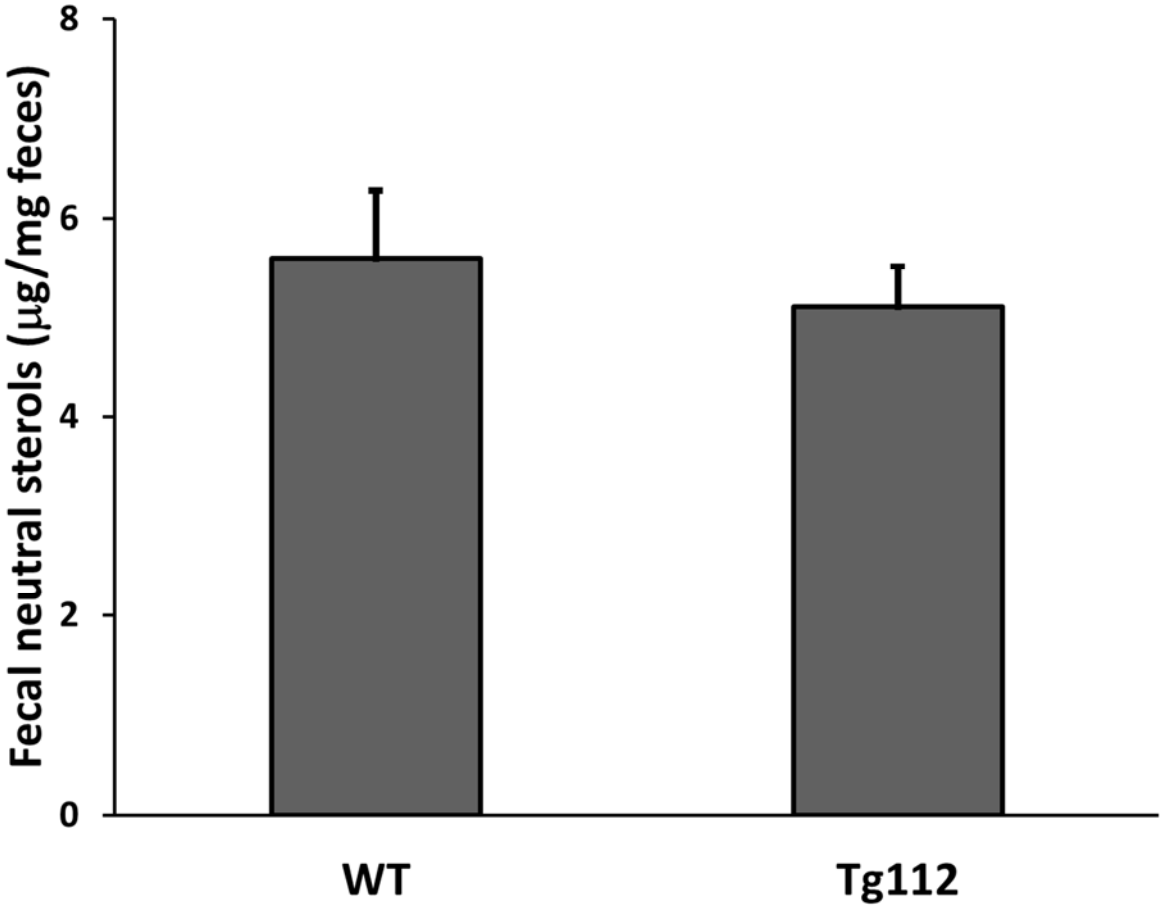

Figure 5B

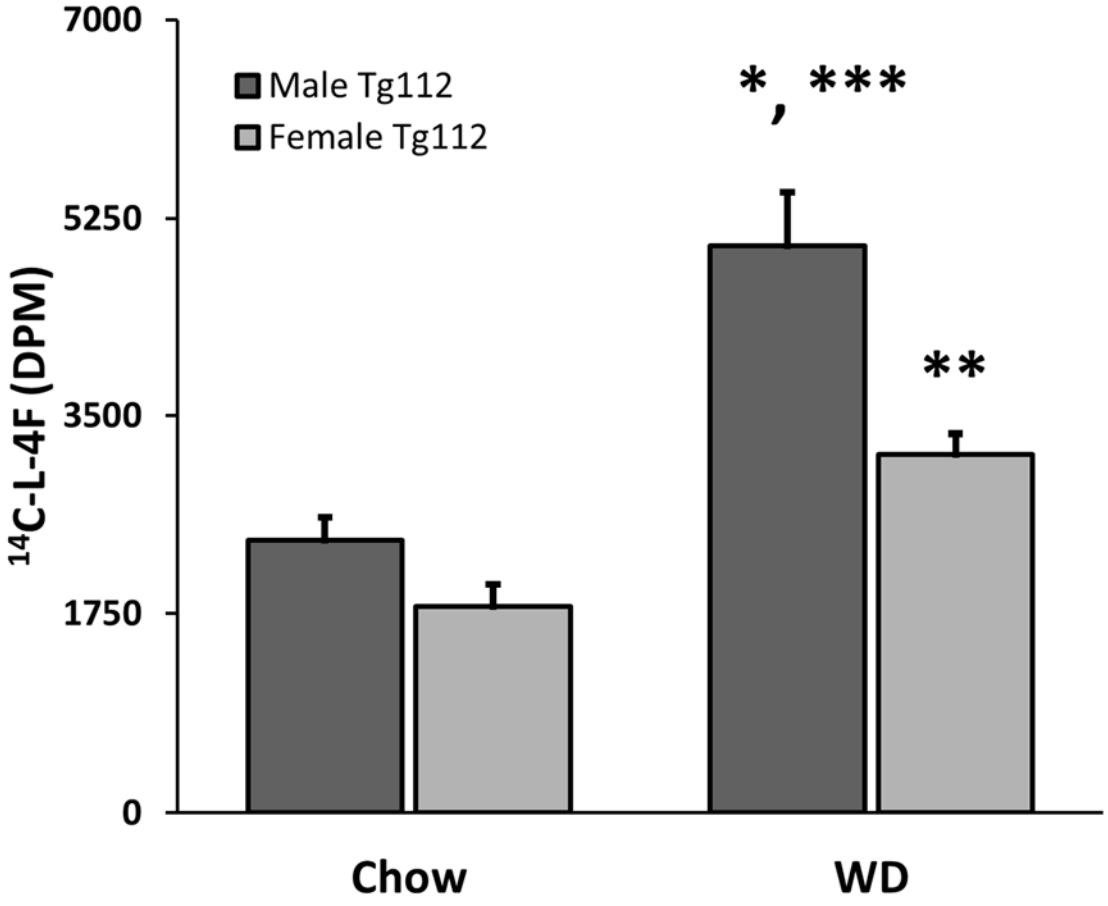
7000
5250
3500
1750
0
^{14}C-L-4F (DPM)
Male Tg112
Female Tg112
*, ***
**
Chow
WD

Figure 5C

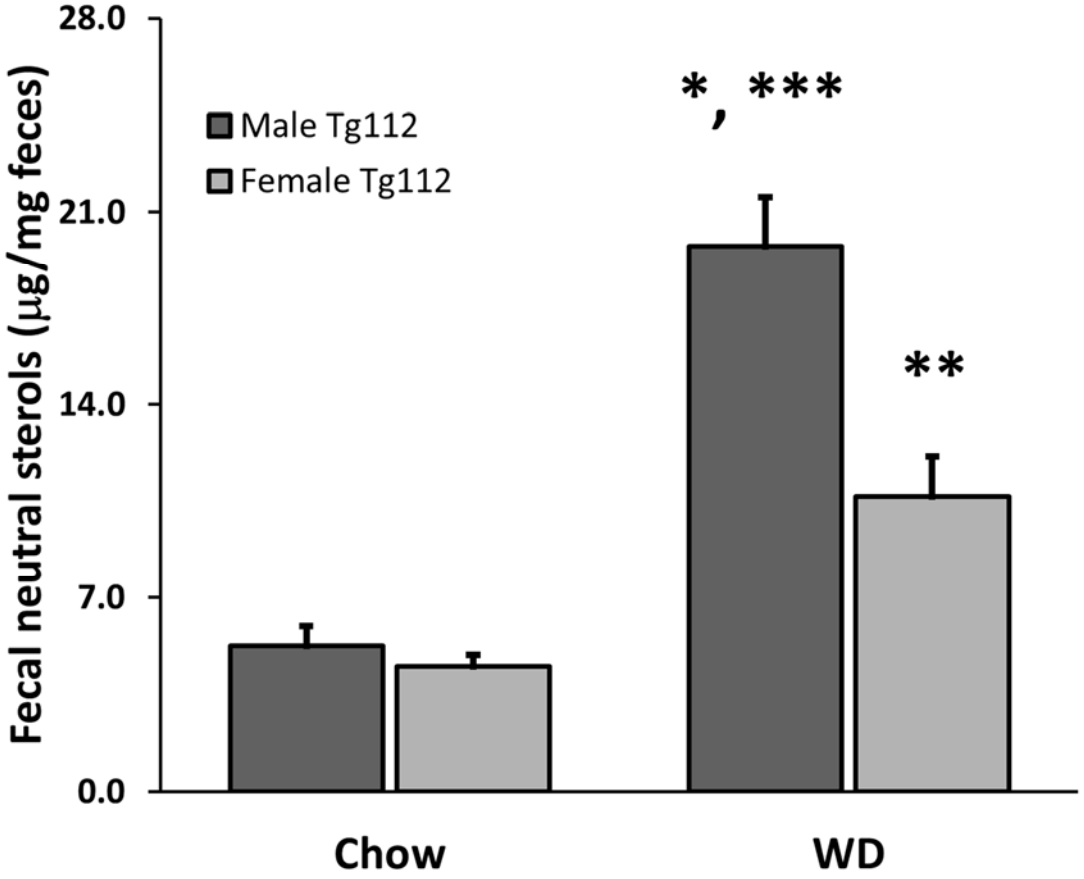
28.0
21.0
14.0
7.0
0.0
Fecal neutral sterols (μg/mg feces)
Male Tg112
Female Tg112
*, ***
**
Chow
WD

Figure 2-5D

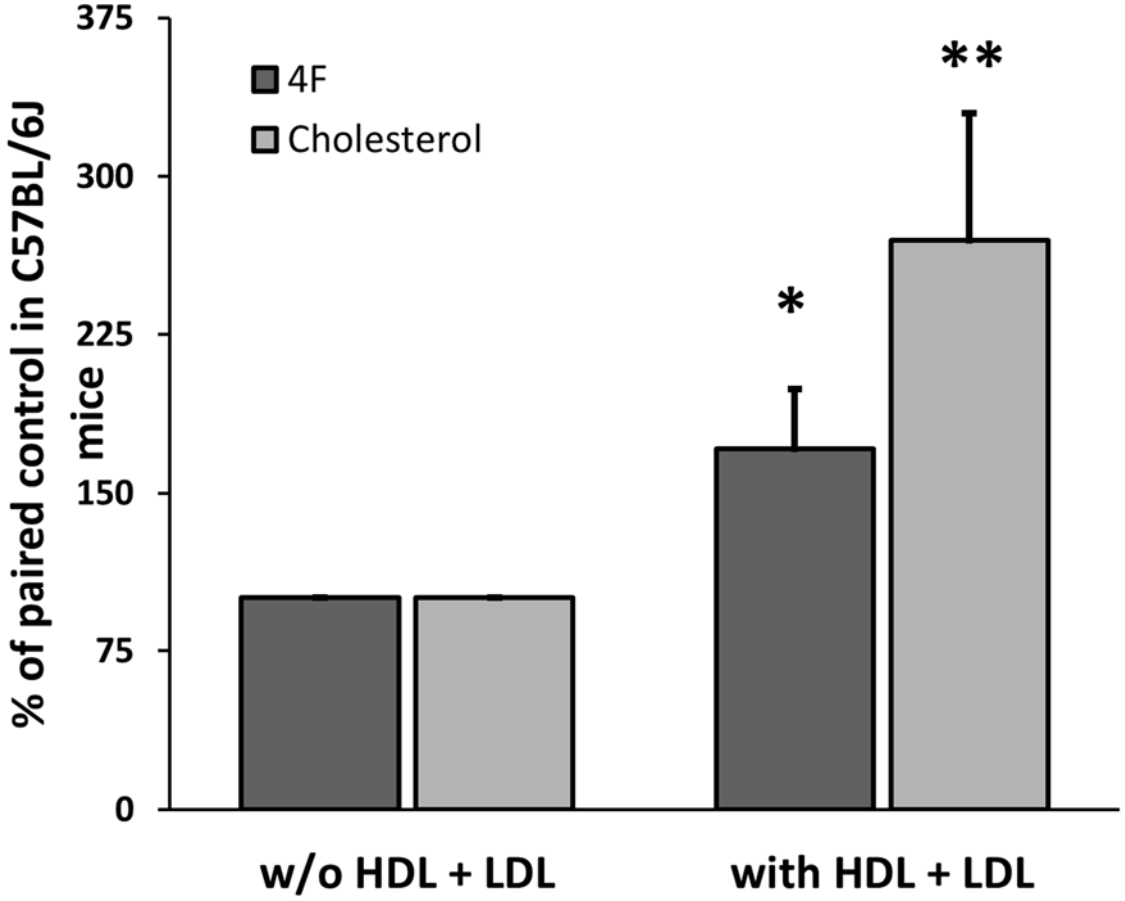
375
300
225
150
75
0
% of paired control in C57BL/6J mice
4F
Cholesterol
*
**
w/o HDL + LDL
with HDL + LDL

Figure 2-6A

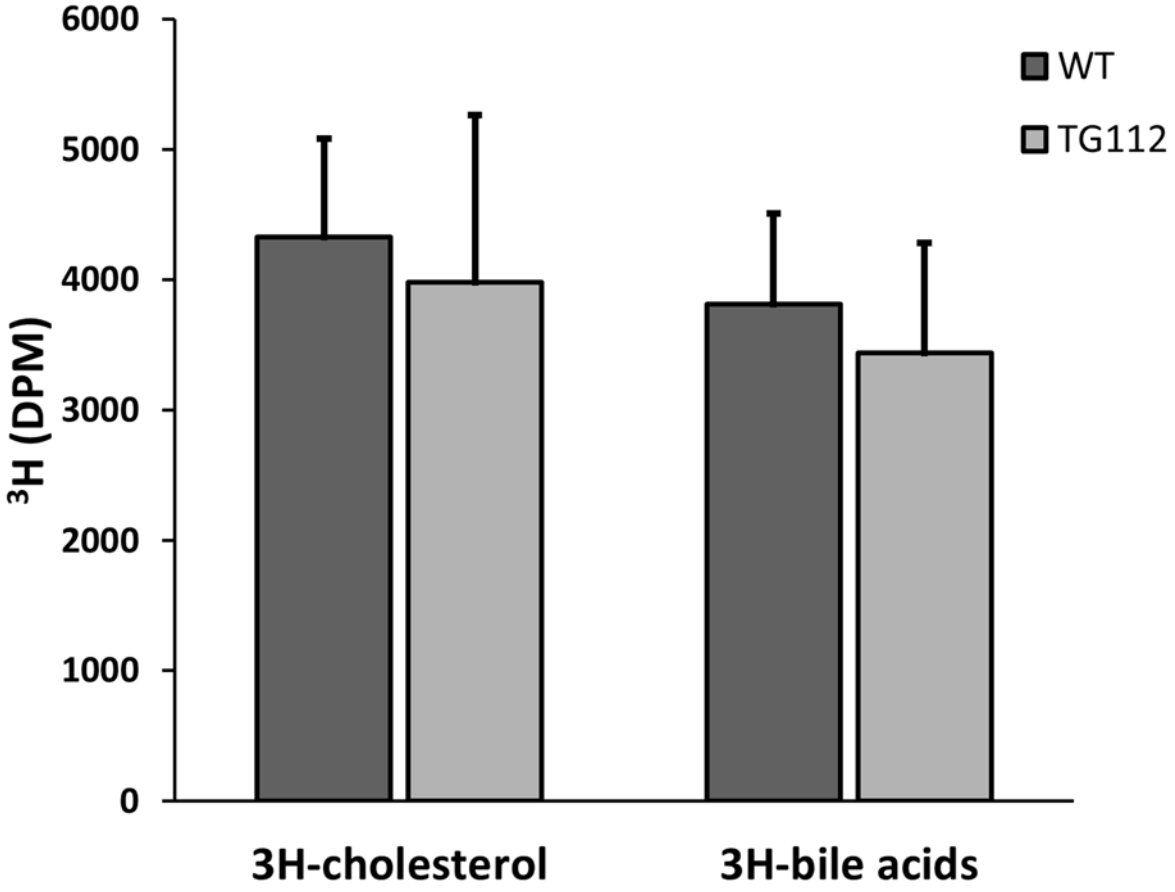
6000
5000
4000
3000
2000
1000
0
^{3}H (DPM)
WT
TG112
3H-cholesterol
3H-bile acids

Figure 2-6B

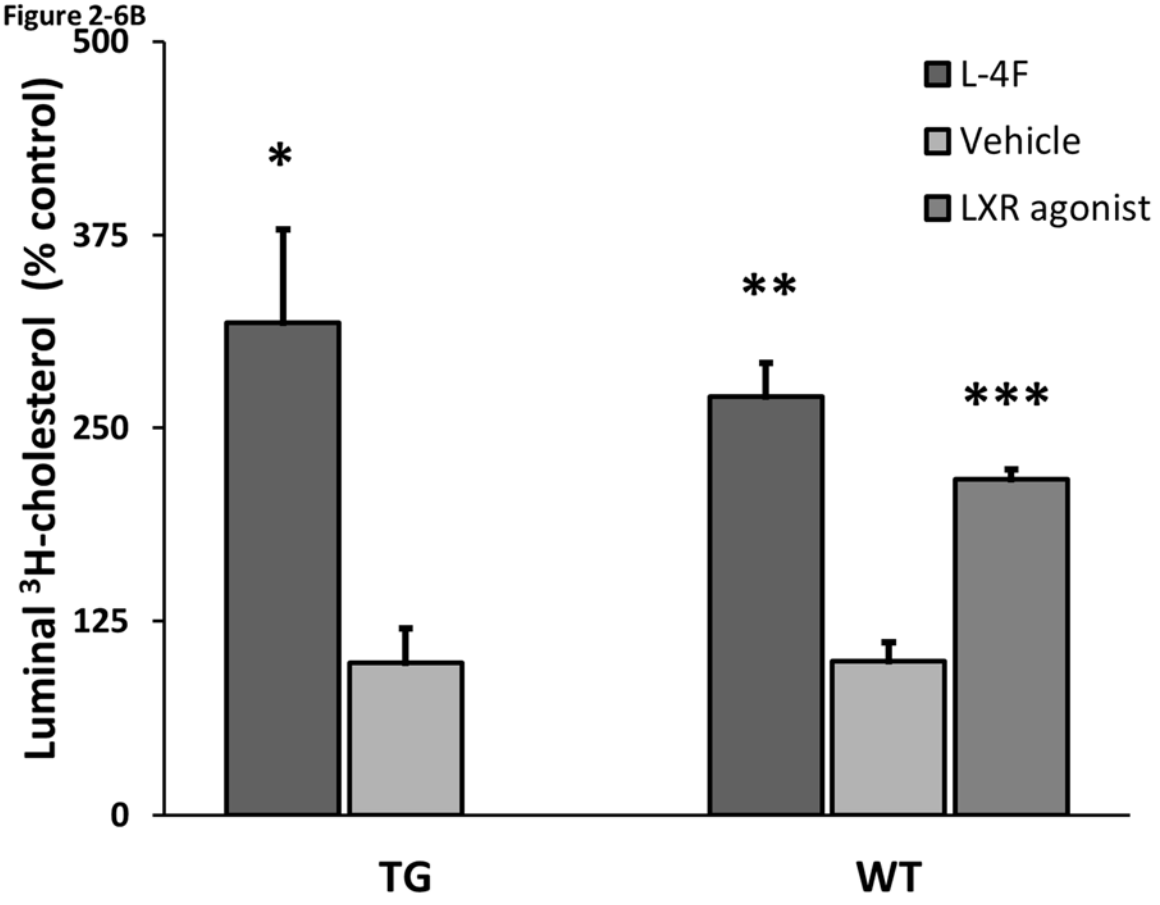
500
375
250
125
0
Luminal ^{3}H-cholesterol (% control)
L-4F
Vehicle
LXR agonist
*
**
***
TG
WT

Figure 2-6C

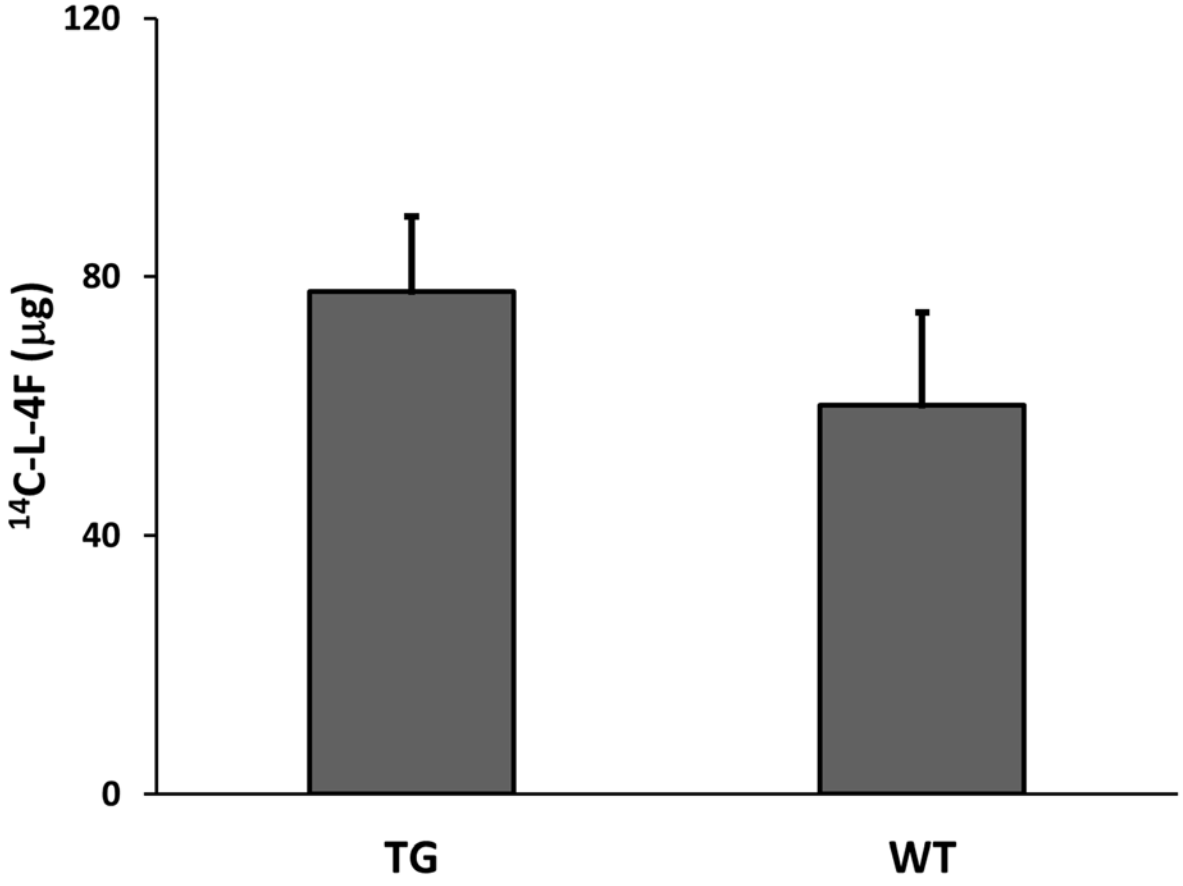

Figure 2-6D

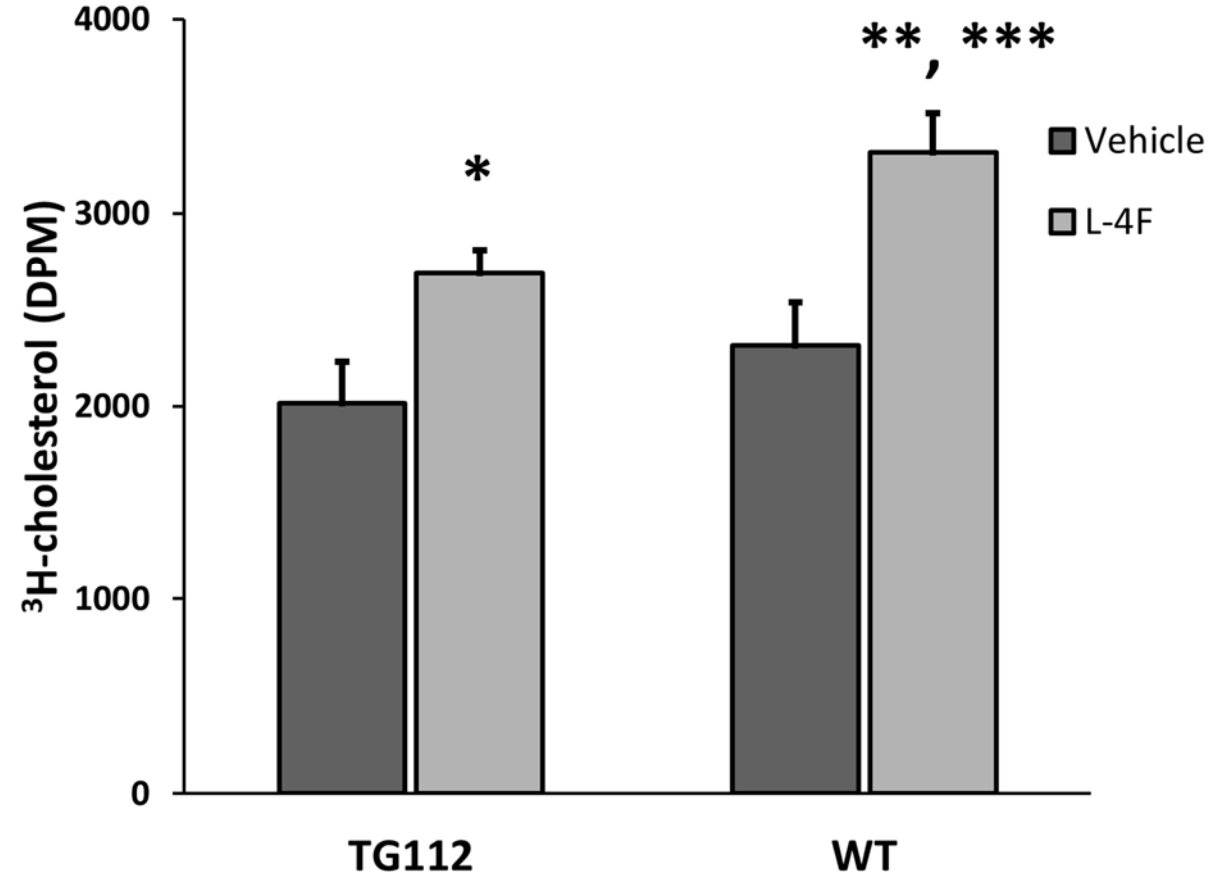
4000
3000
2000
1000
0
^{3}H-cholesterol (DPM)
*
, *
Vehicle
L-4F
TG112
WT

Figure 2-7A

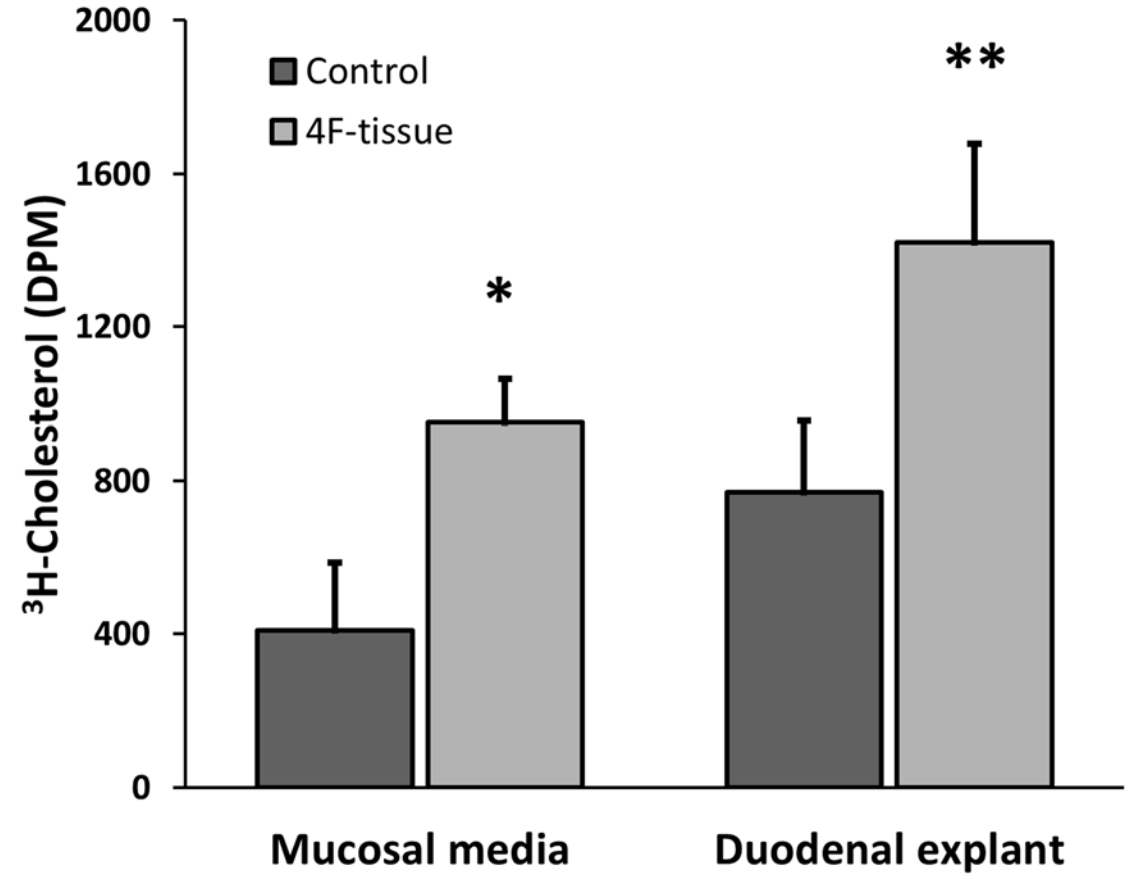
2000
1600
1200
800
400
0
^{3}H-Cholesterol (DPM)
Control
4F-tissue
*
**
Mucosal media
Duodenal explant

Figure 7B

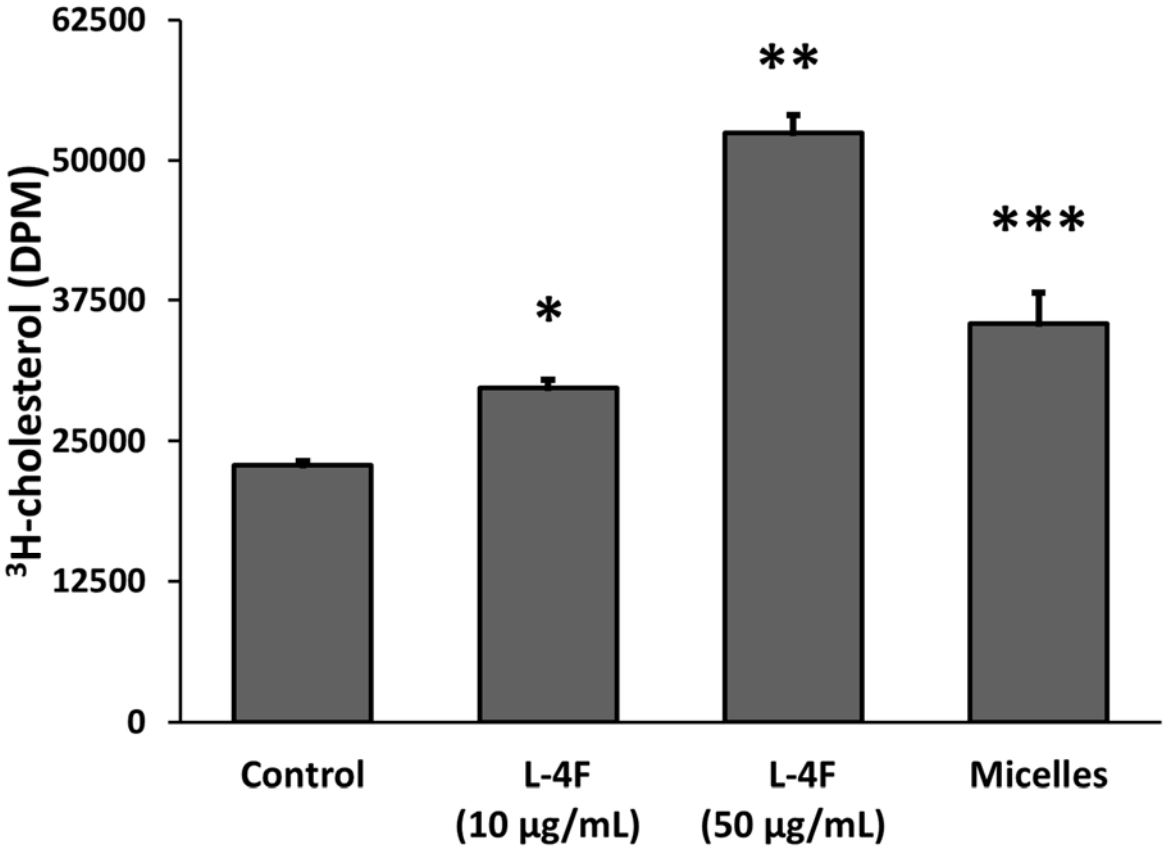
62500
50000
37500
25000
12500
0
^{3}H-cholesterol (DPM)
*
**
***
Control
L-4F (10 µg/mL)
L-4F (50 µg/mL)
Micelles

Figure 7C

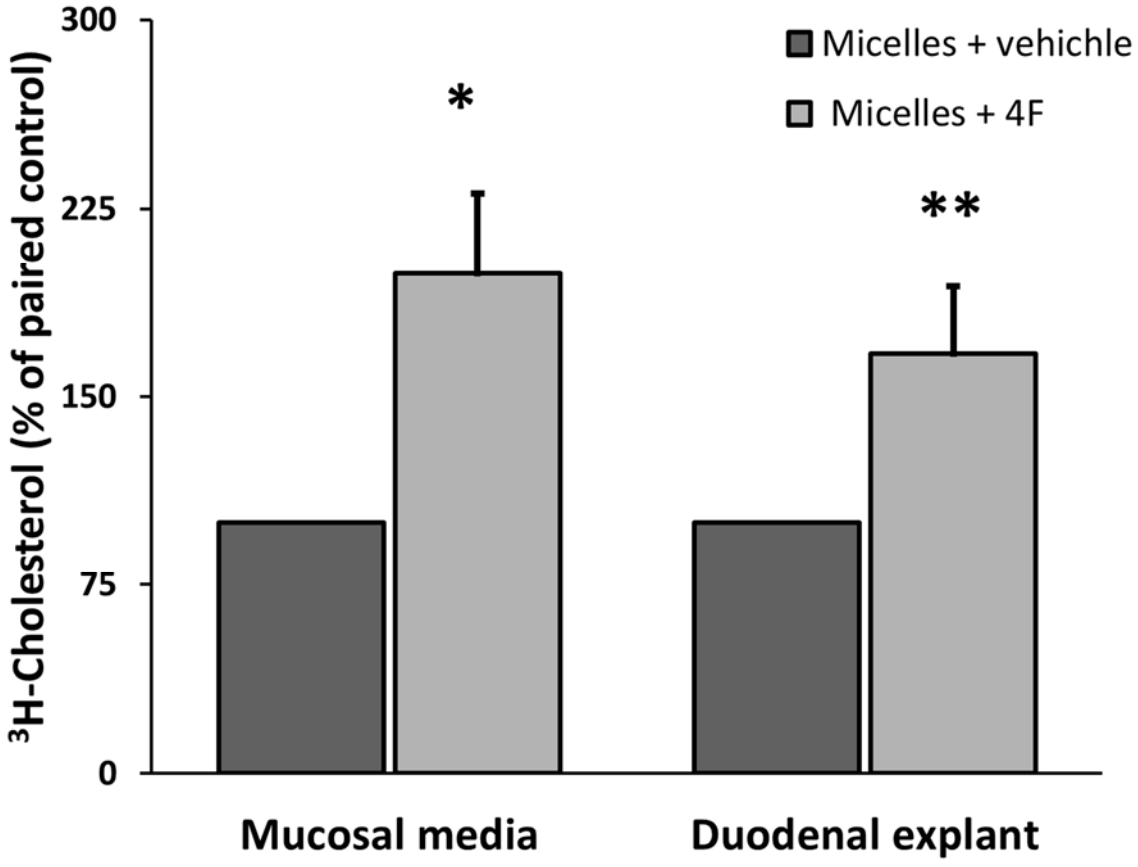
300
225
150
75
0
^{3}H-Cholesterol (% of paired control)
Micelles + vehichle
Micelles + 4F
*
**
Mucosal media
Duodenal explant

Chapter 3: COX2 dependent dysregulation of inflammatory signaling is rescued by apoA-I mimetic therapy in mouse models of IBD

Abstract

Inflammatory bowel disease (IBD) is a multi-factorial inflammatory disorder of the intestinal tract that exhibits high morbidity with very limited therapeutic options. ApoA-I mimetics including both 4F and Tg6F are potent anti-atherogenic and anti-inflammatory peptides, but they have not been studied as therapies for IBD. We have reported that the intestine is the site of action of the atheroprotective effects of 4F, where it modulates the trans-intestinal efflux of cholesterol. We thus sought to determine whether orally administered 4F could inhibit the development of IBD in two independent mouse models. Our laboratory previously reported that mice with complete or myeloid-conditional cyclooxygenase 2 (COX2) knock-out develop severe Crohn's disease-like inflammation in their ileo-ceco-colic junctions when fed a cholate-containing diet. 4F treatment dramatically inhibited intestinal inflammation in myeloid conditional COX2 knock-out mice challenged with 0.2% cholate-containing diet: significantly improving survival, gross pathology, H&E score, inflammatory cytokine profiles, macrophage and neutrophil infiltration, and markers of systemic inflammation. In parallel, we examined the effect of 4F on the development of colitis in $IL10^{-/-}$ mice fed the COX inhibitor piroxicam. As in the COX2 and cholate model, 4F treatment significantly improved various markers of disease including colon length, clinical colitis scores, and colon H&E scores. Because we observed that both cholate and piroxicam increase intestinal barrier permeability and translocation of LPS into portal vein serum in COX2 and IL10 KO mice respectively, while also observing that both antibiotic treatment and MyD88 inhibition abrogate intestinal inflammation in the COX2 and cholate IBD model, we further examined the inflammatory profiles of LPS-activated but 4F-treated primary macrophages from both types of mice. While both COX2 KO and IL10 KO + piroxicam enhance the pro-inflammatory effects of LPS activation,

co-treatment with 4F significantly inhibits the pro-inflammatory phenotype of these LPS-activated macrophages, as assessed by cytokine RNA expression as well as by the levels of pro-inflammatory lipid signals. These results suggest that 4F may protect against IBD in these models in part by suppressing toll-like receptor signaling. We also examined the effect of 4F treatment on the levels of inflammatory lipid signaling mediators present in both plasma and intestinal tissue in both models, observing that 4F treatment shifted the balance of pro-inflammatory and inflammation resolving lipid signals towards a less inflammatory phenotype in both tissue and plasma. Additional work ex vivo established that 4F can directly clear pro-inflammatory lipid signals from intestinal explants while also mediating the trans-intestinal transport of these lipid signals from lipoproteins into the intestinal lumen; strongly suggesting that 4F treatment directly clears pro-inflammatory lipid signals in vivo. As the apoA-I mimetic Tg6F also inhibits the development of intestinal inflammation in the COX2 KO and cholate model, these findings suggest that apoA-I mimetic peptides may provide an important new therapy for the treatment of IBD.

Introduction

Inflammatory bowel disease (IBD), inclusive of Crohn's disease (CD) and ulcerative colitis (UC), is a chronic and relapsing inflammatory disorder of the gastrointestinal tract. IBD consists of a dysregulated mucosal immune response to gut microbiota, brought about by host and/or environmental triggers in genetically susceptible individuals.(1, 2) However, there exists no single pathogenic mechanism for IBD. Approximately 200 genetic susceptibility loci have been identified for IBD.(3) The candidate genes broadly implicate several distinct functional categories, including epithelial barrier function, innate immunity, T cell signaling, and autophagy; but even within a category, the underlying pathways are largely distinct.(3, 4) The range of environmental factors associated with the development of IBD is also complex; antibiotic use, childbirth mode, breastfeeding, air pollution, NSAID use, hypoxia or high altitude, diet, and urban environments have all been associated with increased risk of disease.(5) In the absence of a single pathogenic mechanism, investigation into the etiology and pathogenesis of IBD requires careful elucidation of the disparate causal contributions of the many susceptibility-linked genes and disease-associated environmental factors.

IBD exhibits high morbidity, but there are currently few effective pharmacological interventions. For example, between 70% and 90% of all CD patients eventually undergo surgery within their lifetime, and approximately 40% will require repeated surgery.(6) Anti-TNF therapies including both infliximab and adalimumab offer a treatment option for IBD that is refractory to conventional therapies including corticosteroids and immunomodulators—leading to mucosal healing and reducing the need for hospitalization and surgery.(7) However, treatment failures with anti-TNF therapies are common. Primary nonresponse was reported in up to 40% of patients in clinical trials, while secondary loss of response was observed in up to 46% of those patients exhibiting a primary response.(8) There exists a pressing need for additional IBD therapies.

Murine models have importantly helped both to illuminate the overall pathogenesis of IBD and to determine the causal contribution to disease of many susceptibility-linked genes.(2) These models have also played an important role in both drug discovery and predicting clinical response.(9) Mirroring the genetic complexity of human disease, there exist over 50 genetic mouse models for IBD. As with humans, disturbances of barrier integrity, or dysregulations of innate or adaptive immune responses, can independently realize IBD-like intestinal inflammation in these models.(10-12) For example, MDR1 is a susceptibility gene for IBD,(13) and its contribution to disease has been studied extensively in the *mdr1a*-deficient mouse model of spontaneous colitis.(14) In turn, several potential drugs including anti-IL17 therapy have been investigated in this model.(15)

COX2 is the inducible form of cyclooxygenase and is responsible for the rate limiting step in the conversion of arachidonic acid to prostanoids (prostacyclins, prostaglandins, and thromboxanes).(16) Multiple genetic susceptibility studies have linked COX2 to an altered risk of developing IBD,(3, 17-20) but the exact nature of the link is not thereby clear—with studies associating COX2 polymorphisms both with increased(17-19) and decreased risk.(20) We previously reported that both COX2 total knock-out (COX2 TKO) and COX2 myeloid-specific knock-out (COX2 MKO) mice or COX2-inhibited (COX2i) mice develop severe CD-like inflammation in their ileo-ceco-colic junctions upon cholate (0.5% w/w) dietary challenge.(21, 22) These results establish that COX2 is protective against CD-like pathology in these models. However, while this earlier work characterized disease phenotype, it did not further investigate the pathogenic mechanism of these models.

The present study makes use of our COX2 and cholate models to investigate the causal contributions to IBD of both COX2 and the environmental trigger cholate, while simultaneously employing these models to investigate the efficacy of apoA-I mimetic peptides as therapies against IBD. There exists a synergy between these two arms of investigation. We here report that apoA-I mimetic peptide therapy significantly inhibits the development of intestinal inflammation in these models. Our

observations regarding the underlying pathogenic mechanism of these mouse models inform our hypotheses regarding the inhibitory mechanisms of these therapies. In turn, we also make use of these effective therapies as investigative tools to help support our claims regarding the mechanism of disease in these models.

ApoA-I mimetic peptides including both 4F and 6F are short amino acid sequences that recapitulate the secondary structure and partial function of apoA-I, the main structural protein of high density lipoprotein (HDL).(23) ApoA-I contains 243 amino acids, while both 4F and 6F contain only 18; but both peptides exhibit the same class A amphipathic helical structure as apoA-I, while also mimicking its ability to bind and solubilize lipids. The 4F peptide was found to be protective in numerous animal models of inflammatory disease, including atherosclerosis,(24-26) arthritis,(27) renal inflammation,(28) hepatic fibrosis,(29) and pulmonary hypertension.(30) Transgenic 6F (Tg6F), extract from tomatoes expressing the 6F peptide, likewise prevented the development of atherosclerosis(31) and systemic inflammation(32) in mouse models. Of particular interest, apoA-I has been shown to inhibit DSS-induced colitis in mice,(33) while 4F has inhibited the development of air-pollution induced inflammation in the small intestine.(34)

We have previously reported that circulating 4F selectively targets the small intestine, where it is transported into the intestinal lumen, is reabsorbed by the intestinal mucosa, and mediates the trans-intestinal efflux of cholesterol.(35) We have also demonstrated that both oral and subcutaneous (SQ) administered 4F reduces the levels of the pro-inflammatory fatty acid metabolites 15HETE, 12HETE, 13HODE, and 9HODE in enterocytes of LDLR-null mice on western diet, while also improving markers of systemic inflammation.(36) Likewise, the intestine has also been identified as the site of action of the systemic anti-inflammatory effects of Tg6F.(32) Given this background, we thus sought to determine whether orally administered 4F and Tg6F could inhibit the development of CD-like inflammation in the COX2 and cholate model.

Overall, we report that while cholate initiates disease by increasing both barrier permeability and the translocation of pathogen-associated molecular patterns (PAMP), disease further requires COX2-dependent dysregulation of the inflammatory response to MyD88-specific TLR ligands. Dysregulation within the macrophage compartment is sufficient to drive disease, and macrophages lacking COX2 activity are more pro-inflammatory upon LPS activation. We developed a LC-MS/MS panel of 40 pro-inflammatory and inflammation resolving signaling lipids and show that the balance of pro-inflammatory and inflammation resolving lipid signals is altered in both ceca and plasma of mice with the disease. Of interest, we observed that ceca from COX2 KO mice exhibit a smaller ratio of the inflammation resolving resolvin D1 (RvD1) to the pro-inflammatory leukotriene B4 (LTB4): a finding consistent with a recent report about the nature of more pro-inflammatory and unstable atherosclerotic lesions.(37)

Both 4F and Tg6F therapy abrogates disease in the COX2 and cholate models. 4F peptide treatment inhibits the pro-inflammatory phenotype of LPS-activated COX2-deficient macrophages, while also rescuing the imbalance of pro-inflammatory lipid signals in ceca and plasma. We demonstrate ex vivo that 4F can directly clear pro-inflammatory lipid signals from intestinal tissue, while also increasing the trans-intestinal transport of these pro-inflammatory signals from HDL and LDL. Last, we show that 4F therapy inhibits disease in the piroxicam-accelerated (PAC) IL10 KO model of colitis, where 4F treatment also lowers levels of pro-inflammatory lipid signals in plasma. As we observe that piroxicam, like cholate, increases both intestinal barrier permeability and PAMP translocation, we demonstrate that 4F suppresses pro-inflammatory signaling from LPS-activated and piroxicam-treated IL10 KO primary macrophages. These results together recommend apoA-I mimetics as potential therapies for IBD including both CD and UC.

Materials and Methods

Mice. COX2 MKO ($COX2^{fl/fl}$; $LysM^{Cre/+}$), COX2 TKO mice ($COX2^{luc/luc}$), and $IL10^{-/-}$ were all bred and maintained as described.(22, 38, 39)

ApoA-I mimetic peptides. D-4F peptide was made synthesized as previously described.(35) For in vivo studies, D-4F was supplied as 500 ug/ml in drinking water, and the mice were allowed to drink ad libitum. For cell culture studies, D-4F was added at 15 ug/ml to the cell culture media. Tg6F and empty vector (EV) extracts were prepared as described previously.(40, 41) For studies involving Tg6F, the final diets contained 0.06% of Tg6F or EV extract by weight.

Basic IBD studies involving the COX2 CCHF and PAC IL10 mouse models. COX2 TKO or MKO mice were challenged with CCHF diet (Envigo TD.90221) for 2 or 7-10 weeks, respectively. Inflammation in the ileo-ceco-colic junctions was assessed by gross pathology, histological scoring of inflammation and epithelial damage (see below), as well as by immunohistochemistry for Ly6G and F4/80, and qPCR for TNFα and IL10. Both immunohistochemistry and qPCR were performed in accord with standard protocols. C57BL/6J mice were fed the selective COX2 inhibitor celecoxib as described,(22) and inflammation was evaluated as above. Piroxicam mixed into chow and fed to $IL10^{-/-}$ mice as described.(39) Colitis was evaluated in these mice as described in the Results.

Barrier permeability, endotoxin, inflammation, and epithelial damage. *Barrier permeability* was measured by determining urinary excretion of sucralose, mannitol, and lactulose over 24 hours in metabolic cages following oral gavage. LC-MS/MS was used to determine the levels of these carbohydrates relative to raffinose used as internal standard. LC-MS/MS methods and dosing are as

described.(42) *Endotoxin* levels in portal vein serum were determined following collection of portal vein plasma from anesthetized mice. Serum was allowed to form over 1 hour at RT. Serum samples were heated to 50 deg for 10 min, and endotoxin levels were determined via LAL assay in accord with the manufacturer's protocol (Kinetic Turbidimetric LAL Assay, Lonza). *Inflammation* was determined by histological score of HE stained sections of ileo-ceco-colic junction. Inflammation was scored 0-4 on three separate fields per sample. *Epithelial damage* was also assessed histologically on the basis of a score of 0-4 in three separate fields per sample.(43)

Antibiotic treatment. Vancomycin, ampicillin, neomycin, and metroniadazole were supplied in drinking water as described.(44)

MyD88 inhibition. The MyD88 inhibitor T6167923 was supplied 3x/week at 250 ug/injection.(45)

Bone marrow derived macrophage studies. Bone marrow derived macrophages were generated as previously described.(46) BMDM were activated with 25 ng/ml LPS and either co-treated with 15 ug/ml D-4F or pre-treated for 2 days with 15 ug/ml D-4F. For analysis of lipids, lysates were collected and assessed as described in Supplementary Methods. Separate wells of the 6-well dishes were set aside for RNA. Pro-inflammatory cytokine gene expression was determined using BIoRad's SYBR green kit in accord with standard protocols. (n=3/group/time point)

Carrageenan hind paw model. Mouse hind paws were injected with carrageenan and paw edema was measured as described.(47) For the study of hind paw swelling in COX2 MKO and FLOX mice, n = 7.

Lipid inflammatory mediators in tissue and plasma of COX2 MKO and FLOX mice. Lipid inflammatory mediators were determined in both tissue and plasma of COX2 MKO and FLOX mice that had been fed a CCHF diet for 8.5 weeks (see Supplemental Methods).

ApoA-I mimetics and COX MKO + CCHF. COX2 MKO mice were challenged with CCHF for 7, 8.5, and 10 weeks (n=7/group/time point), and the effect of D-4F (500 ug/ml) on intestinal inflammation was determined as noted above. In brief, gross pathology, histopathology (HE inflammatory score and muscle thickness), IHC for Ly6G and F4/80, and qPCR for expression of *Tnfα* and *Il10* were determined. Lipid inflammatory mediators in both plasma and intestinal tissue were determined, also as described. Tg6F or EV extract (0.06% w/w) in combination with CCHF diet were fed to both FLOX and COX2 MKO for 8.5 weeks (n=8/group), and drug treatment was assessed by gross pathology and histopathology.

Total cholesterol and PON. Both plasma TC and PON1 activity were determined as previously reported by our lab.(48)

Ussing chamber experiments. These experiments were performed in accord with our previously published methods, except for the minor modifications detailed in the Results herein.(35)

Binding affinity studies. Binding affinities between 4F and both cholate and 15HETE were determined by surface plasmon resonance in accord with methods previously detailed by our lab.(49)

Assessment of colitis in PAC IL10 model. During evaluation of the severity of colitis in the PAC IL10 model, we followed previously published procedures and criteria.(39)

ApoA-I mimetic 4F and PAC IL10. The protocol for this study is given in Figure 6.

Statistics. P-values were determined by double sided unpaired or, where specified, paired T-tests, with significance set at $p < 0.05$. Variation is reported as SEM.

Results

Dysregulated inflammatory response to PAMP drives intestinal inflammation in the COX2 and cholate models of IBD.

Consistent with our prior reports, both COX2 TKO and COX2i but not wild-type (WT) mice developed severe chronic inflammation in their ileo-ceco-colic junctions when challenged with a cholate-containing high fat diet for 2 weeks.(21, 22) Disease was characterized by severe inflammatory lesions in both the submucosa and muscularis propria together with sporadic foci of mucosal ulceration, as well as by thickening of the intestinal wall (**Figure 1A**). While both a cholate-containing chow (CCC) diet and a cholate-containing high fat (CCHF) diet induce histologically comparable disease, CCHF diet accelerates the disease time course compared to CCC (2-3 weeks *vs.* 4-12 weeks, for full induction).(21) In order to economize the lengths of our animal experiments, we conducted our studies with CCHF diet.

Within our models, loss of COX2 activity is necessary but not sufficient for the development of IBD. Chow-fed COX2 TKO mice exhibit reduced viability together with, for example, renal alterations characteristic of renal dysplasia,(50) but they do not spontaneously develop chronic inflammation in their ileo-ceco-colic junctions (data not shown, 21). Rather, CD-like inflammation is initiated in these mice by an environmental trigger (viz., 0.5% dietary cholate). In this respect, our models mirror the etiology of CD itself, in which genetic susceptibility combines with environmental triggers to produce disease. Because the production of cholate is increased by diets high in fat and cholesterol,(51) while diets high in fat and cholesterol increase the risk of developing CD,(49) the manner in which cholate here triggers disease is of potential significance regarding the pathogenesis of CD. We thus sought to determine the mechanism by which dietary cholate initiates disease in our COX2 models.

When we fed COX2 TKO and COX2i mice CCHF for 2 weeks, we observed sporadic ulceration of the epithelia in the ileo-ceco-colic junctions of the experimental mice (see Figure 1A). Bile acids including cholic acid pose a significant risk of cellular toxicity, in part as a result of their detergent capacity to alter cell membrane integrity.(52, 53) In turn, epithelial damage can disrupt epithelial barrier function, while damage-associated molecular patterns (DAMP) themselves(54) or disrupted barrier function can be a cause of gut inflammation.(55) Several studies have moreover identified increased intestinal permeability as a primary etiologic factor in CD.(56, 57) By contrast, COX2 expression is strongly induced in both intestinal and esophageal epithelial cells by non-conjugated bile acids like cholic acid,(58-61) while COX2 and COX2-derived PGE2 play important roles in gastrointestinal mucosal defense(62) including protecting against intestinal ulceration.(63, 64) We thus initially hypothesized that in the absence of COX2 activity, dietary cholate damages intestinal epithelium and increases barrier permeability in a manner consistent with the initiation of inflammation in our models.

Epithelial damage can cause intestinal inflammation, but intestinal inflammation can itself cause epithelial damage including ulceration.(65) If epithelial damage or altered barrier function are a cause of intestinal inflammation in our models, these alterations must precede the development of inflammation. We thus conducted a time course experiment in which we monitored epithelial damage, changes in barrier permeability, translocation of endotoxin into portal vein serum, and ileo-ceco-colic inflammation over time (**Figure 1B**). C57BL/6 mice were fed either CCHF or CCHF containing the COX2 inhibitor celecoxib (CX) and sacrificed at 2, 7, 11, and 14 days. Whole intestinal barrier permeability was measured by determining the urinary excretion of orally gavaged sucralose (by LC-MS/MS method), across the 24 hours prior to sacrifice.(42, 66) At each time point, portal vein serum was collected from the mice for endotoxin analysis and ceca were collected for subsequent histological determination of epithelial damage and inflammation.

We observed that CCHF significantly increased whole intestinal barrier permeability by approximately 3-fold in CX-treated mice ($p = 0.02$), as assessed by urinary excretion of sucralose (see Figure 1B, top left). The effects of CCHF on permeability peaked at 7 days with permeability at 14 days not differing significantly from day 7 ($p = 0.5$). In this same experiment, we also determined urinary excretion of lactulose and mannitol, whose ratio assesses increase in the permeability of the small bowel. We observed only an approximate 2-fold increase in permeability (data not shown), suggesting that at least some of the observed increase in sucralose permeability was due to alteration in the distal bowel.(66) In order to rule out the possibility that the observed increase in barrier permeability was due to possible off-target effects of celecoxib in this model,(67, 68) we also determined the effect of CCHF on permeability in COX2 TKO mice across 14 days and obtained comparable results (**Supplemental Figure 1**).

The increase in barrier permeability in CX-treated mice was mirrored by a significant increase ($p < 0.01$ at 7d) in the translocation of endotoxin into portal vein serum, as determined by limulus amebocyte lysate assay (see Figure 1B, top right).(69) The increases in both barrier permeability and endotoxin translocation preceded the development of histologically assessed inflammation in the ileo-ceco-colic junctions of CX-treated mice. Thus, the time course of these changes is consistent with the hypothesis that CCHF initiates CD-like inflammation by functional alteration of the intestinal barrier, leading to influx of pathogen-associated molecular patterns (PAMP). However, while we observed at 14 days sporadic epithelial ulceration in CX treated mice (see Figure 1B, bottom left), these changes did not precede the development of inflammation. This result suggests that DAMP associated with epithelial ulceration do not initiate the intestinal inflammation of these models. In this case, the epithelial ulceration appears to be a consequence rather than a cause of the inflammation.

To our surprise, CCHF equally and significantly increased whole intestinal permeability in C57BL/6J mice through 7 days ($p < 0.05$ compared to 0d; $p = 0.75$ compared to CX-treated mice). While

permeability significantly decreased in control mice compared to CX-treated mice by day 14 ($p < 0.05$; see Figure 1B, top left), the initial increase in permeability in control mice was also accompanied by increased translocation of endotoxin into portal vein serum (see Figure 1B, top right). Nonetheless, only CX-treated mice and not control mice develop ileo-ceco-colic inflammation and epithelial ulceration (see Figure 1B, bottom left). The COX2-independent effect of CCHF on barrier permeability and translocation of PAMP puts pressure on our hypothesis regarding the initiation of inflammation in our models.

We nonetheless continued to investigate this hypothesis, by stepping back to determine the dependence of the intestinal inflammation of our models on gut microbiota. Gut microbiota have been shown to play an essential role in the initiation of intestinal inflammation in many mouse models of IBD.(11) We thus pre-treated both TKO and CX-treated mice for 1 week with ampicillin, neomycin, metroniadazole, and vancomycin—an antibiotic cocktail that has been demonstrated to ablate intestinal bacteria in mice.(44) While continuing to treat the mice with these antibiotics (AB), we then challenged with CCHF or CCHF + CX for 2 weeks, respectively (**Figure 1C**). We observed that AB treatment completely abrogated inflammation in the ileo-ceco-colic junctions of both TKO and CX-treated mice, as assessed by gross pathology. Histological assessment gave comparable results (data not shown). However, gut microbiota can convert cholate to deoxycholate, and deoxycholate has itself been shown to cause greater intestinal epithelial damage than cholate.(70, 71) We thus sought to rule out the possibility that AB treatment inhibited inflammation by blocking the conversion of cholate to deoxycholate. We determined the effects of both dietary cholate and deoxycholate on barrier permeability in AB-treated TKO mice—a treatment we carried forward in order to ensure that dietary cholate did not convert to deoxycholate, thereby confounding our results. We observed no difference between the effects of dietary cholate and deoxycholate on intestinal barrier permeability (**Supplemental Figure 2**). These results are thus consistent with PAMP initiating the inflammation of our models.

LPS induces the production of pro-inflammatory signals by stimulating the LBP/CD14/MD-2/TLR4 cell surface complex. In turn, this complex signals through the adaptor protein MyD88 to trigger the nuclear translocation of NFκB and the transcription of pro-inflammatory target genes.(72) We had observed LPS in portal vein serum following CCHF challenge (see Figure 1B). We thus inhibited MyD88 with the small molecule T6167923 in TKO mice,(45) while challenging these mice with CCHF for 2 weeks (**Figure 1D**). As with AB treatment, MyD88 inhibition abrogated gross pathological evidence of ileo-ceco-colic inflammation. Histological assessment mirrored this result (**Supplemental Figure 3**). The results of Figures 1C and 1D together indicate that intestinal inflammation depends upon TLR and MyD88-dependent PAMP signaling in our models, while the results of Figure 1B suggest a role for LPS.

However, it remains the case that CCHF increases barrier permeability and translocation of PAMP equally in control and CX-treated mice (see Figure 1B). If it is nonetheless true that PAMP translocation and TLR/MyD88 signaling initiates disease in our models, there must exist a differential response to bacteria-dependent TLR ligands in the absence of COX2 activity—a response that is more pro-inflammatory and/or less inflammation resolving than the control response. Consistent with our prior report,(22) myeloid-conditional COX2 knock-out mice ($COX2^{fl/fl}$; $LysM^{cre/+}$) develop ileo-ceco-colic inflammation comparable to that of TKO and COX2i, upon 7 or 10 week CCHF challenge (**Supplemental Figure 4**). The LysM promotor of these conditional knock-outs is expressed in close to 100% of mature non-splenic macrophages and approximately 60% of neutrophils.(73) We thus conducted a small pilot study using neutrophil-specific COX2 KO mice ($COX2^{fl/fl}$; $MRP8^{Cre/+}$)—mice whose Cre promotor is almost unexpressed in mature macrophages.(73) Following 7 wk CCHF challenge, we did not observe any gross pathological or histological evidence of ileo-ceco-colic inflammation (data not shown). These results led us to investigate dysregulated responses to PAMP within the macrophage compartment. We thus generated bone-marrow derived macrophages (BMDM) from MKO mice, or treated primary peritoneal macrophages (PM) with the COX2 inhibitor SC236. We then activated the macrophages with LPS and

determined the expression of NFκB pro-inflammatory target genes using qPCR. We validated the loss of COX2 activity by monitoring the levels of COX2 metabolites including PGE2, PGD2, PGJ2, and 15dPGJ2 via LC-MS/MS (**Supplemental Figure 5**). We observed that the expressions of pro-inflammatory genes including TNFα and IL1β were significantly higher in the absence of COX2 activity in both BMDM (**Figure 1E**) and PM (data now shown) at 12 hours post-LPS. Dysregulation of PAMP-dependent pro-inflammatory signaling within the macrophage compartment could thus partially explain the differential response to CCHF between control and TKO/COX2i/MKO mice.

MKO mice challenged with CCHF exhibit an imbalance of pro-inflammatory and inflammation-resolving lipid signals in both tissue and plasma.

COX2 is upregulated during acute inflammation in response to pro-inflammatory stimuli including TNFα, IL1β, and LPS,(74) and its role during the initiation of inflammation has been well characterized. COX2 mediates the conversion of arachidonic acid to PGH2, while tissue specific synthases convert PGH2 to the major prostaglandins (PGE2, PGD2, PGI2, and PGF2α) as well as to thromboxane A2 (TXA2)--all of which can be produced in macrophages.(75) These prostanoids all can act as pro-inflammatory autacoids and signal in paracrine fashion.(76) PGE2 for example helps promote both vasodilation and the attraction and activation of neutrophils and macrophages.(77)

Less well appreciated, COX2 also mediates the cessation and resolution of acute inflammation.(78) COX2 TKO inhibited the resolution of acute inflammation in a carrageenan-induced hind paw model,(47) while COX2i impaired resolution in a carrageenan-induced model of pleurisy.(79) In part, this may be due to an increased production of pro-inflammatory lipoxygenase (LOX) products, as arachidonic acid (AA) that would otherwise pass through the COX2 pathway shunts instead through LOX including 5-lipoxygenase (5LOX) and 12 or 15-lipoxygenase (12/15LOX in mice).(80) LOX-mediated AA

products include leukotrienes B4, C4, and E4 (LTB4, LTC4, LTE4) as well as 5, 12, and 15 HETE—all of which can exhibit pro-inflammatory effects (see Supplemental Table 1 for details). But distinct COX2 products have also been identified as directly anti-inflammatory—including PGD2 in contexts(81) but especially its degradation product 15d-PGJ2, which can act as a negative regulator of NFκB.(82)

The resolution of inflammation involves the cessation of neutrophil influx and the macrophage-mediated clearance of apoptotic cells and debris in a process known as efferocytosis. To some extent, resolution merely involves the downregulation and loss of pro-inflammatory signals. But resolution also involves active signal-mediated responses—including the active inhibition of neutrophil migration as well as the nonphlogistic recruitment of macrophages and the stimulation of efferocytosis.(83) These resolving signals are largely lipid mediators and include AA-derived lipoxins (LXA4, LXB4) as well as the omega-3 docosahexaenoic acid (DHA) and eicosapentaenoic acid (EPA) derived maresins (MaR1), resolvins (RvD-series and E-series), and protectins (PD1 and PDx).(84, 85) COX2 itself has been implicated in the production of resolving signals. Prostaglandins produced early in inflammation, for example, can trigger a lipid-mediator class switch within the LOX pathway, from the production of pro-inflammatory LTB4 to the pro-resolving LXA4(86)—an eicosanoid which promotes resolution by reducing vascular permeability,(87) promoting the nonphlogistic infiltration of macrophages,(88) and stimulating efferocytosis.(89) While LXA4 is often produced through combination of 15LOX and 5LOX activity, macrophage COX2 itself can also directly mediate the intracellular production of LXA4 through COX-dependent production of 15HETE.(80)

The murine carrageenan hind paw model has long been used to investigate both the underlying mechanisms of and possible interventions against acute inflammation.(90-92) The introduction of carrageenan into the foot pad of the mouse causes edema, whose degree serves as a non-invasive marker across both the initiation and resolution of inflammation. The inflammatory response of C57BL/6J mice in this model is biphasic, with an early peak at between 2-6 hours and a later peak at 72

hour; while resolution to baseline occurs by around 144 hours.(93) Neutrophil infiltration peaks at around 24 hours, while COX2 protein expression begins at 24 and peaks at 72 hours.(93) The effect of COX2 TKO on both phases of the inflammatory response in this model has been investigated,(47) as has the effect of COX2 MKO on the early phase of an air-pouch model of acute inflammation.(94) However, there are no reports of the effect of COX2 MKO on the biphasic response of the carrageenan model. We thus assessed paw edema in both C57BL/6J FLOX and COX2 MKO mice across both phases of the inflammatory response (0-144 hours) triggered by carrageenan (**Figure 2A**). Consistent with the published characterizations of this model, we observed in control FLOX mice a biphasic response, with an early response at 2 hours and a late response at 72 hours, and with significant resolution from that late response by 144 hours ($p < 0.01$). In contrast, while the early response in COX2 MKO mice was significantly delayed ($p < 0.01$) but of equal magnitude, the late response remained significantly greater than that in FLOX mice ($p < 0.01$ across all time points from 10 hrs). More importantly, the late response in COX2 MKO mice failed to resolve across the full 144 hours of the experiment. Thus, the late inflammatory response in COX2 MKO mice appeared to be both more pro-inflammatory and less inflammation resolving than that in FLOX mice.

During acute inflammation, early edema is followed by neutrophil infiltration, which is in turn followed by macrophage recruitment and efferocytosis. The peak of macrophage infiltration thus coincides with the clearance of neutrophils.(83) We also observed that the ileo-ceco-colic junctions of MKO mice on CCHF diet contained a significant co-presence of both macrophages and neutrophils, suggestive of a failure of efferocytosis (see Figures 3D-E). The initial observations presented in Figures 2A and 3D-E led us to conjecture that COX2 MKO mice would exhibit an altered balance of pro-inflammatory, anti-inflammatory, and inflammation resolving lipid mediators compared to chow and FLOX + CCHF controls. In particular, we hypothesized that these signals would be both more pro-inflammatory and less inflammation resolving than those of FLOX mice challenged with CCHF.

In order to test this hypothesis, we developed an MRM LC-MS/MS method capable of measuring a large panel of pro-inflammatory, anti-inflammatory, and inflammation resolving lipid signals (see **Supplemental Methods** for details). In brief, the method includes most of the bioactive signaling metabolites of AA, DHA, and EPA in the COX and LOX pathways, together with various pathway markers and stable degradation products (**Supplemental Table 1**). The bioactive lipids here measured directly or indirectly include the above COX-dependent prostanoids together with the anti-inflammatory Δ12-PGJ2 and 15d-PGJ2; the pro-inflammatory LOX products LTB4 and LTC4, 5 and 12 and 15HETE, 9 and 13 HODE, and 5-oxeETE; and the pro-resolving LOX products LXA4, LXB4, RvD1-5, MaR1, PDx, and RvE1 (**Table 1**). Overall, the method contains 2 separate MRM transitions for each 39 distinct lipid metabolites and 19 exact or class specific deuterated internals standards (**Supplemental Table 2**). The liquid chromatographic method provides good resolution and separation of all peaks across 14 min (**Supplemental Figure 6**). Lower limits of quantitation and detection (LLOQ, LLOD), upper limits of quantitation (ULOQ), and linearities of response were determined for each analyte (**Supplemental Table 3**). Lipids are isolated from samples using solid phase extraction (SPE); and sample preparation methods were validated for intestinal tissue, plasma, cell culture lysate, and cell culture media by determination of precision and extraction efficiency (**Supplemental Tables 4-5**).

We fed COX2 MKO and FLOX mice with CCHF diet for 8.5 weeks. We isolated plasma and ileo-ceco-colic junctions from these mice together with COX2 MKO plus chow controls. We extracted the lipid contents by SPE and determined by LC-MS/MS the levels of the above referenced lipids in both tissue (**Table 2**) and plasma (**Table 3**). As we had previously observed that COX2 MKO increased the pro-inflammatory cytokine phenotype of primary macrophages, we were particularly interested in determining how COX2 MKO would alter the in vivo lipid signaling phenotype in response to CCHF challenge.

In both intestinal tissue and plasma, COX2 MKO significantly increased the levels of multiple LOX and COX-dependent pro-inflammatory signals compared to FLOX controls (**Figures 2B-2C**). In intestinal tissue, COX2 MKO significantly increased the LOX signals 12HETE, 15HETE, and 13HODE, as well as COX-dependent PGE3 together with the PGI2 degradation product 6ketoPGF1α. In plasma, COX2 MKO significantly increased the LOX signals 12HETE and 5HETE, together with the COX signal PGF2α as well as the degradation product 13,14-dihydro-15-PGF2α ($p < 0.05$). More interestingly, COX2 MKO significantly increased the total level of LOX pro-inflammatory signals in both tissue and plasma, while also significantly increasing pro-inflammatory COX signals in tissue ($p<0.05$) and borderline-significantly increasing ($p < 0.1$) these signals in plasma.

As noted above, both PGE2 and PGD2 can have pro- or anti-inflammatory effects depending upon temporal and cellular context. We here observed that COX2 MKO significantly increased both PGE2 and its stable metabolite 15ketoPGE2 in intestinal tissue, together with PGE2 in plasma. Moreover, COX2 MKO significantly increased the total of PGE2, PGD2, and their metabolites in both intestinal tissue and plasma (**Figure 2D**). These results were counter to our observation of the effect of COX2 MKO on PGE2 and PGD2 in LPS-activated BMDM (see Supplemental Figure 5), suggesting that other cell types were responsible for these in vivo results.

Interestingly, COX2 MKO significantly reduced pro-resolving LOX signals at the same time that it increased pro-inflammatory LOX and COX signals in the ileo-ceco-junctions of CCHF-challenged mice (**Figure 2E**). While the 5LOX product RvD1 was only borderline-significantly reduced ($p = 0.1$), both the 5LOX product LXA4 and the total of 5LOX resolving products (LX + RvD series) were both significantly decreased ($p < 0.05$). Also of interest, the ratios of both LXA4 and 5LOX-associated resolving products to pro-inflammatory leukotriene LTB4 and the degradation product 6trans12epiLTB4 were both significantly suppressed by COX2 MKO. It was recently reported that this ratio of 5LOX-associated pro-resolving mediators to LTB4 was lower in unstable compared to stable atherosclerotic plaques.(37) Our

observations regarding signaling lipids in inflamed intestinal tissue are intriguingly in-line with the observations regarding atherosclerotic plaque stability and inflammation.

The apoA-I mimetics 4F and Tg6F inhibit the development of intestinal inflammation in the COX2 and cholate model of IBD.

The apoA-I mimetic peptide 4F is an effective anti-inflammatory agent that selectively targets the intestine (see Introduction). We thus first challenged MKO mice with CCHF and treated with oral 4F (500 ug/ml drinking water) for 7 and 10 weeks. 4F synthesized from L amino acids (L-4F) and from D amino acids (D-4F) have both been used in biological studies. D-4F and L-4F were shown to have the same *in vitro* and *in vivo* properties, indicating that stereo-specificity is not essential to the activity of the peptide.(95, 96) However, we here used the D form of this peptide in order to limit proteolytic degradation and increase oral bioavailability.(97)

Oral D-4F therapy protected against ileo-ceco-colic inflammation in MKO mice challenged with CCHF for either 7 or 10 weeks (**Figure 3**). 4F treatment blocked the increase in ileo-ceco-colic junction thickness otherwise triggered by CCHF diet (**Figure 3A**). 4F likewise significantly improved H&E inflammatory score ($p < 0.001$), (**Figure 3B**), while also blocking the CCHF-mediated increase in muscle thickness (**Figure 3C**). 4F treatment returned these measures to their no-disease baselines, indicating that 4F treatment largely or completely blocked the development of disease in this model.

We previously reported that MKO mice begin to die from burst ceca after approximately 10-11 weeks of CCHF diet. Consistent with this prior report, approximately 50% of our untreated MKO mice died by 10 weeks of CCHF challenge. In contrast, and consistent with the results of Figures 2A-C, no 4F-treated mice died within this period (**Supplemental Figure 7**).

Both F4/80+ macrophages and Ly6G+ neutrophils are extensively co-present in the inflammatory lesions of MKO mice challenged with CCHF diet, as determined by IHC (**Figures 3D-E**). By contrast, we did not observe a significant influx of either CD4+ or CD8+ T-cells over the controls (data not shown). 4F treatment significantly inhibited the influx of both F4/80+ macrophages and Ly6G+ neutrophils into the ileo-ceco-colic junctions of these mic e ($p < 0.001$) (see Figures 3D-E). 4F-treated mice also expressed significantly less TNFα in their ileo-ceco-colic junctions ($p < 0.01$), as determined by qPCR (**Figure 3F**).

In order to determine whether the protective effect of 4F in this model extended to other apoA-I mimetic peptides, we challenged MKO and floxed control mice (FLOX) with CCHF diet and treated with 0.06% Tg6F (w/w) for 8.5 weeks. Comparable to the effects of 4F, Tg6F therapy rescued gross pathology and significantly improved H&E score (**Figure 3G** and **Supplemental Figure 8**). These last results suggest that apoA-I mimetic peptides as a class may be protective against intestinal inflammation in the COX2 and cholate model of IBD. (may be add a little more about the translational potential of Tg6F in the near future)

4F treatment suppresses the pro-inflammatory phenotype of LPS-activated macrophages while improving the balance of inflammatory lipid signals in CCHF-challenged COX2 MKO mice.

We have argued that dysregulated TLR-dependent inflammatory signaling is a differential cause of intestinal inflammation in CCHF-challenged COX2 KO compared to WT mice. This inflammation is both bacteria and MyD88 dependent, while COX2 MKO increases the expression of pro-inflammatory cytokines in LPS-activated macrophages (see Figure 1). COX2 MKO also alters the balance of pro-inflammatory and inflammation resolving lipid signals in intestinal tissue and plasma of CCHF-fed mice, suggesting dysregulated inflammatory lipid signaling may act as a complimentary driver of disease in

these mice (see Figure 2). We thus framed our investigation into the protective mechanism of 4F therapy in terms of these earlier observations. We asked, in other words, whether 4F treatment could rescue these cytokine and lipid signaling phenotypes. In turn, we hoped that this investigation into the protective mechanism of 4F would lend support to the causal hypotheses of our earlier studies.

CCHF diet increased the expression of the pro-inflammatory cytokine TNFα in the ileo-ceco-colic junctions of MKO mice (see Figure 3F), while COX2 MKO increased its expression in LPS-activated BMDM (see Figure 1E). Because 4F had inhibited TNFα expression in vivo (see Figure 2F), we sought to determine whether 4F treatment could directly suppress pro-inflammatory cytokine expression in our primary macrophage models.

It has previously been reported that 7 day pre-treatment with 4F inhibits TLR expression in human monocyte-derived macrophages, while also suppressing the pro-inflammatory response to LPS.(98, 99) It has also been shown that 4F binds LPS with high affinity.(100) We thus both pre-treated and co-treated LPS-activated COX2 MKO BMDM with 4F (15 ug/ml) and assessed the expression of NFκB pro-inflammatory target genes including TNFα and IL1β. BMDM require at least 6 day stimulation with MCSF in order to differentiate from isolated bone marrow cells (**Supplemental Figure 9**). PM cultures are comparably time-constrained. In order to ensure macrophage viability across the experimental time course, we limited 4F pre-treatment to 2 days prior to LPS administration (25ng/ml).

We observed that co-treatment with 4F significantly inhibited the expression of IL1β and TNFα in both COX2 MKO BMDM across multiple time points through 24 hours (**Figure 4A**), while pre-treatment had no effect (data not shown). While 4F co-treatment partially or fully rescued the pro-inflammatory effects of COX2 MKO on IL1β and TNFα expression, respectively, at 12 hours compared to FLOX, 4F co-treatment also significantly inhibited the expression of these pro-inflammatory markers in FLOX BMDM. This result indicates that the anti-inflammatory effects of 4F in this system are independent of any dysregulation consequent to COX2 MKO.

We also assessed the effects of 4F pre- and co-treatment on lipid inflammatory mediators in cell lysate. We had previously observed that LPS stimulated the production of COX metabolites including PGE2 and PGD2 in FLOX BMDM, while COX2 MKO severely inhibited this induction effect (see Supplemental Figure 5). In contrast, neither LPS nor LPS plus COX2 MKO altered the levels of total LOX metabolites (**Supplemental Figure 10**). We here observed that 4F co-treatment but not pre-treatment significantly reduced the levels of LPS-induced COX metabolites including PGE2 and PGD2 (**Figure 4B**). Because 4F can clear lipid inflammatory mediators directly from tissue (see Figure 5A), we considered the hypothesis that 4F was clearing these COX metabolites from the BMDM. However, 4F co-treatment did not alter the levels of total LOX metabolites (see Supplemental Figure 10). Comparing the monohydroxylated COX and LOX AA-metabolites 11HETE and 15HETE, respectively, we observed that 4F treatment significantly lowered the levels of 11- but not 15HETE (**Figure 4C**). 4F has high binding affinity to monodydroxylated metabolites of arachidonic acid including 15HETE.(101) If 4F were somehow lowering the level of 11HETE by binding and thereby clearing this lipid species (see Figure 5B), 4F should affect 15HETE as well. This differential effect on the levels of 11- and 15HETE (together with the result from the experiment of Figure 4A) thus suggests that 4F inhibits the pro-inflammatory effects of LPS in this model by directly interfering with LPS-dependent signaling rather than by clearing any resultant pro-inflammatory mediators downstream.

We next determined the consequence of oral 4F therapy on the levels of lipid inflammatory mediators in the ileo-ceco-colic junctions of COX2 MKO mice challenged with CCHF. We challenged both COX2 MKO and FLOX mice with CCHF for 8.5 weeks, while administering oral D-4F (500 ug/ml) in drinking water to some of the COX2 MKO mice. At the end of the study, we collected intestinal tissue and determined the levels of lipid inflammatory mediators (**Supplemental Table 6**). Of note, 4F treatment significantly reduced the levels of the pro-inflammatory LOX products 12HETE and 13HODE, while also significantly reducing the total level of all pro-inflammatory LOX metabolites (**Figure 4D**). 4F

therapy thus partially rescued the pro-inflammatory effect of COX2 MKO on these LOX lipid mediators. By contrast, while COX2 MKO increased the levels of several of the pro-inflammatory COX mediators including those associated with PGE2 and PGD2, 4F therapy largely failed to reduce these lipid levels—only decreasing 13,14-dihydro-15keto-PGD2. 4F also lowered the levels of PGJ2 and Δ12-PGJ2, without affecting the level of the more anti-inflammatory 15d-PGJ2. However, by comparison, the concentrations of the PGD2 metabolites were several hundred fold lower than those of the pro-inflammatory mediators. Interestingly, while 4F did not significantly increase the level of any individual pro-resolving LOX mediator, the total level of these signals did increase with marginal significance ($p < 0.1$).

We also investigated the effects of oral D-4F on plasma lipids in CCHF-fed COX2 MKO mice. We first determined the effect of 4F both on total cholesterol (TC) and on PON1 activity as a measure of HDL function (**Figure 4E**).(102) Interestingly, 4F significantly reduced TC by approximately 50%, returning it towards the chow baseline. We previously reported that 4F can enhance the trans-intestinal efflux of cholesterol,(35) and we have recently shown that Tg6F increases fecal neutral sterol excretion into feces when fed to LDLR-/- fed a western diet.(41) While others have reported that oral D-4F does not reduce total cholesterol of mice on western diet,(103) the prior group had administered 10-fold less D-4F in drinking water; and we have subsequently demonstrated that the effects of 4F therapy are highly dose-dependent.(104) Consistent with prior reports, 4F therapy also here significantly improved PON1 activity in plasma.(102)

We next determined the effect of 4F on broad classes of lipids in MKO + CCHF mice. We made use of SCIEX's Lipidyzer lipidomic platform to determine the concentrations of 1103 lipid species from 13 lipid classes covering lyso-phosphatidylcholines (LPC), lyso-phosphatidylethanolamines (LPE), phosphatidylcholines (PC), phosphatidylethanolamines (PE), sphingomyelins (SM), cholesterol esters (CE), ceramides (CER), dihydroceramides (DCER), hexosylceramides (HCER) and lactosylceramides

(LCER), diacylglycerols (DAG), triacylglycerols (TAG), and free fatty acids (FFA). We observed significant reductions in total TAG, DAG, CE, LPE, CER, and HCER—with the greatest fold changes associating with TAG (4 fold, $p < 0.00001$)) and DAG (2 fold, $p < 0.005$) (**Supplemental Figure 11**).

Finally, we determined the effect of 4F on the levels of lipid inflammatory mediators present in plasma of COX2 MKO mice challenged with CCHF (**Supplemental Table 7**). More extensively than in intestinal tissue itself (cf. Supplemental Table 6 and Figure 5A), 4F rescued the pro-inflammatory effect of COX2 MKO on the levels of LOX inflammatory mediators. In particular, 4F significantly reduced the level of every pro-inflammatory LOX mediator that had been significantly elevated by COX2 MKO. At the same time, 4F reduced the level of most additional pro-inflammatory mediators in this class. (**Figure 4F**). In contrast to the effect of 4F in intestinal tissue, 4F also significantly suppressed most pro-inflammatory COX2 mediators including PGE2 and PGD2 and associated metabolites, again rescuing the level of every mediator that had been elevated by COX2 MKO (**Figure 4G**). Unlike the effect of 4F in tissue, however, there were no trending effects on the total level of pro-resolving LOX mediators (see Supplemental Table 7).

4F can directly clear lipid pro-inflammatory mediators from intestinal tissue and plasma.

COX2 MKO alters the inflammatory signaling phenotype of LPS-activated macrophages and CCHF-challenged mice, resulting in higher levels of cytokine and lipid pro-inflammatory mediators and lower levels of lipid resolving mediators (at least in intestinal tissue). In turn, 4F therapy blocks the development of intestinal inflammation while also largely rescuing these pro-inflammatory shifts in the levels of inflammatory mediators. These results in synergy support the hypothesis that dysregulated inflammatory signaling is a causal contributor to disease in COX2 MKO mice challenged with CCHF diet.

It remains possible nonetheless that the lipid inflammatory mediators serve more as markers of disease and less as cause. If disease itself produces the shift in lipid mediators rather than the converse, 4F could rescue the pro-inflammatory phenotype of these signals by inhibiting disease through some other mechanism. By contrast, were 4F to directly clear or inhibit these pro-inflammatory mediators, it would be more plausible that 4F inhibits disease because it clears or inhibits these mediators. It is this latter possibility that more strongly supports the above hypothesis.

Interestingly, there exists a differential effect of 4F on lipid inflammatory mediators in intestinal tissue. While 4F lowers the levels of the pro-inflammatory lipoxygenase mediators that are increased by COX2 MKO (see Figure 4D), it does not significantly reduce any of the pro-inflammatory COX mediators that are likewise elevated by COX2 MKO (**Figure 5A**). This selective reduction of lipid pro-inflammatory mediators in intestinal tissue argues against the possibility of a general cause—that these elevated mediators are all markers of disease, and that 4F lowers the levels of these mediators by inhibiting disease. Rather, the fact that 4F affects some elevated mediators but not others raises the possibility that 4F is directly rather than indirectly producing this reduction in pro-inflammatory mediators.

We previously employed Ussing chambers to study the effect of 4F on trans-intestinal cholesterol efflux (TICE) ex vivo.(35) We once again turned to this means of investigating epithelial transport in intestinal explants to ask the question whether 4F could directly clear pro-inflammatory LOX mediators from intestinal tissue. We took small intestinal explants from COX2 MKO mice that had been fed CCHF for 8.5 weeks and mounted them in Ussing chambers. While limiting our analysis to those mediators whose actual concentrations in tissue or plasma were most reduced by 4F (15HETE, 12HETE, 5HETE, 13HODE, 9HODE; see Supplemental Tables 6 and 7), we observed that mucosal side (i.e. luminal side) D-4F significantly increased the clearance into the mucosal media of all mediators except 15HETE (?)(**Figure 5B**). This ex vivo experiment establishes proof of principle that luminal 4F can directly clear lipid inflammatory mediators from intestinal tissue.

We also sought to determine whether luminal 4F could induce the trans-intestinal transport of lipid inflammatory mediators associated with lipoproteins. We previously reported that the above inflammatory mediators associate with lipoproteins including HDL.(49, 105) We have also demonstrated that 4F enhances TICE, while showing ex vivo that luminal 4F can increase the trans-intestinal efflux of lipoprotein-associated cholesterol.(35) We now asked whether luminal 4F could affect not only the trans-intestinal transport of cholesterol, but of other lipoprotein-associated lipid species as well. We thus combined deuterated forms of the 15HETE, 12HETE, and 13HODE with HDL and LDL, and we loaded this mixture into the serosal sides of Ussing chambers. We added micelles or 4F plus micelles to the mucosal media, and we determined whether any of the tagged inflammatory mediators were transported across intestinal explants into the mucosal chamber. Interestingly, we not only observed in this system the trans-intestinal efflux of cholesterol (data not shown), but we also observed the trans-intestinal transport of these tagged inflammatory mediators (**Figure 5C**, left panel). This result is striking in itself, as none of the literature on TICE reports about the possibility of trans-intestinal transport from the circulation into the intestinal lumen of any other lipid species beyond cholesterol. It thus appears as if there may exist trans-intestinal lipid transport (TILT) of a broader range of lipid classes. Just as noteworthy, mucosal-side 4F significantly increased TILT of 15HETE-d and 12HETE-d (**Figure 5C**, right panel). As before, this ex vivo experiment establishes proof of principle that luminal 4F can directly enhance the trans-intestinal lipid transport, and thereby possible clearance, of lipoprotein-associated inflammatory mediators.

4F treatment inhibits development of colitis in the piroxicam-accelerated IL10$^{-/-}$ model

We have demonstrated that the apoA-I mimetics 4F and Tg6F protect against intestinal inflammation in the COX2 and cholate model of IBD (see Figure 3). While we have argued in favor of a

protective mechanism that involves the rescue of dysregulated levels of inflammatory mediators, we nonetheless sought to demonstrate that the protective effects of these peptides were not model specific.

We have already pointed out how dietary cholate is required for the initiation of inflammation in the COX2 model (see Figure 1). We have also previously reported that 4F binds to cholesterol with high affinity, with a K_D in the low nanomolar range (approximately 11 nM).(101) We thus first considered the possibility that 4F might be protective merely by binding and thereby somehow inactivating the dietary cholate. In order to investigate this possibility, we determined the binding affinity between D-4F and cholate. As positive control, we first determined the binding affinity between 4F and 15HETE. Consistent with our prior report,(101) the binding affinity here was high, with K_D equal to approximately 30 nM. By contrast, the binding affinity between 4F and cholate is approximately 10,000 fold weaker, with K_D in the high micromolar range (**Supplemental Figure 12**). Moreover, even if 4F could bind and thereby somehow inactivate cholate, the molar ratios between 4F and cholate do not favor this possible protective mechanism. We administered 500 ug/ml of 4F to the mice. At a molecular weight of approximately 2400 for 4F, and assuming a daily consumption of 2.5 ml water, this amounts to approximately 0.5 micromoles 4F/day. By contrast, the mice were fed 0.5% (w/w) cholate in their diet. At a molecular weight of approximately 408 for cholate, and assuming a daily consumption of 4 g of diet, this amounts to approximately 50 micromoles cholate/day—a 100-fold excess.

We nonetheless assessed the efficacy of 4F therapy in a second mouse model of IBD, the piroxicam accelerated (PAC) $IL10^{-/-}$ model of IBD.(39, 106) IL10 is an immunoregulatory cytokine with anti-inflammatory properties that also plays a role in intestinal homeostasis by maintaining tolerance against bacterial antigens and molecular patterns.(107) Mice deficient of IL10 develop spontaneous colitis, but the incidence of colitis is low, limiting the use of $IL10^{-/-}$ mice alone as an experimental model of IBD. Piroxicam (PX) is an NSAID that inhibits both COX1 and COX2, thereby reducing the level of PGE2

in the colons of PX-treated mice.(106) PX also exhibits off-target cellular toxicity, directly damaging enterocytes and inducing apoptosis in epithelial cells of $IL10^{-/-}$ mice.(108) $IL10^{-/-}$ mice that are fed 200 ppm (200 mg/kg) PX in chow for 9 days develop colitis that is characterized by pronounced hyperplasia and focal transmural inflammation reminiscent of human CD.(39) In the PAC $IL10^{-/-}$ model, disease is usually assessed at day 14 (5 days post-PX) by determining colon length, severity of colitis, and histopathological score.(39)

We treated PAC $IL10^{-/-}$ mice with oral D-4F and determined efficacy at day 14 (for experimental protocol, **Figure 6A**). As we had observed in the COX2 MKO and cholate model, 4F therapy significantly inhibited disease. PX significantly decreased colon length by approximately 25%, while 4F therapy largely rescued this effect, limiting this reduction to approximately 6% while significantly increasing colon length from PX baseline by approximately 21% (**Figure 6B,** left panel). We assessed colitis severity on a 12 point scale by assessing the thickening of the mucosa, vascularity, granularity, and feces consistency.(39) As with colon length, 4F therapy significantly improved colitis disease score relative to PX baseline (**Figure 6B**, right panel). Finally, we scored histological sections from a central 3 cm segment of the colons of the mice by assessing the degree of lesions, hyperplasia, ulceration, and % area involved (0-3 for each, 12 points maximum). 4F therapy again inhibited disease and significantly improved histological score from PX baseline (**Figure 6C**).

We earlier detailed the pathogenic mechanism by which dietary cholate initiates disease in COX2 KO mice (see Figure 1). Overall, we have suggested the picture of a multi-hit model in which cholate alters barrier function and increases translocation of PAMP, while loss of COX2 results in loss of tolerance by altering the levels and balance of inflammatory mediators. The PAC $IL10^{-/-}$ model itself depends on a multi-hit mechanism, and disease in this model as in our COX2 model depends upon the presence of gut microbiota to initiate disease.(39) Given the off-target epithelial toxicity of PX, as well as the role of PGE2 in maintaining intestinal epithelial homeostasis, it has been conjectured that PX

accelerates disease by impairing barrier function, in a manner comparable to what we observed for cholate.(108) However, there have been no reports on the direct effect of PX on barrier permeability itself in IL10$^{-/-}$ mice. We thus assessed the effect of PX on the urinary excretion of sucralose in Il10$^{-/-}$ across 9 days of PX challenge. Interestingly, we observed a biphasic response, with an early significant increase in permeability (day 0-3), followed by a plateau (day 3-7), followed by a late significant increase in permeability (day 7-9) (**Figure 6D, left panel**). It is probable that the early increase is the result of PX itself, while the later increase results from disease that is increasingly developed around day 7-9. We also observed an influx of endotoxin into portal vein serum at day 9 (**Figure 6D, right panel**).

The symmetries between the two models of IBD led us to investigate the protective mechanism of 4F therapy in the PAC IL10$^{-/-}$ model by first examining the effect of 4F co-treatment on the LPS induction of inflammatory mediators in IL10$^{-/-}$ peritoneal macrophages treated with PX. We had previously observed that LPS increased the levels of COX-dependent AA metabolites including PGE2 and PGD2 across 24 hours, while 4F co-treatment significantly inhibited these inductive effects (see Figure 4B). In this study, we monitored the levels of COX inflammatory mediators as markers of LPS induction. We again observed that 4F co-treatment significantly reduced the levels of these LPS-induced inflammatory mediators (**Figure 6E**).

We next determined the levels of lipid inflammatory mediators in colon tissue from PAC IL10$^{-/-}$ mice treated with 4F. As in the ileo-ceco-colic junctions of COX2 MKO mice challenged with CCHF, PX caused a significant increases in multiple pro-inflammatory mediators in the colons of IL10$^{-/-}$mice (**Supplemental Table 8**). These ranged from LOX products 12HETE, 15HETE, 5HETE, LTB4, LTE4; as well as COX products TXB2, PGE2, and PGD2. Also as before, 4F therapy rescued these increases with respect to most pro-inflammatory LOX products (**Figure 6F**), without inhibiting the significant increases in COX products (**Figure 6G**). While we here observed significant increases in pro-inflammatory COX products including PGE2 and PGD2 as the result of PX, it is worth noting that we determined the levels of these

lipid inflammatory mediators on day 14, 5 days post-PX. Interestingly, while 4F therapy did not significantly alter the levels of pro-resolving LOX products, we did observe that the ratio of RvD1 to LTB4 and 6trans12epiLTB4 was significantly reduced in the tissue of IL10+PX mice compared to IL10-/- mice alone ($p < 0.001$), with 4F therapy improving this ratio with marginal significance ($p<0.1$) (**Figure 6H**). We had previously observed a comparable shift in the balance of inflammation resolving and pro-inflammatory mediators in the ileo-ceco-colic junctions of MKO mice challenged with CCHF, suggesting that this sort of shift might be characteristic of IBD more generally.

Finally, we determined the effect of 4F on the levels of lipid inflammatory mediators in the plasmas of $IL10^{-/-}$+PX mice (**Table 4**). 4F therapy significantly reduced the levels of the pro-inflammatory LOX mediators LTC4, LTE4, 13HODE, 9HODE, 12HETE; as well as the pro-inflammatory COX mediators PGF2α, and 13,14-dihydro-PGF2α. 4F therapy also significantly reduced the PGE2 metabolites 15ketePGE2, while all other PGE2 and PGD2 associated signals trended lower. 4F therapy also significantly reduced the DHA pathway markers 17HDHA and 14HDHA. Except for the effects here upon 17HDHA and 14HDHA, these results are consistent with the effects of 4F on plasma that we had observed in COX2 MKO mice fed CCHF (see Supplementary Table 7). This data is particularly striking in that the levels of every detectable inflammatory mediator that was analyzed were either significantly lower or trending lower compared to the no-4F control. In this respect, the effects of 4F on plasma inflammatory mediators differ from the effects on intestine-associated mediators. The broad nature of the effects on plasma suggests a broad clearance mechanism capable of affecting all plasma-associated mediators together. We have suggested one such possible mechanism, in the form of TILT (see Figure 5C). By contrast, 4F exhibits differential effects on lipid inflammatory mediators in intestinal tissue, preferentially lowering LOX rather than COX metabolites.

Discussion

Dietary cholate alters intestinal barrier function in C57BL/6J mice by increasing intestinal barrier permeability and inducing the translocation of PAMP, but WT mice are nonetheless able to maintain tolerance when challenged with CCHF diet. By contrast, COX2 TKO and MKO mice develop severe inflammation in their ileo-ceco-colic junctions. The intestinal inflammation is both gut microbiota and MyD88-dependent, indicating that PAMP/TLR signaling is an essential component of the overall pathogenic mechanism. COX2 thus appears to help maintain tolerance by somehow limiting or damping the inflammatory consequences of these innate immune pathways. Consistent with this hypothesis, we observed that loss of COX2 dysregulates the levels of cytokine pro-inflammatory mediators in LPS-activated macrophages. COX2 MKO in CCHF-challenged mice also increases the levels of lipid pro-inflammatory mediators in intestinal tissue and plasma, while reducing the levels of pro-resolving mediators in tissue.

Of note, pro-inflammatory COX prostanoids were elevated in disease, a result on its face in tension with the partial knock-out of COX2 in this model. However, while myeloid COX2 had been ablated, COX2 remained in other cell types including endothelial cells. We had observed that COX2 MKO macrophages expressed elevated levels of IL1beta. In turn, IL1beta has been shown to induce both COX2 and COX2-prostanoid production in endothelial cells. Our results are consistent with this biology.

ApoAI mimetic therapy inhibits disease in the COX2 MKO and CCHF model. Moreover, 4F rescues the inflammatory mediator phenotypes of macrophages, intestinal tissue, and plasma that had been altered by COX2 MKO. 4F therapy directly inhibits pro-inflammatory cytokine expression in LPS-activated macrophages, most likely by interfering with LPS activation itself. 4F can also directly clear lipid pro-inflammatory mediators associated with both intestinal tissue and lipoproteins. These observations taken together strengthen the hypotheses that dysregulated levels of inflammatory mediators are pathogenic for disease in the COX2 MKO model, while rescue of these signal levels is

protective. There exists, in other words, a synergy between the investigations into pathogenic and protective mechanisms in this model.

In two separate mouse models of IBD, we have highlighted the possible role of changes in barrier permeability in the early pathogenesis of disease. Increased intestinal permeability has been proposed as a primary etiologic factor in IBD.(56) However, the inflammatory process itself can increase intestinal permeability.(109) There thus remains debate whether changes in barrier permeability are early events in pathogenesis or mere secondary phenomena.(110, 111) We demonstrate here how CCHF increases barrier permeability and induces translocation of PAMPs prior to the development of inflammation in the COX2 models. We also demonstrate how disease is dependent in this model on both gut microbiota and MyD88 signaling (see Figure 1). These results together suggest a pathogenic mechanism in which CCHF alters permeability and increases translocation of PAMPs that in turn signal through TLR/MyD88 to initiate the disease process. Interestingly, piroxicam in the PAC IL10-/- model produces an early (0d-2d) increase intestinal permeability, a change that also precedes the first appearance of disease in this model (see Figure 6D).(39) In parallel, these investigations into barrier permeability have also characterized a role for environmental triggers including NSAIDs and dietary factors as early modifiers of intestinal barrier permeability.

We investigated the effects of LPS and COX2 MKO in primary macrophage cultures, but there exist additional PAMPs that also signal through TLR/MyD88. These include lipoteichoic acid (LTA), a component of the cell wall of gram+ bacteria, as well as peptidoglycan (PG).(72) Nothing in the present study excludes additional PAMPs from playing a role in initiating disease in the COX2 models. However, COX2 MKO did increase the expression of NFκB target genes in macrophages upon LPS activation (see Figure 1E). The cyclopentenone prostaglandins (cyPGs) PGJ2 and 15d-PGJ2 have been identified as negative regulators of NFκB.(112, 113) We had observed that the levels of PGJ2 and 15d-PGJ2 increased from 4 Hr in FLOX BMDM activated with LPS, while COX2 MKO largely abolished these mediators (see

Supplemental Figure 5). It is thus possible that a loss of negative feedback control of NFκB partially explains the pro-inflammatory effects of COX2 MKO in macrophages. Because both LTA and PG also partially signal through NFκB,(72) we would expect COX2 MKO to affect the inflammatory response to these PAMPs comparably to manner in which it affects the response to LPS. As PAMP signal through TLR/MyD88/NFκB in additional cell types besides macrophages, we might also expect loss of COX2 in these other cell types to enhance NFκB target gene expression upon PAMP stimulation—perhaps partially explaining why COX2 TKO has accelerated disease compared to COX2 MKO upon CCHF challenge.

Upon CCHF challenge COX2 MKO increased the intestinal level of total pro-inflammatory LOX mediators, while also increasing the levels 15HETE, 12HETE, and 13HODE (see Figure 2B). Interestingly, the COX inhibitor PX also increased the level of total pro-inflammatory LOX mediators as well 15HETE, 12HETE, 5HETE, 5oxoETE, and LTs B4 and C4 in the colons of $IL10^{-/-}$ mice (see Figure 6F). The total level of pro-inflammatory COX mediators also increased in the diseased intestine of both models, as did the levels of PGE2 and total PGE2/D2 associated mediators; while PGE3 and 6ketoPGF1alpha on the one hand, and 11HETE and TXB2 on the other, were elevated in the COX2 MKO and PAC $IL10^{-/-}$ models respectively. This overall pro-inflammatory eicosanoid signature is surprisingly similar to that identified in the colons of human UC patients, for which a recent study reported higher levels of 15HETE, 12HETE, 5 HETE, 11 HETE, PGE2, and TXB2.(114) This signature—with elevations of both total pro-inflammatory LOX and COX mediators as well as 15HETE, 12HETE, and PGE2—may thus constitute a more general signature for IBD.

We also observed that disease associated with an altered balance of pro-resolving mediators to pro-inflammatory leukotrienes in both models, while further associating with lower levels of both LXA4 and total 5LOX-associated resolving mediators in the ileo-ceco-colic junctions of COX2 MKO mice on CCHF diet (see Figures 2E and 6H). Lipoxins including LXA4 can trigger a number of resolving and anti-

inflammatory functions blocking neutrophil migration, stimulating efferocytosis, and down regulating both CCL8 by epithelial cells and superoxide production by neutrophils.(113) RvD1 has also been shown to downregulate adhesion receptors, inhibit ROS and pro-inflammatory cytokine, block PMN migration, while also stimulating efferocytosis.(115) By contrast, LTB4 is a potent pro-inflammatory mediator involved in neutrophil recruitment.(116) Altered balance of 5LOX-associated resolving mediators to LTB4 has been associated with plaque instability in atherosclerosis(37) and could possibility explain the build-up of neutrophils in the COX2 MKO model (see Figure 3E). Loss of 5LOX-associated resolving mediators has been associated with atherosclerotic progression(117) and could account for the apparent failure of macrophages to clear neutrophils in the COX2 model (see Figures 3D and 3E). Loss of COX2 activity in macrophages leads to a reduction in intracellular LXA4 production while increasing 5LOX-dependent LTB4 under some activation conditions,(80) offering a possible link between COX2 MKO and COX inhibition and the altered ratios of resolving mediators to LTB4.

The increases in pro-inflammatory mediators in intestinal tissue were mirrored by comparable increases in plasma levels of these same mediators in the COX2 MKO model. Total pro-inflammatory LOX mediators together with 12 and 5HETE, total pro-inflammatory COX mediators together with PGF2alpha and TXB2, and PGE2 were all elevated in plasma compared to FLOX+CCHF. These plasma-associated inflammatory mediators may thus be of interest as possible IBD biomarkers. It has not been established whether plasma-associated inflammatory mediators can also feed back into intestinal tissue and play a role driving disease.

We have here reported that apoA-I mimetic therapy strongly inhibits disease in two independent mouse models with characteristics reminiscent of human CD. 4F was previously reported to ameliorate the phenotypic and histopathological features of DSS-induced UC,(33) while the bihelical apoA-I mimetic 5A has also been shown to inhibit disease progression in this model.(118) Given the cost associated with administering the synthetic peptide 4F at its optimal effective dose range for

inflammatory disorders including the IBD models here (> 40 mg/kg),(23, 104) transgenic tomato plants expressing the apoA-I mimetic 6F were constructed by our laboratory.(119) Cost of production of Tg6F is substantially lower than for 4F, indicating that Tg6F may be a more viable apoA-I mimetic translational option against IBD.

Consistent with prior reports,(120, 121) we show here that for both COX2 MKO and IL10$^{-/-}$ macrophages, 4F inhibits LPS-dependent induction and activation of NFκB target genes including TNFα, IL1β, and COX2, as assessed by either RNA expression or lipid mediator levels (see Figures 4A-B and 6E). Of greater interest, we also show that 4F therapy rescues the levels of pro-inflammatory LOX mediators in the intestinal tissue in both the COX2 MKO and PAC IL10 models, without comparably reducing the elevated levels of pro-inflammatory COX mediators (see Figure 4D together with Supplementary Table 6, as well as Figures 6F-G). These differential effects, combined with our observation that 4F can directly clear pro-inflammatory LOX mediators from intestinal tissue, suggests that the elevated levels of these mediators in intestinal tissue may be causative for disease in these models. Of interest, elevated levels of 12HETE have been associated with human IBD.(114). 12HETE has been shown to enhance vascular permeability and neutrophil recruitment,(122) while 12HETE also serves as a pathway marker for the production of hepoxilin A3, a pro-inflammatory lipid mediator also implicated in neutrophil recruitment by the intestinal mucosa.(123, 124) 4F rescues the elevated levels of 12HETE in the COX2 MKO model, suggesting that 12HETE may play an important role in the pathogenesis of disease in this model.

4F therapy dramatically reduced the levels of lipid inflammatory mediators in both models of IBD (see Supplementary Table 7 as well as Table 4). Of great interest, we demonstrate ex vivo that lipid inflammatory mediators can be transported across intestinal explants from lipoproteins into mucosal media, indicating that trans-intestinal lipid transport (TILT) may involve lipid species over and above cholesterol. We moreover demonstrate that mucosal-side 4F can enhance the trans-intestinal transport of these same mediators (see Figure 5C). It is possible that TILT is responsible for the broad reduction of

lipid inflammatory mediators observed in plasma effected by 4F. 4F also lowered total cholesterol in the plasma of COX2 MKO mice fed CCHF (see Figure 4E). We have previously demonstrated that 4F can enhance the trans-intestinal transport of cholesterol. It may be the case that 4F mediates the reduction of plasma cholesterol and plasma lipid inflammatory mediators through the same trans-intestinal mechanism.

The current study contains several limitations. First, while we demonstrate that intestinal inflammation in the COX2 TKO model depends upon MyD88 signaling, we do not show that MyD88 signaling in the macrophage compartment is necessary for disease in COX2 MKO mice. Nonetheless, we argue to the in vivo significance of our in vitro macrophage observations by way of our more general result regarding MyD88. Second, while we demonstrate that COX2 MKO alters the levels of inflammatory mediators in CCHF-fed mice, we do not show how loss of COX2 itself could produce these alterations. It is possible that loss of COX2 is directly responsible for at least some of these changes—we have cited several studies linking loss of COX2 activity with both increased pro-inflammatory LOX mediators and reduced pro-resolving LOX mediators in vivo. It is nonetheless consistent with our observations here that the changes in lipid mediator levels are not directly mediated by loss of COX2 in the myeloid compartment. Third, while we partially have made use of 4F as an investigative tool to argue for the causal significance of various changes in lipid mediator profile, more work is required to fully establish a causative role for either elevated pro-inflammatory LOX signals. Related, while loss of resolving signals can rationalize the build up of neutrophils in the ceca of COX2 MKO mice, we have not here demonstrated that resolving signals including LXA4 and RvD1 are protective in these models. Finally, we do not resolve the question whether the observed changes in plasma inflammatory mediators are mere markers of disease, or whether elevated levels of plasma pro-inflammatory mediators can feed back into disease and play a driving role.

Nonetheless, this present study is one of the few to approach mouse models of IBD through a broad lipidomic approach focused on inflammatory mediators. We moreover highlight the importance of alterations in barrier permeability for IBD, while detailing some aspects of the possible protective role of COX2 in this disease. Finally, we offer further evidence of the possible translational value of apoA-I mimetics as therapy for IBD, while adding importantly to our understanding of the possible protective mechanisms of these important anti-inflammatory agents.

Supplemental Materials and Methods

MRM LC-MS/MS Pro-Inflammatory and Inflammation Resolving Lipid Signaling Panel

Overview

Several groups have recently developed ESI LC-MS/MS methods for collectively analyzing various AA, DHA, and EPA-derived signaling lipids (AA and EPA-derived eicosanoids as well as DHA-derived docosanoids), which cover a range of pro-inflammatory, anti-inflammatory, and inflammation resolving bioactive lipids.(117, 125-129) Each of these groups uses multiple reaction monitoring (MRM) in negative ion mode coupled together with liquid chromatography as the basis for identification and quantification. Chromatography is performed on C18 column variants, with gradient elutions consisting of water and either methanol or acetonitrile, all together with formic or acetic acid. Some number of deuterated internal standards are used to compensate for variability in sample preparation, injection volume, and ionization efficiency. Most all sample preparation methods involve some form of solid-phase extraction (SPE).

We settled upon the analytes of our lipid panel by cross-reference to the above cited methods, together with a more general search of the literature regarding eicosanoid, anti-inflammatory lipid, and specialized pro-resolving lipid mediator (SPM) biology.(83, 113, 115, 130) At base, we sought to analyze the bioactive lipids detailed in the body of this paper (see Table 1). However, several of these lipids are unstable or with short half-lives in either tissue or plasma. For example, PGI2 is bioactive but unstable and rapidly hydrolyzes to 6ketoPGF1α. Likewise, PGE2 is converted to both 15ketoPGE2 and 13,14-dihydro-15keto-PGE2 in plasma. In these cases, we substituted or supplemented our analysis of a particular bioactive lipid with analysis of its degradation products (see Supplemental Table 1 for a complete list). We also included various pathway markers in our analysis, for example: 14-HDHA and

17-HDHA as markers for the DHA → MaR1, and RvD-14 and PD1/PDx pathways, respectively(131); and 11 HETE as a monohydroxylated marker of COX activity.(80)

The method covers 39 distinct bioactive lipids, degradation products, and pathway markers. We divided the bioactive lipids into pro-inflammatory, anti-inflammatory, and pro-resolving functional categories by literature search (see Supplemental Table 1), while further indexing these as being COX or LOX products and as being derived from AA, DHA, or EPA (see Supplemental Table 1). We assigned each analyte to one of 19 distinct structurally identical or class-specific deuterated internal standards (see Supplemental Table 2). In the cases in which a particular analyte lacked a structurally identical internal standard, we assigned an internal standard that both shared the same basic structure and co-eluted within 0.5 min of the analyte in question. For example, we assigned PGE2-d4 both to PGE2 and to PGF2α, which elutes within 0.3 min of PGE2-d4 and differs from PGE2 only by substitution of a ketone for a hydroxyl group within the cyclopentane ring (see Supplemental Table 2).

We built the method with two distinct MRM transitions for each analyte and internal standard, while MS/MS settings were optimized for declustering potential (DP), entrance potential (EP), collision energy (CE), and cell exit potential (CXP) by manual tuning (see below, and Supplemental Table 2). In the case of isobaric parent ions, distinct compounds were resolved by the use of either a unique MS2 fragment ion or by chromatographic separation. For example, the LOX products 15HETE and 12HETE both have a parent mass to charge (m/z) of 319.1, but these two species can be resolved through the use of the unique fragments of 219.1 for 15HETE and 184 for 12HETE. Chromatography on a Phenomenex Kinetex C18 column using a water and acetonitrile gradient gave sharp peak resolution (see Supplemental Figure 6). In order to ensure adequate dwell time for each MRM channel while also ensuring adequate data coverage of each chromatographic peak, we made use of scheduled MRM to activate only the requisite MRM channels within a 60 second window around each peak. For each

analyte, we determined the LLOD, LLOQ, and ULOQ, while also determining the linearity of the associated standard curve (see Supplemental Table 3).

We prepared tissue, plasma, and lysate samples first by combination with methanol and the anti-oxidant BHT, and then by SPE using Oasis HLB cartridges. Post SPE, samples were reconstituted in methanol for LCMS analysis. We validated our sample preparation methods for each matrix by determining precision for each biologically available analyte across 5 identical extractions of a particular sample (see Supplemental Table 4), while also determining the precision and extraction efficiency of each internal standard within each matrix (see Supplemental Table 5). In accord with FDA guidelines, we set a CV of 15% as our cutoff for precision, while also ascertaining that recovery was consistent, precise, and reproducible.(132)

Chemicals

18-hydroxyeicosapentaenoic acid (18-HEPE); 6-keto-prostaglandin F1α (6kPGF$_{1\alpha}$); resolvin E1 (RvE1); resolvin E1 deuterated (RvE1-d4); thromboxane B3 (TXB$_3$); thromboxane B2 (TXB$_2$); thromboxane B2 deuterated (TXB$_2$-d4); prostaglandin E3 (PGE$_3$); 20-hydroxy-leukotriene B4 (LTB4); prostaglandin F2α (PGF$_{2\alpha}$); prostaglandin E2 (PGE$_2$); prostaglandin E2 deuterated (PGE$_2$-d4); resolvin D3 (RvD3); resolvin D3 deuterated (RvD3-d5); lipoxin B4 (LXB4), prostaglandin D2 (PGD$_2$); prostaglandin D2 deuterated (PGD$_2$-d4); resolvin D2 (RVD2); resolvin D2 deuterated (RvD2-d5); leukotriene C4 (LTC4); leukotriene C4 deuterated (LTC4-d5); 15-keto-prostaglandin E2 (15keto-PGE$_2$); leukotriene E4 (LTE4); lipoxin A4 (LxA4); lipoxin A4 deuterated (LxA4-d5); 15-epi-lipoxin A4 (15epi-LXA4); resolvin D1 (RvD1); resolvin D1 deuterated (RvD1-d5); 13, 14-dihydro-15-keto prostaglandin F2α (13,14-dihydro-15keto-PGF$_{2\alpha}$); 13, 14-dihydro-15-keto prostaglandin F2α deuterated (13,14-dihydro-15-keto-PGF$_{2\alpha}$-d4); 13, 14-dihydro-15-keto prostaglandin E2 (13,14-dihydro-15keto-PGE$_2$); 13, 14-dihydro-15-keto prostaglandin E2 deuterated (13,14-dihydro-15-keto-PGE$_2$-d4); resolvin D4 (RvD4); 13, 14-dihydro-15-keto prostaglandin D2 (13,14-

dihydro-15keto-PGD_2); prostaglandin J2 (PGJ_2); Δ_{12}-Prostaglandin J2 (Δ_{12}-PGJ_2); 7(S)-maresin (MaR1); 7(S)-maresin deuterated (MaR1-d5); 10(S),17(S)-protectin (PDx); 6-trans-12-epi leukotriene B4 (6trans-12epi-LTB4); resolvin D5 (RvD5); leukotriene B4 (LTB4); leukotriene B4 deuterated (LTB4-d4); 15-deoxy-$\Delta_{12,14}$-Prostaglandin J2 (15d-PGJ_2); 15-deoxy-$\Delta_{12,14}$-Prostaglandin J2 deuterated (15d-PGJ_2-d4); 13-hydroxyoctadecadienoic acid (13-HODE), 9-HODE, 13-HODE-d4; 15-hydroxyeicosatetraenoic acid (15-HETE) and 12-HETE, 5-HETE, 15-HETE-d8, 12-HETE-d8, 5-HETE-d8, and 11-HETE; 17S-hydroxydocosahexaenoic acid (17S-HDHA) and 14S-HDHA; 5-oxoeicosatetraenoic acid (5-oxoETE); and 5-oxoeicosatetraenoic acid deuterated (5-oxoETE-d7) were purchased from Cayman Chemicals (Ann Arbor, MI, USA).

Liquid Chromatography

Chromatography was performed on an Agilent 1290 UHPLC system using a Phenomenex Kinetex C18 column (2.6 uM particle size, 2.1 mm ID x 150 mm) and gradient elution. Solvent A was 75/25/0.1 (H2O/acetonitrile/formic acid) and Solvent B was 100/0.1 (acetonitrile/formic acid), and the gradient was as follows: 0-8.5 min, 0-85%B; 8.5-9.5 min, 85-100%B; 9.5-10.5 min, 100%B; 10.5-12 min, 100-0% B; 12-14 min, 0%B; with an additional 1 min equilibration at the starting conditions prior to each run. The column oven was set to 40 deg C, while the flow rate was 350 ul/min. 5 ul of sample was injected for each run.

MS/MS

Mass spectrographic analysis was performed on a SCIEX 5500 QTrap run in negative ion mode and controlled by Analyst 1.6.2 software. Two separate MRM transitions were determined for each compound, and DP, EP, CE, and CXP for each compound were all manually optimized by tuning on direct infusions of approximately 50 ng compound/ml 50%B (see Supplemental Table 2 for final settings). The

source settings were optimized by tuning on a mix of analytes while also flowing in 50%B at 350 ul/min, with temperature set at x, GS1 at x, GS2 at x, CAD gas a medium and CUR gas at 25. Scheduled MRM was employed, with the window for each MRM channel set at 60 seconds around the retention times (RT) of each compound (see Supplemental Table 2 for RT). LLOD, LLOQ, ULOQ, and linearity of response for each analyte were determined (see Supplemental Table 3).

Sample preparation

Lipids were extracted from 50 mg of intestinal tissue by first adding 500 ul MS-grade H20 together with 50 ul of 20 ng/ml internal standard mix as well as a final concentration of 20 uM BHT. The tissue was homogenized, 1 ml of methanol was added, the tissue was vortexed, and the sample was spun down at 15000 RPM for 10 min at 4 deg. The supernatant was removed and brought up to 10 ml with pH 3-4 HCl-acidified H2O. SPE was performed on an Oasis HLB 3 cc column in accord with the manufacturer's protocol. The sample was eluted with 2 ml methanol, dried down under argon, and brought up again in 100 ul methanol for LCMS analysis. The final concentrations of internal standards in the samples were 10 ng/ml.

Lipids were extracted from 100 ul of plasma by first adding 50 ul of 20 ng/ml internal standard mix together with 150 ul of methanol. BHT was added to a final concentration of 20 uM. The sample was vortexed and spun down at 15000 RPM for 10 min at 4 deg. The supernatant was combined with 1.8 ml of HCl-acidified H2O (pH = 3-4); SPE was performed on 3 cc Oasis HLB cartridges; and samples were eluted with methanol, dried down under argon, and brought up in 100 ul of methanol for LCMS analysis.

Cells grown in culture were first washed of media 2x with cold PBS. The cells were then scraped and collected in 50 mM pH 7.4 phosphate buffer and kept at -80 for subsequent lipid analysis. For 300 ul of lysate, sufficient for macrophages grown in a well of a 6 well plate, 50 ul of 20 ng/ml internal

standard together with 150 ul of methanol was added as well as 20 uM BHT (final concentration). The samples were otherwise extracted as plasma.

1 ml of cell culture media was combined with 50 ul of internal standard mix together with 450 ul of methanol and 20 uM BHT (final concentration). The samples were vortexed, spun down, and supernatant was brought up to 5 ml with H2O. The samples were acidified to pH 3-4 using formic acid and otherwise extracted as above.

Each sample preparation method was independently validated by determining precision and recovery, as described above (see Supplemental Tables 4 and 5 for partial data).

Data analysis

Data analysis was performed using MultiQuant software, with the concentration of each analyte being determined relative to its internal standard and against standard curves. Final data was normalized to either tissue weight, plasma volume, media volume, or for lysate protein concentration as determined by Bradford from a small aliquot of each lysate. For comparison between groups (see Figures 2, 4, and 6), significance was determined by Student's unpaired T-test, with significance set at $p < 0.05$.

1. Sartor, R. B. 2006. Mechanisms of disease: pathogenesis of Crohn's disease and ulcerative colitis. *Nat Clin Pract Gastroenterol Hepatol* **3**: 390-407.

2. Xavier, R. J., and D. K. Podolsky. 2007. Unravelling the pathogenesis of inflammatory bowel disease. *Nature* **448**: 427-434.

3. Liu, J. Z., S. van Sommeren, H. Huang, S. C. Ng, R. Alberts, A. Takahashi, S. Ripke, J. C. Lee, L. Jostins, T. Shah, S. Abedian, J. H. Cheon, J. Cho, N. E. Daryani, L. Franke, Y. Fuyuno, A. Hart, R. C. Juyal, G. Juyal, W. H. Kim, A. P. Morris, H. Poustchi, W. G. Newman, V. Midha, T. R. Orchard, H. Vahedi, A. Sood, J. J. Y. Sung, R. Malekzadeh, H.-J. Westra, K. Yamazaki, S.-K. Yang, C. International Multiple Sclerosis Genetics, I. B. D. G. C. International, J. C. Barrett, A. Franke, B. Z. Alizadeh, M. Parkes, T. B K, M. J. Daly, M. Kubo, C. A. Anderson, and R. K. Weersma. 2015. Association analyses identify 38 susceptibility loci for inflammatory bowel disease and highlight shared genetic risk across populations. *Nature Genetics* **47**: 979.

4. Lee, J. C., D. Biasci, R. Roberts, R. B. Gearry, J. C. Mansfield, T. Ahmad, N. J. Prescott, J. Satsangi, D. C. Wilson, L. Jostins, C. A. Anderson, U. I. G. Consortium, J. A. Traherne, P. A. Lyons, M. Parkes, and K. G. C. Smith. 2017. Genome-wide association study identifies distinct genetic contributions to prognosis and susceptibility in Crohn's disease. *Nature Genetics* **49**: 262.

5. Ananthakrishnan, A. N., C. N. Bernstein, D. Iliopoulos, A. Macpherson, M. F. Neurath, R. A. R. Ali, S. R. Vavricka, and C. Fiocchi. 2017. Environmental triggers in IBD: a review of progress and evidence. *Nature reviews. Gastroenterology & hepatology*.

6. Lewis, R. T., and D. J. Maron. 2010. Efficacy and Complications of Surgery for Crohn's Disease. *Gastroenterology & Hepatology* **6**: 587-596.

7. Peyrin-Biroulet, L. 2010. Anti-TNF therapy in inflammatory bowel diseases: a huge review. *Minerva gastroenterologica e dietologica* **56**: 233-243.

8. Kopylov, U., and E. Seidman. 2016. Predicting durable response or resistance to antitumor necrosis factor therapy in inflammatory bowel disease. *Therapeutic Advances in Gastroenterology* **9**: 513-526.

9. Maxwell, J. R., and J. L. Viney. 2009. Overview of mouse models of inflammatory bowel disease and their use in drug discovery. *Current protocols in pharmacology* **Chapter 5**: Unit5.57.

10. Mizoguchi, A. 2012. Animal Models of Inflammatory Bowel Disease. *In* Progress in Molecular Biology and Translational Science. P. M. Conn, editor. Academic Press. 263-320.

11. Elson, C. O., Y. Cong, V. J. McCracken, R. A. Dimmitt, R. G. Lorenz, and C. T. Weaver. 2005. Experimental models of inflammatory bowel disease reveal innate, adaptive, and regulatory mechanisms of host dialogue with the microbiota. *Immunol Rev* **206**: 260-276.

12. Wirtz, S., and M. F. Neurath. 2007. Mouse models of inflammatory bowel disease. *Advanced drug delivery reviews* **59**: 1073-1083.

13. Gaya, D. R., R. K. Russell, E. R. Nimmo, and J. Satsangi. 2006. New genes in inflammatory bowel disease: lessons for complex diseases? *Lancet (London, England)* **367**: 1271-1284.

14. Dommels, Y. E., C. A. Butts, S. Zhu, M. Davy, S. Martell, D. Hedderley, M. P. Barnett, W. C. McNabb, and N. C. Roy. 2007. Characterization of intestinal inflammation and identification of related gene expression changes in mdr1a(−/−) mice. *Genes & Nutrition* **2**: 209-223.

15. Willis, C. R., A. Seamons, J. Maxwell, P. M. Treuting, L. Nelson, G. Chen, S. Phelps, C. L. Smith, T. Brabb, B. M. Iritani, and L. Maggio-Price. 2012. Interleukin-7 receptor blockade suppresses adaptive and innate inflammatory responses in experimental colitis. *Journal of inflammation (London, England)* **9**: 39.

16. Herschman, H. R. 1996. Prostaglandin synthase 2. *Biochim Biophys Acta* **1299**: 125-140.

17. Cox, D. G., J. B. Crusius, P. H. Peeters, H. B. Bueno-de-Mesquita, A. S. Pena, and F. Canzian. 2005. Haplotype of prostaglandin synthase 2/cyclooxygenase 2 is involved in the susceptibility to inflammatory bowel disease. *World J Gastroenterol* **11**: 6003-6008.

18. Ostergaard, M., A. Ernst, R. Labouriau, E. Dagiliene, H. B. Krarup, M. Christensen, N. Thorsgaard, B. A. Jacobsen, U. Tage-Jensen, K. Overvad, H. Autrup, and V. Andersen. 2009. Cyclooxygenase-2, multidrug resistance 1, and breast cancer resistance protein gene polymorphisms and inflammatory bowel disease in the Danish population. *Scand J Gastroenterol* **44**: 65-73.

19. Andersen, V., E. Nimmo, H. B. Krarup, H. Drummond, J. Christensen, G. T. Ho, M. Ostergaard, A. Ernst, C. Lees, B. A. Jacobsen, J. Satsangi, and U. Vogel. 2011. Cyclooxygenase-2 (COX-2) polymorphisms and risk of inflammatory bowel disease in a Scottish and Danish case-control study. *Inflamm Bowel Dis* **17**: 937-946.

20. de Vries, H. S., R. H. te Morsche, M. G. van Oijen, I. D. Nagtegaal, W. H. Peters, and D. J. de Jong. 2010. The functional -765G-->C polymorphism of the COX-2 gene may reduce the risk of developing crohn's disease. *PLoS One* **5**: e15011.

21. Lin, J. A., J. Watanabe, N. Rozengurt, A. Narasimha, M. G. Martin, J. Wang, J. Braun, R. Langenbach, and S. T. Reddy. 2007. Atherogenic diet causes lethal ileo-ceco-colitis in cyclooxygenase-2 deficient mice. *Prostaglandins Other Lipid Mediat* **84**: 98-107.

22. Watanabe, J., J. A. Lin, A. J. Narasimha, A. Shahbazian, T. O. Ishikawa, M. G. Martin, H. R. Herschman, and S. T. Reddy. 2010. Novel anti-inflammatory functions for endothelial and myeloid cyclooxygenase-2 in a new mouse model of Crohn's disease. *Am J Physiol Gastrointest Liver Physiol* **298**: G842-850.

23. Navab, M., S. T. Reddy, D. Meriwether, S. I. Fogelman, and A. M. Fogelman. 2015. ApoA-I Mimetic Peptides: A Review of the Present Status. *In* Apolipoprotein Mimetics in the Management of Human Disease. G. M. Anantharamaiah and D. Goldberg, editors. Springer International Publishing, Cham. 15-27.

24. Navab, M., G. M. Anantharamaiah, S. Hama, D. W. Garber, M. Chaddha, G. Hough, R. Lallone, and A. M. Fogelman. 2002. Oral administration of an Apo A-I mimetic Peptide synthesized from D-amino

acids dramatically reduces atherosclerosis in mice independent of plasma cholesterol. *Circulation* **105**: 290-292.

25. Navab, M., G. M. Anantharamaiah, S. Hama, G. Hough, S. T. Reddy, J. S. Frank, D. W. Garber, S. Handattu, and A. M. Fogelman. 2005. D-4F and statins synergize to render HDL antiinflammatory in mice and monkeys and cause lesion regression in old apolipoprotein E-null mice. *Arterioscler Thromb Vasc Biol* **25**: 1426-1432.

26. Wool, G. D., V. G. Cabana, J. Lukens, P. X. Shaw, C. J. Binder, J. L. Witztum, C. A. Reardon, and G. S. Getz. 2011. 4F Peptide reduces nascent atherosclerosis and induces natural antibody production in apolipoprotein E-null mice. *FASEB J* **25**: 290-300.

27. Charles-Schoeman, C., M. L. Banquerigo, S. Hama, M. Navab, G. S. Park, B. J. Van Lenten, A. C. Wagner, A. M. Fogelman, and E. Brahn. 2008. Treatment with an apolipoprotein A-1 mimetic peptide in combination with pravastatin inhibits collagen-induced arthritis. *Clin Immunol* **127**: 234-244.

28. Buga, G. M., J. S. Frank, G. A. Mottino, A. Hakhamian, A. Narasimha, A. D. Watson, B. Yekta, M. Navab, S. T. Reddy, G. M. Anantharamaiah, and A. M. Fogelman. 2008. D-4F reduces EO6 immunoreactivity, SREBP-1c mRNA levels, and renal inflammation in LDL receptor-null mice fed a Western diet. *J Lipid Res* **49**: 192-205.

29. DeLeve, L. D., X. Wang, G. C. Kanel, R. D. Atkinson, and R. S. McCuskey. 2008. Prevention of hepatic fibrosis in a murine model of metabolic syndrome with nonalcoholic steatohepatitis. *Am J Pathol* **173**: 993-1001.

30. Sharma, S., S. Umar, F. Potus, A. Iorga, G. Wong, D. Meriwether, S. Breuils-Bonnet, D. Mai, K. Navab, D. Ross, M. Navab, S. Provencher, A. M. Fogelman, S. Bonnet, S. T. Reddy, and M. Eghbali. 2014. Apolipoprotein A-I Mimetic Peptide 4F Rescues Pulmonary Hypertension by Inducing MicroRNA-193-3p. *Circulation* **130**: 776-785.

31. Chattopadhyay, A., M. Navab, G. Hough, F. Gao, D. Meriwether, V. Grijalva, J. R. Springstead, M. N. Palgnachari, R. Namiri-Kalantari, F. Su, B. J. Van Lenten, A. C. Wagner, G. M. Anantharamaiah, R. Farias-Eisner, S. T. Reddy, and A. M. Fogelman. 2013. A novel approach to oral apoA-I mimetic therapy. *J Lipid Res* **54**: 995-1010.

32. Navab, M., G. Hough, G. M. Buga, F. Su, A. C. Wagner, D. Meriwether, A. Chattopadhyay, F. Gao, V. Grijalva, J. S. Danciger, B. J. Van Lenten, E. Org, A. J. Lusis, C. Pan, G. M. Anantharamaiah, R. Farias-Eisner, S. S. Smyth, S. T. Reddy, and A. M. Fogelman. 2013. Transgenic 6F tomatoes act on the small intestine to prevent systemic inflammation and dyslipidemia caused by Western diet and intestinally derived lysophosphatidic acid. *J Lipid Res* **54**: 3403-3418.

33. Gkouskou, K. K., M. Ioannou, G. A. Pavlopoulos, K. Georgila, A. Siganou, G. Nikolaidis, D. C. Kanellis, S. Moore, K. A. Papadakis, D. Kardassis, I. Iliopoulos, F. A. McDyer, E. Drakos, and A. G. Eliopoulos. 2016. Apolipoprotein A-I inhibits experimental colitis and colitis-propelled carcinogenesis. *Oncogene* **35**: 2496-2505.

34. Li, R., K. Navab, G. Hough, N. Daher, M. Zhang, D. Mittelstein, K. Lee, P. Pakbin, A. Saffari, M. Bhetraratana, D. Sulaiman, T. Beebe, L. Wu, N. Jen, E. Wine, C.-H. Tseng, J. A. Araujo, A. Fogelman, C. Sioutas, M. Navab, and T. K. Hsiai. 2015. Effect of Exposure to Atmospheric Ultrafine Particles on Production of Free Fatty Acids and Lipid Metabolites in the Mouse Small Intestine. *Environmental Health Perspectives* **123**: 34-41.

35. Meriwether, D., D. Sulaiman, A. Wagner, V. Grijalva, I. Kaji, K. J. Williams, L. Yu, S. Fogelman, C. Volpe, S. J. Bensinger, G. M. Anantharamaiah, I. Shechter, A. M. Fogelman, and S. T. Reddy. 2016. Transintestinal transport of the anti-inflammatory drug 4F and the modulation of transintestinal cholesterol efflux. *J Lipid Res* **57**: 1175-1193.

36. Navab, M., S. T. Reddy, G. M. Anantharamaiah, G. Hough, G. M. Buga, J. Danciger, and A. M. Fogelman. 2012. D-4F-mediated reduction in metabolites of arachidonic and linoleic acids in the small

intestine is associated with decreased inflammation in low-density lipoprotein receptor-null mice. *Journal of Lipid Research* **53**: 437-445.

37. Fredman, G., J. Hellmann, J. D. Proto, G. Kuriakose, R. A. Colas, B. Dorweiler, E. S. Connolly, R. Solomon, D. M. Jones, E. J. Heyer, M. Spite, and I. Tabas. 2016. An imbalance between specialized pro-resolving lipid mediators and pro-inflammatory leukotrienes promotes instability of atherosclerotic plaques. *Nat Commun* **7**: 12859.

38. Ishikawa, T. O., N. K. Jain, M. M. Taketo, and H. R. Herschman. 2006. Imaging cyclooxygenase-2 (Cox-2) gene expression in living animals with a luciferase knock-in reporter gene. *Mol Imaging Biol* **8**: 171-187.

39. Holgersen, K., P. H. Kvist, H. Markholst, A. K. Hansen, and T. L. Holm. 2014. Characterisation of enterocolitis in the piroxicam-accelerated interleukin-10 knock out mouse--a model mimicking inflammatory bowel disease. *J Crohns Colitis* **8**: 147-160.

40. Chattopadhyay, A., V. Grijalva, G. Hough, F. Su, P. Mukherjee, R. Farias-Eisner, G. M. Anantharamaiah, K. F. Faull, L. H. Hwang, M. Navab, A. M. Fogelman, and S. T. Reddy. 2015. Efficacy of tomato concentrates in mouse models of dyslipidemia and cancer. *Pharmacol Res Perspect* **3**: e00154.

41. Mukherjee, P., G. Hough, A. Chattopadhyay, M. Navab, H. R. Fogelman, D. Meriwether, K. Williams, S. Bensinger, T. Moller, K. F. Faull, A. J. Lusis, M. L. Iruela-Arispe, K. I. Bostrom, P. Tontonoz, S. T. Reddy, and A. M. Fogelman. 2017. Transgenic tomatoes expressing the 6F peptide and ezetimibe prevent diet-induced increases of IFN-β and cholesterol 25-hydroxylase in jejunum. *Journal of Lipid Research* **58**: 1636-1647.

42. Kubica, P., A. Kot-Wasik, A. Wasik, J. Namiesnik, and P. Landowski. 2012. Modern approach for determination of lactulose, mannitol and sucrose in human urine using HPLC-MS/MS for the studies of intestinal and upper digestive tract permeability. *J Chromatogr B Analyt Technol Biomed Life Sci* **907**: 34-40.

43. Jilling, T., J. Lu, M. Jackson, and M. S. Caplan. 2004. Intestinal Epithelial Apoptosis Initiates Gross Bowel Necrosis in an Experimental Rat Model of Neonatal Necrotizing Enterocolitis. *Pediatr Res* **55**: 622-629.

44. Ivanov, II, L. Frutos Rde, N. Manel, K. Yoshinaga, D. B. Rifkin, R. B. Sartor, B. B. Finlay, and D. R. Littman. 2008. Specific microbiota direct the differentiation of IL-17-producing T-helper cells in the mucosa of the small intestine. *Cell Host Microbe* **4**: 337-349.

45. Olson, M. A., M. S. Lee, T. L. Kissner, S. Alam, D. S. Waugh, and K. U. Saikh. 2015. Discovery of small molecule inhibitors of MyD88-dependent signaling pathways using a computational screen. *Sci Rep* **5**: 14246.

46. York, A. G., K. J. Williams, J. P. Argus, Q. D. Zhou, G. Brar, L. Vergnes, E. E. Gray, A. Zhen, N. C. Wu, D. H. Yamada, C. R. Cunningham, E. J. Tarling, M. Q. Wilks, D. Casero, D. H. Gray, A. K. Yu, E. S. Wang, D. G. Brooks, R. Sun, S. G. Kitchen, T. T. Wu, K. Reue, D. B. Stetson, and S. J. Bensinger. 2015. Limiting Cholesterol Biosynthetic Flux Spontaneously Engages Type I IFN Signaling. *Cell* **163**: 1716-1729.

47. Wallace, J. L., A. Bak, W. McKnight, S. Asfaha, K. A. Sharkey, and W. K. MacNaughton. 1998. Cyclooxygenase 1 contributes to inflammatory responses in rats and mice: implications for gastrointestinal toxicity. *Gastroenterology* **115**: 101-109.

48. Guirgis, F. W., C. Leeuwenburgh, V. Grijalva, J. Bowman, C. Kalynych, L. Moldawer, F. A. Moore, and S. T. Reddy. 2017. HDL Cholesterol Efflux is Impaired in Older Patients with Early Sepsis: A Subanalysis of a Prospective Pilot Study. *Shock (Augusta, Ga.)*.

49. Meriwether, D., S. Imaizumi, V. Grijalva, G. Hough, L. Vakili, G. M. Anantharamaiah, R. Farias-Eisner, M. Navab, A. M. Fogelman, S. T. Reddy, and I. Shechter. 2011. Enhancement by LDL of transfer of L-4F and oxidized lipids to HDL in C57BL/6J mice and human plasma. *J Lipid Res* **52**: 1795-1809.

50. Loftin, C. D., H. F. Tiano, and R. Langenbach. 2002. Phenotypes of the COX-deficient mice indicate physiological and pathophysiological roles for COX-1 and COX-2. *Prostaglandins & Other Lipid Mediators* **68-69**: 177-185.

51. Vlahcevic, Z. R., W. M. Pandak, and R. T. Stravitz. 1999. Regulation of bile acid biosynthesis. *Gastroenterol Clin North Am* **28**: 1-25, v.

52. Hofmann, A. F. 1999. Bile Acids: The Good, the Bad, and the Ugly. *News Physiol Sci* **14**: 24-29.

53. Carey, M. C., J. C. Montet, M. C. Phillips, M. J. Armstrong, and N. A. Mazer. 1981. Thermodynamic and molecular basis for dissimilar cholesterol-solubilizing capacities by micellar solutions of bile salts: cases of sodium chenodeoxycholate and sodium ursodeoxycholate and their glycine and taurine conjugates. *Biochemistry* **20**: 3637-3648.

54. Boyapati, R. K., A. G. Rossi, J. Satsangi, and G. T. Ho. 2016. Gut mucosal DAMPs in IBD: from mechanisms to therapeutic implications. *Mucosal Immunology* **9**: 567.

55. Strober, W., I. Fuss, and P. Mannon. 2007. The fundamental basis of inflammatory bowel disease. *J Clin Invest* **117**: 514-521.

56. Munkholm, P., E. Langholz, D. Hollander, K. Thornberg, M. Orholm, K. D. Katz, and V. Binder. 1994. Intestinal permeability in patients with Crohn's disease and ulcerative colitis and their first degree relatives. *Gut* **35**: 68-72.

57. Soderholm, J. D., G. Olaison, K. H. Peterson, L. E. Franzen, T. Lindmark, M. Wiren, C. Tagesson, and R. Sjodahl. 2002. Augmented increase in tight junction permeability by luminal stimuli in the non-inflamed ileum of Crohn's disease. *Gut* **50**: 307-313.

58. Zhang, Z., H. Sheng, J. Shao, R. D. Beauchamp, and R. N. DuBois. 2000. Posttranscriptional regulation of cyclooxygenase-2 in rat intestinal epithelial cells. *Neoplasia* **2**: 523-530.

59. Zhang, F., K. Subbaramaiah, N. Altorki, and A. J. Dannenberg. 1998. Dihydroxy bile acids activate the transcription of cyclooxygenase-2. *J Biol Chem* **273**: 2424-2428.

60. Zhang, F., N. K. Altorki, J. R. Mestre, K. Subbaramaiah, and A. J. Dannenberg. 1999. Curcumin inhibits cyclooxygenase-2 transcription in bile acid- and phorbol ester-treated human gastrointestinal epithelial cells. *Carcinogenesis* **20**: 445-451.

61. Zhang, F., N. K. Altorki, Y. C. Wu, R. A. Soslow, K. Subbaramaiah, and A. J. Dannenberg. 2001. Duodenal reflux induces cyclooxygenase-2 in the esophageal mucosa of rats: evidence for involvement of bile acids. *Gastroenterology* **121**: 1391-1399.

62. Wallace, J. L., and P. R. Devchand. 2005. Emerging roles for cyclooxygenase-2 in gastrointestinal mucosal defense. *Br J Pharmacol* **145**: 275-282.

63. Schmassmann, A., B. M. Peskar, C. Stettler, P. Netzer, T. Stroff, B. Flogerzi, and F. Halter. 1998. Effects of inhibition of prostaglandin endoperoxide synthase-2 in chronic gastro-intestinal ulcer models in rats. *Br J Pharmacol* **123**: 795-804.

64. Okayama, M., S. Hayashi, Y. Aoi, H. Nishio, S. Kato, and K. Takeuchi. 2007. Aggravation by selective COX-1 and COX-2 inhibitors of dextran sulfate sodium (DSS)-induced colon lesions in rats. *Dig Dis Sci* **52**: 2095-2103.

65. Pallone, F., and G. Monteleone. 2001. Mechanisms of tissue damage in inflammatory bowel disease. *Current opinion in gastroenterology* **17**: 307-312.

66. Meddings, J. B., and I. Gibbons. 1998. Discrimination of site-specific alterations in gastrointestinal permeability in the rat. *Gastroenterology* **114**: 83-92.

67. Petruzzelli, M., M. Vacca, A. Moschetta, R. Cinzia Sasso, G. Palasciano, K. J. van Erpecum, and P. Portincasa. 2007. Intestinal mucosal damage caused by non-steroidal anti-inflammatory drugs: Role of bile salts. *Clinical Biochemistry* **40**: 503-510.

68. Oyama, K., T. Fujimura, I. Ninomiya, T. Miyashita, S. Kinami, S. Fushida, T. Ohta, and M. Koichi. 2005. A COX-2 inhibitor prevents the esophageal inflammation-metaplasia-adenocarcinoma sequence in rats. *Carcinogenesis* **26**: 565-570.

69. Volynets, V., A. Reichold, G. Bardos, A. Rings, A. Bleich, and S. C. Bischoff. 2016. Assessment of the Intestinal Barrier with Five Different Permeability Tests in Healthy C57BL/6J and BALB/cJ Mice. *Dig Dis Sci* **61**: 737-746.

70. Vyvoda, O. S., R. Coleman, and G. Holdsworth. 1977. Effects of different bile salts upon the composition and morphology of a liver plasma membrane preparation. Deoxycholate is more membrane damaging than cholate and its conjugates. *Biochim Biophys Acta* **465**: 68-76.

71. Coleman, R., S. Iqbal, P. P. Godfrey, and D. Billington. 1979. Membranes and bile formation. Composition of several mammalian biles and their membrane-damaging properties. *Biochem J* **178**: 201-208.

72. Lu, Y.-C., W.-C. Yeh, and P. S. Ohashi. 2008. LPS/TLR4 signal transduction pathway. *Cytokine* **42**: 145-151.

73. Abram, C. L., G. L. Roberge, Y. Hu, and C. A. Lowell. 2014. Comparative analysis of the efficiency and specificity of myeloid-Cre deleting strains using ROSA-EYFP reporter mice. *Journal of immunological methods* **408**: 89-100.

74. Diaz, A., K. P. Chepenik, J. H. Korn, A. M. Reginato, and S. A. Jimenez. 1998. Differential regulation of cyclooxygenases 1 and 2 by interleukin-1 beta, tumor necrosis factor-alpha, and transforming growth factor-beta 1 in human lung fibroblasts. *Exp Cell Res* **241**: 222-229.

75. Agarwal, S., G. V. Reddy, and P. Reddanna. 2009. Eicosanoids in inflammation and cancer: the role of COX-2. *Expert Review of Clinical Immunology* **5**: 145-165.

76. Ricciotti, E., and G. A. FitzGerald. 2011. Prostaglandins and inflammation. *Arterioscler Thromb Vasc Biol* **31**: 986-1000.

77. Kalinski, P. 2012. Regulation of immune responses by prostaglandin E2. *J Immunol* **188**: 21-28.

78. Wallace, J. L. 2006. COX-2: A Pivotal Enzyme in Mucosal Protection and Resolution of Inflammation. *TheScientificWorldJOURNAL* **6**.

79. Gilroy, D. W., P. R. Colville-Nash, D. Willis, J. Chivers, M. J. Paul-Clark, and D. A. Willoughby. 1999. Inducible cyclooxygenase may have anti-inflammatory properties. *Nat Med* **5**: 698-701.

80. Norris, P. C., D. Gosselin, D. Reichart, C. K. Glass, and E. A. Dennis. 2014. Phospholipase A2 regulates eicosanoid class switching during inflammasome activation. *Proc Natl Acad Sci U S A* **111**: 12746-12751.

81. Angeli, V., C. Faveeuw, O. Roye, J. Fontaine, E. Teissier, A. Capron, I. Wolowczuk, M. Capron, and F. Trottein. 2001. Role of the parasite-derived prostaglandin D2 in the inhibition of epidermal Langerhans cell migration during schistosomiasis infection. *J Exp Med* **193**: 1135-1147.

82. Straus, D. S., G. Pascual, M. Li, J. S. Welch, M. Ricote, C. H. Hsiang, L. L. Sengchanthalangsy, G. Ghosh, and C. K. Glass. 2000. 15-deoxy-delta 12,14-prostaglandin J2 inhibits multiple steps in the NF-kappa B signaling pathway. *Proc Natl Acad Sci U S A* **97**: 4844-4849.

83. Serhan, C. N. 2014. Pro-resolving lipid mediators are leads for resolution physiology. *Nature* **510**: 92-101.

84. Serhan, C. N., S. Yacoubian, and R. Yang. 2008. Anti-inflammatory and proresolving lipid mediators. *Annu Rev Pathol* **3**: 279-312.

85. Serhan, C. N., R. Yang, K. Martinod, K. Kasuga, P. S. Pillai, T. F. Porter, S. F. Oh, and M. Spite. 2009. Maresins: novel macrophage mediators with potent antiinflammatory and proresolving actions. *The Journal of Experimental Medicine* **206**: 15-23.

86. Levy, B. D., C. B. Clish, B. Schmidt, K. Gronert, and C. N. Serhan. 2001. Lipid mediator class switching during acute inflammation: signals in resolution. *Nat Immunol* **2**: 612-619.

87. Takano, T., C. B. Clish, K. Gronert, N. Petasis, and C. N. Serhan. 1998. Neutrophil-mediated changes in vascular permeability are inhibited by topical application of aspirin-triggered 15-epi-lipoxin A4 and novel lipoxin B4 stable analogues. *J Clin Invest* **101**: 819-826.

88. Maddox, J. F., and C. N. Serhan. 1996. Lipoxin A4 and B4 are potent stimuli for human monocyte migration and adhesion: selective inactivation by dehydrogenation and reduction. *J Exp Med* **183**: 137-146.

89. Godson, C., S. Mitchell, K. Harvey, N. A. Petasis, N. Hogg, and H. R. Brady. 2000. Cutting edge: lipoxins rapidly stimulate nonphlogistic phagocytosis of apoptotic neutrophils by monocyte-derived macrophages. *J Immunol* **164**: 1663-1667.

90. Levy, L. 1969. Carrageenan paw edema in the mouse. *Life Sci* **8**: 601-606.

91. Sugishita, E., S. Amagaya, and Y. Ogihara. 1981. Anti-inflammatory testing methods: comparative evaluation of mice and rats. *J Pharmacobiodyn* **4**: 565-575.

92. Henriques, M. G., P. M. Silva, M. A. Martins, C. A. Flores, F. Q. Cunha, J. Assreuy-Filho, and R. S. Cordeiro. 1987. Mouse paw edema. A new model for inflammation? *Braz J Med Biol Res* **20**: 243-249.

93. Posadas, I., M. Bucci, F. Roviezzo, A. Rossi, L. Parente, L. Sautebin, and G. Cirino. 2004. Carrageenan-induced mouse paw oedema is biphasic, age-weight dependent and displays differential nitric oxide cyclooxygenase-2 expression. *British Journal of Pharmacology* **142**: 331-338.

94. Narasimha, A. J., J. Watanabe, T. O. Ishikawa, S. J. Priceman, L. Wu, H. R. Herschman, and S. T. Reddy. 2010. Absence of myeloid COX-2 attenuates acute inflammation but does not influence development of atherosclerosis in apolipoprotein E null mice. *Arterioscler Thromb Vasc Biol* **30**: 260-268.

95. Getz, G. S., G. D. Wool, and C. A. Reardon. 2009. Apoprotein A-I mimetic peptides and their potential anti-atherogenic mechanisms of action. *Curr Opin Lipidol* **20**: 171-175.

96. Van Lenten, B. J., A. C. Wagner, M. Navab, G. M. Anantharamaiah, S. Hama, S. T. Reddy, and A. M. Fogelman. 2007. Lipoprotein inflammatory properties and serum amyloid A levels but not cholesterol levels predict lesion area in cholesterol-fed rabbits. *J Lipid Res* **48**: 2344-2353.

97. Bruno, B. J., G. D. Miller, and C. S. Lim. 2013. Basics and recent advances in peptide and protein drug delivery. *Therapeutic delivery* **4**: 1443-1467.

98. Smythies, L. E., C. R. White, A. Maheshwari, M. N. Palgunachari, G. M. Anantharamaiah, M. Chaddha, A. R. Kurundkar, and G. Datta. 2010. Apolipoprotein A-I mimetic 4F alters the function of human monocyte-derived macrophages. *Am J Physiol Cell Physiol* **298**: C1538-1548.

99. White, C. R., L. E. Smythies, D. K. Crossman, M. N. Palgunachari, G. M. Anantharamaiah, and G. Datta. 2012. Regulation of pattern recognition receptors by the apolipoprotein A-I mimetic peptide 4F. *Arterioscler Thromb Vasc Biol* **32**: 2631-2639.

100. Sharifov, O. F., G. Anantharamaiah, and H. Gupta. 2015. Effects of ApoA-I Mimetic Peptide L-4F in LPS-Mediated Inflammation. *In* Apolipoprotein Mimetics in the Management of Human Disease. Springer. 63-88.

101. Van Lenten, B. J., A. C. Wagner, C. L. Jung, P. Ruchala, A. J. Waring, R. I. Lehrer, A. D. Watson, S. Hama, M. Navab, G. M. Anantharamaiah, and A. M. Fogelman. 2008. Anti-inflammatory apoA-I-mimetic peptides bind oxidized lipids with much higher affinity than human apoA-I. *J Lipid Res* **49**: 2302-2311.

102. Vakili, L., K. D. Navab, M. Shabihkhani, N. Pourtabatabaei, S. Vazirian, Z. Barseghian, S. Seyedali, and G. Hough. 2014. Systemic Inflammation, Intestine, and Paraoxonase-1. *In* Oxidative Stress and Inflammation in Non-communicable Diseases - Molecular Mechanisms and Perspectives in Therapeutics. J. Camps, editor. Springer International Publishing, Cham. 83-88.

103. Ou, J., J. Wang, H. Xu, Z. Ou, M. G. Sorci-Thomas, D. W. Jones, P. Signorino, J. C. Densmore, S. Kaul, K. T. Oldham, and K. A. Pritchard. 2005. Effects of D-4F on Vasodilation and Vessel Wall Thickness in Hypercholesterolemic LDL Receptor Null and LDL receptor/ApoA-I Double Knockout Mice on Western Diet. *Circulation research* **97**: 1190-1197.

104. Navab, M., S. T. Reddy, G. M. Anantharamaiah, S. Imaizumi, G. Hough, S. Hama, and A. M. Fogelman. 2011. Intestine may be a major site of action for the apoA-I mimetic peptide 4F whether administered subcutaneously or orally. *J Lipid Res* **52**: 1200-1210.

105. Morgantini, C., D. Meriwether, S. Baldi, E. Venturi, S. Pinnola, A. C. Wagner, A. M. Fogelman, E. Ferrannini, A. Natali, and S. T. Reddy. 2014. HDL lipid composition is profoundly altered in patients with type 2 diabetes and atherosclerotic vascular disease. *Nutr Metab Cardiovasc Dis* **24**: 594-599.

106. Berg, D. J., J. Zhang, J. V. Weinstock, H. F. Ismail, K. A. Earle, H. Alila, R. Pamukcu, S. Moore, and R. G. Lynch. 2002. Rapid development of colitis in NSAID-treated IL-10-deficient mice. *Gastroenterology* **123**: 1527-1542.

107. Keubler, L. M., M. Buettner, C. Hager, and A. Bleich. 2015. A Multihit Model: Colitis Lessons from the Interleukin-10-deficient Mouse. *Inflammatory bowel diseases* **21**: 1967-1975.

108. Hale, L. P., M. R. Gottfried, and A. Swidsinski. 2005. Piroxicam treatment of IL-10-deficient mice enhances colonic epithelial apoptosis and mucosal exposure to intestinal bacteria. *Inflammatory bowel diseases* **11**: 1060-1069.

109. Bruewer, M., A. Luegering, T. Kucharzik, C. A. Parkos, J. L. Madara, A. M. Hopkins, and A. Nusrat. 2003. Proinflammatory cytokines disrupt epithelial barrier function by apoptosis-independent mechanisms. *J Immunol* **171**: 6164-6172.

110. Cobrin, G. M., and M. T. Abreu. 2005. Defects in mucosal immunity leading to Crohn's disease. *Immunol Rev* **206**: 277-295.

111. Targan, S. R., and L. C. Karp. 2005. Defects in mucosal immunity leading to ulcerative colitis. *Immunol Rev* **206**: 296-305.

112. Poligone, B., and A. S. Baldwin. 2001. Positive and Negative Regulation of NF-κB by COX-2: ROLES OF DIFFERENT PROSTAGLANDINS. *Journal of Biological Chemistry* **276**: 38658-38664.

113. Lawrence, T., D. A. Willoughby, and D. W. Gilroy. 2002. Anti-inflammatory lipid mediators and insights into the resolution of inflammation. *Nat Rev Immunol* **2**: 787-795.

114. Masoodi, M., D. S. Pearl, M. Eiden, J. K. Shute, J. F. Brown, P. C. Calder, and T. M. Trebble. 2013. Altered Colonic Mucosal Polyunsaturated Fatty Acid (PUFA) Derived Lipid Mediators in Ulcerative Colitis: New Insight into Relationship with Disease Activity and Pathophysiology. *PLOS ONE* **8**: e76532.

115. Buckley, C. D., D. W. Gilroy, and C. N. Serhan. 2014. Proresolving lipid mediators and mechanisms in the resolution of acute inflammation. *Immunity* **40**: 315-327.

116. Lämmermann, T., P. V. Afonso, B. R. Angermann, J. M. Wang, W. Kastenmüller, C. A. Parent, and R. N. Germain. 2013. Neutrophil swarms require LTB4 and integrins at sites of cell death in vivo. *Nature* **498**: 371.

117. Viola, J. R., P. Lemnitzer, Y. Jansen, G. Csaba, C. Winter, C. Neideck, C. Silvestre-Roig, G. Dittmar, Y. Doring, M. Drechsler, C. Weber, R. Zimmer, N. Cenac, and O. Soehnlein. 2016. Resolving Lipid Mediators Maresin 1 and Resolvin D2 Prevent Atheroprogression in Mice. *Circ Res* **119**: 1030-1038.

118. Nowacki, T. M., A. T. Remaley, D. Bettenworth, M. Eisenblatter, T. Vowinkel, F. Becker, T. Vogl, J. Roth, U. J. Tietge, A. Lugering, J. Heidemann, and J. R. Nofer. 2016. The 5A apolipoprotein A-I (apoA-I) mimetic peptide ameliorates experimental colitis by regulating monocyte infiltration. *Br J Pharmacol* **173**: 2780-2792.

119. Chattopadhyay, A., M. Navab, G. Hough, F. Gao, D. Meriwether, V. Grijalva, J. R. Springstead, M. N. Palgnachari, R. Namiri-Kalantari, F. Su, B. J. Van Lenten, A. C. Wagner, G. M. Anantharamaiah, R. Farias-Eisner, S. T. Reddy, and A. M. Fogelman. 2013. A novel approach to oral apoA-I mimetic therapy. *Journal of Lipid Research* **54**: 995-1010.

120. Ma, J., X. L. Liao, B. Lou, and M. P. Wu. 2004. Role of apolipoprotein A-I in protecting against endotoxin toxicity. *Acta Biochim Biophys Sin (Shanghai)* **36**: 419-424.

121. Gupta, H., L. Dai, G. Datta, D. W. Garber, H. Grenett, Y. Li, V. Mishra, M. N. Palgunachari, S. Handattu, S. H. Gianturco, W. A. Bradley, G. M. Anantharamaiah, and C. R. White. 2005. Inhibition of

lipopolysaccharide-induced inflammatory responses by an apolipoprotein AI mimetic peptide. *Circ Res* **97**: 236-243.

122. Rossaint, J., and A. Zarbock. 2013. Tissue-Specific Neutrophil Recruitment into the Lung, Liver, and Kidney. *Journal of Innate Immunity* **5**: 348-357.

123. Szabady, R., and B. McCormick. 2013. Control of Neutrophil Inflammation at Mucosal Surfaces by Secreted Epithelial Products. *Frontiers in Immunology* **4**.

124. Pazos, M., D. Siccardi, K. L. Mumy, J. D. Bien, S. Louie, H. N. Shi, K. Gronert, R. J. Mrsny, and B. A. McCormick. 2008. Multi-Drug Resistance Transporter 2 Regulates Mucosal Inflammation by Facilitating the Synthesis of Hepoxilin A(3). *Journal of immunology (Baltimore, Md. : 1950)* **181**: 8044-8052.

125. Masoodi, M., A. A. Mir, N. A. Petasis, C. N. Serhan, and A. Nicolaou. 2008. Simultaneous lipidomic analysis of three families of bioactive lipid mediators leukotrienes, resolvins, protectins and related hydroxy-fatty acids by liquid chromatography/electrospray ionisation tandem mass spectrometry. *Rapid Commun Mass Spectrom* **22**: 75-83.

126. Dalli, J., and C. N. Serhan. 2012. Specific lipid mediator signatures of human phagocytes: microparticles stimulate macrophage efferocytosis and pro-resolving mediators. *Blood* **120**: e60-72.

127. Colas, R. A., M. Shinohara, J. Dalli, N. Chiang, and C. N. Serhan. 2014. Identification and signature profiles for pro-resolving and inflammatory lipid mediators in human tissue. *Am J Physiol Cell Physiol* **307**: C39-54.

128. Le Faouder, P., V. Baillif, I. Spreadbury, J. P. Motta, P. Rousset, G. Chene, C. Guigne, F. Terce, S. Vanner, N. Vergnolle, J. Bertrand-Michel, M. Dubourdeau, and N. Cenac. 2013. LC-MS/MS method for rapid and concomitant quantification of pro-inflammatory and pro-resolving polyunsaturated fatty acid metabolites. *J Chromatogr B Analyt Technol Biomed Life Sci* **932**: 123-133.

129. Homann, J., J. Suo, M. Schmidt, N. de Bruin, K. Scholich, G. Geisslinger, and N. Ferreiros. 2015. In Vivo Availability of Pro-Resolving Lipid Mediators in Oxazolone Induced Dermal Inflammation in the Mouse. *PLoS One* **10**: e0143141.

130. Buczynski, M. W., D. S. Dumlao, and E. A. Dennis. 2009. Thematic Review Series: Proteomics. An integrated omics analysis of eicosanoid biology. *J Lipid Res* **50**: 1015-1038.

131. Mozurkewich, E. L., M. Greenwood, C. Clinton, D. Berman, V. Romero, Z. Djuric, C. Qualls, and K. Gronert. 2016. Pathway Markers for Pro-resolving Lipid Mediators in Maternal and Umbilical Cord Blood: A Secondary Analysis of the Mothers, Omega-3, and Mental Health Study. *Front Pharmacol* **7**: 274.

132. Health, U. D. o., and H. Services. 2001. Guidance for industry, bioanalytical method validation. *http://www.fda.gov/cder/guidance/index.htm*.

Legends

Figure 3-1 Dysregulated inflammatory response to PAMP drives intestinal inflammation in the COX2 and cholate models of IBD. A: (*Left panel*) C57BL/6J mice treated with the COX2 inhibitor celecoxib (CX) were challenged with CCHF for 2 weeks. These mice developed severe inflammatory disease in their ileo-ceco-colic junctions, characterized by marked inflammatory lesions, sporadic foci of ulceration, and thickening of the intestinal wall. COX2 TKO responded comparably to CCHF. (*Right panel*) CCHF significantly increased the thickness of the ileo-ceco-colic junctions of both COX2 TKO and CX-treated mice (*, $p < 0.001$) **B**: C57BL/6J mice were fed CCHF diet and either treated (CX) or not treated (No-CX) with CX for 2 weeks. At multiple time points, mice were assessed and sacrificed (n = 4 mice/group/time point). (*Upper left panel*) Barrier permeability was assessed by 24 hr urinary sucralose excretion following oral gavage. CCHF significantly increased permeability in both CX and No-CX mice by 7 days (*, each compared to time 0, $p < 0.01$), with no difference between the goups ($p = .75$). By 14 days, permeability had improved in No-CX mice compared to CX (**, $p < 0.05$). (*Upper right panel*) Inflammation significantly increased in CX-treated mice from 7 -11 and 11-14 days (*, $p < 0.001$). (*Lower left panel*) Endotoxin in portal vein serum increased in both CX and No-CX mice by 7 days (*, compared to time 0, $p < 0.01$). (*Lower right panel*). Epithelial damage (scored 0-4) did not significantly emerge in CX-treated mice until day 14 (*, $p < 0.001$). **C**: WT and COX2 TKO were treated with vancomycin, ampicillin, neomycin, and metroniadazole for 7 days. COX2 TKO and WT mice were then continued on antibiotics (AB) across 14 days of CCHF challenge (left panel), while additional WT mice were kept on AB and then fed either CCHF or CCHF+CX (right panel). AB treatment rescued the development of intestinal inflammation in both COX2 TKO and CX groups (n=5/group) (*, $p < 0.001$). **D**: COX2 TKO (COX2 KO) and WT mice were challenged with CCHF diet across 14 days, while some mice in each group (n=7) receiving 3x/wk i.p. injections of the MyD88 inhibitor T6167923 (0.25 mg/injection). MyD88 inhibition

significantly inhibited the development of intestinal inflammation in COX2 TKO mice (*, $p < 0.01$). E: Bone-marrow derived macrophages were generated from COX2 MKO and FLOX mice (n=3 group/time point). The BMDM were activated with LPS (25 ng/ml media). After various time points, rna was isolated from cell lysates and expression of pro-inflammatory cytokines was determined by qPCR. COX2 MKO significantly enhanced the expression of IL1beta and TNFalpha at 10 hours and IL1beta at 24 hrs compared to FLOX (*, $p < 0.01$).

Figure 3-2 COX2 MKO mice challenged with CCHF exhibit dysregulated levels of pro-inflammatory and inflammation resolving lipid signals in tissue and plasma. **A**: COX2 MKO (MKO) and FLOX (Control) mice were injected with carrageenan and paw edema was determined as a measure of inflammation (n = 5). The initial phase of inflammation was delayed in COX2 MKO compared to FLOX (*, $p < 0.01$) and remained greater than FLOX across all time points from 10 hours (***, $p < 0.01$). The response in FLOX mice resolved at 144 compared to 72 hours (**, $p < 0.01$). **B-C**: Pro-inflammatory LOX and COX mediators were determined in the ileo-ceco-colic junctions (B) and plasmas (C)of COX2 MKO and FLOX mice fed CCHF for 8.5 weeks (n=8). All significant differences between the two groups within this broad category of pro-inflammatory mediators are reported here, as a percentage increase from FLOX (*, $p < 0.05$; &, $p < 0.1$). **D**: PGE2, PGD2, and associated metabolites were determined for both tissue and plasma in the experiment above. All significant differences are reported here, as a % of FLOX (*, $p < 0.05$). E: COX2 MKO significantly lowers the level of the pro-resolving LOX mediators (SPM) LXA4 as well as total SPM and significantly reduces the ratio of LXA4 as well as 5LOX pro-resolving mediators to LTB4 (*, $p < 0.05$; &, $p < 0.1$).

Figure 3-3 ApoA-I mimetics inhibit the development of intestinal inflammation in the COX2 MKO and CCHF model of IBD. A-F: COX2 MKO mice were challenged with CCHF for 7 and 10 weeks, and the effect of oral D-4F (500 ug/ml water) on the development of intestinal inflammation was determined (n = 7 mice/group/time point). (A) 4F significantly reduced the thickness of the ileo-ceco-colic junctions of these mice at 7 and 10 weeks, returning the thickness to its pre-disease baseline (see Fig 1A). (B) (*Left panel*) Representative images of effect of CCHF and 4F on inflammation in ileo-ceco-colic junctions of COX2 MKO mice. (*Right panel*) CCHF significantly increases intestinal inflammation as scored in histological sections (*, $p < 0.001$), while 4F significantly inhibited this increase (**, $p < 0.001$). (C) 4F significantly reduced muscle thickening in COX2 MKO + CCHF mice (*, $p < 0.001$). (D-E) 4F treatment significantly reduced infiltration of macrophages (F4/80+) and neutrophils (Ly6G+) into the ileo-ceco-junctions of COX2 MKO mice on CCHF diet (*, $p < 0.001$). (F) 4F significantly inhibited expression of TNFα but significantly increased expression of IL10 in the ceca of COX2 MKO mice fed CCHF for 7 weeks ($p < 0.01$). **G**: COX2 MKO and FLOX mice were challenged with CCHF, and the effect of Tg6F on intestinal inflammation was determined (n = 8/group). Tg6F significantly suppressed thickening of ileo-ceco-colic junctions in both FLOX (*, $p < 0.05$) and COX2 MKO (**, $p < 0.001$). Tg6F also improved a 12 point HE inflammatory score that assigned up to 3 points to area affected, degree of infiltration, muscle thickness, and ulceration (***, $p < 0.01$).

Figure 3-4 4F treatment improves the inflammatory mediator profile of macrophages, intestinal tissue, and plasma. A: BMDM from both FLOX and COX2 MKO mice were activated with LPS and co-treated with 15 ug/ml D-4F. 4F significantly suppressed both IL1β (*left*) and TNFα (*right*) expression across multiple time points in both FLOX and COX2 MKO cultures. (n=3/group/time pt) **B**: 4F co-treatment significantly reduced the levels of PGE2 and PGD2 in both COX2 MKO and FLOX BMDM

cultures across all time points from 10 hours on ($p < 0.05$). **C**: 4F co-treatment selectively inhibited the COX metabolite 11HETE without altering the LOX metabolite 15HETE in LPS-activated COX2 MKO and FLOX BMDM. D: The effect of 4F on the intestinal lipid inflammatory mediator profile of COX2 MKO mice fed CCHF for 8.5 weeks was determined (see Supplemental Table 6). In intestinal tissue, 4F rescued the pro-inflammatory effect of COX2 MKO on LOX metabolites with respect to 12HETE, 13HODE, and total LOX metabolites (*, compared to FLOX, $p < 0.05$; **, compared to MKO+CCHF, $p < 0.05$). **E**: The effect of 4F therapy on plasma TC (*left*) and PON1 activity (*right*) was determined for the plasmas from the 7 and 10 week studies. 4F significantly reduced TC and significantly enhanced PON at both time points (*, $p < 0.01$). **F**: The effect of 4F on the plasma lipid inflammatory mediator profile of COX2 MKO mice fed CCHF for 8.5 weeks was determined (see Supplemental Table 7). 4F significantly reduced a broad class of pro-inflammatory LOX mediators that were elevated by COX2 MKO (*, compared to FLOX+CCHF, $p < 0.05$; **, compared to MKO+CCHF, $p < 0.05$). **G**: 4F therapy likewise reduced in plasma most elevated pro-inflammatory COX mediators (*, compared to FLOX+CCHF, $p < 0.05$; **, compared to MKO+CCHF, $p < 0.05$).

Figure 3-5 4F can directly clear lipid pro-inflammatory mediators from intestinal tissue and plasma. A: 4F displays a differential effect upon pro-inflammatory mediators in intestinal tissue of COX2 MKO mice fed CCHF. While 4F clears elevated pro-inflammatory LOX mediators (see figure 4D), 4F here does not affect pro-inflammatory COX mediators that are increased with disease (*, compared to FLOX+CCHF, $p < 0.05$). B: Paired intestinal explants from COX2 MKO mice that had been fed CCHF for 8.5 weeks were mounted in Ussing chambers and 4F added to the mucosal media. Clearance of pro-inflammatory LOX mediators into the mucosal chamber was determined by LCMS. (n=6, *, $p < 0.05$; #, $p < 0.1$; paired T-test). C: Explants from C57BL/6J mice were loaded into Ussing chambers (n=6) and HDL and LDL were

pre-loaded with 1 ug each deuterated 15- and 12-HETE together with deuterated 13HODE per 2.5mgHDL+5mgLDL. The entire 7.5 mg of lipoprotein was added to the serosal media, and baseline trans-intestinal transport of deuterated lipid was monitored via LCMSMS (*left*). We observed a baseline transintestinal transport of these tagged lipids. In a repeat experiment, we sought to determine the effect of 4F on this transport by adding 50 ug/ml D-4F to mucosal media in the presence of micelles. 4F significantly enhanced the trans-intestinal transport of both 12- and 15-HETE-d (*, $p < 0.01$).

Figure 3-6 4F treatment inhibits the development of colitis in the piroxicam-accelerated IL10$^{-/-}$model. We sought to determine whether 4F could protect against intestinal inflammation in the PAC IL10 model of colitis. A: The protocol of the study is presented here. B: PX significantly decreased colon length (*left*) and increased colitis score (*right*), while 4F therapy largely rescued these effects (*, $p < 0.001$; **, $p < 0.01$).The effect of both PAC and 4F on the development of colitis was determined by assessing colon length and colitis score. C: Disease significantly increased H&E score (*left*) , while 4F therapy largely rescued this effect. (*, $p < 0.001$; **, $p < 0.01$). Representative images of IL10-/-, PAC IL10 -/- and 4F treated PAC IL10-/- are given. Red arrow points to a focus of inflammation. D: The effect of PX on barrier permeability in each of 6 mice ("ms1" for mouse 1, etc.) was determined by measuring urinary sucralose excretion as before. PX increased barrier permeability in all mice in a biphasic manner (*left*) , with an early significant increase over time 0 (*, $p < 0.01$, paired T-test), and a late increase over day 7 (**, $p < 0.01$, paired T-test). Increase in barrier permeability was accompanied by a significant increase in the translocation of endotoxin into portal vein serum (*, $p < 0.02$). E: The effect of 4F on pro-inflammatory COX mediators in BMDM from IL10-/- mice with and without piroxicam was determined following LPS activation. COX mediators were measured by LC-MS/MS. 4F significantly inhibited pro-inflammatory mediator levels in both groups for all times past 4 hours ($p < 0.001$). F: The

effect of 4F on inflammatory mediators in the colons of the mice from (A) was determined (see Supplemental Table 8). As with 4F in the COX2 CCHF model, 4F rescued the PX-induced elevations of pro-inflammatory LOX mediators in tissue. [*, $p < 0.05$ (IL10-PX v IL10). **, $p < 0.05$ (IL10-PX v IL10-PX-4F)].G: Also as in the case of the COX2 CCHF model, 4F does not rescue elevated pro-inflammatory COX products in tissue. (*, $p < 0.05$, IL10-PX v IL10) H: Interestingly, inflamed colon in this model exhibited a significant reduction in the ratio of pro-resolving RvD1 to LTB4 (*: $p< 0.001$ compared to IL10. #: $p < 0.1$ compared to IL10+PX).

Table 3-1 Bioactive lipid inflammatory mediators analyzed by LC-MS/MS. The table lists all of the bioactive inflammatory mediators determined in this study by LC-MS/MS. For a complete list of all measured analytes, see Supplemental Table 1. (Bold = bioactive lipid that is measure directly in panel. [lipid] = bioactive lipid that is measured indirectly in panel. *Italics* = lipid analyte used in part as a pathway marker.

Table 3-2 Effect of COX2 MKO and CCHF on lipid inflammatory mediators in ileo-ceco-colic junctions of mice. COX2 MKO and FLOX mice were fed with CCHF diet for 8.5 weeks (8 mice/group). We extracted by SPE the lipid contents from these intestinal tissues together with tissues from an equal number of COX2 MKO mice fed a chow diet, and we determined by LC-MS/MS the levels of the analytes of our lipid inflammatory mediator panel. Results are here reported as ng/50 mg tissue. (Key: *: $p < 0.05$, significant compared to MKO+CHOW. **: $p < 0.05$, significant compared to FLOX+CCHF &: $p < 0.1$ compared to FLOX+CCHF. $: $p < 0.1$ compared to MKO + CHOW. ND = not detected.)

Table 3-3 Effect of COX2 MKO and CCHF on lipid inflammatory mediators in plasma of mice. COX2 MKO and FLOX mice were fed with CCHF diet for 8 weeks (8 mice/group). We extracted by SPE the lipid contents from these plasmas together with plasmas from an equal number of COX2 MKO mice fed a chow diet, and we determined by LC-MS/MS the levels of the analytes of our lipid inflammatory mediator panel. Results are here reported as ng/100 ul plasma. (Key: *: $p < 0.05$, significant compared to MKO+CHOW. **: $p < 0.05$, significant compared to FLOX+CCHF &: $p < 0.1$ compared to FLOX+CCHF. ND = not detected.)

Figure 3-1

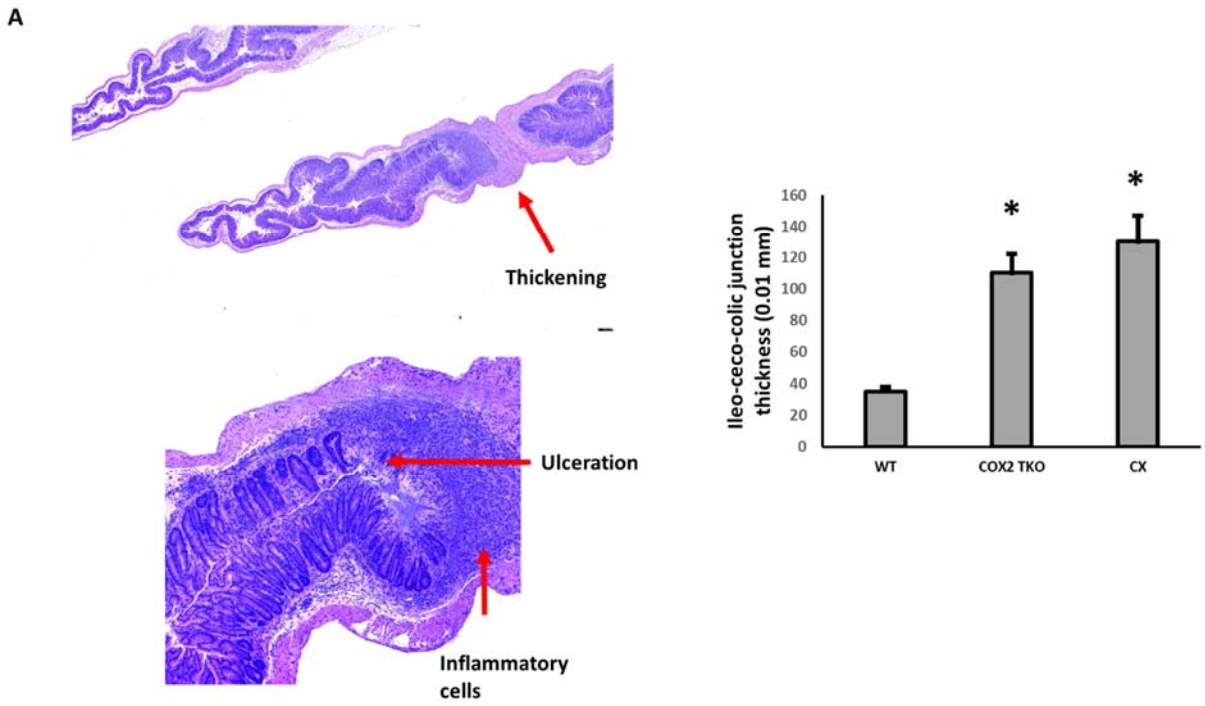
A
Thickening
Ulceration
Inflammatory cells
Ileo-ceco-colic junction thickness (0.01 mm)
160
140
120
100
80
60
40
20
0
*
*
WT
COX2 TKO
CX

B

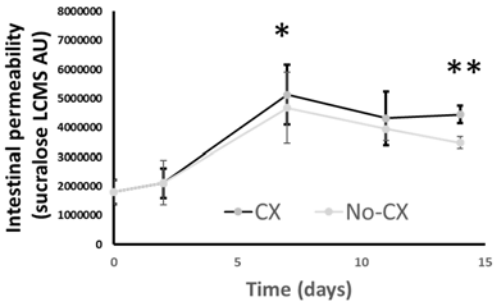
Intestinal permeability (sucralose LCMS AU)
8000000
7000000
6000000
5000000
4000000
3000000
2000000
1000000
0
*
**
CX
No-CX
0
5
10
15
Time (days)

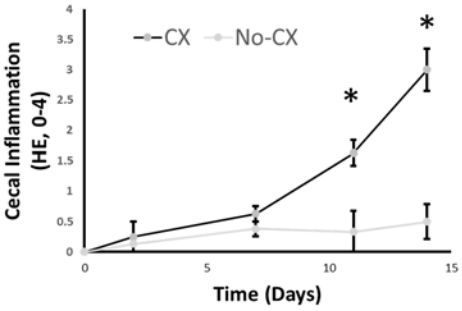
Cecal Inflammation (HE, 0-4)
4
3.5
3
2.5
2
1.5
1
0.5
0
CX
No-CX
*
*
0
5
10
15
Time (Days)

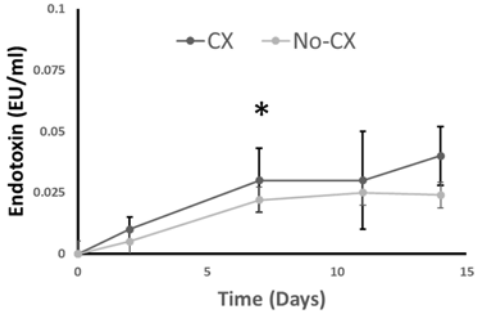
Endotoxin (EU/ml)
0.1
0.075
0.05
0.025
0
CX
No-CX
*
0
5
10
15
Time (Days)

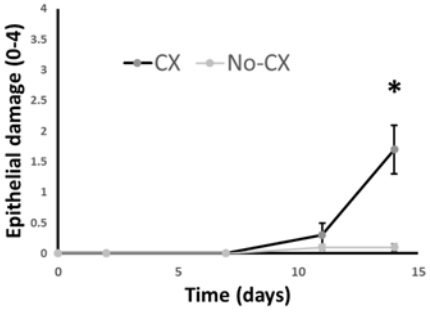
Epithelial damage (0-4)
4
3.5
3
2.5
2
1.5
1
0.5
0
CX
No-CX
*
0
5
10
15
Time (days)

C

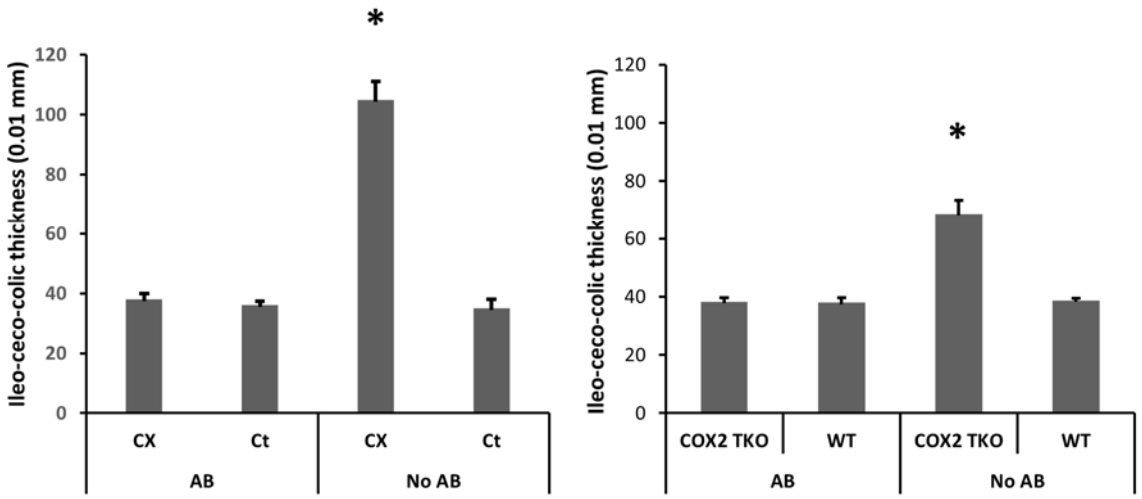
*
Ileo-ceco-colic thickness (0.01 mm)
120
100
80
60
40
20
0
CX
Ct
CX
Ct
AB
No AB
*
Ileo-ceco-colic thickness (0.01 mm)
120
100
80
60
40
20
0
COX2 TKO
WT
COX2 TKO
WT
AB
No AB

D

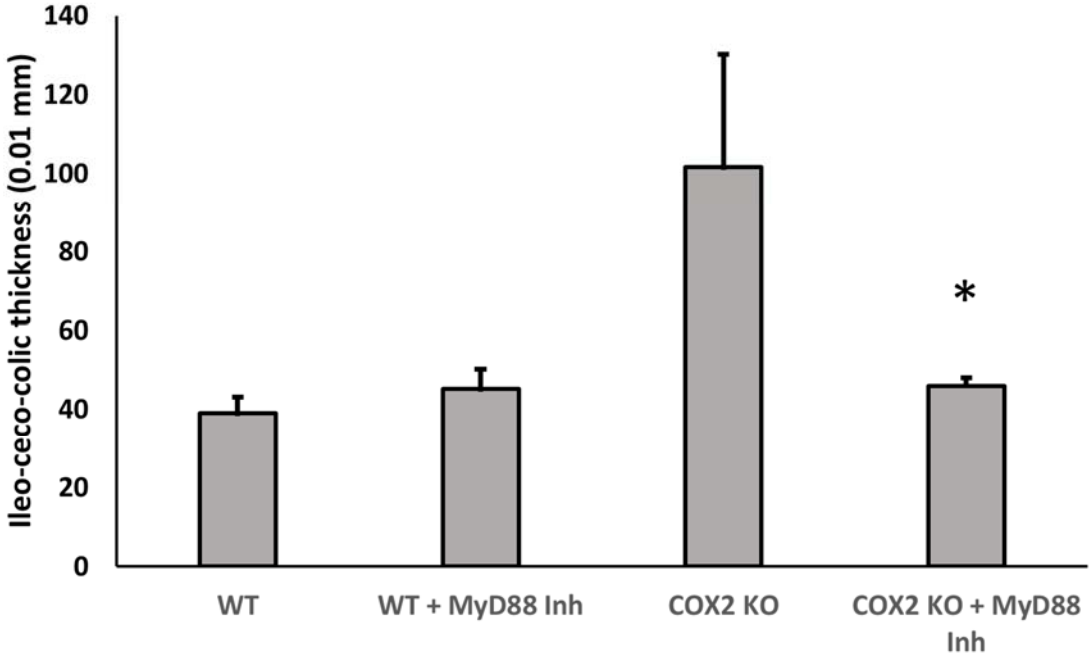
140
120
100
80
60
40
20
0
Ileo-ceco-colic thickness (0.01 mm)
*
WT
WT + MyD88 Inh
COX2 KO
COX2 KO + MyD88 Inh

E

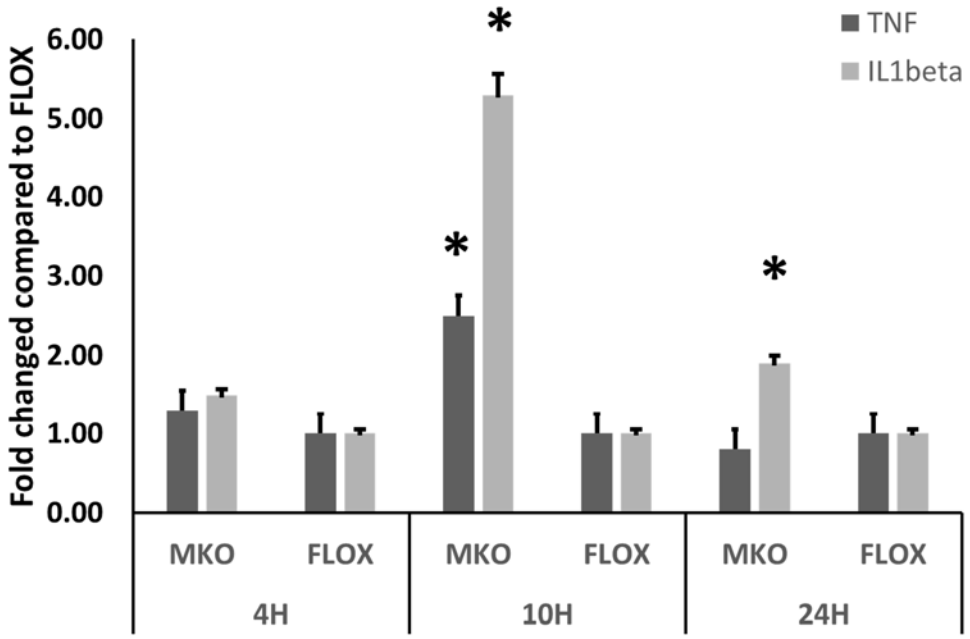
Fold changed compared to FLOX
6.00
5.00
4.00
3.00
2.00
1.00
0.00
TNF
IL1beta
*
*
*
MKO
FLOX
MKO
FLOX
MKO
FLOX
4H
10H
24H

Figure 3-2

A

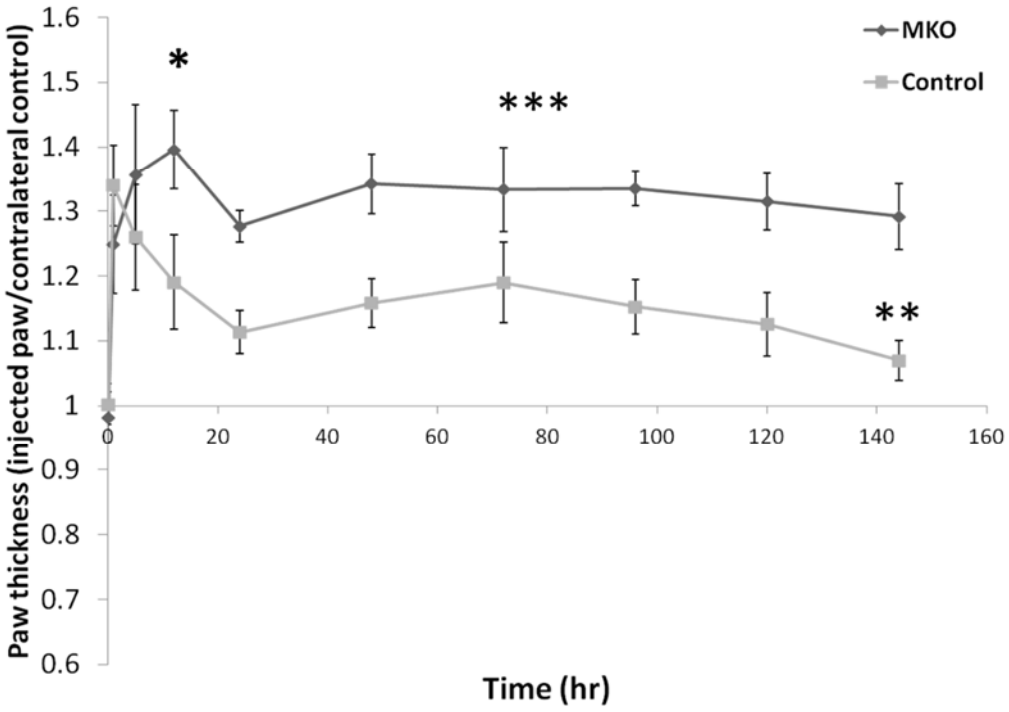
MKO
Control
*
***
**
Paw thickness (injected paw/contralateral control)
Time (hr)
1.6
1.5
1.4
1.3
1.2
1.1
1
0.9
0.8
0.7
0.6
0
20
40
60
80
100
120
140
160

B

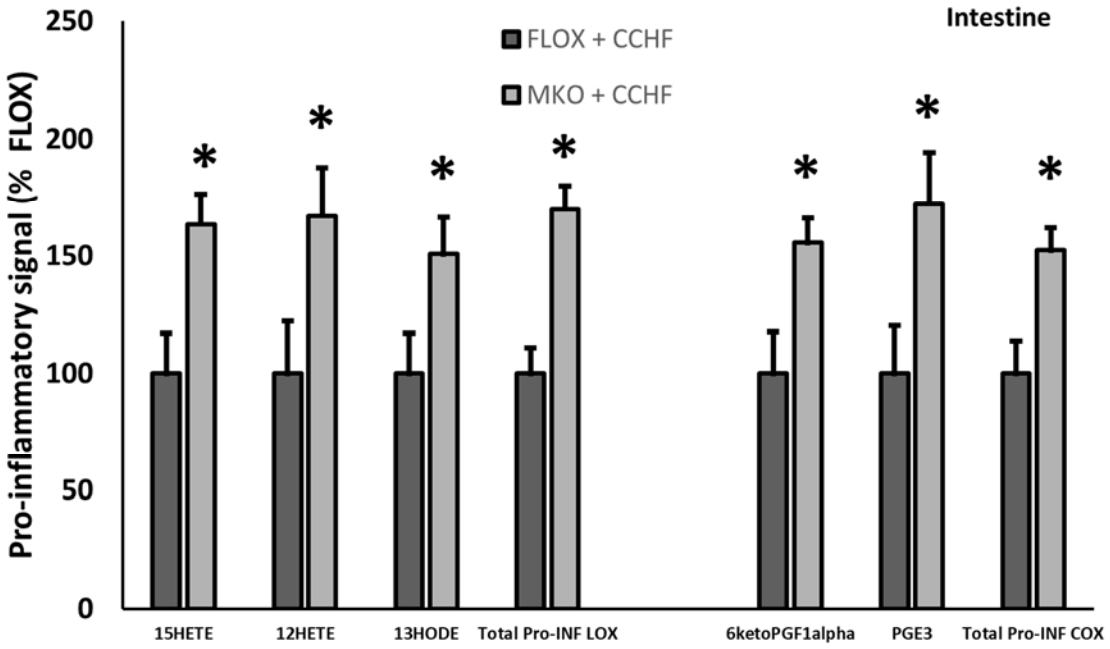
Intestine
FLOX + CCHF
MKO + CCHF
Pro-inflammatory signal (% FLOX)
250
200
150
100
50
0
*
15HETE
12HETE
13HODE
Total Pro-INF LOX
6ketoPGF1alpha
PGE3
Total Pro-INF COX

C

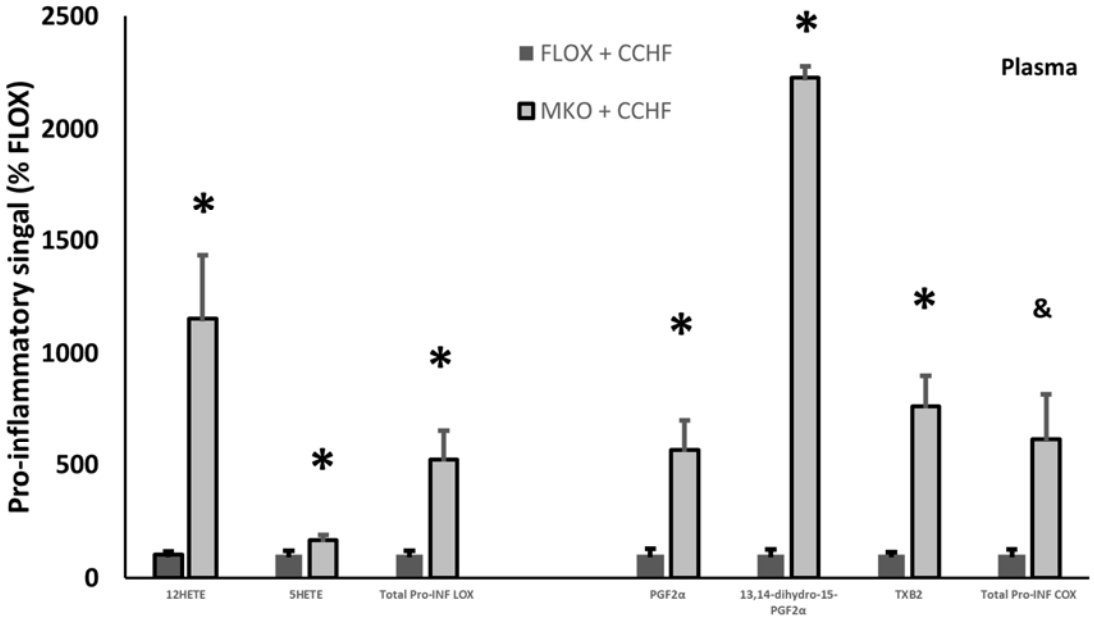
Pro-inflammatory singal (% FLOX)
2500
2000
1500
1000
500
0
FLOX + CCHF
MKO + CCHF
Plasma
*
*
*
*
*
*
&
12HETE
5HETE
Total Pro-INF LOX
PGF2α
13,14-dihydro-15-PGF2α
TXB2
Total Pro-INF COX

D

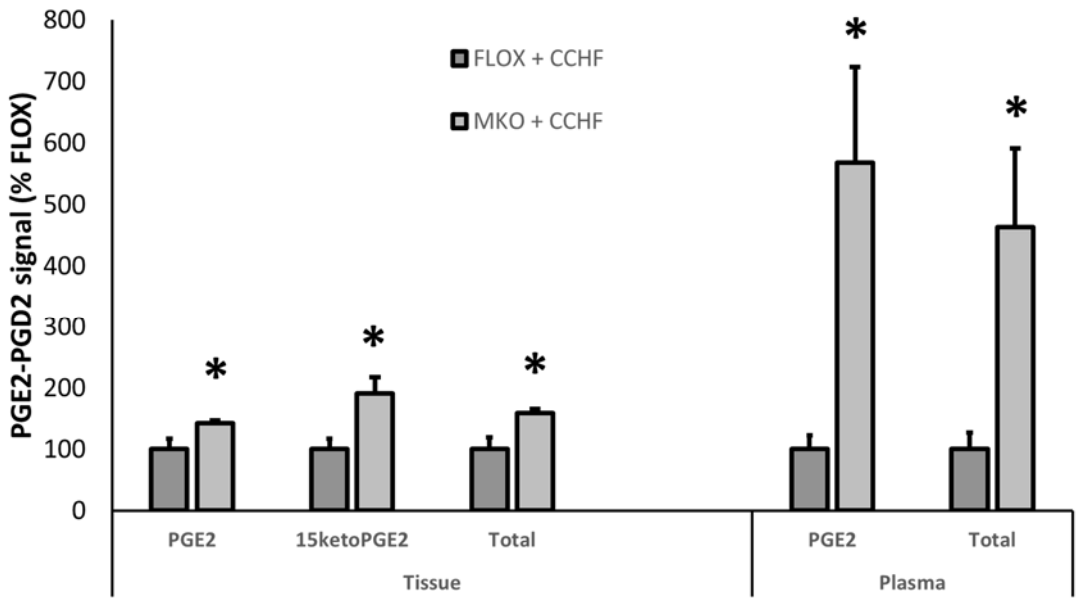
PGE2-PGD2 signal (% FLOX)
800
700
600
500
400
300
200
100
0
FLOX + CCHF
MKO + CCHF
*
*
*
*
*
PGE2
15ketoPGE2
Total
PGE2
Total
Tissue
Plasma

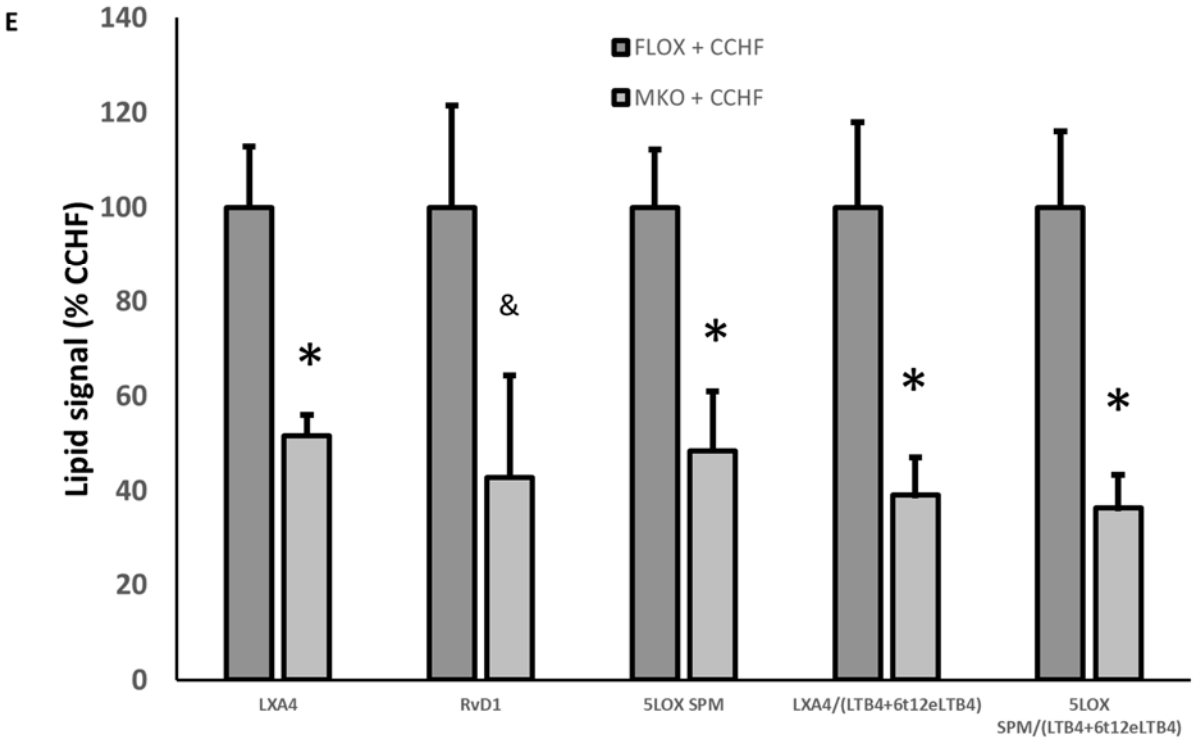
E
140
120
100
80
60
40
20
0
Lipid signal (% CCHF)
FLOX + CCHF
MKO + CCHF
*
&
*
*
*
LXA4
RvD1
5LOX SPM
LXA4/(LTB4+6t12eLTB4)
5LOX SPM/(LTB4+6t12eLTB4)

Figure 3-3

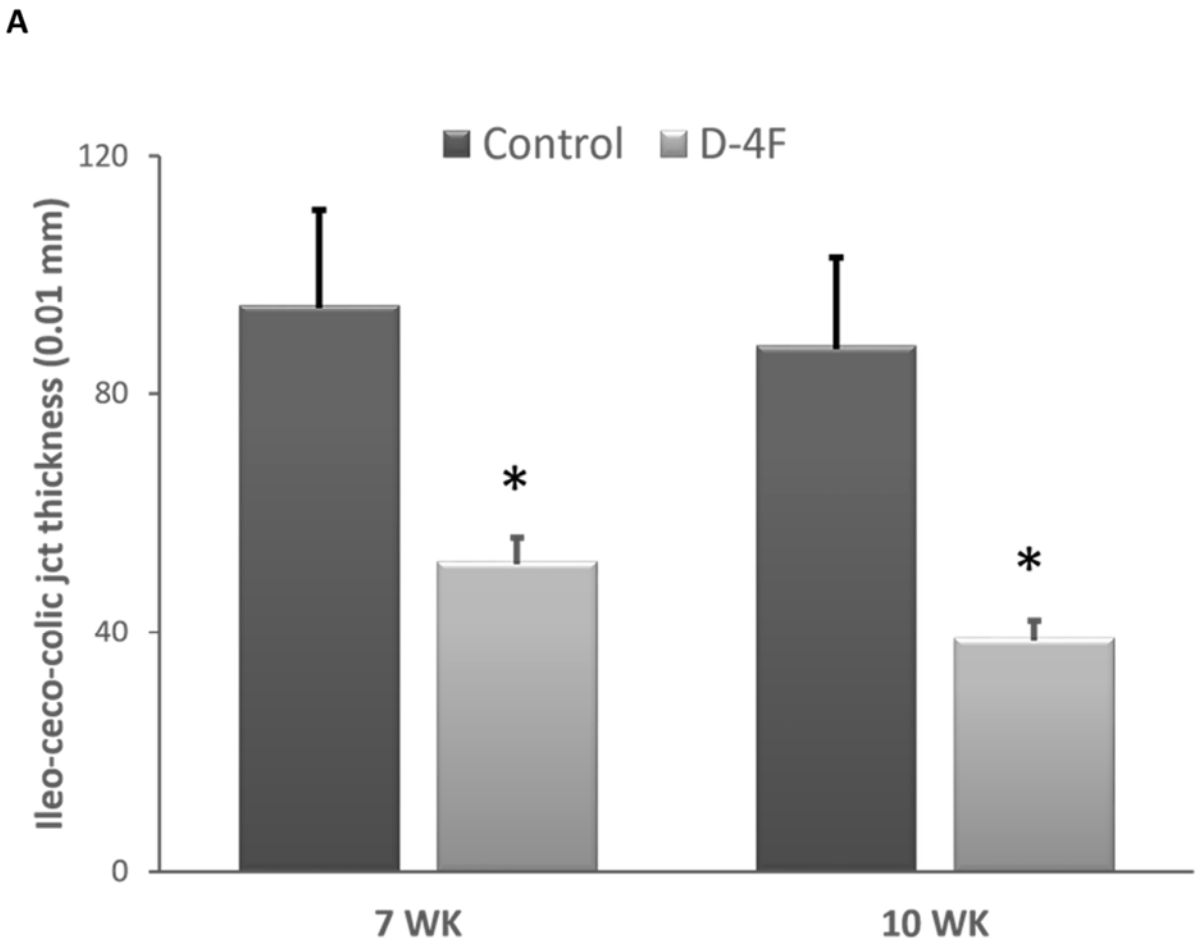
A
Control
D-4F
120
80
40
0
Ileo-ceco-colic jct thickness (0.01 mm)
*
*
7 WK
10 WK

B

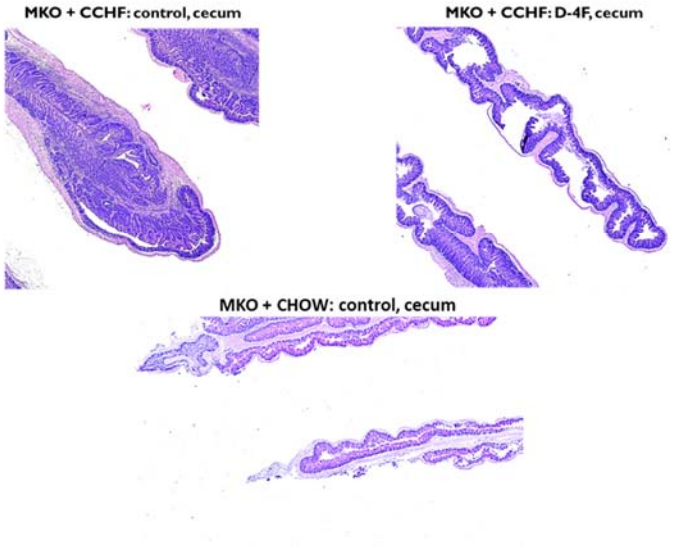
MKO + CCHF: control, cecum
MKO + CCHF: D-4F, cecum
MKO + CHOW: control, cecum

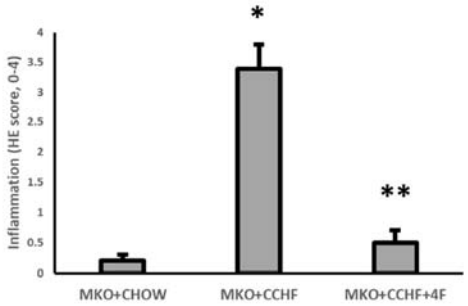
Inflammation (HE score, 0-4)
4
3.5
3
2.5
2
1.5
1
0.5
0
*
**
MKO+CHOW
MKO+CCHF
MKO+CCHF+4F

C

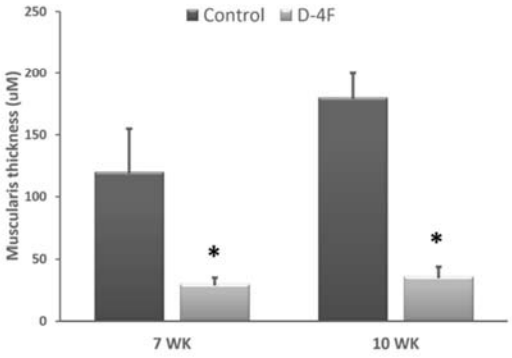
Control
D-4F
250
200
150
100
50
0
Muscularis thickness (uM)
*
*
7 WK
10 WK

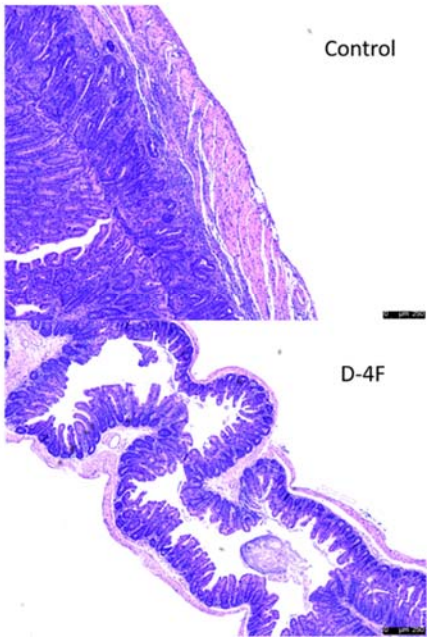
Control
D-4F

D

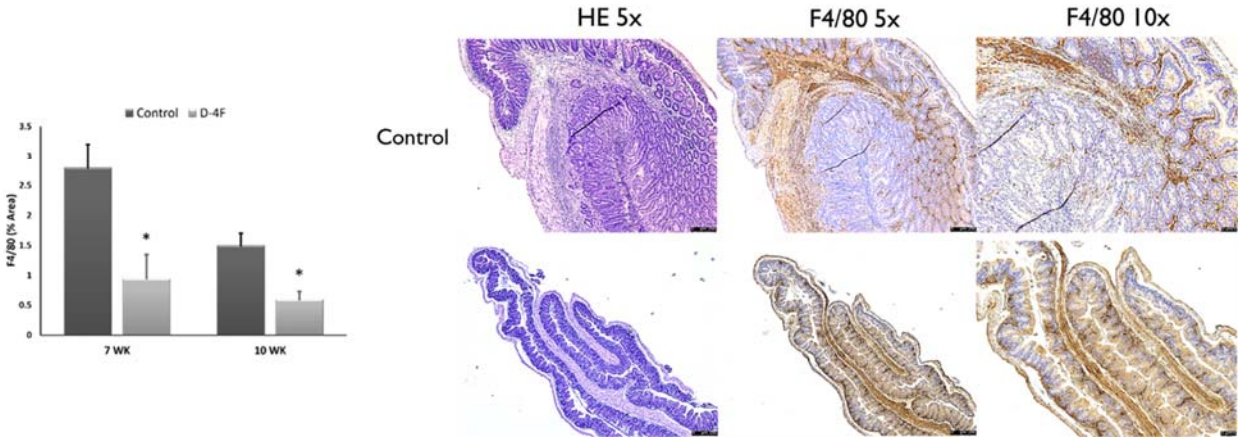
Control
D-4F
F4/80 (% Area)
3.5
3
2.5
2
1.5
1
0.5
0
*
*
7 WK
10 WK
HE 5x
F4/80 5x
F4/80 10x
Control

E

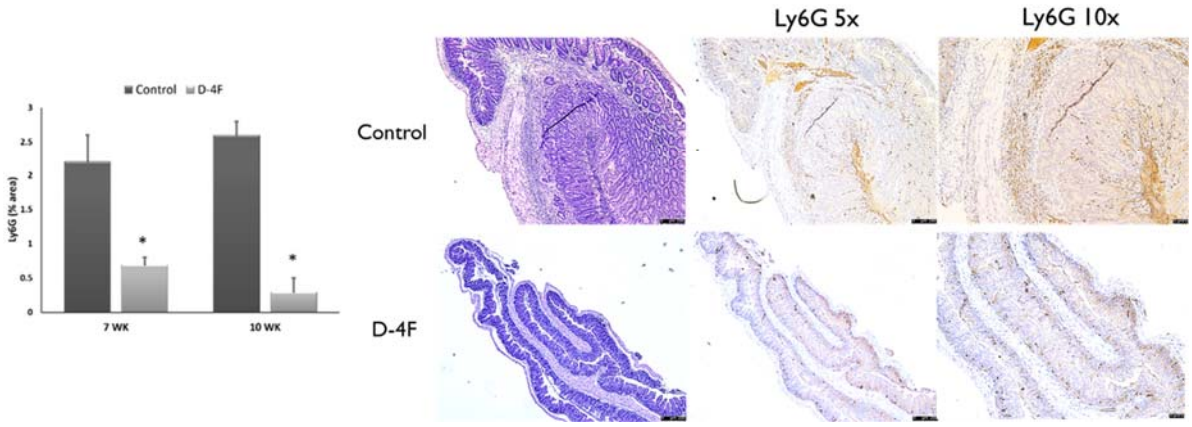

F

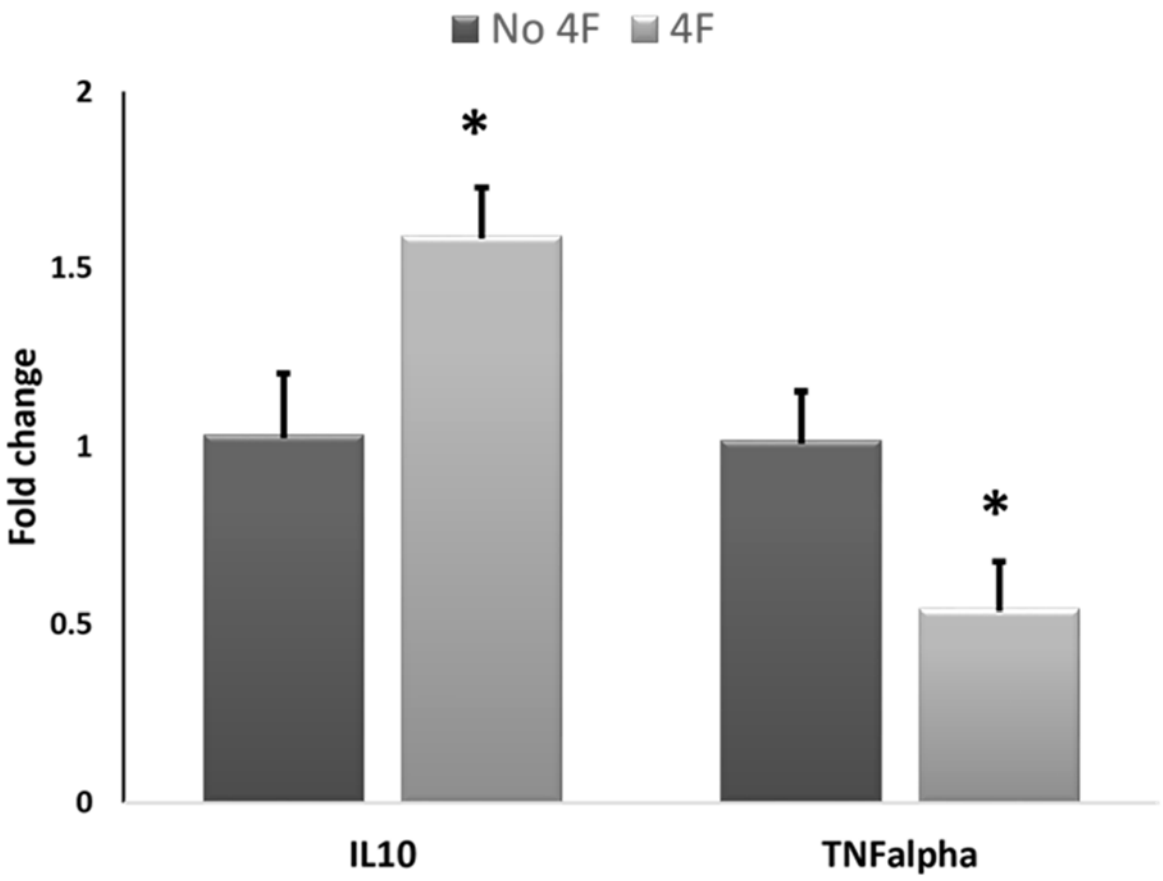

G

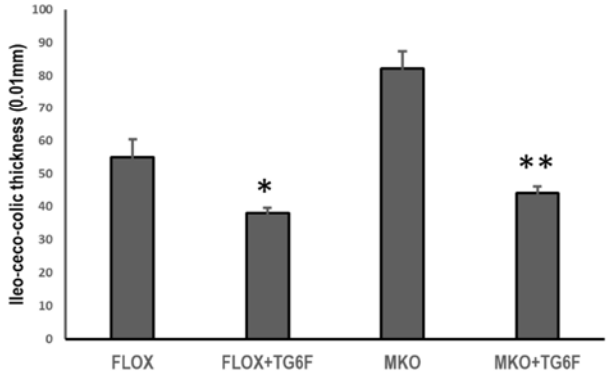
Ileo-ceco-colic thickness (0.01mm)
100
90
80
70
60
50
40
30
20
10
0
*
**
FLOX
FLOX+TG6F
MKO
MKO+TG6F

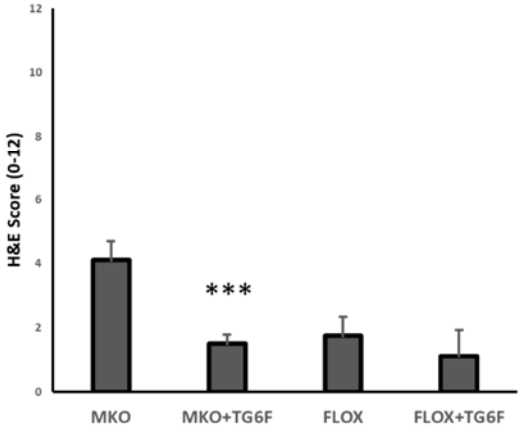
H&E Score (0-12)
12
10
8
6
4
2
0
***
MKO
MKO+TG6F
FLOX
FLOX+TG6F

Figure 3-4

A

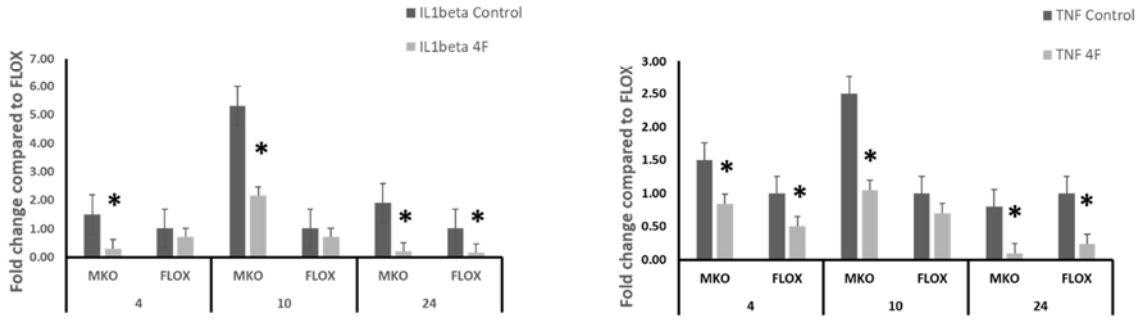
IL1beta Control
IL1beta 4F
Fold change compared to FLOX
7.00
6.00
5.00
4.00
3.00
2.00
1.00
0.00
MKO
FLOX
MKO
FLOX
MKO
FLOX
4
10
24
TNF Control
TNF 4F
Fold change compared to FLOX
3.00
2.50
2.00
1.50
1.00
0.50
0.00
MKO
FLOX
MKO
FLOX
MKO
FLOX
4
10
24

B

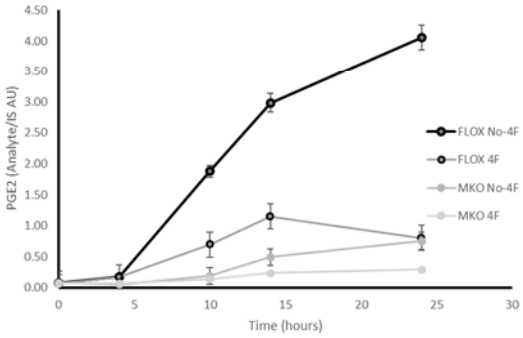
PGE2 (Analyte/IS AU)
4.50
4.00
3.50
3.00
2.50
2.00
1.50
1.00
0.50
0.00
0
5
10
15
20
25
30
Time (hours)
FLOX No-4F
FLOX 4F
MKO No-4F
MKO 4F

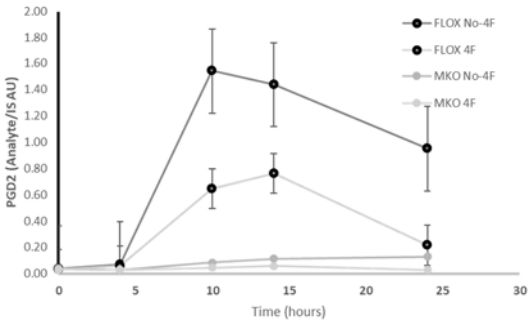
PGD2 (Analyte/IS AU)
2.00
1.80
1.60
1.40
1.20
1.00
0.80
0.60
0.40
0.20
0.00
0
5
10
15
20
25
30
Time (hours)
FLOX No-4F
FLOX 4F
MKO No-4F
MKO 4F

C

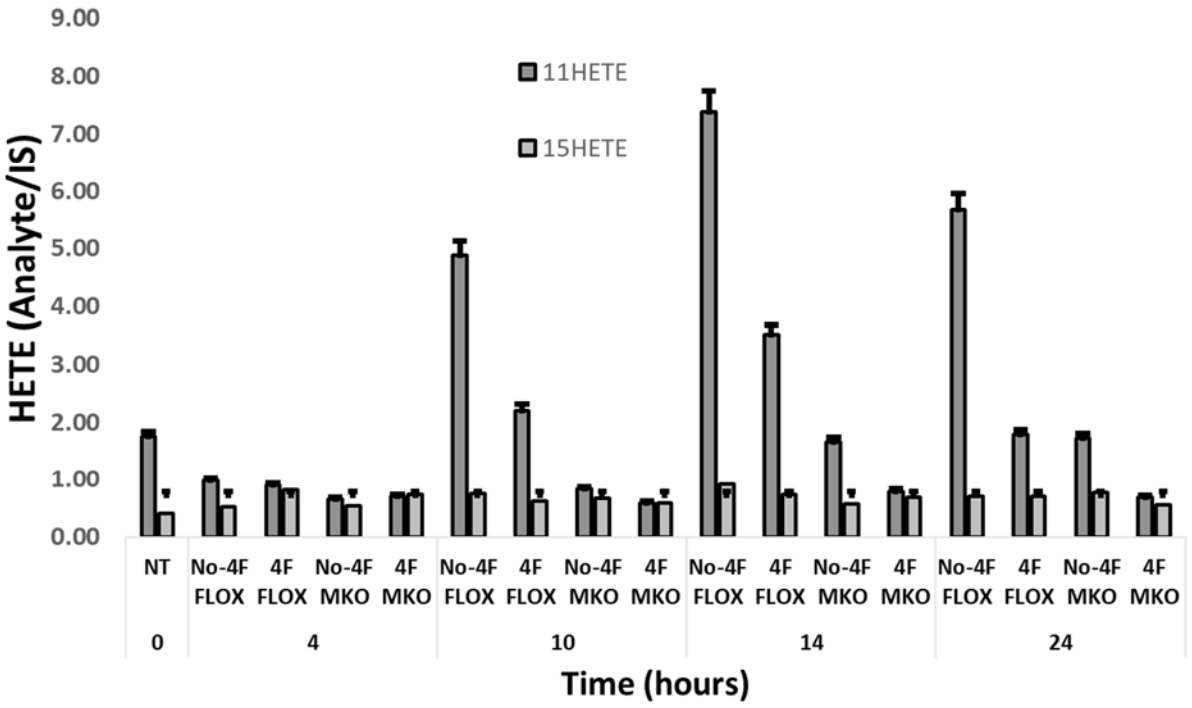
9.00
8.00
7.00
6.00
5.00
4.00
3.00
2.00
1.00
0.00
HETE (Analyte/IS)
11HETE
15HETE
NT
No-4F FLOX
4F FLOX
No-4F MKO
4F MKO
0
4
10
14
24
Time (hours)

D

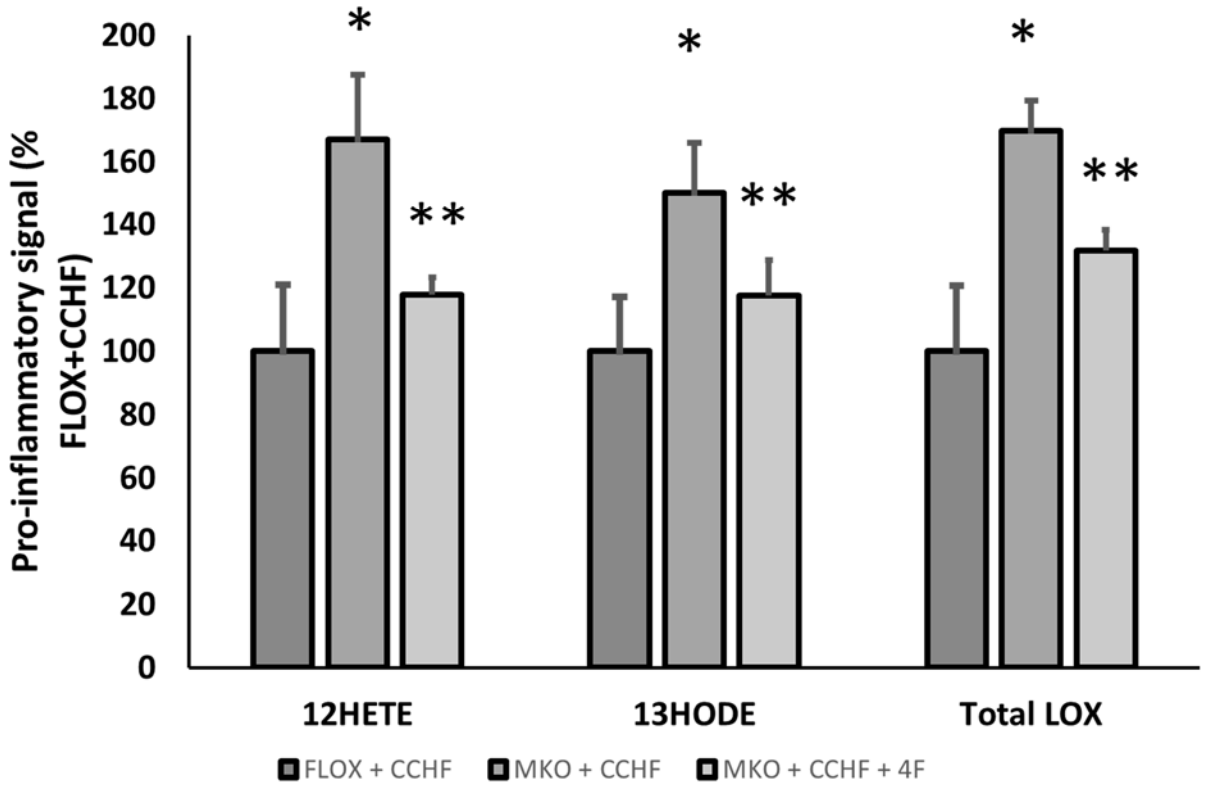
Pro-inflammatory signal (% FLOX+CCHF)
200
180
160
140
120
100
80
60
40
20
0
*
**
*
**
*
**
12HETE
13HODE
Total LOX
FLOX + CCHF
MKO + CCHF
MKO + CCHF + 4F

E

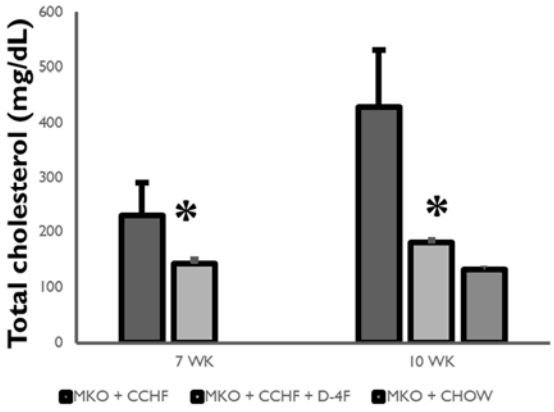
Total cholesterol (mg/dL)
600
500
400
300
200
100
0
*
*
7 WK
10 WK
MKO + CCHF
MKO + CCHF + D-4F
MKO + CHOW

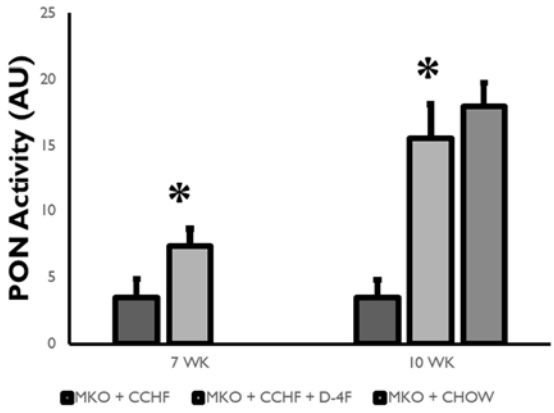
PON Activity (AU)
25
20
15
10
5
0
*
*
7 WK
10 WK
MKO + CCHF
MKO + CCHF + D-4F
MKO + CHOW

F

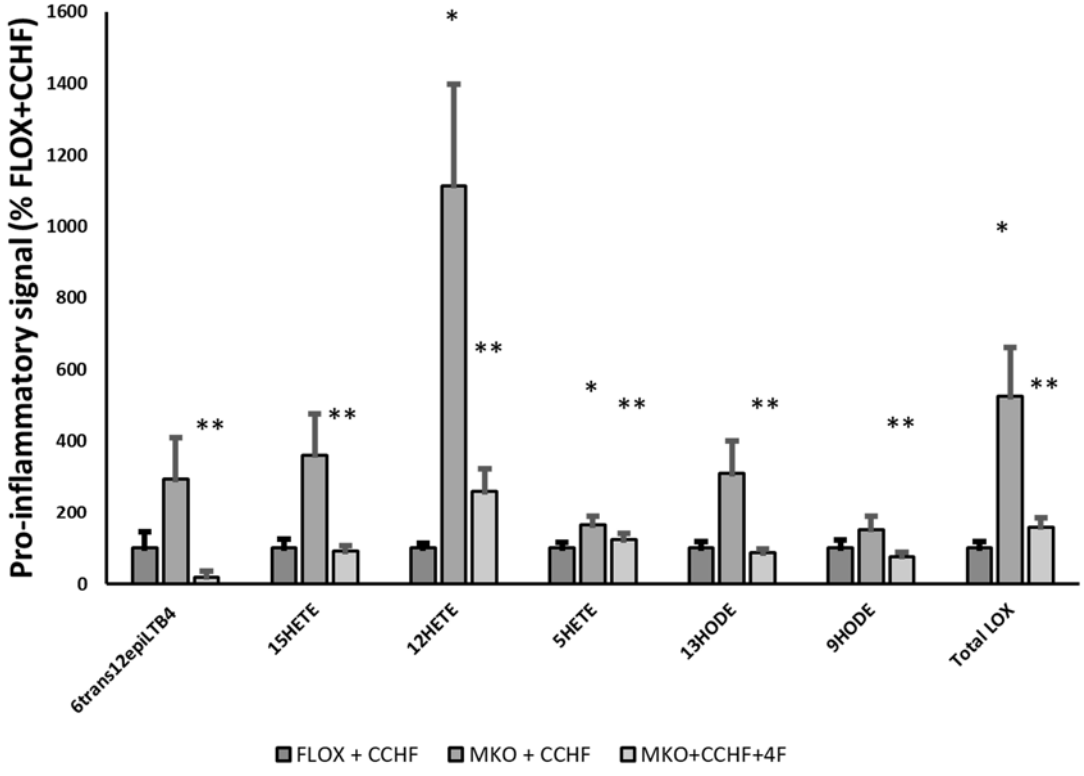
Pro-inflammatory signal (% FLOX+CCHF)
1600
1400
1200
1000
800
600
400
200
0
6trans12epiLTB4
15HETE
12HETE
5HETE
13HODE
9HODE
Total LOX
FLOX + CCHF
MKO + CCHF
MKO+CCHF+4F

G

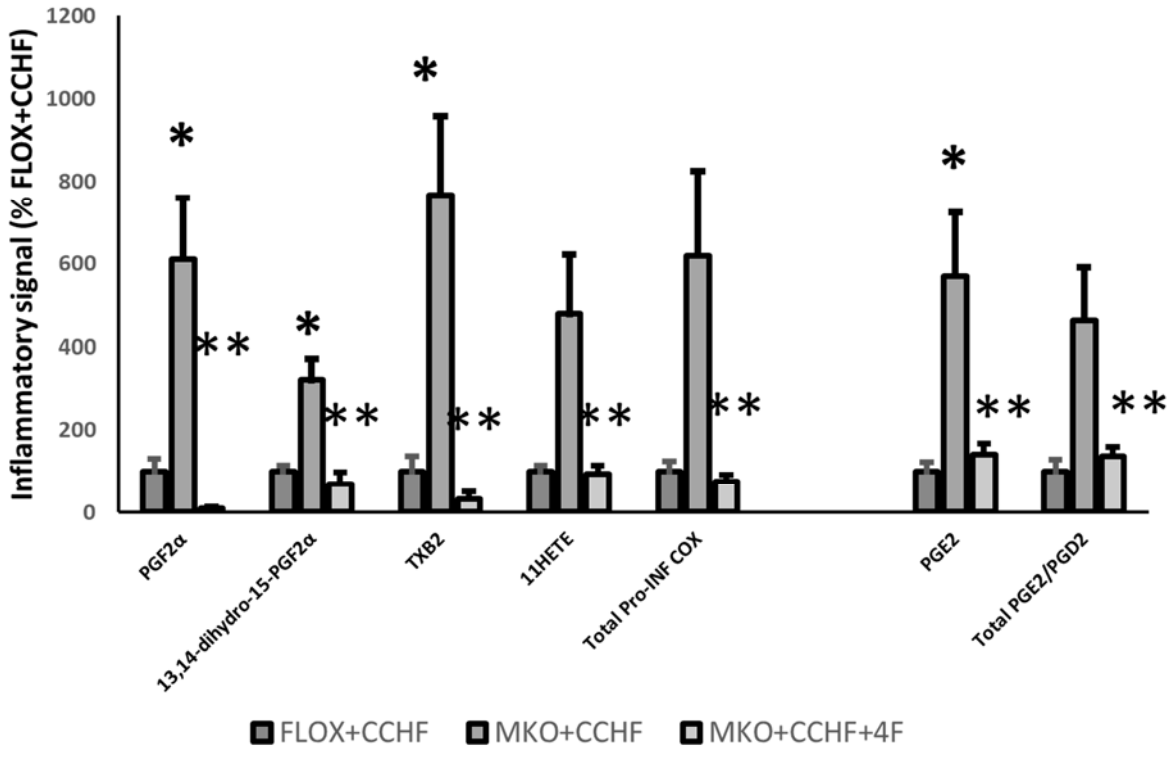
Inflammatory signal (% FLOX+CCHF)
1200
1000
800
600
400
200
0
PGF2α
13,14-dihydro-15-PGF2α
TXB2
11HETE
Total Pro-INF COX
PGE2
Total PGE2/PGD2
FLOX+CCHF
MKO+CCHF
MKO+CCHF+4F

Figure 3-5

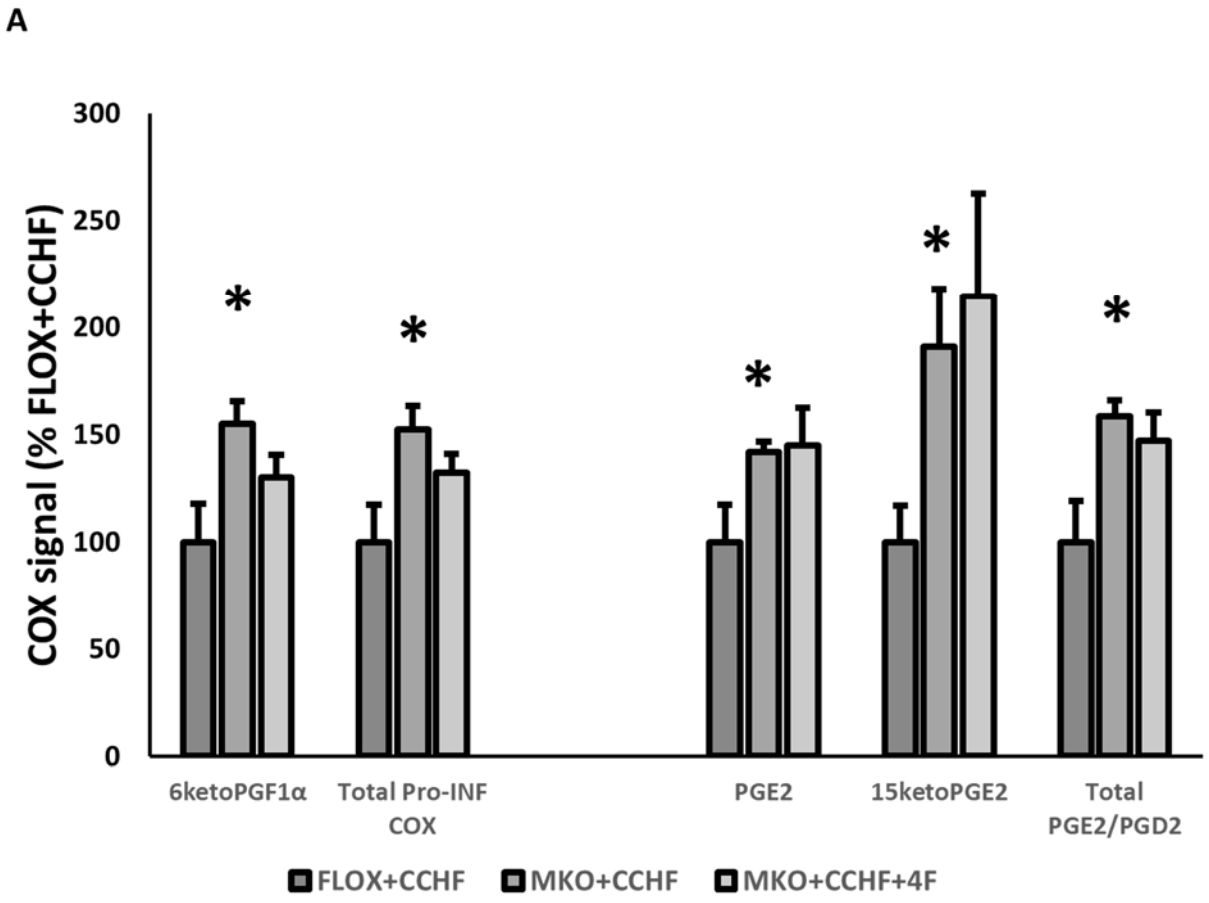
A
COX signal (% FLOX+CCHF)
300
250
200
150
100
50
0
*
*
*
*
*
6ketoPGF1α
Total Pro-INF COX
PGE2
15ketoPGE2
Total PGE2/PGD2
FLOX+CCHF
MKO+CCHF
MKO+CCHF+4F

B

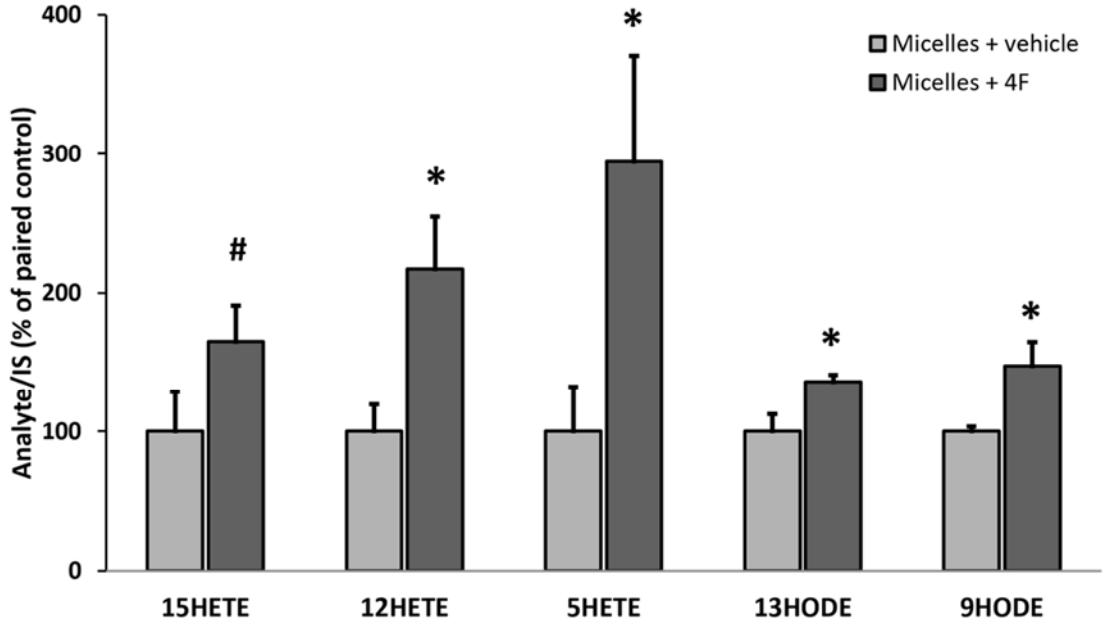
400
300
200
100
0
Analyte/IS (% of paired control)
Micelles + vehicle
Micelles + 4F
#
*
*
*
*
15HETE
12HETE
5HETE
13HODE
9HODE

C

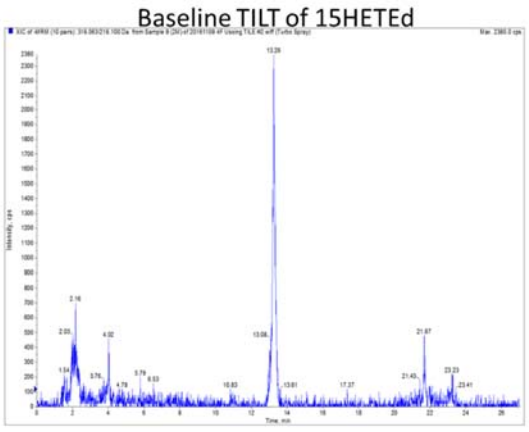
Baseline TILT of 15HETEd

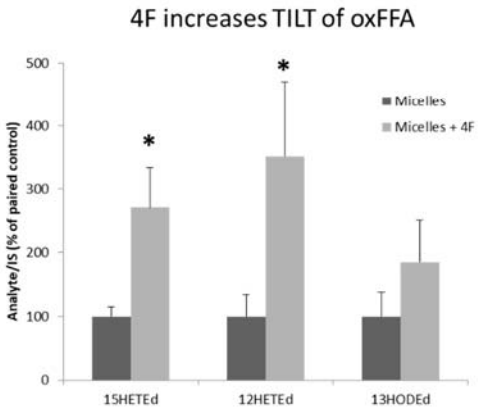
4F increases TILT of oxFFA
Analyte/IS [% of paired control)
500
400
300
200
100
0
*
*
Micelles
Micelles + 4F
15HETEd
12HETEd
13HODEd

A

- IL10$^{-/-}$ mice (approx. 3-4 months of age) were treated with the COX inhibitor piroxicam for 9 days to induce colitis. Colitis was assessed at day 14.
- Mice receiving **D-4F** in drinking water (**500 ug/ml**) were pre-treated for 7 days and were treated across the entire 14 day induction of colitis.

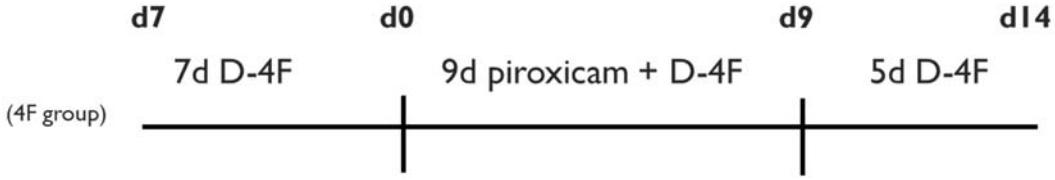

- Groups: **IL10 only**
  IL10 + piroxicam
  IL10 + piroxicam + 4F

B

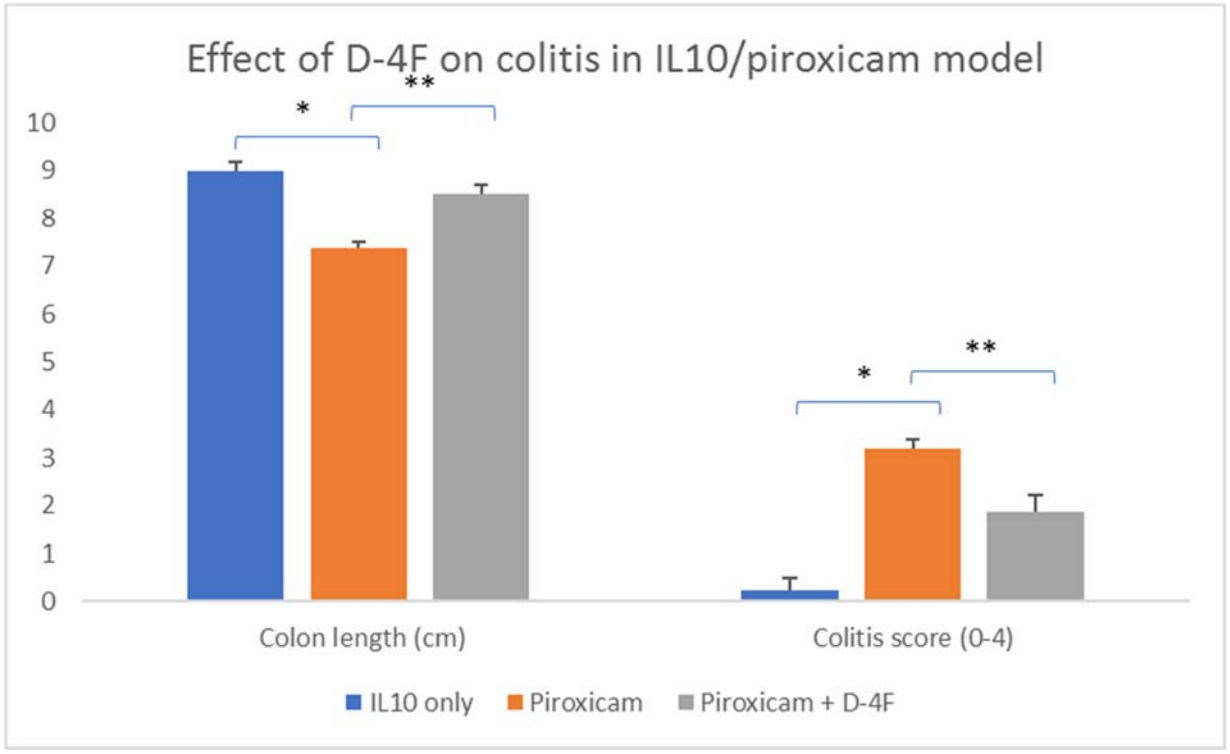
Effect of D-4F on colitis in IL10/piroxicam model
10
9
8
7
6
5
4
3
2
1
0
*
**
*
**
Colon length (cm)
Colitis score (0-4)
IL10 only
Piroxicam
Piroxicam + D-4F

C

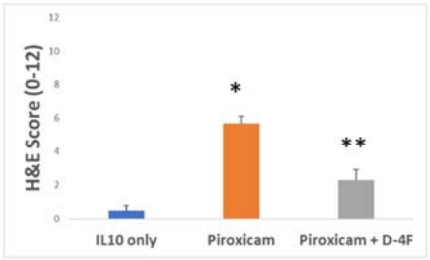
H&E Score (0-12)
12
10
8
6
4
2
0
*
**
IL10 only
Piroxicam
Piroxicam + D-4F

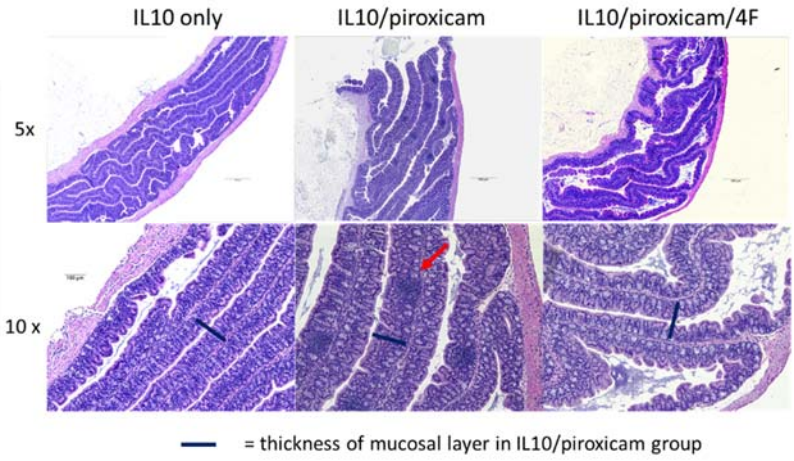
IL10 only
IL10/piroxicam
IL10/piroxicam/4F
5x
10 x
= thickness of mucosal layer in IL10/piroxicam group

D

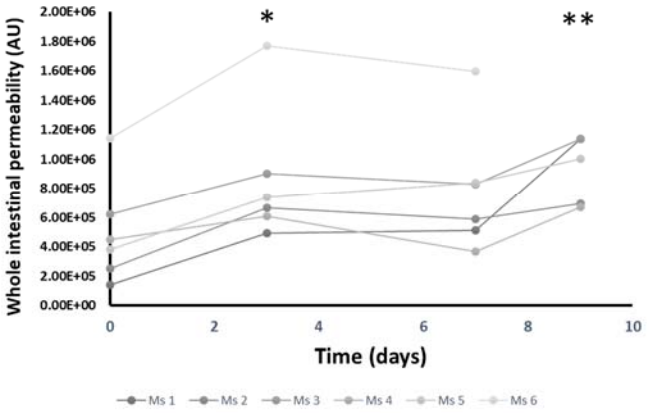

Paired TTest

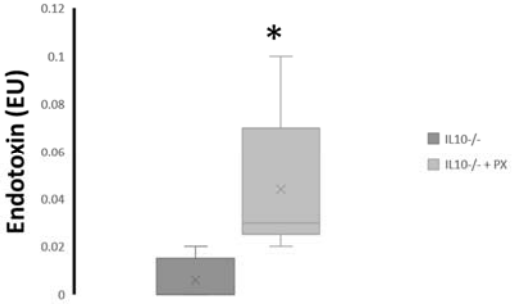

Unpaired TTest

E

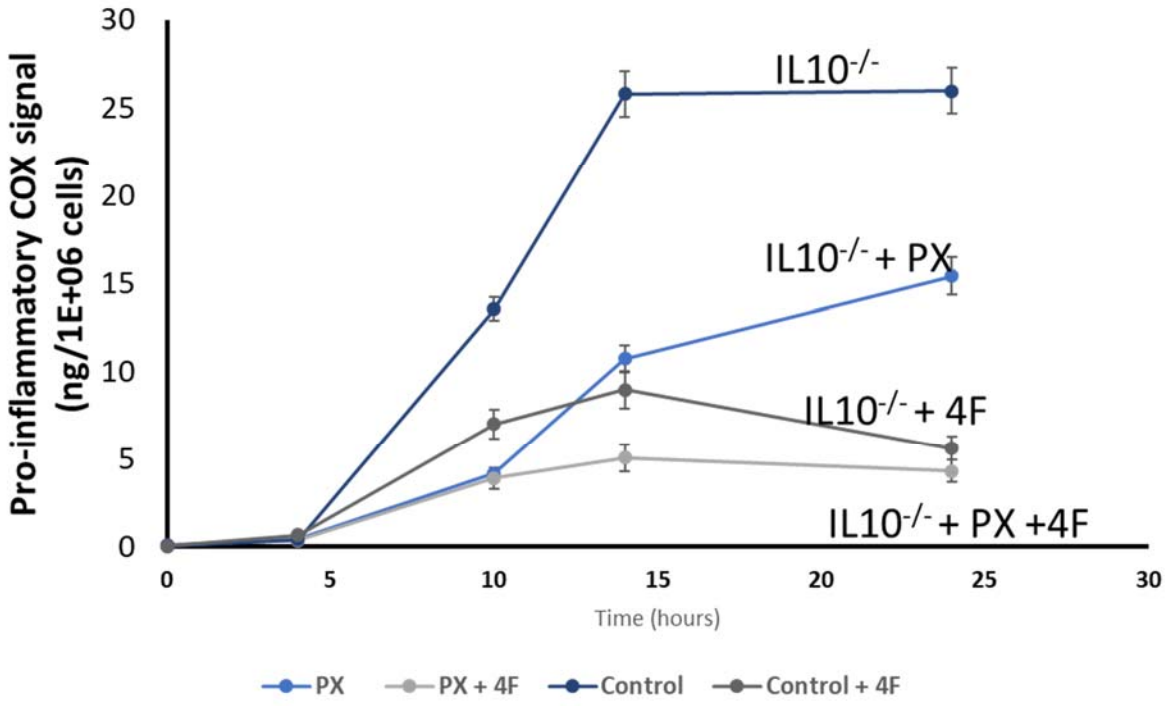
Pro-inflammatory COX signal (ng/1E+06 cells)
30
25
20
15
10
5
0
0
5
10
15
20
25
30
Time (hours)
IL10-/-
IL10-/- + PX
IL10-/- + 4F
IL10-/- + PX +4F
PX
PX + 4F
Control
Control + 4F

F

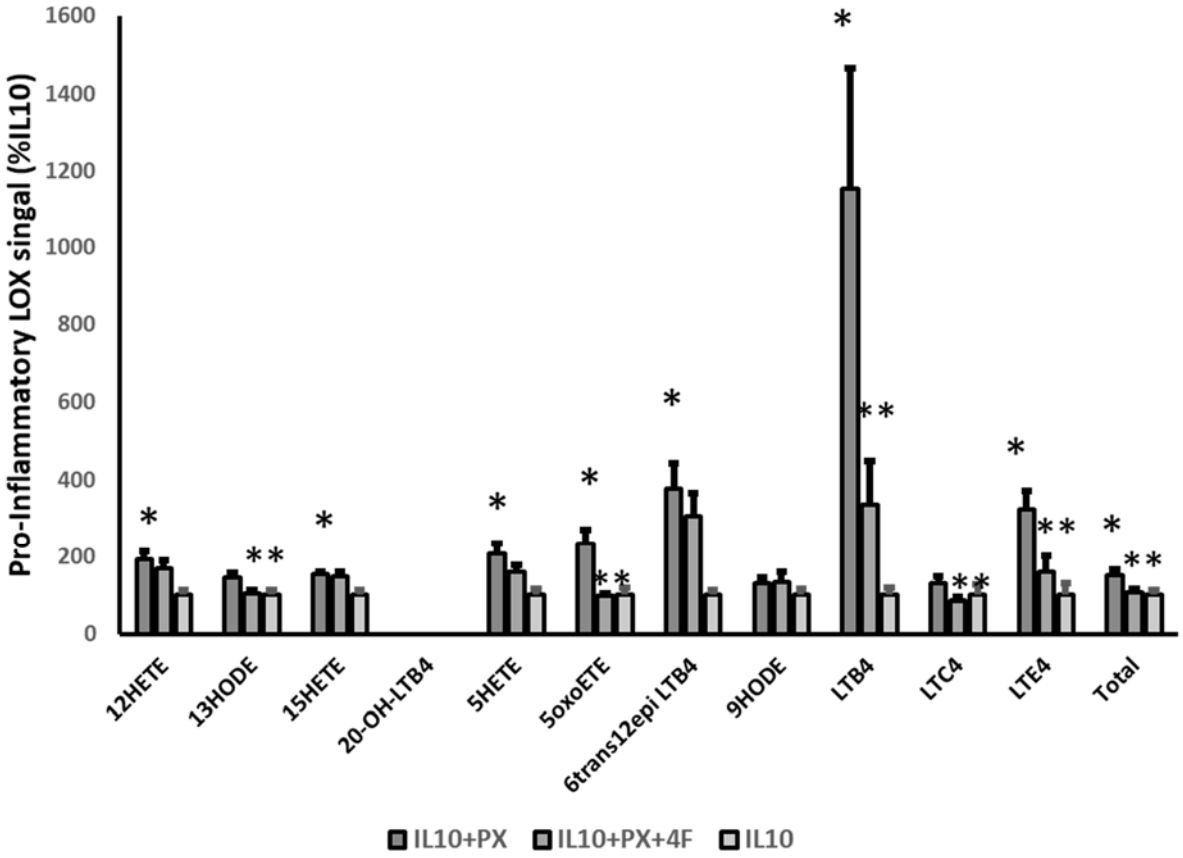
Pro-Inflammatory LOX singal (%IL10)
1600
1400
1200
1000
800
600
400
200
0
12HETE
13HODE
15HETE
20-OH-LTB4
5HETE
5oxoETE
6trans12epi LTB4
9HODE
LTB4
LTC4
LTE4
Total
IL10+PX
IL10+PX+4F
IL10

G

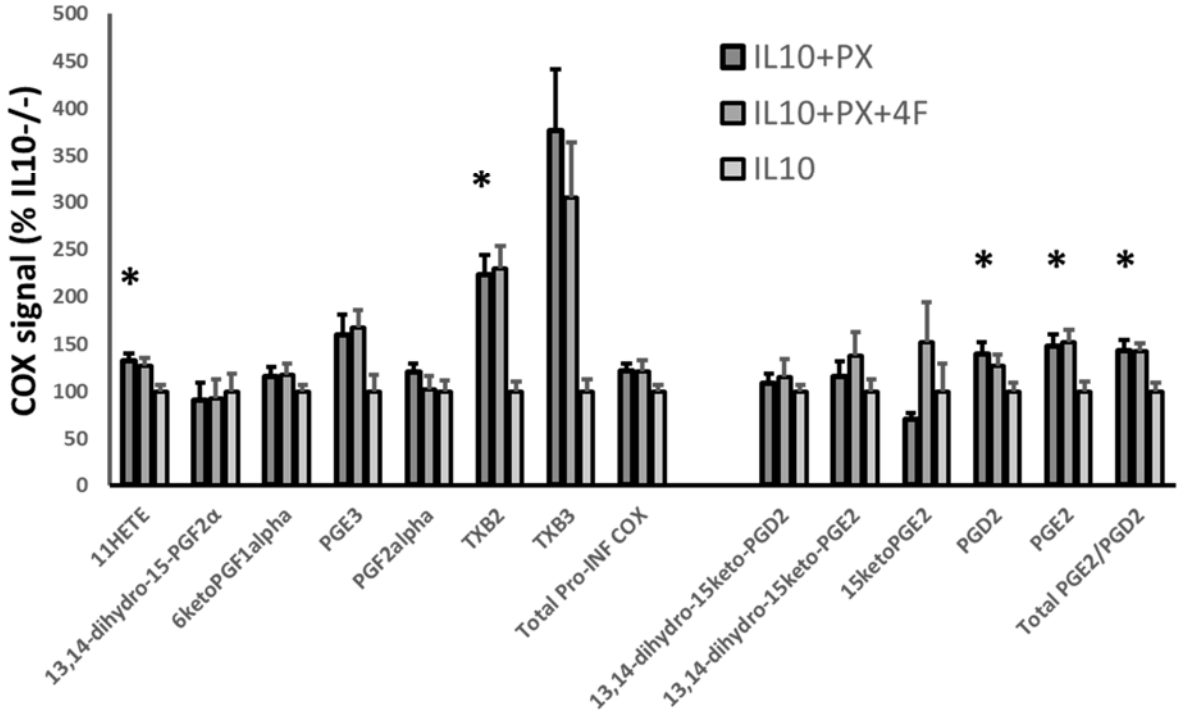
COX signal (% IL10-/-)
500
450
400
350
300
250
200
150
100
50
0
IL10+PX
IL10+PX+4F
IL10
*
*
*
*
*
11HETE
13,14-dihydro-15-PGF2α
6ketoPGF1alpha
PGE3
PGF2alpha
TXB2
TXB3
Total Pro-INF COX
13,14-dihydro-15keto-PGD2
13,14-dihydro-15keto-PGE2
15ketoPGE2
PGD2
PGE2
Total PGE2/PGD2

Table 3-1

Analyte	Precursor	Status	Function
Anti-INF COX			
Δ12-PGJ2	AA, PGD2, PGJ2	bioactive, *PGD2/J2 marker*	Anti-INF: PPARgamma agonist; *PGD2/J2/15dPGJ2 marker*
15-deoxy-Δ12,14-PGJ2	AA, PGJ2	bioactive	Anti-INF: negative regulator of NFkB, PPARgamma agonist, Nrf2 activator
PGE2-PGD2			
PGE2	AA	bioactive	Pro-INF: vascular leakage; pro-RES: class-switching
PGD2	AA	bioactive	Pro-INF: PMN chemotaxis through DP1 DP2; pro-RES: class-switching; anti-INF: Nrf2 activator
Pro-INF COX products			
[PGI2]	AA	[bioactive but unstable]	Pro-INF: vasodilation
PGF2alpha	AA	bioactive**, unstable**	Pro-INF: RA, ath
[TXA2]	AA	[bioactive but unstable]	Pro-INF: microvascular constriction, PMN adherence (overall:vasoconstriction and platelet aggregation)
TXB2	AA, TXA2	bioactive, *TXA2 product*	Pro-INF: PMN chemotaxis and adherence (maybe through TXA2)
11HETE	AA	bioactive, *COX pathway marker*	Pro-INF: leukocyte regulation; *COX activity marker*
PGE3	EPA	bioactive	Pro-INF: induce COX2 and IL6 in macrophage
TXB3	EPA	bioactive but less than TXA2/B2, *TXA3 product*	Pro-INF: induce COX2 and IL6 in macrophage
Pro-INF LOX products			
LTB4	AA, LTA4	bioactive	Pro-INF: vascular leakage; leukocyte chemotaxis and adhesion
LTC4	AA, LTA4	bioactive, *glutathione conjugate of LTA4*	Pro-INF: vascular permeability (macrophage product)
5HETE	AA	bioactive*; pathway marker, 5LOX*	pro-INF: PMN chemotaxis and degranulation
12HETE	AA	bioactive	pro-INF: neutrophil chemotaxis and adhesion
15HETE	AA	bioactive*; pathway marker, LX*	pro-INF: activator of LT biosynthesis; *LX pathway marker*
5-oxoETE	AA,5HETE (dehydrogenase)	bioactive	pro-INF: PMN chemotaxis and degranulation
13HODE	LA	bioactive	pro-INF: PMN chemotaxis
9HODE	LA	bioactive	pro-INF: PMN chemotaxis
Pro-RES LOX products			
LXA4	AA; 15HETE[5LOX]; LTA4[15	bioactive	pro-RES and anti-INF: promote M1 to M2; NFkB negative regulator; inhibit neutrophil chemotaxis and adhesion
LXB4	AA	bioactive	pro-RES and anti-INF: promote M1 to M2; NFkB negative regulator; inhibit neutrophil chemotaxis and adhesion
MaR1	DHA;	bioactive	pro-RES; tissue regeneration; M1 to M2; inhibit neutrophil migration; increase efferocytosis
RvD1	DHA[15LOX,5LOX]	bioactive	pro-RES: limit neutrophil infiltration
RvD2	DHA	bioactive	pro-RES: enhanace survival in sepsis; protect against colitis
RvD3	DHA	bioactive	pro-RES: limit leukocyte migration, enhance macrophage efferocytosis
RvD4	DHA	bioactive	pro-RES: limit leukocyte migration, enhance macrophage efferocytosis
RvD5	DHA	bioactive	pro-RES: enhance bacterial containment and phagocytosis
PDx (10S,17S-DiHDHA)	DHA	bioactive	pro-RES: inhibit neutrophil infiltration and platelet aggregation
RvE1	EPA	bioactive	pro-RES: reduce PMN infiltration; promote resolution in colitis model

Table 3-2

Pro-inflammatory LOX														
		LTE4	**LTC4**	**LTB4**	**6trans12epi LTB4**	**20-OH-LTB4**	**15HETE**	**12HETE**	**5HETE**	**5oxoETE**	**13HODE**	**9HODE**	**Total**	
MKO+CHOW	**AVG**	**3.25**	**0.15**	**0.18**	**1.44**	**ND**	**40.81**	**107.96**	**13.39**	**10.61**	**681.26**	**212.20**	**1071.25**	
	SEM	2.36	0.08	0.07	0.21		4.93	15.18	3.96	2.69	82.21	35.07	90.95	
FLOX+CCHF	**AVG**	**3.98**	**0.02**	**0.52**	**5.58$**	**ND**	**52.95**	**240.10**	**21.30**	**15.04**	**511.51**	**154.31**	**965.84**	
	SEM	1.76	0.02	0.28	1.82		9.42	53.70	6.52	4.83	87.30	23.69	105.95	
MKO+CCHF	**AVG**	**2.34**	**0.11**	**0.50**	**8.00***	**ND**	**85.13*,****	**401.23*,****	**19.30**	**9.81**	**768.60****	**213.91**	**1640.09*,****	
	SEM	0.34	0.07	0.16	1.67		6.96	49.51	2.62	1.79	80.23	27.04	98.39	
Pro-inflammatory COX														
		PGF2α	**13,14-dihydro-15-PGF2α**	**6ketoPGF1α**	**TXB2**	**11HETE**	**TXB3**	**PGE3**	**Total**					
MKO+CHOW	**AVG**	**13.95**	**3.05**	**885.35**	**28.27**	**302.95**	**0.53**	**2.42**	**1236.39**					
	SEM	3.13	1.69	214.45	10.16	83.88	0.13	0.67	189.26					
FLOX+CCHF	**AVG**	**23.47**	**3.58**	**874.68**	**41.63**	**208.46**	**0.20***	**0.89***	**1152.93**					
	SEM	6.43	0.47	155.46	10.71	28.54	0.06	0.18	158.55					
MKO+CCHF	**AVG**	**29.15***	**4.80**	**1355.14*,****	**70.41***	**346.85**	**0.32**	**1.55****	**1755.11*,****					
	SEM	2.57	1.04	92.25	11.55	57.39	0.06	0.20	109.29					
PGE2/PGD2														
		PGE2	**13,14-dihydro-15keto-PGE2**	**15ketoPGE2**	**13,14-dihydro-15keto-PGD2**	**PGD2**	**Total**							
MKO+CHOW	**AVG**	**130.10**	**18.66**	**4.82**	**0.00**	**22.97**	**173.31**							
	SEM	22.82	9.01	0.44	0.00	8.16	38.73							
FLOX+CCHF	**AVG**	**154.85**	**26.59**	**3.00***	**0.43***	**67.82**	**259.71**							
	SEM	27.19	7.08	0.51	0.11	20.35	49.33							
MKO+CCHF	**AVG**	**219.60*,****	**39.75**	**5.72****	**0.61***	**109.33***	**412.12*,****							
	SEM	7.25	8.48	0.81	0.13	14.88	18.50							
Anti-inflammatory COX														
		PGJ2	**Δ12-PGJ2**	**15d-PGJ2**	**Total**									
MKO+CHOW	**AVG**	**0.31**	**0.35**	**0.20**	**0.85**									
	SEM	0.06	0.05	0.04	0.12									
FLOX+CCHF	**AVG**	**2.02***	**1.58***	**0.64**	**4.25***									
	SEM	0.56	0.40	0.20	1.14									
MKO+CCHF	**AVG**	**2.55***	**2.01***	**0.90***	**5.47***									
	SEM	0.32	0.25	0.12	0.62									
Pro-resolving LOX														
		LXA4	**LXB4**	**14HDHA**	**MaR1-**	**17HDHA**	**PDx**	**RVD1**	**RVD2**	**RVD3**	**RVD4**	**RVD5**	**RVE1**	**Total**
MKO+CHOW	**AVG**	**0.152**	**0.733**	**56.156**	**0.845**	**27.671**	**1.853**	**0.016**	**ND**	**ND**	**ND**	**0.233**	**ND**	**86.71**
	SEM	0.050	0.063	2.636	0.066	1.744	0.057	0.006				0.012		3.88
FLOX+CCHF	**AVG**	**0.31$**	**0.991**	**55.139**	**1.945**	**30.669**	**3.349**	**0.015**	**ND**	**ND**	**ND**	**0.346**	**ND**	**92.67**
	SEM	0.039	0.180	10.156	0.644	6.343	0.898	0.004				0.093		18.11
MKO+CCHF	**AVG**	**0.16****	**1.127**	**60.143**	**1.668**	**26.294**	**3.261**	**0.006&**	**ND**	**ND**	**ND**	**0.476**	**ND**	**74.92**
	SEM	0.015	0.229	5.691	0.414	5.571	0.713	0.003				0.100		18.91

Table 3-3

Pro-inflammatory LOX														
		LTE4	**LTC4**	**LTB4**	**6trans12 epiLTB4**	**20OH-LTB4**	**15HETE**	**12HETE**	**5HETE**	**5oxoETE**	**13HODE**	**9HODE**	**Total**	
MKO+CHOW	**AVG**	**ND**	**ND**	**ND**	**0.01**	**ND**	**0.26**	**19.94**	**0.36**	**0.06**	**16.41**	**3.56**	**34.00**	
	SEM				0.00		0.03	2.12	0.06	0.01	2.28	0.61	5.34	
FLOX+CCHF	**AVG**	**ND**	**ND**	**ND**	**0.02**	**ND**	**0.30**	**6.19***	**0.53**	**0.15**	**24.03**	**6.67**	**30.00**	
	SEM				0.01		0.08	0.89	0.09	0.04	4.38	1.54	5.15	
MKO+CCHF	**AVG**	**ND**	**ND**	**ND**	**0.04**	**ND**	**1.07**	**69.00*,****	**0.88*,****	**0.16***	**74.55**	**10.15***	**157.42*,****	
	SEM				0.02		0.34	17.55	0.12	0.05	21.71	2.50	40.95	
Pro-inflammatory COX														
		PGF2α	**13,14-dihydro-15-PGF2α**	**6ketoPGF1α**	**TXB2**	**11HETE**	**TXB3**	**PGE3**	**Total**					
MKO+CHOW	**AVG**	**0.04**	**0.02**	**0.13**	**2.56**	**1.23**	**ND**	**ND**	**3.98**					
	SEM	0.02	0.01	0.02	0.44	0.14			0.60					
FLOX+CCHF	**AVG**	**0.03**	**0.04**	**0.08**	**0.91**	**0.95**	**ND**	**ND**	**1.96***					
	SEM	**0.008**	0.01	0.01	0.32	0.12			0.46					
MKO+CCHF	**AVG**	**0.17*,****	**0.12*,****	**1.78**	**6.96****	**4.54[&]**	**ND**	**ND**	**12.13[&]**					
	SEM	0.04	0.02	0.82	1.74	1.35			4.04					
PGE2/PGD2														
		PGE2	**13,14-dihydro-15keto-PGE2**	**15ketoPGE2**	**13,14-dihydro-15keto-PGD2**	**PGD2**	**Total**							
MKO+CHOW	**AVG**	**0.100**	**0.062**	**0.000**	**0.000**	**0.043**	**0.21**							
	SEM	0.016	0.011	0.000	0.000	0.006	0.03							
FLOX+CCHF	**AVG**	**0.044**	**0.035**	**0.000**	**0.000**	**0.031**	**0.11**							
	SEM	0.010	0.016	0.000	0.000	0.006	0.03							
MKO+CCHF	**AVG**	**0.25****	**0.092**	**0.006**	**0.032**	**0.121**	**0.51[&]**							
	SEM	0.068	0.033	0.004	0.023	0.034	0.14							
Anti-inflammatory COX														
		PGJ2	**Δ12-PGJ2**	**15d-PGJ2**	**Total**									
MKO+CHOW	**AVG**	**ND**	**ND**	**ND**	**ND**									
	SEM													
FLOX+CCHF	**AVG**	**ND**	**ND**	**ND**	**ND**									
	SEM													
MKO+CCHF	**AVG**	**ND**	**ND**	**ND**	**ND**									
	SEM													
Pro-resolving LOX														
		LXA4	**LXB4**	**14HDHA**	**MaR1**	**17HDHA**	**PDx**	**RVD1**	**RVD2**	**RVD3**	**RVD4**	**RVD5**	**RVE1**	**Total**
MKO+CHOW	**AVG**	**ND**	**ND**	**3.62**	**ND**	**0.21**	**0.01**	**0.01**	**ND**	**ND**	**ND**	**ND**	**ND**	**3.86**
	SEM			0.53		0.04	0.01	0.00						0.57
FLOX+CCHF	**AVG**	**ND**	**ND**	**2.68**	**ND**	**0.28**	**0.01**	**0.01**	**ND**	**ND**	**ND**	**ND**	**ND**	**2.98**
	SEM			1.43		0.08	0.01	0.00						1.50
MKO+CCHF	**AVG**	**ND**	**ND**	**3.88**	**ND**	**0.40**	**0.03**	**0.01**	**ND**	**ND**	**ND**	**ND**	**ND**	**4.32**
	SEM			1.49		0.29	0.02	0.01						1.74

Table 3-4

Pro-INF LOX							***Pro-INF COX***					
	IL10+PX		IL10+PX+4F					IL10+PX		IL10+PX+4F		
	AVG	SEM	**AVG**	SEM	*TTEST*			**AVG**	SEM	**AVG**	SEM	*TTEST*
20-OH-LTB4	**ND**		**ND**				**6ketoPGF1α**	**0.08**	0.06	**0.02**	0.00	0.319
LTC4	**0.03**	0.00	**0.00**	0.00	3.05E-06		**TXB3**	**ND**		**ND**		
LTE4	**0.02**	0.00	**0.00**	0.00	2.42E-05		**TXB2**	**1.41**	0.52	**0.67**	0.27	0.270
6trans12epi LTB4	**2.71**	1.90	**0.07**	0.01	0.159		**PGE3**	**ND**		**ND**		
LTB4	**ND**		**ND**				**PGF2α**	**0.17**	0.04	**0.05**	0.01	0.043
13HODE	**86.81**	32.72	**15.37**	1.51	0.037		**13,14-dihydro-15-PGF2α**	**0.03**	0.00	**0.01**	0.00	0.041
9HODE	**82.48**	35.90	**12.76**	1.72	0.054		**11HETE**	**7.63**	4.09	**0.88**	0.16	0.164
15HETE	**10.13**	4.96	**1.22**	0.17	0.116		**Total**	**9.28**	3.95	**1.63**	0.33	0.109
12HETE	**34.95**	8.19	**8.72**	2.12	0.004							
5HETE	**33.05**	15.77	**5.82**	1.12	0.110		***Pro-RES LOX***					
5-oxoETE	**1.06**	0.62	**0.11**	0.02	*0.059*			IL10+PX		IL10+PX+4F		
Total	**154.83**	49.41	**43.93**	4.93	0.033			**AVG**	SEM	**AVG**	SEM	*TTEST*
							RvE1	**ND**		**ND**		
PGE2/PGD2							**RvD3**	**ND**		**ND**		
	IL10+PX		IL10+PX+4F				**LXB4**	**ND**		**ND**		
	AVG	SEM	**AVG**	SEM	*TTEST*		**RvD2**	**ND**		**ND**		
PGE2	**0.36**	0.17	**0.07**	0.01	0.144		**LXA4**	**0.36**	0.18	**0.07**	0.01	0.176
PGD2	**0.34**	0.16	**0.07**	0.01	0.143		**15epi-LXA4**	**0.26**	0.12	**0.05**	0.01	0.140
15ketoPGE2	**0.04**	0.01	**0.02**	0.00	0.029		**RvD1**	**0.13**	0.06	**0.02**	0.00	0.110
13,14-dihydro-15keto-PGE2	**ND**		**ND**				**RvD4**	**ND**		**ND**		
13,14-dihydro-15keto-PGD2	**0.13**	0.05	**0.02**	0.00	*0.095*		**MaR1-**	**2.67**	1.52	**0.05**	0.02	0.147
Total	**0.84**	0.38	**0.42**	0.13	0.134		**PDx**	**3.22**	1.85	**0.07**	0.02	0.151
							RvD5	**2.11**	1.11	**0.10**	0.02	0.131
Anti-INF COX							**17HDHA**	**14.49**	1.95	**6.52**	1.46	0.027
	IL10+PX		IL10+PX+4F				**14HDHA**	**11.17**	2.23	**4.42**	0.72	0.036
	AVG	SEM	**AVG**	SEM	*TTEST*		**Total**	**26.44**	4.22	**10.97**	4.48	0.03
PGJ2	**0.03**	0.00	**0.02**	0.00	0.166							
Δ12-PGJ2	**0.98**	0.45	**0.18**	0.03	0.138							
15-deoxy-Δ12,14-PGJ2	**ND**		**ND**									
Total	**9.914**	4.579	**1.833**	0.293	0.139							

Supplemental Legends

Supplemental Figure 3-1. CCHF increases barrier permeability in both COX TKO and WT mice. Both COX2 TKO (COX2 KO) and litter-mate control mice (WT) were challenged with CCHF diet over 16 days. Barrier permeability was determined in the same mice over time by measuring via LC-MS/MS the level of sucralose excreted in urine over 24 hrs following oral gavage. Permeability significantly increased in both groups over the first 4 days (*, $p < 0.001$). By day 16, permeability had improved in WT mice compared to COX2 TKO (**, $p < 0.01$).

Supplemental Figure 3-2. Cholate and deoxycholate affect barrier permeability equally in both COX2 TKO and WT mice. COX2 TKO and WT were pre-treated with antibiotics and then a chow diet containing either cholate or deoxycholate (0.5% w/w) while antibiotics were continued. Barrier permeability was determined at multiple time points by measuring via LCMSMS the urinary excretion of lactulose and mannitol. Both diets affected all mice equally through 10 days, with the barrier permeability of all groups significantly elevated from time 0 (*, $p< 0.001$). Permeability was not significantly different between any groups through day 10. At day 14, barrier permeability for WT mice fed either cholate or deoxycholate improved compared to the respective COX2 TKO control (**, $p < 0.05$).

Supplemental Figure 3-3. MyD88 inhibition rescued intestinal inflammation in COX2 TKO mice as assessed by histological score. COX2 TKO and WT mice were fed CCHF diet for 14 days and treated with either vehicle or the MyD88 inhibitor T6167923 3x/wk i.p. (250 ug/injection). MyD88 inhibition significantly suppressed the development of inflammation in the ileo-ceco-colic junctions of COX2 TKO mice (*, $p < 0.001$).

Supplemental Figure 3-4. COX2 MKO mice develop severe inflammation in their ileo-ceco-colic junctions when challenged with CCHF diet for 7-10 weeks. COX2 MKO (MKO) and floxed control mice (FLOX) mice were fed CCHF for 10 weeks. CCHF induced severe inflammation in the ileo-ceco-colic junctions of MKO mice, while neither FLOX+CCHF nor MKO+CHOW developed intestinal inflammation (representative images).

Supplemental Figure 3-5. COX2 MKO suppresses the levels of COX metabolites including 15d-PGJ2 in LPS-activated BMDM. BMDM were isolated from FLOX and COX2 MKO mice and activated with LPS (25 ng/ml). At various time points, lysate was collected, lipids were extracted, and the levels of COX inflammatory mediators was determined by LC-MS/MS (see Figure 2 and Supplemental Methods for details). Consistent with the loss of myeloid COX2, total COX inflammatory mediators (*left panel*) were significantly suppressed at all time points (*, $p < 0.01$). NFkB negative regulator 15d-PGJ2 was also significantly suppressed by COX2 MKO at all time points from 10 hours (*, $p < 0.01$) (*right panel*).

Supplemental Figure 3-6. Liquid chromatography provides good peak resolution and separation of all lipid analytes measured in this study. The complete chromatogram of all analytes of the lipid inflammatory mediator panel are given herein. The LC method is overlaid on the elution pattern, and examples of classes of compounds eluted in the distinct phases of the method are detailed. Sterically hindered and hydrophilic compounds are eluted first, with more hydrophobic compounds requiring increasing strength of the elution solvent to be pushed off the column.

Supplemental Figure 3-7. D-4F completely protected COX2 MKO mice on CCHF from disease-induced mortality. Through 10 weeks, only 8 of 14 COX2 MKO mice on CCHF diet survived, while all 14 of 14 mice receiving oral D-4F were protected from disease-induced mortality during this time frame.

Supplemental Figure 3-8. Tg6F protects against intestinal inflammation in COX2 MKO mice on CCHF diet. COX2 MKO mice were challenged with CCHF for 8.5 weeks, and the effect of Tg6F on intestinal inflammation was determined. Tg6F protected against inflammation in the ileo-ceco-colic junctions, as here represented by H&E images.

Supplemental Figure 3-9. Bone marrow cells differentiate to F4/80+ macrophages after 6 days treatment with MCSF. Bone marrow was isolated from a COX2 MKO mouse and cultured for six days in the presence of 25 ng/ml rMCSF. After six days, living cells were FACS analyzed for expression of F4/80. In this instance, 86% of cells were F4/80+.

Supplemental Figure 3-10. Total inflammatory LOX mediator level is unaffected by LPS, COX2 KO, and 4F co-treatment. Both COX2 MKO and FLOX BMDM were activated with LPS and co-treated with 4F. Total level of inflammatory pro-inflammatory LOX mediators was determined by LC-MS/MS. Total LOX mediator level remain unchanged across all conditons.

Supplemental Figure 3-11. 4F therapy lowered broad classes of plasma lipids in COX2 MKO mice challenged with CCHF. MKO mice were fed CCHF for 8.5 weeks and the effect of 4F on broad classes of plasma lipids was determined on SCIEX's Lididyzer platform. 4F significantly reduced total TAG, DAG, CE, HCER, CER, and LPE classes (for meaning of abbreviations, see main text).

Supplemental Figure 3-12. 4F does not have high binding affinity to cholate. The binding affinity between 4F and cholate was determined by surface plasmon resonance. The high-binding 15 HETE was used as a positive control. In this study, 15HETE (KD = 30 nM) is approximately 30,000 fold more avid for 4F than cholate (KD = 160 uM).

Supplemental Table 3-1. Bioactive lipids, degradation products, and pathway markers determined by LC-MS/MS. All bioactive lipids, degradation products, and pathways markers analyzed by the LC-MS/MS method explained in the Supplemental Methods are listed herein. The particular analytes, their fatty acid precursors, their statuses (bioactive, pathway marker, degradation product), and their functions (pro or anti-inflammatory or inflammation resolving, or both pro- and anti-inflammatory) are detailed.

Supplemental Table 3-2. Complete lipid panel with complete MS settings, assigned internal standards, and LC retention times. This table contains all of the optimized MS/MS settings for each analyte, together with the internal standards assigned to each lipid of interest listed in Supplementary Table 1. Isobaric compounds share a color. For compounds of the same color, specificity is generated by either unique fragment ions or by sufficient chromatographic separation. An example of an assignment of internal standards to two analytes is given.

Supplemental Table 3-3. Validation of LC-MS/MS method. Lower limit of detection (LLOD), lower limit of quantitation (LLOQ), upper limit of quantitation (ULOQ), and linearity of response are detailed for each of the analytes of interest in this method. A representative standard curve is provided.

Supplemental Table 3-4. **Precision of extractions from intestinal tissue and plasma.** Precision was determined for our sample preparation methods for intestinal tissue and plasma, with respect to all biologically available analytes within each matrix, as described in the Supplemental Methods. Precision is here reported as CV (%).

Supplemental Table 3-5. **Precision and extraction efficiency of internal standards in intestinal tissue and plasma.** Precision with respect to the area under the curve for each internal standard in both intestinal tissue and plasma was determined and reported as CV (%). Extraction efficiency for each internal standard was determined as the ratio of the recovery of 10 ng/ml IS from each matrix to the signal intensity of 10 ng/ml of each internal standard in methanol.

Supplemental Table 3-6. The effect of oral D-4F on lipid inflammatory mediators in intestinal tissue of COX2 MKO mice fed CCHF. MKO and FLOX mice were challenged with CCHF for 8.5 weeks, and the effect of 4F on the inflammatory lipid profile of MKO+CCHF mice was investigated. Intestinal lipids were extracted from MKO + chow, MKO+CCHF, MKO+CCHF+4F, and FLOX+CCHF mice (n=7/group), and lipid inflammatory mediator levels were determined as described.

Supplemental Table 3-7. The effect of oral D-4F on lipid inflammatory mediators in plasma of COX2 MKO mice fed CCHF. MKO and FLOX mice were challenged with CCHF for 8.5 weeks, and the effect of 4F on the plasma lipid inflammatory mediator profile of MKO+CCHF mice was investigated. Intestinal lipids were extracted from MKO + chow, MKO+CCHF, MKO+CCHF+4F, and FLOX+CCHF mice (n=7/group), and lipid inflammatory mediator levels were determined as described.

Supplemental Table 3-8. The effect of oral D-4F on intestinal inflammatory mediators in PAC IL10 model of colitis. Following the experiment of Figure 6A, lipids were extracted from the colons of the mice, and lipid inflammatory mediators were determined as before by LC-MS/MS. P-values are included in the table for every analyte; where $p < 0.05$, significance is marked with an underline.

Supplemental Figure 3-1

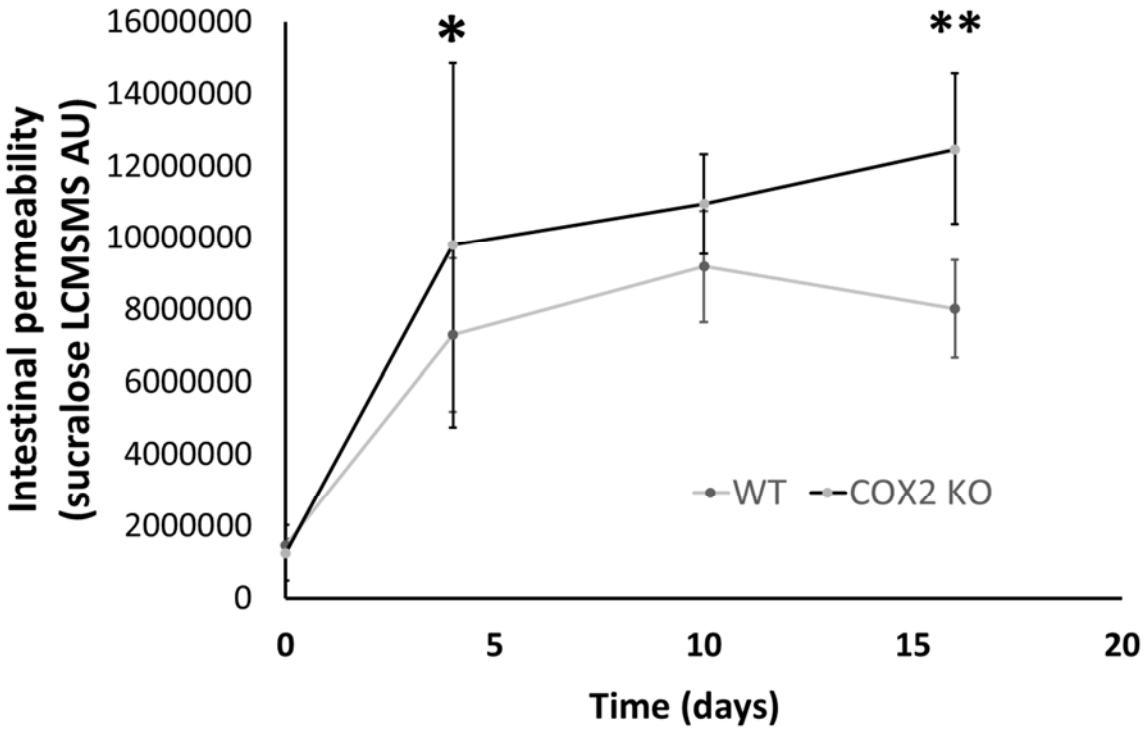

Supplemental Figure 3-2

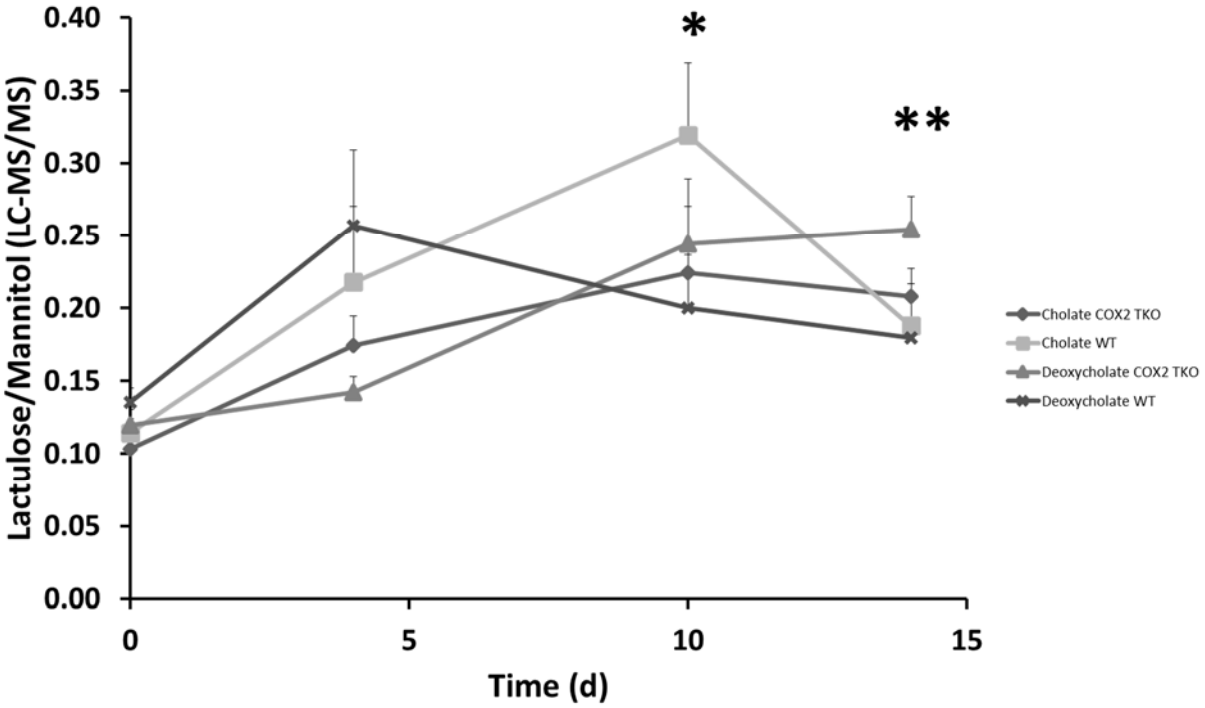

Supplemental Figure 3-3

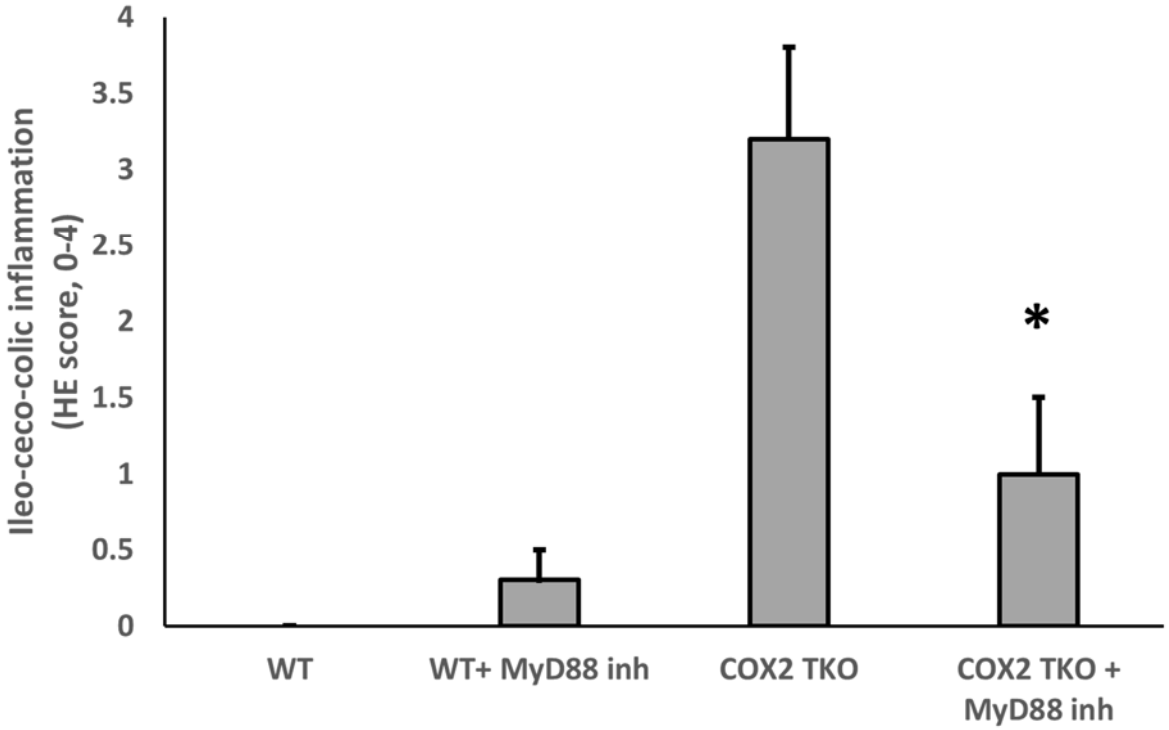

Supplemental Figure 3-4

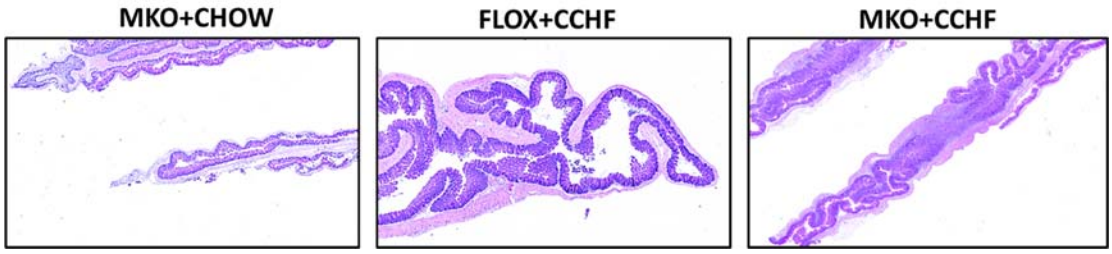

Supplemental Figure 3-5

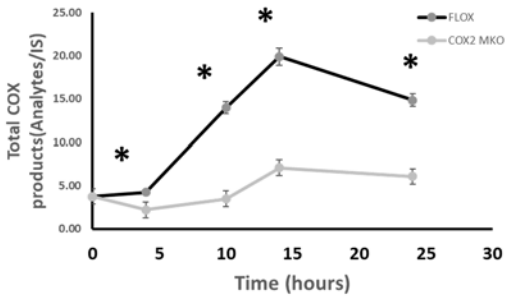

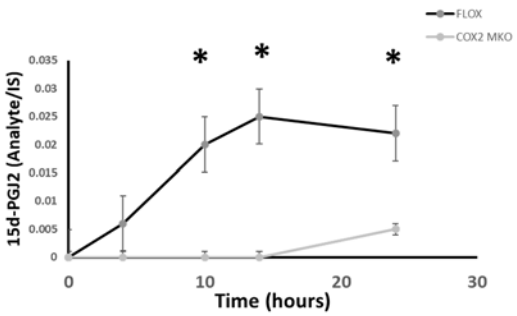

Supplemental Figure 3-6

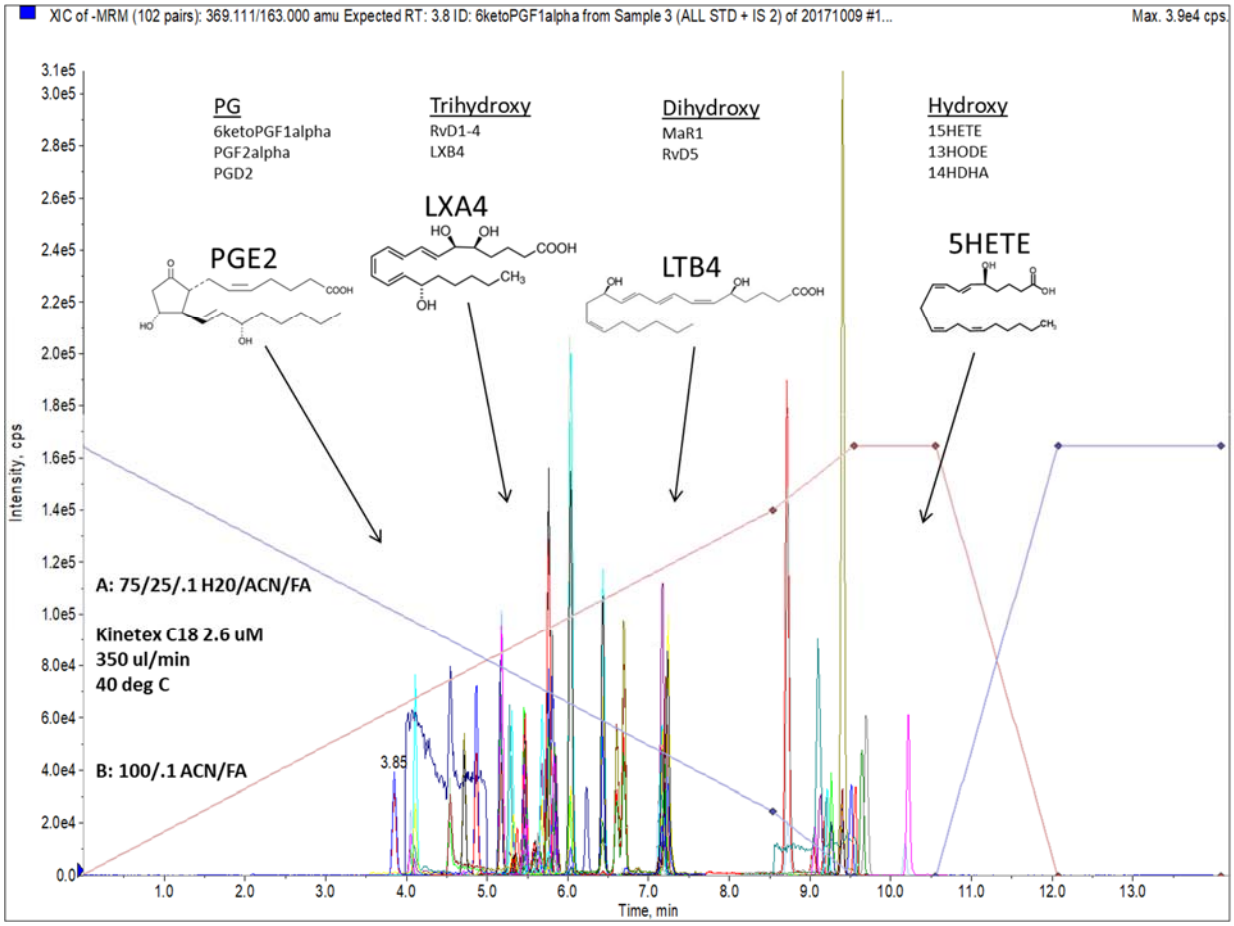

Supplemental Figure 3-7

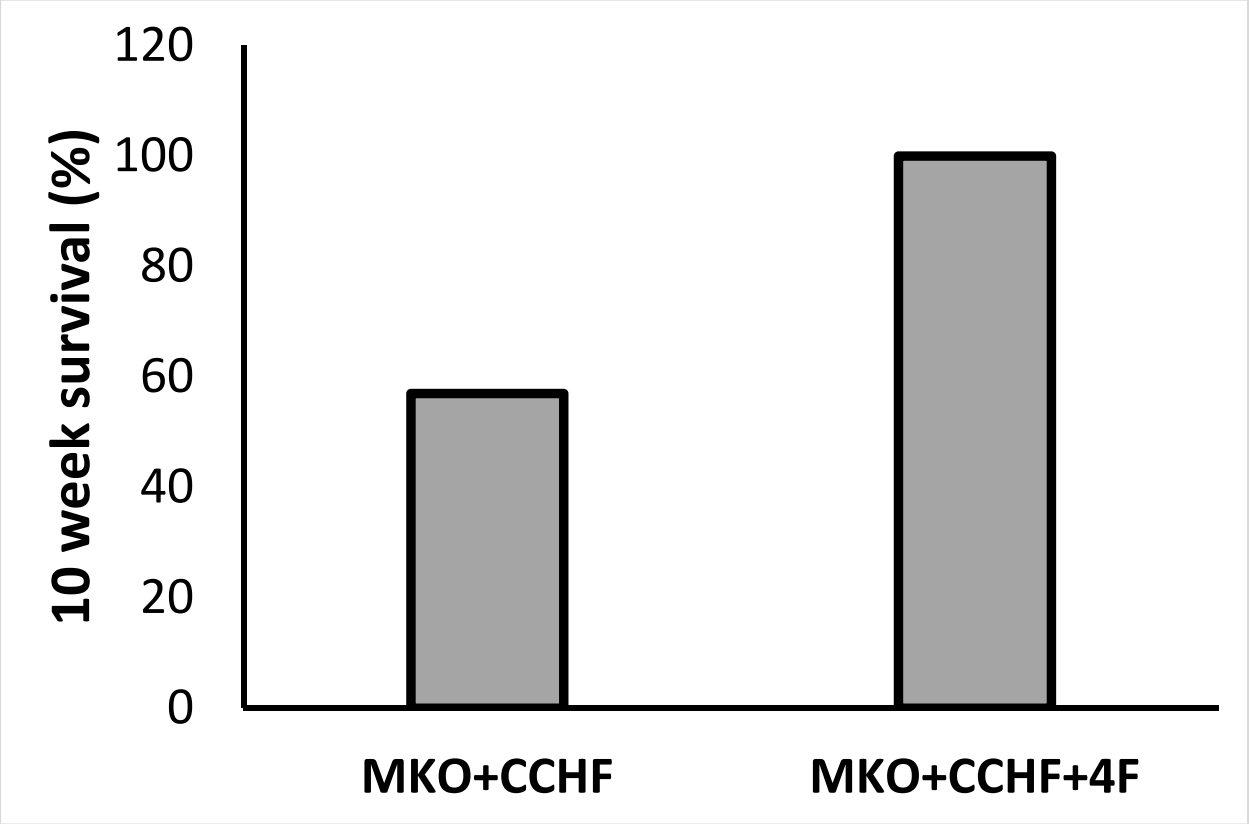

Supplemental Figure 3-8

COX2 MKO + CCHF

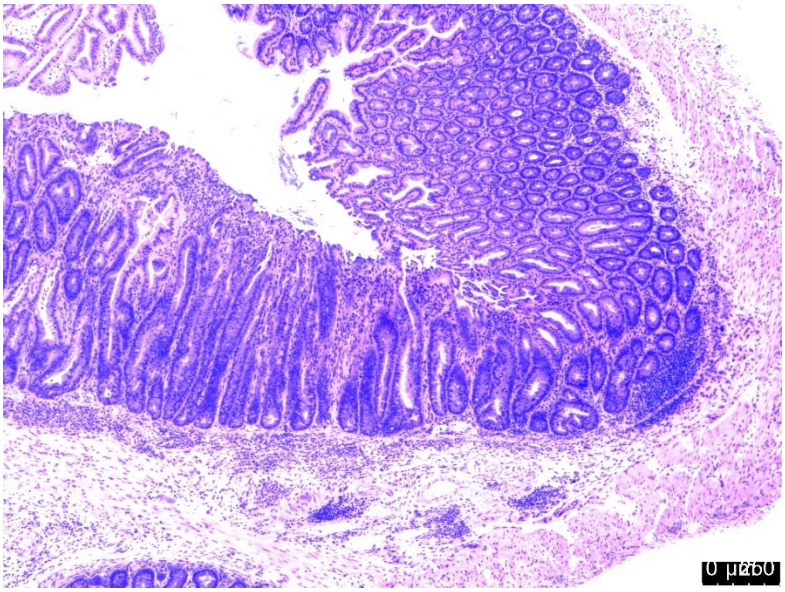

COX2 MKO + CCHF + Tg6F

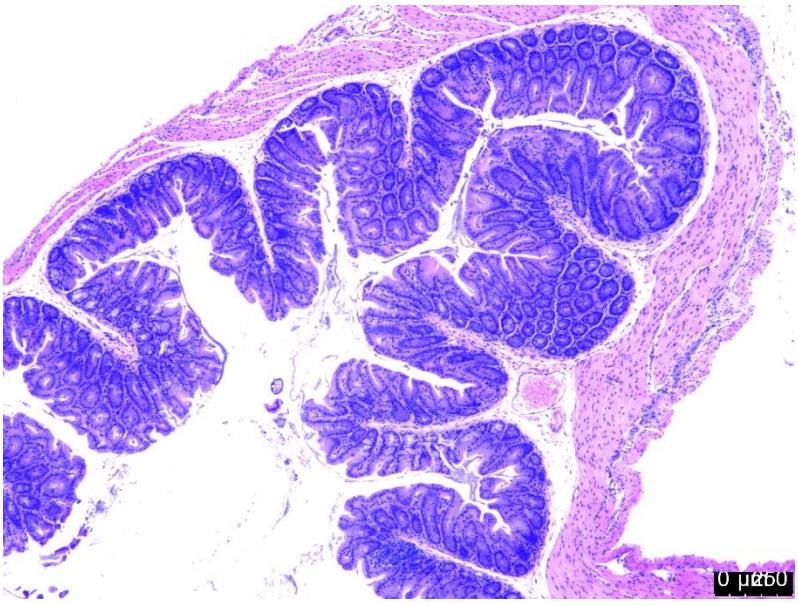

Supplemental Figure 3-9

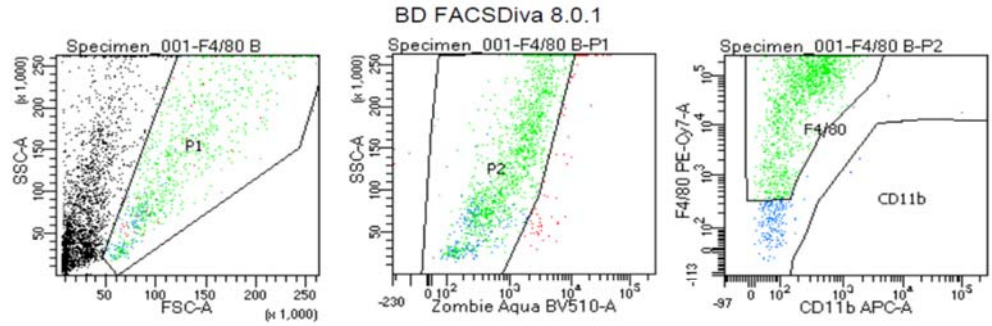

Tube: F4/80 B

Population	#Events	%Parent	%Total
All Events	6,678	####	100.0
P1	1,559	23.3	23.3
P2	1,477	94.7	22.1
F4/80	1,274	86.3	19.1
CD11b	2	0.1	0.0

COX2 MKO BMDM
D6: 86% F4/80

Supplemental Figure 3-10

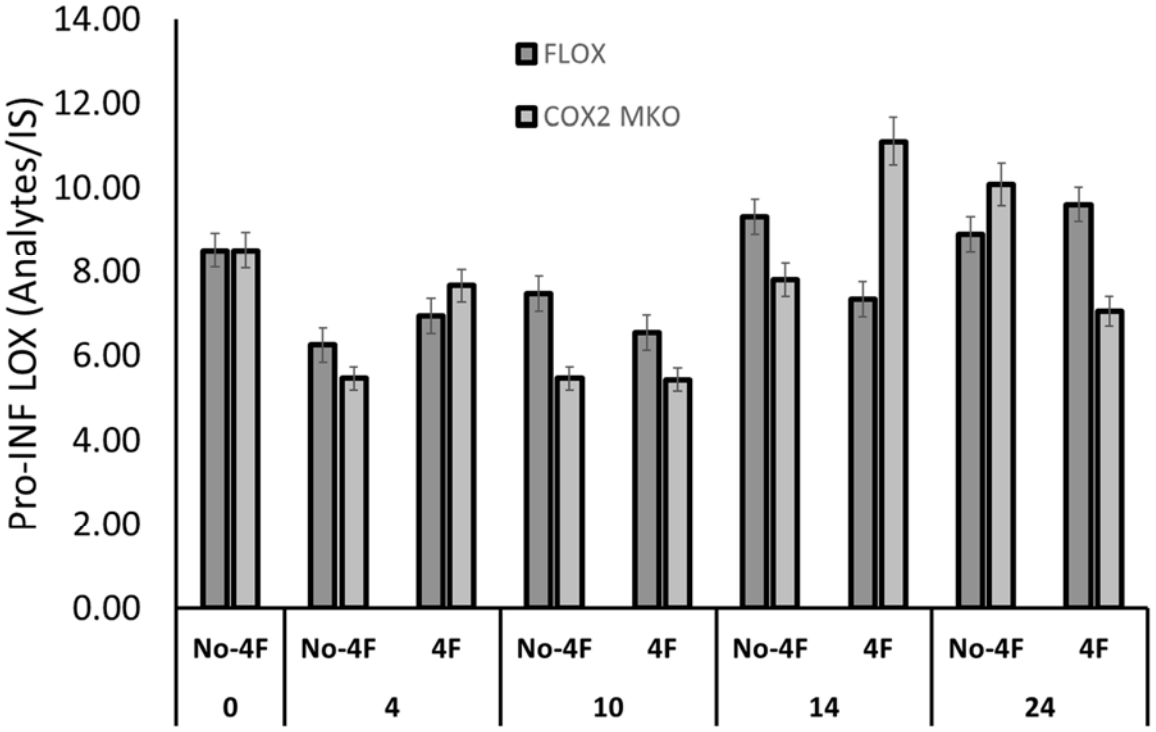

Supplemental Figure 3-11

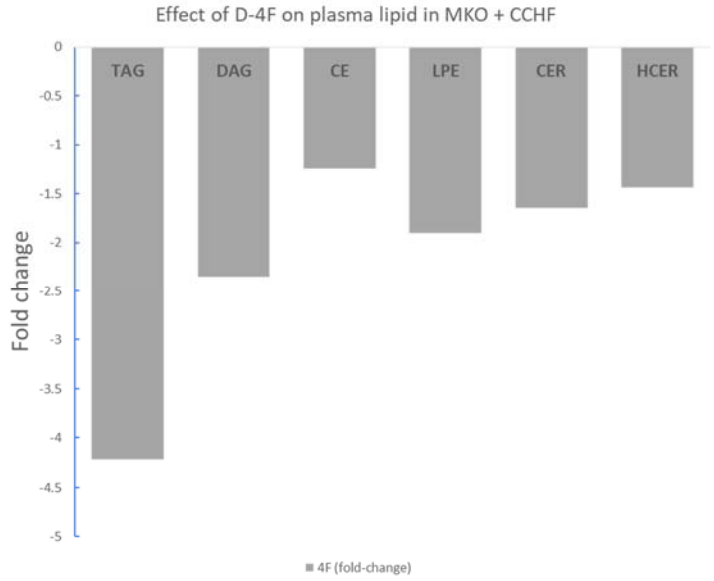

	Fold change	p-value
TAG	-4.216	0.000001
DAG	-2.356	0.0052
CE	-1.243	0.0002
LPE	-1.9	0.0002
CER	-1.649	0.0294
HCER	-1.437	0.0145
PE	-1.835	0.0609
PC	-1.756	0.2384
LPC	-1.241	0.6381
SM	-1.179	0.3065
FFA	1.2049	0.3703
LCER	ND	
DCER	ND	

Supplemental Figure 3-12

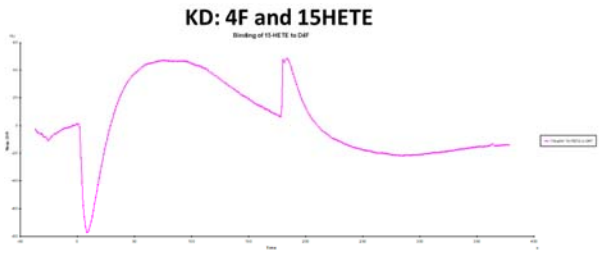

	ka (1/Ms)	kd (1/s)	Rmax (RU)	RI (RU)	Conc of analyte	KA (1/M)	KD (M)	Req (RU)	kobs (1/s)
10ng/ml 15-HETE to D4F	9.64e5	0.0321	286	-95	31.25n	3e7	**3.33e-8**	139	0.0622

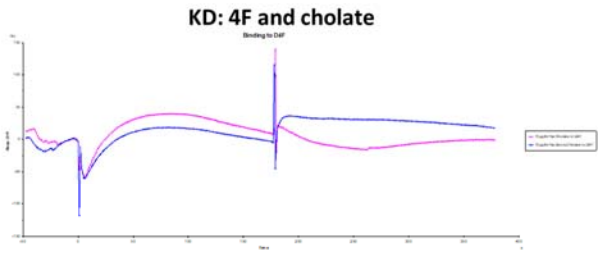

	ka (1/Ms)	kd (1/s)	Rmax (RU)	RI (RU)	Conc of analyte	KA (1/M)	KD (M)	Req (RU)	kobs (1/s)
10µg/ml Na Cholate to D4F	261	0.0426	834	-61.3	23226n	6.13e3	**1.63e-4**	104	0.0487

Supplemental Table 3-1

Analyte	Precursor	Status	Function
COX			
Anti-INF COX			
PGJ2	AA, PGD2	nonezymatic metabolite of PGD2, **unstable**	inhibit platelet aggregation; *PGD2, 15dPGJ2 marker*
Δ12-PGJ2	AA, PGD2, PGJ2	bioactive, *PGD2/J2 marker*	Anti-INF: PPARgamma agonist; *PGD2/J2/15dPGJ2 marker*
15-deoxy-Δ12,14-PGJ2	AA, PGJ2	bioactive	Anti-INF: negative regulator of NFkB, PPARgamma agonist (PPARgamma reduces INF response of endo cells; increase PON1), Nrf2 activator
13-oxo-DHA	DHA	bioactive	Anti-INF: negative regulator of NFkB, PPARgamma agonist
13-oxo-DPA	DPA	bioactive	Anti-INF: negative regulator of NFkB, PPARgamma agonist
Pro-INF and pro-RES COX			
PGE2	AA	bioactive	Pro-INF: vascular leakage; pro-RES: class-switching
15ketoPGE2	AA, PGE2	*PGE2 marker, 15hydroxyPGDH product*	*PGE2 marker*
13,14-dihydro-15keto-PGE2	AA, PGE2	*PGE2 marker, 15hydroxyPGDH product*	*PGE2 marker*
PGD2	AA	bioactive	Pro-INF: PMN chemotaxis through DP1 DP2; pro-RES: class-switching; anti-INF: Nrf2 activator
13,14-dihydro-15keto-PGD2	AA, PGD2	*PGD2 marker, 15hydroxyPGDH product*	*PGD2 marker*
Further COX products (larely pro-INF)			
[PGI2]	AA	[bioactive but unstable]	Pro-INF: vasodilation
6ketoPGF1alpha	AA, PGI2	*hydrolysis product of PGI2, plasma*	*PGI2 marker*
PGF2alpha	AA	bioactive, **unstable**	Pro-INF: RA, ath
13,14-dihydro-15-keto Prostaglandin F2α	AA, PGF2alpha	*product of PGF2alpha, plasma*	*PGF2alpha marker*
[TXA2]	AA	[bioactive but unstable]	Pro-INF: microvascular constriction, PMN adherence (overall:vasoconstriction and platelet aggregation)
TXB2	AA, TXA2	bioactive, *TXA2 product*	Pro-INF: PMN chemotaxis and adherence (maybe through TXA2)
11HETE	AA	*pathway marker (COX)*	*COX activity marker*
15HETE	AA	*Precursor; pathway marker (COX, 15LOX, LX)*	Anti-INF: LX precursor
PGE3	EPA	bioactive	Pro-INF: induce COX2 and IL6 in macrophage
TXB3	EPA	bioactive but less than TXA2/B2, *TXA3 product*	Pro-INF: induce COX2 and IL6 in macrophage

LOX			
Pro-INF LOX products			
LTB4	AA, LTA4	bioactive	Pro-INF: vascular leakage; leukocyte chemotaxis and adhesion
6trans12epi LTB4	AA, LTA4	*non-enzymatic hydrolysis product of LTA4*	*LT marker*
20-OH-LTB4	AA, LTB4	*LTB4 metabolite (LTB4 20 hydroxylase)*	*LTB4 marker*
LTC4	AA, LTA4	bioactive, *glutathione conjugate of LTA4*	Pro-INF: vascular permeability (macrophage product)
LTE4	AA, LTA4	*plasma marker of LTD4*	*LTD4 marker, plasma and urine*
5HETE	AA	*bioactive; pathway marker, 5LOX*	pro-INF: PMN chemotaxis and degranulation
12HETE	AA	bioactive	pro-INF: neutrophil chemotaxis and adhesion
15HETE	AA	*pathway marker, LX*	
5-oxoETE	AA,5HETE (dehydrogenase)	bioactive	pro-INF: PMN chemotaxis and degranulation
13HODE	LA	bioactive	pro-INF: PMN chemotaxis
9HODE	LA	bioactive	pro-INF: PMN chemotaxis
Pro-RES LOX products			
LXA4	AA; 15HETE[5LOX]; LTA4[15LOX]	bioactive	pro-RES and anti-INF: promote M1 to M2; NFkB negative regulator; inhibit neutrophil chemotaxis and adhesion
15epi-LXA4	AA; 15HETE[5LOX]; LTA4[15LOX]	bioactive	pro-RES and anti-INF: promote M1 to M2; NFkB negative regulator; inhibit neutrophil chemotaxis and adhesion
5,15-diHETE	AA; 5HETE[15LOX]	bioactive; *pathway marker, LX*;	*pathway marker, LX*; proINF: PMN degranulation and chemotaxis
LXB4	AA	bioactive	pro-RES and anti-INF: promote M1 to M2; NFkB negative regulator; inhibit neutrophil chemotaxis and adhesion
MaR--1	DHA;	bioactive	pro-RES; tissue regeneration; M1 to M2; inhibit neutrophil migration; increase efferocytosis
14S-HDHA (14S-HDoHE)	DHA	*pathway marker, MaR1; oxidation product*	*Mar1 marker*
RvD1	DHA[15LOX,5LOX]	bioactive	pro-RES: limit neutrophil infiltration
RvD2	DHA	bioactive	pro-RES: enhanace survival in sepsis; protect against colitis
RvD3	DHA	bioactive	pro-RES: limit leukocyte migration, enhance macrophage efferocytosis
RvD4	DHA	bioactive	
RvD5	DHA	bioactive	pro-RES: enhance bacterial containment and phagocytosis
17S-HDHA (17S-HDoHE)	DHA	*pathway marker, RvD PD*	*RvD and PD marker*
PDx (10S,17S-DiHDHA)	DHA	bioactive	pro-RES: inhibit neutrophil infiltration and platelet aggregation
RvE1	EPA	bioactive	pro-RES: reduce PMN infiltration; promote resolution in colitis model
18HEPE	EPA	*pathway marker, RvE*	*RvE marker*

Supplemental Table 3-2

COMPLETE LIPID PANEL: IS, RT, MS/MS

Analyte	Internal Standard	MW	RT	MS1	DP	EP	MS2-1	CE	CXP	MS2-2	CE	CXP
18HEPE	RvE1-d4	318.5	1.52	317.102	-90	-10	113	-22	-5	248.9	-10	-11
6ketoPGF1alpha	RvE1-d4	370.5	3.78	369.111	-145	-10	163	-36	-7	245.2	-36	-9
RvE1-d4		354.5	3.95	353.121	-120	-10	109.1	-26	-5	197.1	-24	-7
RvE1	**RvE1-d4**	350.5	3.98	349.12	-130	-10	107.1	-26	-5	161	-26	-5
TXB3	TXB2-d4	368.5	4.03	367.016	-110	-10	169.2	-24	-7	195.1	-16	-9
20-OH-LTB4	RvE1-d4	352.5	4.05	351.099	-100	-10	195.1	-24	-9	333.1	-22	-13
TXB2-d4		374.5	4.46	373.105	-135	-10	173.1	-22	-7	199.1	-18	-9
TXB2	**TXB2-d4**	370.5	4.48	369.074	-105	-10	169.1	-24	-7	195.2	-20	-7
PGE3	PGE2-d4	350.5	4.67	349.147	-80	-10	269.1	-22	-13	313.2	-16	-11
PGF2alpha	PGE2-d4	354.5	4.80	353.163	-145	-10	309.2	-26	-11	193.1	-34	-7
PGE2-d4		356.5	5.09	355.3	-95	-10	319.2	-18	-11	275.2	-24	-11
PGE2*	**PGE2-d4**	352.5	5.11	351.3	-100	-10	315.3	-17	-11.5	271.2	-24.4	-10
RvD3-d5		381.5	5.22	380.141	-140	-10	152.1	-26	-7	115.1	-26	-5
RvD3	**RvD3-d5**	376.5	5.25	375.022	-70	-10	147.1	-26	-7	103.1	-34	-5
LXB4	RvD3-d5	352.5	5.28	351.127	-120	-10	227.1	-22	-9	315.2	-20	-5
PGD2-d4		356.5	5.38	355.2	-95	-10	275.2	-24	-11	319.2	-16	-13
PGD2*	**PGD2-d4**	352.5	5.39	351.2	-65	-10	97	-40	-5	189.2	-26	-7
RvD2-d5		381.5	5.40	380.148	-95	-10	175.1	-32	-7	141	-22	-5
RvD2	**RvD2-d5**	376.5	5.41	375.101	-90	-10	175.1	-30	-7	141	-22	-7
LTC4-d5		630.8	5.44	629.116	-95	-10	272.1	-34	-11	142.9	-48	-7
LTC4	**LTC4-d5**	625.8	5.47	624.133	-100	-10	272.1	-30	-7	143.1	-42	-5
15keto PGE2	PGE2-d4	350.5	5.61	349.159	-115	-10	331.1	-16	-5	235.1	-20	-9
LTE4	LTC4-d5	439.6	5.67	438.122	-100	-10	333.2	-24	-13	235.2	-28	-9
LXA4-d5		357.5	5.70	356.189	-95	-10	115.1	-20	-5	222.2	-28	-9
LXA4	**LXA4-d5**	352.5	5.70	351.159	-90	-10	115	-20	-5	217.2	-28	-9
15epi-LXA4	LXA4-d5	352.5	5.72	351.128	-95	-10	115	-20	-5	217.1	-28	-9
RvD1-d5		381.5	5.76	380.159	-100	-10	141	-20	-7	220.2	-30	-9
13,14-dihydro-15-keto PGF2α-d4		358.5	5.77	357.18	-180	-10	113.1	-36	-5	197.2	-36	-9
RvD1	**RvD1-d5**	376.5	5.78	375.002	-50	-10	103	-24	-3	140.9	-20	-5
13,14-dihydro-15-PGF2α	**13,14-dihydro-15-keto PGF2α-d4**	354.5	5.80	353.167	-130	-10	113	-38	-5	183.1	-36	-9
13,14-dihydro-15keto-PGE2	**13,14-dihydro-15-keto PGE2-d4**	352.5	5.98	351.164	-100	-10	333.2	-18	-13	175.1	-32	-7
13,14-dihydro-15-keto PGE2-d4		356.5	6.02	355.152	-100	-10	337.3	-18	-11	179.1	-32	-7
RvD4	RvD1-d5	376.5	6.18	375.021	-90	-10	103	-26	-5	101.1	-32	-5
13,14-dihydro-15keto-PGD2	13,14-dihydro-15-keto PGE2-d4	352.5	6.41	351.127	-110	-10	333.3	-16	-3	207	-26	-7
PGJ2	13,14-dihydro-15-keto PGE2-d4	334.5	6.55	333.123	-105	-10	315.1	-14	-11	189.2	-22	-7
Δ12-PGJ2	13,14-dihydro-15-keto PGE2-d4	334.5	6.64	333.144	-145	-10	315.1	-14	-13	271.2	-22	-11
MaR1-d5		366.5	7.06	364.202	-130	-10	123	-24	-5	93	-44	-9
MaR1-	**MaR1-d5**	360.5	7.11	359.124	-115	-10	93.1	-42	-5	123.1	-22	-19
PDx (10S,17S-DiHDHA)	MaR1-d5	358.5	7.12	359.119	-65	-10	153.1	-24	-5	93.1	-40	-11
6trans12epi LTB4	LTB4-d4	336.5	7.12	335.157	-145	-10	195.2	-22	-7	317.2	-20	-11
RvD5	LTB4-d4	362.5	7.14	359.104	-100	-10	199.1	-22	-9	140.9	-20	-5
LTB4-d4		340.5	7.16	339.181	-125	-10	197.1	-22	-9	321.1	-20	-13
LTB4	**LTB4-d4**	336.5	7.20	335.155	-115	-10	195.1	-20	-7	317.2	-20	-5
15d-PGJ2-d4		320.5	8.66	319.2	-130	-10	275.2	-20	-11	80	-88	-5
15-deoxy-Δ 12, 14-PGJ2	**15d-PGJ2-d4**	316.4	8.69	315.3	-130	-10	271.1	-20	-11	203.1	-30	-7
13HODE-d4		300.5	9.02	299.066	-220	-10	198	-28	-9			
13HODE	**13HODE-d4**	296.5	9.06	295.09	-180	-10	295.09	-28	-9			
9HODE	13HODE-d4	296.5	9.09	295.108	-145	-10	170.8	-26	-27			
15HETE-d8		328.5	9.17	327.146	-150	-10	226	-18	-9			
15HETE	**15HETE-d8**	328.5	9.23	319.063	-170	-10	219.1	-18	-9			
17S-HDHA (17S-HDoHE)	15HETE-d8	344.5	9.24	343.147	-100	-10	281.3	-20	-11	245.1	-16	-9
14S-HDHA (14S-HDoHE)	15HETE-d8	344.5	9.37	343.167	-115	-10	281.2	-18	-11	161.2	-20	-5
11HETE	12HETE-d8	320.5	9.38	319.148	-95	-10	167	-24	-7	149	-28	-23
12HETE-d8		328.5	9.47	327.117	-145	-10	184	-22	-5			
12HETE	**12HETE-d8**	320.5	9.53	319.039	-30	-10	178.8	-20	-5			
5HETE-d8		328.5	9.61	327.139	-145	-10	115.9	-24	-5			
5HETE	**5HETE-d8**	328.5	9.67	319.087	-160	-10	115	-20	-5			
5-oxo-ETE-d7		325.5	10.15	324.22	-120	-10	210.2	-26	-9	120	-18	-5
5-oxoETE	**5-oxo-ETE-d7**	318.5	10.2	317.154	-125	-10	113	-20	-5	203.2	-26	-9

39 ANALYTES
19 INTERNAL STANDARDS (IS)
--Either exact or class specific.
Examples given below.

Analyte	IS	MW	RT
PGF2alpha	PGE2-d4	354.5	4.80
PGE2-d4		356.5	5.09
PGE2*	**PGE2-d4**	352.5	5.11

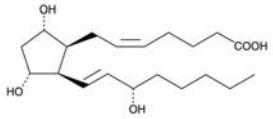

PGF2alpha

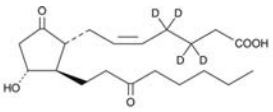

PGE2-d4

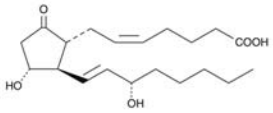

PGE2

Supplemental Table 3-3

Analyte	Internal S	MW	RT	MS1	LLOD (ng	LLOQ (ng	ULOQ (ng	Crv fit (r)
18HEPE	RvE1-d4	318.5	1.52	317.102	NA	NA	NA	NA
6-keto-PGF	RvE1-d4	370.5	3.78	369.111	<0.078	0.15	>80	0.997
RvE1-d4		354.5	3.95	353.121				
RvE1	RvE1-d4	350.5	3.98	349.12	<0.078	0.31	>80	0.994
TXB3	TXB2-d4	368.5	4.03	367.016	0.078	0.625	>80	0.997
20-OH-LTE	RvE1-d4	362.5	4.05	361.099	<0.078	0.15	>80	0.996
TXB2-d4		374.5	4.46	373.105				
TXB2	TXB2-d4	370.5	4.48	369.074	<0.31	0.31	>80	0.99
PGE3	PGE2-d4	350.5	4.67	349.147	<0.15	0.15	>80	0.999
PGF2alph	PGE2-d4	354.5	4.80	353.163	<0.078	0.15	>80	0.997
PGE2-d4		356.5	5.09	355.3				
PGE2*	PGE2-d4	352.5	5.11	351.3	<0.078	0.15	>80	0.993
RvD3-d5		381.5	5.22	380.141				
RvD3	RvD3-d5	376.5	5.25	375.022	<0.078	0.15	>80	0.983
LXB4	RvD3-d5	352.5	5.28	351.127	<0.078	0.31	>80	0.99
PGD2-d4		356.5	5.38	355.2				
PGD2*	PGD2-d4	352.5	5.39	351.2	<0.078	0.15	>80	0.99
RvD2-d5		381.5	5.40	380.148				
RvD2	RvD2-d5	376.5	5.41	375.101	< 15	0.15	>80	0.996
LTC4-d5		630.8	5.44	629.116				
LTC4	LTC4-d5	625.8	5.47	624.133	<0.078	0.15	>80	0.997
15-keto-PG	PGE2-d4	350.5	5.61	349.159	<0.078	0.31	>80	0.997
LTE4	LTC4-d5	439.6	5.67	438.122	<0.078	0.31	>80	0.983
LXA4-d5		357.5	5.70	356.189				
LXA4	LXA4-d5	352.5	5.70	351.159	<0.078	0.31	>80	0.99
15epi-LXA-	LXA4-d5	352.5	5.72	351.128	<0.078	0.15	>80	0.998
RvD1-d5		381.5	5.76	380.159				
13,14-dihydro-15-ket		358.5	5.77	357.18				
RvD1	RvD1-d5	376.5	5.78	375.062	< 15	0.15	>80	0.998
13,14-dihy	13,14-dihy	354.5	5.80	353.167	<0.078	0.15	>80	0.995
13,14-dihy	13,14-dihy	362.5	5.98	361.164	<0.078	0.15	>80	0.993
13,14-dihydro-15-ket		356.5	6.02	355.152				
RvD4	RvD1-d5	376.5	6.18	375.021	<0.078	0.15	>80	0.99
13,14-dihy	13,14-dihy	362.5	6.41	361.127	<0.078	0.15	>80	0.99
PGJ2	13,14-dihy	334.5	6.55	333.123	<0.078	0.15	>80	0.99
Δ12-PGJ2	13,14-dihy	334.5	6.64	333.144	< 15	0.15	>80	0.998
MaR1-d5		365.5	7.06	364.202				
MaR1-	MaR1-d5	360.5	7.11	359.124	0.078	0.31	>80	0.996
PDx (10S,	MaR1-d5	360.5	7.12	359.119	<0.078	0.15	>80	0.997
6trans-12e	LTD4-d4	336.5	7.12	335.157	<0.078	0.15	>80	0.99
RvD5	LTB4-d4	360.5	7.14	359.104	<0.078	0.15	>80	0.99
LTB4-d4		340.5	7.16	339.181				
LTB4	LTB4-d4	336.5	7.20	335.155	<0.078	0.31	>80	0.99
15d-PGJ2-d4		320.5	8.66	319.2				
15-deoxy-Δ	15d-PGJ2	316.4	8.69	315.3	< 15	0.15	>80	0.998
13HODE-d4		300.5	9.02	299.066				
13HODE	13HODE-d	296.5	9.06	295.09	< 15	0.31	>80	0.994
9HODE	13HODE-c	296.5	9.09	295.108	<0.078	0.31	>80	0.991
15HETE-d8		328.5	9.17	327.146				
15-HETE	15HETE-d8	328.5	9.23	319.063	<0.078	0.31	>80	0.99
17S-HDHA	15-HETE-d8	344.5	9.24	343.147	<0.078	0.15	>80	0.99
14S-HDHA	15-HETE-d8	344.5	9.37	343.167	<0.078	0.31	>80	0.99
11HETE	12-HETE-d	320.5	9.38	319.148	< 15	0.31	>80	0.998
12HETE-d8		328.5	9.47	327.117				
12-HETE	12HETE-d	328.5	9.53	319.039				
5HETE-d8		328.5	9.61	327.139				
5-HETE	5HETE-d8	320.5	9.67	319.087	<0.078	0.15	>80	0.995
5-oxo-ETE-d7		325.5	10.15	324.22				
5-oxoETE	5-oxo-ETE	318.5	10.2	317.154	<0.078	0.31	>80	0.98

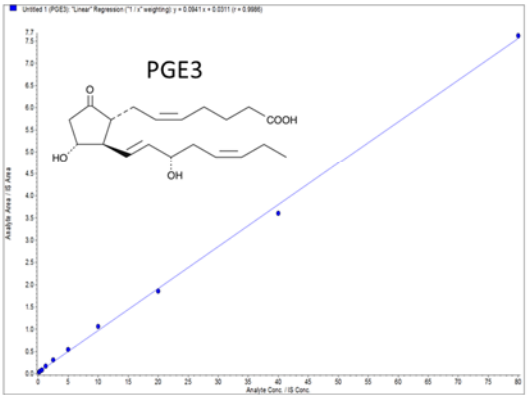

Analyte	IS	MW	RT	MS1	LLOD (ng/ml)	LLOQ (ng/ml	ULOQ (ng/ml)	Crv fit (r)
PGE3	PGE2-d4	350.5	4.67	349.147	<0.078	0.15	>80	0.999

Supplemental Table 3-4

Tissue

Analyte	IS	CV(%)
6ketoPGF1alpha	RvE1-d4	8.93
RvE1	RvE1-d4	NA
TXB3	TXB2-d4	3.42
20-OH-LTB4	RvE1-d4	14.94
TXB2	TXB2-d4	4.24
PGE3	PGE2-d4	3.23
PGF2alpha	PGE2-d4	4.85
PGE2*	PGE2-d4	2.37
RvD3	RvD3-d5	NA
LXB4	RvD3-d5	12.08
PGD2*	PGD2-d4	4.04
RvD2	RvD2-d5	NA
LTC4	LTC4-d5	13.47
15ketoPGE2	PGE2-d4	**43.89**
LTE4	LTC4-d5	17.50
LXA4	LXA4-d5	18.07
15epi-LXA4	(No IS)	NA
RvD1	RvD1-d5	10.55
13,14-dihydro-15-PGF2α	13,14-dihydro-15-keto PGF2α-d4	6.14
13,14-dihydro-15keto-PGE2	13,14-dihydro-15-keto PGE2-d4	0.29
RvD4	RvD1-d5	NA
PGJ2	13,14-dihydro-15-keto PGE2-d4	11.59
13,14-dihydro-15keto-PGD2	13,14-dihydro-15-keto PGE2-d4	6.89
Δ12-PGJ2	13,14-dihydro-15-keto PGE2-d4	14.51
MaR1-	MaR1-d5	5.56
PDx (10S,17S-DiHDHA)	MaR1-d5	4.91
6trans12epi LTB4	LTB4-d4	13.29
RvD5	LTB4-d4	3.14
LTB4	LTB4-d4	2.94
15-deoxy-Δ12,14-PGJ2	15d-PGJ2-d4	15.96
13HODE	13HODE-d4	1.32
9HODE	13HODE-d4	3.01
17S-HDHA (17S-HDoHE)	15HETEd8	9.95
15HETE	15HETEd8	11.30
14S-HDHA (14S-HDoHE)	15HETEd8	4.94
11HETE	12HETE-d8	4.98
12HETE	12HETE-d8	1.26
5HETE	5HETE-d8	6.30
5-oxoETE	5-oxo-ETE-d7	14.47

Plasma

	CV (%)	Extraction efficiency of IS (%)
11HETE	2.92	81.73
12HETE	7.39	81.73
13,14-dihydro-15keto-PGD2	ND	41.15
13,14-dihydro-15keto-PGE2	10.07	41.15
13,14-dihydro-15-PGF2α	5.52	87.57
13HODE	5.60	61.22
14S-HDHA (14S-HDoHE)	10.33	85.01
15-deoxy-Δ12,14-PGJ2	ND	25.39
15epi-LXA4	ND	71.61
15HETE	7.38	85.01
15ketoPGE2	ND	80.09
17S-HDHA (17S-HDoHE)	11.98	85.01
20-OH-LTB4	ND	97.63
5HETE	7.71	73.15
5-oxoETE	16.40	68.73
6ketoPGF1alpha	9.00	97.63
6trans12epi LTB4	12.02	77.51
9HODE	11.02	61.22
LTB4	12.79	77.51
LTC4	ND	79.79
LTE4	ND	79.79
LXA4	ND	71.61
LXB4	ND	78.08
MaR1-	ND	80.46
PDx (10S,17S-DiHDHA)	ND	80.46
PGD2	12.59	42.81
PGE2	8.90	80.09
PGE3	ND	80.09
PGF2alpha	11.29	80.09
PGJ2	ND	41.15
RvD1	16.89	63.04
RvD2	ND	70.42
RvD3	ND	78.08
RvD4	ND	63.04
RvD5	ND	77.51
RvE1	ND	97.63
TXB2	11.18	36.14
TXB3	ND	36.14
Δ12-PGJ2	ND	41.15

Supplemental Table 3-5

	Tissue		Plasma	
Internal Standard	CV (%)	Ext. efficiency (%)	CV (%)	Ext. efficiency
RvE1-d4	3.04	74.88	7.91	113.08
TXB2-d4	1.15	35.42	5.91	75.90
PGE2-d4	13.84	64.18	6.21	93.67
RvD3-d5	16.31	64.07	8.56	106.99
PGD2-d4	13.81	46.98	8.44	72.86
RvD2-d5	24.95	49.68	7.01	103.78
LTC4-d5	14.09	11.91	14.12	92.02
13,14-dihydro-15-keto PGF2α-d4	8.08	61.30	7.98	99.70
LXA4-d5	22.32	48.68	7.05	89.13
RvD1-d5	22.59	51.06	7.80	103.59
13,14-dihydro-15-keto PGE2-d4	9.88	51.91	5.93	70.37
MaR1-d5	12.39	56.98	10.21	98.06
LTB4-d4	16.73	54.22	6.44	97.96
15d-PGJ2-d4	17.02	22.31	9.14	10.07
13HODE-d4	4.22	34.16	0.78	87.14
15HETEd8	14.80	48.88	6.05	98.04
12HETE-d8	14.42	43.02	5.88	93.38
5HETE-d8	14.97	56.13	7.30	99.47
5-oxo-ETE-d7	0.47	36.95	2.96	48.04

Supplemental Table 3-6

Pro-inflammatory LOX														
		LTE4	**LTC4**	**LTB4**	**6trans12epi LTB4**	**20-OH-LTB4**	**15HETE**	**12HETE**	**5HETE**	**5oxoETE**	**13HODE**	**9HODE**	**Total**	
MKO+CHOW	**AVG**	**3.25**	**0.15**	**0.18**	**1.44**	**ND**	**40.81**	**107.96**	**13.39**	**10.61**	**681.26**	**212.20**	**1071.25**	
	SEM	2.36	0.08	0.07	0.21		4.93	15.18	3.96	2.69	82.21	35.07	120.21	
FLOX+CCHF	**AVG**	**3.98**	**0.02**	**0.52**	**5.58[&]**	**ND**	**52.95**	**240.10**	**21.30**	**15.04**	**511.51**	**154.31**	**965.84**	
	SEM	1.76	0.02	0.28	1.82		9.42	53.70	6.52	4.83	87.30	23.69	232.82	
MKO+CCHF	**AVG**	**2.34**	**0.11**	**0.50**	**8.00***	**ND**	**85.13*,****	**401.23*,****	**19.30**	**9.81**	**768.60****	**213.91**	**1640.09*,****	
	SEM	0.34	0.07	0.16	1.67		6.96	49.51	2.62	1.79	80.23	27.04	106.49	
MKO+CCHF	**AVG**	**2.30**	**NA**	**1.34**	**7.40**	**ND**	**75.91**	**283.95*****	**23.79**	**9.77**	**601.64*****	**165.75**	**1273.92*****	
	SEM	**0.66**	**0.00**	**0.48**	**1.88**		**4.55**	**13.24**	**3.93**	**1.20**	**57.06**	**21.88**	**65.34**	
Pro-inflammatory COX														
		PGF2α	**13,14-dihydro-15-PGF2α**	**6ketoPGF1α**	**TXB2**	**11HETE**	**TXB3**	**PGE3**	**Total**					
MKO+CHOW	**AVG**	**13.95**	**3.05**	**885.35**	**28.27**	**302.95**	**0.53**	**2.42**	**1236.39**					
	SEM	3.13	1.69	214.45	10.16	83.88	0.13	0.67	189.26					
FLOX+CCHF	**AVG**	**23.47**	**3.58**	**874.68**	**41.63**	**208.46**	**0.20***	**0.89***	**1152.93**					
	SEM	6.43	0.47	155.46	10.71	28.54	0.06	0.18	199.39					
MKO+CCHF	**AVG**	**29.15***	**4.80**	**1355.14*,****	**70.41***	**346.85**	**0.32**	**1.55****	**1755.11*,****					
	SEM	2.57	1.04	92.25	11.55	57.39	0.06	0.20	127.89					
MKO+CCHF+4F	**AVG**	**31.00**	**4.44**	**1138.67**	**59.85**	**298.66**	**0.27**	**1.28**	**1524.94**					
	SEM	2.23	0.83	90.40	5.86	33.06	0.03	0.27	101.98					
PGE2/PGD2														
		PGE2	**13,14-dihydro-15keto-PGE2**	**15ketoPGE2**	**13,14-dihydro-15keto-PGD2**	**PGD2**	**Total**							
MKO+CHOW	**AVG**	**130.10**	**18.66**	**4.82**	**0.00**	**22.97**	**173.31**							
	SEM	22.82	9.01	0.44	0.00	8.16	38.73							
FLOX+CCHF	**AVG**	**154.85**	**26.59**	**3.00***	**0.43***	**67.82**	**259.71**							
	SEM	27.19	7.08	0.51	0.11	20.35	49.33							
MKO+CCHF	**AVG**	**219.60*,****	**39.75**	**5.72****	**0.61***	**109.33***	**412.12*,****							
	SEM	7.25	8.48	0.81	0.13	14.88	18.50							
MKO+CCHF+4F	**AVG**	**224.16**	**29.36**	**6.44**	**0.34*****	**104.95**	**381.55**							
	SEM	27.34	3.95	1.43	0.04	8.67	34.58							
Anti-inflammatory COX														
		PGJ2	**Δ12-PGJ2**	**15d-PGJ2**	**Total**									
MKO+CHOW	**AVG**	**0.31**	**0.35**	**0.20**	**0.85**									
	SEM	0.06	0.05	0.04	0.12									
FLOX+CCHF	**AVG**	**2.02***	**1.58***	**0.64**	**4.25***									
	SEM	0.56	0.40	0.20	1.14									
MKO+CCHF	**AVG**	**2.55***	**2.01***	**0.90***	**5.47***									
	SEM	0.32	0.25	0.12	0.62									
MKO+CCHF+4F	**AVG**	**1.48*****	**1.26*****	**0.98**	**3.73*****									
	SEM	0.22	0.18	0.08	0.46									
Pro-resolving LOX														
		LXA4	**LXB4**	**14HDHA**	**MaR1**	**17HDHA**	**PDx**	**RVD1**	**RVD2**	**RVD3**	**RVD4**	**RVD5**	**RVE1**	**Total**
MKO+CHOW	**AVG**	**0.152**	**0.733**	**56.156**	**0.845**	**27.671**	**1.853**	**0.016**	**ND**	**ND**	**ND**	**0.233**	**ND**	**86.71**
	SEM	0.050	0.063	2.636	0.066	1.744	0.057	0.006				0.012		3.88
FLOX+CCHF	**AVG**	**0.31[$]**	**0.991**	**55.139**	**1.945**	**30.669**	**3.349**	**0.015**	**ND**	**ND**	**ND**	**0.346**	**ND**	**92.67**
	SEM	0.039	0.180	10.156	0.644	6.343	0.898	0.004				0.093		18.11
MKO+CCHF	**AVG**	**0.16****	**1.353**	**60.143**	**1.668**	**26.294**	**3.261**	**0.006[&]**	**ND**	**ND**	**ND**	**0.476**	**ND**	**74.92**
	SEM	**0.015**	**0.049**	**5.691**	**0.414**	**5.571**	**0.713**	**0.003**				**0.100**		18.91
MKO+CCHF+4F	**AVG**	**0.21**	**1.05**	**74.00**	**2.16**	**37.61**	**4.32**	**0.01**	**0.12**	**ND**	**ND**	**0.62**	**ND**	**127.52[#]**
	SEM	**0.04**	**0.13**	**7.39**	**0.47**	**2.94**	**0.71**	**0.00**	**0.02**			**0.09**		11.44

Supplemental Table 3-7

Pro-inflammatory LOX														
		LTE4	**LTC4**	**LTB4**	**6trans12epi LTB4**	**20OH-LTB4**	**15HETE**	**12HETE**	**5HETE**	**5oxoETE**	**13HODE**	**9HODE**	**Total**	
MKO+CHOW	**AVG**	**ND**	**ND**	**ND**	**0.01**	**ND**	**0.26**	**19.94**	**0.36**	**0.06**	**16.41**	**3.56**	**34.00**	
	SEM				0.00		0.03	2.12	0.06	0.01	2.28	0.61	5.34	
FLOX+CCHF	**AVG**	**ND**	**ND**	**ND**	**0.02**	**ND**	**0.30**	**6.19***	**0.53**	**0.15**	**24.03**	**6.67**	**30.00**	
	SEM				0.01		0.08	0.89	0.09	0.04	4.38	1.54	5.15	
MKO+CCHF	**AVG**	**ND**	**ND**	**ND**	**0.04**	**ND**	**1.07**	**69.00*,****	**0.88*,****	**0.16***	**74.55**	**10.15***	**157.42*,****	
	SEM				0.02		0.34	17.55	0.12	0.05	21.71	2.50	40.95	
MKO + CCHF + 4F	**AVG**	**NA**	**NA**	**NA**	**0.003*****	**NA**	**0.27*****	**16.13*****	**0.66*****	**0.14**	**20.76*****	**5.07*****	**47.52*****	
	SEM				0.003		0.048	3.910	0.095	0.069	2.705	0.791	7.628	
Pro-inflammatory COX														
		PGF2α	**13,14-dihydro-15-PGF2α**	**6ketoPGF1α**	**TXB2**	**11HETE**	**TXB3**	**PGE3**	**Total**					
MKO+CHOW	**AVG**	**0.04**	**0.02**	**0.13**	**2.56**	**1.23**	**ND**	**ND**	**3.98**					
	SEM	0.02	0.01	0.02	0.44	0.14			0.60					
FLOX+CCHF	**AVG**	**0.03**	**0.04**	**0.08**	**0.91**	**0.95**	**ND**	**ND**	**1.96***					
	SEM	**0.008**	0.01	0.01	0.32	0.12			0.46					
MKO+CCHF	**AVG**	**0.17*,****	**0.12*,****	**1.78**	**6.96****	**4.54[&]**	**ND**	**ND**	**12.13[&]**					
	SEM	0.04	0.02	0.82	1.74	1.35			4.04					
MKO + CCHF + 4F	**AVG**	**0*** **	**0.026*****	**0.25[#]**	**0.29*****	**0.89*****	**NA**	**NA**	**1.46*****					
	SEM	0.00	0.01	0.07	0.16	0.19			0.33					
PGE2/PGD2														
		PGE2	**13,14-dihydro-15keto-PGE2**	**15ketoPGE2**	**13,14-dihydro-15keto-PGD2**	**PGD2**	**Total**							
MKO+CHOW	**AVG**	**0.100**	**0.062**	**0.000**	**0.000**	**0.043**	**0.21**							
	SEM	0.016	0.011	0.000	0.000	0.006	0.03							
FLOX+CCHF	**AVG**	**0.044**	**0.035**	**0.000**	**0.000**	**0.031**	**0.11**							
	SEM	0.010	0.016	0.000	0.000	0.006	0.03							
MKO+CCHF	**AVG**	**0.25****	**0.092**	**0.006**	**0.032**	**0.121**	**0.51[&]**							
	SEM	0.068	0.033	0.004	0.023	0.034	0.14							
MKO + CCHF + 4F	**AVG**	**0.062*****	**0.035**	**0.001**	**0.008**	**0.049[#]**	**0.15*****							
	SEM	0.011	0.010	0.001	0.008	0.010	0.024							
Anti-inflammatory COX														
		PGJ2	**Δ12-PGJ2**	**15d-PGJ2**	**Total**									
MKO+CHOW	**AVG**	**ND**	**ND**	**ND**	**ND**									
	SEM													
FLOX+CCHF	**AVG**	**ND**	**ND**	**ND**	**ND**									
	SEM													
MKO+CCHF	**AVG**	**ND**	**ND**	**ND**	**ND**									
	SEM													
MKO + CCHF + 4F	**AVG**	**ND**	**ND**	**ND**	**ND**									
	SEM													
Pro-resolving LOX														
		LXA4	**LXB4**	**14HDHA**	**MaR1**	**17HDHA**	**PDx**	**RVD1**	**RVD2**	**RVD3**	**RVD4**	**RVD5**	**RVE1**	**Total**
MKO+CHOW	**AVG**	**ND**	**ND**	**3.62**	**ND**	**0.21**	**0.01**	**0.01**	**ND**	**ND**	**ND**	**ND**	**ND**	**3.86**
	SEM			0.53		0.04	0.01	0.00						0.57
FLOX+CCHF	**AVG**	**ND**	**ND**	**2.68**	**ND**	**0.28**	**0.01**	**0.01**	**ND**	**ND**	**ND**	**ND**	**ND**	**2.98**
	SEM			1.43		0.08	0.01	0.00						1.50
MKO+CCHF	**AVG**	**ND**	**ND**	**3.88**	**ND**	**0.40**	**0.03**	**0.01**	**ND**	**ND**	**ND**	**ND**	**ND**	**4.32**
	SEM			1.49		0.29	0.02	0.01						1.74
MKO + CCHF + 4F	**AVG**	**ND**	**ND**	**3.720**	**ND**	**0.219**	**0.012**	**0.010**	**ND**	**ND**	**ND**	**ND**	**ND**	**3.960**
	SEM			0.698		0.059	0.005	0.001						0.716

Supplemental Table 3-8

Pro-inflammatory LOX															
		12HETE	13HODE	15HETE	20-OH-LTB4	5HETE	5oxoETE	6trans12epi LTB4	9HODE	LTB4	LTC4	LTE4	Total		
IL10+PX	AVG	**100.1864**	**649.9629**	**36.1296**	**ND**	**7.343705**	**5.79136**	**0.554818**	**257.6375**	**0.57657**	**0.397281**	**2.658975**	**1117.907**		
	SEM	10.81897	60.02646	1.900285		0.963924	0.916129	0.096909	35.31335	0.155281	0.054057	0.395416	94.49674		
IL10+PX+4F	AVG	**87.46349**	**470.3724**	**34.56993**	**ND**	**5.605692**	**2.377679**	**0.449521**	**267.5777**	**0.16748**	**0.258885**	**1.325573**	**786.6759**		
	SEM	10.75304	35.97726	3.114647		0.649486	0.201952	0.088237	50.61475	0.057011	0.033443	0.327687	60.56826		
IL10	AVG	**52.03024**	**451.1757**	**23.60197**	**ND**	**3.540868**	**2.475791**	**0.14739**	**200.3926**	**0.049968**	**0.307262**	**0.822888**	**734.5447**		
	SEM	5.644736	51.55797	2.749026		0.578416	0.479318	0.019933	29.0203	0.00865	0.080549	0.249781	87.7534		
Ttest	4FvPX	0.476175	0.051634	0.691301		0.169155	0.003918	0.451297	0.880291	0.03046	0.054033	0.026708	0.033709		
	IL10vPX	0.01143	0.093205	0.003896		0.034857	0.033493	0.016628	0.342399	0.033666	0.361172	0.01001	0.029725		
Pro-inflammatory COX															
		11HETE	13,14-dihydro-15-PGF2α	6ketoPGF1α	PGE3	PGF2α	TXB2	TXB3	Total						
IL10+PX	AVG	**188.084**	**1.274**	**961.114**	6.167	**42.529**	**50.776**	**0.555**	**1250.500**						
	SEM	9.982	0.258	74.832	0.795	3.420	4.913	0.097	88.492						
IL10+PX+4F	AVG	**179.530**	**1.307**	**972.988**	6.455	**36.347**	**52.307**	**0.450**	**1249.328**						
	SEM	11.669	0.283	99.733	0.695	4.977	5.606	0.088	117.610						
IL10	AVG	**141.287**	**1.404**	**824.154**	3.840	**35.302**	**22.797**	**0.147**	**1028.931**						
	SEM	9.433	0.265	60.779	0.697	4.336	2.558	0.020	72.555						
Ttest	4FvPX	0.593	0.933	0.927	0.789	0.339	0.843	0.451	0.994						
	IL10vPX	0.013	0.775	0.246	0.082	0.170	0.003	0.017	0.125						
PGE2/PGD2															
		13,14-dihydro-15keto-PGD2	13,14-dihydro-15keto-PGE2	15ketoPGE2	PGD2	PGE2	Total								
IL10+PX	AVG	**0.124**	**6.176**	**2.221**	**115.579**	**183.165**	**307.265**								
	SEM	0.012	0.880	0.171	10.263	14.986	24.220								
IL10+PX+4F	AVG	**0.132**	**7.317**	**4.725**	**105.156**	**188.349**	**305.680**								
	SEM	0.021	1.331	1.320	10.149	15.287	19.502								
IL10	AVG	**0.114**	**5.316**	**3.112**	**82.644**	**123.504**	**214.689**								
	SEM	0.008	0.711	0.921	8.321	12.937	20.623								
Ttest	4FvPX	0.744	0.501	0.103	0.485	0.814	0.960								
	IL10vPX	0.590	0.491	0.238	0.058	0.016	0.030								
Anti-inflammatory COX															
		15-deoxy-Δ12,14-PGJ2	PGJ2	Δ12-PGJ2	Total										
IL10+PX	AVG	**32.5989**	**0.732276**	**ND**	**1.22049**										
	SEM	23.04806	0.180635		0.563581										
IL10+PX+4F	AVG	**0.068453**	**3.621917**	**ND**	**55.35209**										
	SEM	0.021388	1.052186		18.12515										
IL10	AVG	**0.666775**	**0.495813**	**ND**	**0.271199**										
	SEM	0.054613	0.003503		0.150986										
Ttest	4FvPX	0.218945	0.062074		0.044113										
	IL10vPX	0.515285	0.537754		0.435946										
Pro-Resolving LOX															
		14S-HDHA (14S-HDoHE)	15epi-LXA4	17S-HDHA (17S-HDoHE)	LXA4	LXB4	MaR1-	PDx (10S,17S-DiHDHA)	RvD1	RvD2	RvD3	RvD4	RvD5	RvE1	Total LOX
IL10+PX	AVG	**24.46778**	**ND**	**19.04**	0.317241	**5.296276**	**0.504185**	**1.235678**	**0.008822**	**ND**	**ND**	**ND**	**0.11999**	**ND**	**53.03741**
	SEM	3.488511		3.119583	0.105277	0.563212	0.09352	0.205752	0.001744				0.031211		7.614881
IL10+PX+4F	AVG	**24.61688**	**ND**	**16.8618**	0.125344	**5.605692**	**0.48445**	**1.25206**	**0.010143**	**ND**	**ND**	**ND**	**0.136798**	**ND**	**48.39245**
	SEM	4.1648		1.940472	0.016059	0.649486	0.086457	0.220187	0.001247				0.03051		6.546206
IL10	AVG	**26.50432**	**ND**	**12.40136**	0.099407	**3.540868**	**0.279022**	**0.757618**	**0.011276**	**ND**	**ND**	**ND**	**0.0669**	**ND**	**43.66077**
	SEM	13.2845		1.736456	0.014436	0.578416	0.037226	0.11111	0.001656				0.009743		15.44542
Ttest	4FvPX	0.978888		0.552617	0.075755	0.763211	0.879134	0.957879	0.540945				0.707267		0.649369
	IL10vPX	0.853439		0.166228	0.161824	0.103854	0.115991	0.201287	0.382386				0.277426		0.552787

Chapter 4: A synergy between disease biology and PK/PD

Introduction

This thesis brings together two independent lines of investigation in synergistic fashion. I first presented, in Chapter 2 together with the Appendix, a partial account of the PKPD of 4F. I showed that 4F associates with the HDL fraction of the plasma in C57BL/6J mice, but that both 4F and 4F-associated HDL are cleared quickly from circulation (Appendix). Interestingly, this clearance is partially the result of selective targeting to the small intestine, where 4F is taken up by the intestinal tissue and transported into the intestinal lumen in a TICE-dependent manner (Chapter 2). 4F in turn can enhance RCT through the TICE pathway, while also directly mediating TICE itself (Chapter 2).

In Chapter 3, I introduced the COX2 KO and CCHF models of IBD, and I began an investigation into the pathogenesis of these models. CCHF initiates chronic intestinal inflammation by altering barrier permeability and increasing the translocation of PAMP in C56BL/6J mice, but only in the absence of COX2 is there a loss of tolerance to these inflammatory stimuli. COX2 MKO increases the levels of pro-inflammatory cytokine mediators in LPS-activated macrophages. More strikingly, in response to CCHF it increases the levels of lipid pro-inflammatory mediators in plasma, while altering the balance of pro-inflammatory and inflammation resolving mediators in intestinal tissue.

These heretofore independent lines of investigation then converged, in the second half of Chapter 3. We had learned that 4F localizes to the intestine, where it increases the clearance of cholesterol (see Chapter 2). We had also determined that 4F can alter the distribution of at least some pro-inflammatory LOX mediators in the circulation (see Appendix). We thus sought to determine whether 4F could protect against intestinal inflammation in the COX2 MKO model. Strikingly, 4F largely abrogated disease. Moreover, 4F rescued the COX2 MKO dependent elevation of lipid pro-inflammatory

mediators in intestinal tissue and plasma, and it appeared to do so directly by increasing the clearance of these mediators from intestinal tissue and lipoproteins. It had been an open question whether the elevations of pro-inflammatory mediators were causes or mere correlates of disease. We now had at least partial evidence that a therapy that inhibits disease also directly counter-acts these elevations—raising the probability that changes in the levels of these pro-inflammatory mediators partially constitute both the pathogenic mechanism of disease and the protective mechanism of 4F. Thus, the payoff from the convergence of these two lines of investigation has been not only the identification of a promising new class of therapies for IBD, but also a deeper understanding of the basic biology of this disease and the protective mechanisms of these therapies—a vivid illustration of the interplay between disease biology and PKPD.

In this concluding chapter, I will revisit these three topics—the PKPD of 4F as presented in Chapter 2 and the Appendix; the pathogenic mechanisms of the COX2 KO and CCHF models; and the protective mechanisms of 4F in both the COX2 CCHF and PAC IL10 models of IBD. I aim to summarize the prior results while adding additional unpublished data. I will moreover detail what I take to be important open questions while laying out some future directions for my work.

§1: Intestinal Clearance of 4F and the Modulation of TICE

In the work of the Appendix, I made several observations about the pharmacokinetics of circulating 4F. While 4F can associate with individual lipoproteins including both LDL and HDL (see Appendix, Figures 1-2 and 9 [A.F1-2,9]), LDL mediates the transfer of 4F to HDL, thereby increasing this latter association (see A.F3,8). The transfer of 4F to HDL by LDL is enhanced in the presence of Inflammatory LOX mediators like 15HETE (see A.F4), which are themselves transferred to HDL by 4F (see A.F5). Thus, 4F largely associates in vivo with the HDL fraction of the plasma of C57BL/6J mice (see

A.F6). 4F is cleared from the plasma quickly, however, with an approximate 75% clearance by 30 minutes (see A.F6). Interestingly, 4F-associated HDL is also cleared quickly from the circulation, with $t_{1/2}$ equal to approximately 24 min (see A.F7).

I began the work of Chapter 2 by further investigating the distribution and excretion of circulating 4F. To my surprise, 4F did not distribute to the kidneys or the liver but rather to the small intestine (see Chapter 2, Figure 1 [2.F1]), where 4F is transported into the intestinal lumen (see 2.F2). 4F enters the lumen by directly and selectively crossing the intestinal epithelium (see 2.F3). The transport process is saturable, and 4F once in the lumen can be taken up by the intestinal mucosa (see 2.F4). Interestingly, the transport of 4F into the lumen can be modulated by TICE (see 2.F5). Overall, the rate of uptake and clearance of 4F by the intestine is consistent with the rate of clearance of 4F from the plasma (compare 2.F1B with A.F6), indicating that intestinal clearance is at least partially responsible for the observations reported in the Appendix.

Since the completion of this work from the first half of Chapter 2, I have continued to investigate the mechanism behind the intestinal clearance of 4F. I had observed that increasing TICE by western diet (WD) in TG112 mice had also increased the trans-intestinal transport of 4F from the circulation (see 2.F5B-C). I had further observed that serosal-side lipoproteins increased the clearance of 4F from intestinal explants mounted in Ussing chambers (see 2.F5C). LXR agonists have been shown to increase TICE.(1) Moreover, I myself had observed that the LXR agonist T0901317 had increased RCT of ^{3}H-cholesterol from macrophages into the intestinal lumen of C57BL/6J mice (see 2.F6B). Thus, I sought to reproduce the effect of WD in TG112 mice on the intestinal clearance of 4F through the use of this LXR agonist. I pre-treated TG112 mice with T0901317 for 7 days, as well as TG112 mice with WD for 6 weeks as positive control. I introduced ^{14}C-L-4F into the circulation of the mice by tail vein injection. To my surprise, while WD increased the clearance of ^{14}C-L-4F into the SI lumen, LXR agonist treatment did not (**Figure 1**). Nonetheless, both WD and T0901317 increased fecal neutral sterol loss (data not shown).

I used this differential effect to further investigate the molecular mechanism of the intestinal transport of 4F. LXR agonists increase the expression of the sterol transporters ABCG5/G8 on the apical surface of enterocytes.(2) These transporters clear phytosterols from enterocytes into the intestinal lumen,(3) but ABCG5/G8 also play an important role in TICE.(4) However, increasing TICE through higher expression of ABCG5/G8 did not increase 4F clearance. Nonetheless, I had reason to suppose that 4F clearance was a transporter-mediated process (see 2.F4A) that could also be modulated by TICE (see above).

I thus considered other enterocyte transporters that could mediate TICE and that might also transport 4F into the lumen. ABCB1, otherwise known as p-glycoprotein (P-gp) or multi-drug resistance 1 (MDR1), is a member of the ABC superfamily of proteins that also includes ABCA1 and ABCG5/G8. Like these other transporters, ABCB1 can efflux intracellular cholesterol. ABCB1 is highly expressed on the apical surface of enterocytes,(3) and ABCB1 has been identified as a transporter in TICE.(5) However, ABCB1 can also transport xenobiotics,(3) and as such it plays an important role in determining both the absorption characteristics of drugs as well as drug resistance.(6, 7) Interestingly, the xenobiotic transport capacity of ABCB1 has been shown to be both cholesterol(8) and cholesterol transport dependent.(9) ABCB1 thus rationalizes as a candidate transporter for 4F. While 4F mimics the secondary structure of apoA-I, it lacks sequence homology. It may thus be a plausible substrate for transport by ABCB1. Moreover, ABCB1 mediates TICE, while increasing the cholesterol and cholesterol transport associated with ABCB1 increases its xenobiotic transfer capacity. As such, transport of 4F by ABCB1 might explain why increasing TICE through WD or supplying lipoproteins to the serosal side of intestinal explants, but not increasing TICE through LXR and ABCG5/G8, also increases 4F clearance.

Tariquidar (TQR) is a third-generation inhibitor of ABCB1(6) with maximal inhibition in vitro at between 100nM and 1 uM.(10) I thus pre-loaded 4F into intestinal explants by IV-administering 4F to mice 30 minutes prior to explantation (see 2.F3B). Explants were pre-treated with 100 nM TQR during

removal of the muscle layer, and TQR was added to the mucosal media of Ussing chambers. As in the experiment of 2.F5D, HDL and LDL were added to the serosal chamber, and the efflux of 4F into the mucosal media was determined over time by LC-MS/MS. TQR significantly inhibited 4F transport into the mucosal media at all time points sampled from 20 minutes on (**Figure 2**). Clearance of 4F from intestinal explants was over 50% inhibited at 60 minutes, indicating that TQR at least partially mediates the clearance of 4F from intestinal tissue.

In overall summary (**Figure 3**), 4F associates with lipoproteins especially HDL in the circulation, from which 4F and 4F-associated HDL are cleared rapidly. 4F is taken up by the small intestine (SI) and transported into the intestinal lumen in a cholesterol and TICE dependent manner. Lipoproteins are a cholesterol source for TICE (see Chapter 2), suggesting that lipoproteins are the vehicle of 4F transport to the SI. After being taken up by enterocytes, 4F is cleared into the intestinal lumen at least partially by ABCB1. Once in the lumen, 4F can be taken up by intestinal tissue by an as yet unknown mechanism.

There remain a number of open questions that require additional experiments; I will here address a few. First, is HDL truly the lipoprotein carrier for 4F to the SI? Some reports have claimed that HDL is not a cholesterol source for TICE,(11) while additional reports have claimed otherwise.(5) Does 4F association in any way potentiate or tag HDL to be taken up by enterocytes? If so, could this explain why 4F-associated HDL appears to be cleared from the circulation of mice? In order to address these questions, I will first return to the Ussing chamber. ^{3}H-cholesterol-hHDL, ^{3}H-cholesterol-hHDL-^{14}C-4F, and ^{14}C-4F will be added to the serosal sides of intestinal explants. Uptake and clearance of ^{3}H, ^{14}C and human apoA-I will be determined, in order to assess whether 4F increases the uptake of cholesterol and HDL, and whether HDL increases the uptake of 4F. Comparable experiments will be performed with other lipoproteins including LDL and VLDL.

Second, inhibition of ABCB1 inhibits 4F clearance, but does activation of ABCB1 increase 4F clearance? And while ABCB1 appears to be involved in the clearance of at least some 4F from intestinal

explants, are there other pathways involved? Is all clearance transporter dependent, and if so, what additional transporters can clear 4F? MRP2 is also a xenobiotic transporter of the ABC family that is expressed apically on enterocytes.(12) Is MRP2 also involved in 4F transport? Additional studies will be performed in Ussing chambers involving ABCB1 activators, as well as inhibitors and activators of MRP2.

Finally, 4F in the lumen of the intestine can get taken up into intestinal tissue (see 2.F4B). This observation suggests that 4F can recirculate between enterocytes and lumen. However, I did not fully establish recirculation as opposed to mere uptake. Moreover, I have not identified the pathway by which 4F might be taken up by enterocytes and transported into the circulation, where at least some oral 4F distributes.(13) There exists a peptide uptake transporter on the apical side of enterocytes (PepT1), but its substrates appear limited to di- and tri-peptides.(14) It is possible that 4F is internalized by an endocytic pathway, like the protein hormone insulin (MW = 5808).(15) Recirculation at least can be investigated in Ussing chambers, by loading 4F into mucosal media; allowing 4F to load the intestinal explants for 30 minutes; clearing the mucosal media of 4F; and then determining whether 4F is nonetheless transported out into mucosal media again (with or without serosal side lipoproteins) after additional time.

In Chapter 2, I further investigated whether 4F could modulate trans-intestinal cholesterol efflux itself. I first established in vivo that 4F could increase RCT from macrophages via the TICE pathway (see Chapter 2, Figures 6A-C [2.F6A-C]), and I also showed that 4F could increase trans-intestinal cholesterol efflux from lipoproteins themselves (see 2.F6D). I next confirmed ex vivo that both tissue and mucosal 4F could increase TICE across intestinal explants (see 2.7A,C), while also demonstrating that 4F increased cholesterol efflux directly from enterocytes (see 2.7B). Independently, I had also observed that 4F could increase cholesterol efflux from macrophages (**Figure 4**). Consistent with the observations in the Appendix and Chapter 2, there exist at least three possible mechanisms by which 4F can enhance TICE

(**Figure 5**). First, 4F might increase the intestinal targeting and uptake of 4F-associated HDL **(I)**. Second, since the transport of 4F through ABCB1 requires the co-transport of cholesterol, 4F efflux itself may directly increase the efflux of cholesterol **(II)**. Finally, 4F might act as a cholesterol acceptor at the ABC transporters ABCG5/G8 **(III)**. In the Discussion of Chapter 2, I have offered the rationale behind hypothesizing (II) or (III).

In Chapter 3, I observed that oral 4F therapy reduced total cholesterol (TC) in the plasma of COX2 MKO mice fed CCHF (see 3.F4E). While this result is consistent with oral 4F increasing TICE and thereby reducing TC, I had not demonstrated in the work of Chapter 2 that oral 4F could modulate the TICE pathway. I thus pre-treated both WT and TG112 mice with oral D-4F (500 ug/ml) for 1 week. I then labeled HDL and LDL with ^{3}H-cholesterol and introduced this lipoprotein mixture into the tail veins of the mice, as in the experiment of 2.F6D. After 1 hour, I collected SI lumen wash and performed a chloroform/methanol extraction. I determined the levels of 3H-bile acids and 3H-cholesterol in the wash of untreated mice (**Figure 6A**), observing that the levels were comparable in both WT and TG112 mice. I then determined the levels of 3H-cholesterol in the lumens of both untreated and 4F-treated mice, observing that oral D-4F significantly increased the amount of labeled cholesterol that had been transported into the SI lumen in both TG112 and WT mice (**Figure 6B**). As TG112 mice largely lack biliary FC excretion, but the levels of labeled FC were comparable in both TG112 and WT mice, this result indicates that oral D-4F increased cholesterol efflux into the SI lumen via the TICE pathway at least in TG112 mice.

The results of Figure 6 together with 3.F4E suggest that oral 4F therapy can reduce TC in mice fed a high fat diet by increasing cholesterol efflux into the SI lumen, and that this increase in cholesterol efflux is at least partially mediated by TICE. This hypothesis is strengthened by our observation that oral Tg6F therapy both reduced TC and increased total neutral sterol loss into the feces in LDLR$^{-/-}$ mice fed a western diet.(16) However, several aspects of this hypothesis remain unproven. First, in the case of the

experiment of Figure 6B, cholesterol efflux into the lumen does not of itself entail net cholesterol excretion: e.g., luminal cholesterol can be reabsorbed. Thus, the effect of oral 4F on total neutral sterol loss to the feces should be observed. Second, even if one allows that increasing luminal cholesterol efflux thereby increases total net cholesterol excretion, I have not established that increasing net cholesterol excretion thereby reduces total circulating cholesterol: for example, cholesterol can be synthesized. Finally, even if one allows that increased cholesterol excretion thereby lowers total plasma cholesterol, I have not established that the amount of cholesterol lost to net efflux is sufficient to account for the amount of total plasma cholesterol reduced by oral 4F. It remains possible that 4F lowers TC not only directly, by increasing 4F-mediated clearance, but also indirectly, by somehow inhibiting e.g. cholesterol biosynthesis. Nonetheless, the finding that sufficiently-dosed oral 4F (together with oral Tg6F) can reduce plasma TC while increasing luminal cholesterol efflux or cholesterol excretion is of considerable potential significance regarding the treatment of dyslipidemia and atherosclerosis.

§2: Pathogenic mechanism of the COX2 and CCHF model of IBD: initiation and resolution of inflammation

When I began my work on the pathogenic mechanism of the COX2 and CCHF models of IBD, I had originally hypothesized that: *in the absence of COX2, cholate challenge damages intestinal epithelium and alters barrier function in a manner that leads to increased translocation of PAMP and to increased inflammation.* I further hypothesized that: *dysregulation of tissue repair and inflammation resolution pathways amplifies tissue damage and the inflammatory response in a mutually reinforcing manner.* I set out to partially test this hypothesis through three aims. **First**, I sought to determine the manner in which dietary cholate initiated inflammation in this model. **Second**, I sought to determine the

role of COX2 in the repair response of intestinal epithelium. And **third**, I sought to determine the effect of COX2 MKO on the balance of lipid pro-inflammatory and pro-resolving mediators in the intestinal tissue and plasma of these models.

I have addressed the first and third aims in the work put forward in Chapter 3. As regards my first aim, I did in fact observe that CCHF increases both barrier permeability and the translocation of PAMP (see Chapter 3, Figure 1 [3.F1]). Moreover, I observed that these changes in barrier function precede the development of intestinal inflammation—a temporal order consistent with these changes serving as an initiating cause of the subsequent inflammation. However, contrary to my original hypothesis, the effect of CCHF on barrier function is not COX2-dependent: CCHF increases barrier permeability equally in WT and COX2 TKO mice. Moreover, in my original hypothesis I assumed that changes in barrier function would be downstream of gross epithelial damage like ulceration. While I did observe that gross epithelial damage accompanied intestinal inflammation, both the changes to barrier function and the initiation of intestinal inflammation itself preceded this epithelial damage: indicating first that CCHF alters barrier function independent of gross epithelial damage, and second that this type of epithelial damage is most likely a partial consequence rather than an initiating cause of the intestinal inflammation.

While CCHF altered barrier function equally in WT and COX2 TKO mice, I nonetheless concluded that these alterations to barrier function initiated disease in the COX2 models. I detailed my reasoning in Chapter 3. In brief, intestinal inflammation in the COX2 and CCHF models is both gut microbiota and MyD88 dependent, indicating that PAMP/TLR/MyD88 signaling constitutes an essential part of disease pathogenesis (see 3.F1). Moreover, I observed that COX2 MKO dysregulates LPS-dependent expression of pro-inflammatory cytokines (see 3.F1), while 4F therapy—which protects against disease in the COX2 MKO and CCHF model—rescues this effect (see 3.F4). Taken together, the data from these sections support the hypothesis that, for the COX2 MKO and CCHF model, CCHF and COX2 MKO combine to

initiate disease as follows. First, CCHF alters barrier permeability and increases the translocation of PAMP including LPS. Second, COX2 MKO dysregulates the inflammatory response to PAMP/TLR/MyD88 signaling (perhaps through loss of feedback inhibition of NFkB), as in the case of LPS-activated CO2 MKO BMDM. Third, this dysregulation initiates an inflammatory response that over its course constitutes loss of tolerance to PAMP, perhaps as the pro-inflammatory signals themselves (e.g., IL1) amplify across successive cells in the absence of negative feedback control (**Figure 7**).

I intend to pursue the following future directions regarding this work. First, while I established the MyD88 as such is necessary for the development of intestinal inflammation in the COX2 TKO and CCHF model, the above hypothesis turns in part on the role of myeloid-specific MyD88 in the COX2 MKO model. Thus, I would like to generate myeloid COX2 and myeloid MyD88 double conditional knock-out mice, by crossing the $COX2^{fl/fl}$ mice with $MyD88^{fl/fl}$ [B6.129P2(SJL)-*Myd88*^{tm1Defr}/J] to generate $COX2^{fl/fl}$;$MyD88^{fl/fl}$ mice. $LysM^{Cre/+}$ will be backcrossed onto this background in order to generate experimental $COX2^{fl/fl}$;$MyD88^{fl/fl}$; $LysM^{Cre/+}$ mice. I will challenge these mice with CCHF and ask whether myeloid-specific MyD88 is itself necessary for the development of intestinal inflammation in the COX2 MKO model. Because COX2 MKO dysregulates TLR/MyD88 pro-inflammatory signaling in macrophages, the necessity of myeloid MyD88 in this model would amount to the necessity of dysregulated myeloid TLR/MyD88 pro-inflammatory signaling in this model. Thus, this result would lend strong support to my claim that COX2-dependent dysregulation of PAMP/TLR/MyD88 pro-inflammatory signaling in macrophages constitutes the differential cause between the opposite responses of COX2 MKO and FLOX to CCHF—my claim, in other words, that this dysregulated pro-inflammatory signaling is an initiating cause of disease in the COX2 MKO model.

Second, I intend to better characterize the full range of dysregulated pro-inflammatory signaling in COX2 MKO primary macrophages. I investigated the effect of LPS alone and observed that expressions of both IL1beta and TNFalpha were elevated. However, neither LPS nor COX2 MKO altered

the levels of lipid pro-inflammatory LOX mediators in cell lysate across 24 hr, while COX2 MKO unsurprisingly reduced the levels of pro-inflammatory COX mediators. However, LPS activation followed by the DAMP ATP, which signals through the purinergic receptor P2X7, elevates the levels pro-inflammatory LOX mediators. COX2i has been shown to elevate the levels of pro-inflammatory LOX mediators further under this double stimulation of macrophages.(17) Does COX2 MKO have the same effect? And what of the effect of COX2 MKO on the lipid and cytokine pro-inflammatory mediator profiles of TLR2, 5, 7, and 9 stimulated macrophages—all of which also signal through MyD88? What of IL1β and TNFα as stimuli—does COX2 MKO also dysregulate the pro-inflammatory response in macrophages to these stimuli? And finally, how does COX2 MKO affect the pro-inflammatory mediator profile in response to additional DAMP like apoptotic cell debris?

Finally, I intend to investigate the mechanism by which COX2 MKO dysregulates pro-inflammatory signaling in the above manners. (a) For example, In the case of the NFkB target genes IL1β and TNFα, I proposed in Chapter 3 that the loss of negative regulators of NFkB like 15d-PGJ2 might be responsible for elevated expression of these cytokines. Does exogenous 15d-PGJ2 rescue these effects, and does inhibiting prostaglandin D2 synthase (15d-PGJ2 being a non-enzymatic product of PGD2) in WT macrophages reproduce them? (b) 13EFOX, a COX2 metabolite of DHA produced in activated macrophages, is also a negative regulator of NFkB.(18) As in the case of 15d-PGJ2: are 13EFOX levels down in COX2 MKO BMDM, and does addition of exogenous 13EFOX rescue the pro-inflammatory effects of COX2 MKO on IL1 and TNF? (c) In the case of possible elevations of pro-inflammatory LOX mediators, has AA that would otherwise have gone through COX2 been shunted through LOX pathways instead (the pathway enzyme levels otherwise being the same), or are we observing a difference in LOX and e.g phospholipase enzymes instead?

I also addressed Aim 3 in Chapter 3 above. In brief, I observed that COX2 MKO elevates the levels of pro-inflammatory LOX and COX mediators in tissue and plasma (see Chapter 3, Figure 2 and associated Tables), while observing the 4F therapy reduced the levels of pro-inflammatory LOX mediators in tissue while also reducing both pro-inflammatory LOX and COX mediators in plasma (see Chapter 3, Figure 4 and associated Tables). In parallel, I observed that COX2 MKO reduced the total levels of pro-resolving LOX mediators in tissue, thereby altering the balance of pro-resolving mediators to LTB4 (see Chapter 3, Figure 2).

These changes may constitute a signature for at least those types of IBD that appear to involve loss of tolerance to pro-inflammatory stimuli like PAMP: the lipid panel results for the PAC 1L10 model broadly mirrored the results for the COX2 MKO model (see Chapter 3, Figure 6 and associated Tables). Moreover, the differential clearance of particular LOX mediators from tissue supports the hypothesis that the elevated levels of this subset of mediators (like 12HETE in the COX2 MKO model and LTB4 in the PAC IL10 model) are causal for disease in their respective models. Nonetheless, several important questions remain open and will thereby constitute the basis of some of my future work.

(1) First, what is the mechanism by which COX2 MKO elevates pro-inflammatory mediators while reducing pro-resolving mediators? For example, does loss of COX2 activity in macrophages and some neutrophils shift the lipid mediator phenotypes of those compartments towards pro-inflammatory LOX mediators? Or, as may be the case for the elevated COX mediators, does loss of COX2 activity by some other mechanism induce chronic inflammation, the result of which is higher aggregate levels of e.g. COX mediators? And related, does loss of COX2 activity directly influence the production of pro-resolving mediators? (2) The first question is thus closely related to the second important question: to what extent are these alterations in the levels of inflammatory mediators (higher pro-inflammatory mediator levels and lower pro-resolving mediator levels) causal for disease, and to what extent are they mere disease markers? At the level of the tissue and plasma, this second question becomes: to what

extent are the tissue changes causal; and even if tissue changes are causal, does this hold equally for changes in plasma levels? (3) And a third question, also related to the second: to what extent is a lack of resolution—dysregulation within resolution pathways themselves—playing a causal role in the disease of the COX2 MKO model, or is disease here largely driven instead by higher levels of lipid and cytokine pro-inflammatory mediators?

As regards the first question, I will approach it in the manner I detailed for Aim 1, above. In particular, I will make use of COX2 MKO and FLOX primary macrophages, and I will ask relative to a range of macrophage stimuli, whether COX2 MKO either raises the levels of lipid pro-inflammatory mediators or lowers the levels of lipid pro-resolving mediators. Of interest, I have conducted a pilot study in collaboration with the Bensinger lab, looking at the effect of activating WT BMDM through TLR2 (PAM3), 3 (PIC), and 4 (LPS) on lipid inflammatory mediator levels at 48 hours. I observed that all three agonists significantly increased the level of the pro-resolving mediator pathway marker 17HDHA at 48 hours in lysate (**Figure 8**), consistent with a recent report.(19) Moreover, the TLR3 agonist PIC increased 14HDHA in media and lysate (data not shown). While TLR3 activation, being limited to viral double-stranded RNA, most likely does not map into the COX2 CCHF IBD model, these experiments do provide evidence of macrophage-specific production of pro-resolving mediator pathway markers, thereby opening the possibility that COX2 MKO might influence this macrophage-specific effect.

As regards the third question, I intend to pursue two separate lines of inquiry. First, the carrageenan hind paw model of acute inflammation has a much faster experimental course than the COX2 MKO model, while also allowing one to monitor resolution non-invasively, by monitoring paw edema. I had moreover already observed that COX2 MKO delays resolution in this model (see Chapter 3, Figure 2A). I thus intend to try to answer question 3 within the hind paw model first, and then see if these results map into the COX2 MKO model. (i) Thus, in this model it would be feasible to determine a lipid mediator time course while contrasting the acute inflammatory response in FLOX paws—which do

resolve—with that of COX2 MKO paws. Does the resolving response associate with elevations of pro-resolving mediators, which are absent in the non-resolving paws? Or, rather, are the non-resolving paws differentially marked by their levels of pro-inflammatory mediators? (ii) Next, if there exist differences in resolving signals between the two groups, are there differences in resolution processes themselves? (a) First, is the resolution time course in the FLOX paws marked by a rise in neutrophils, followed by macrophages that clear the neutrophils; and is the sustained inflammation of the COX2 MKO paws marked by a co-presence of macrophages and neutrophils? (b) Second, are the COX2 MKO macrophages isolated from the swollen paw pads somehow functionally different from FLOX macrophages—e.g., less capable of efferocytosing apoptotic cells? (iii) And finally, do additions of exogenous pro-resolving mediators rescue the resolution response of the COX2 MKO paws (100 ng/resolving mediator i.p.)(20)?

With these results in hand, I then intend to work back into the COX2 MKO and CCHF model of IBD. If the protracted paw swelling of the COX2 MKO model is indeed marked by a loss of resolution function, rather than merely by an excess of pro-inflammatory function, it would be more likely that chronic inflammation of the COX2 MKO and CCHF model was comparably driven. Moreover, I have already observed that there is alteration in the balance of pro-resolving mediators to LTB4 in the intestinal tissue of this model. I have also observed that inflamed intestinal tissue is marked by the co-presence of both macrophages and neutrophils. (i) Thus, what is the capacity of the COX2 MKO macrophages in this model for resolution functions like efferocytosis? I would begin with COX2 MKO BMDM and assess cell-autonomous effects of COX2 KO, by determining whether COX2 MKO reduces the capacity of BMDM to efferocytose apoptotic Jurkat cells. (ii) Second, I would assess context-dependent effects upon efferocytosis, by isolating macrophages from inflamed intestine and likewise determining their efferocytosis capacity—as we had previously done with respect to the capacity of COX2 MKO intestinal macrophages to uptake LDL.(21) (iii) Finally, I would determine whether adding back RvD1

and LXA4 (the two pro-resolving mediators that taken together were significantly reduced in the inflamed intestinal tissue of COX2 MKO mice) could either prevent or rescue the chronic intestinal inflammation in the COX2 MKO and CCHF model—by injecting i.p. 100 ng/each mediator, 3x/wk; starting either at week 0 or week 5 of a 10 week study.(20)

§3: Pathogenic mechanism of the COX2 and CCHF model of IBD: intestinal epithelial tissue repair

Unlike Aims 1 and 3, I did not address Aim 2 in Chapter 3. Nonetheless, I have done work to address the question whether COX2 mediates the intestinal epithelial response to tissue damage. I would like to detail that work here, while laying out the future directions that I will be pursuing as regards this topic.

I had originally hypothesized that CCHF would directly damage intestinal epithelium in a COX2-dependent manner. CCHF did increase intestinal barrier permeability and damage barrier function, which changes may of themselves constitute a type of minor epithelial damage. Nonetheless, CCHF did not directly cause gross epithelial damage in COX2 TKO mice. However, ulceration and other forms of gross epithelial damage did associate with the intestinal inflammation of the COX2 TKO and CCHF model (see Chapter 3, Figure 1). While intestinal inflammation itself rather than CCHF is the most likely cause of this ulceration (see §2 above, as well as Chapter 3, Figure 1), both COX2 TKO and COX2 MKO mice begin to die of ruptured ceca at between 2-3 weeks and 7-10 weeks of CCHF challenge (**Figure 9**). This exaggerated phenotype suggests that both COX2 TKO and MKO might inhibit the tissue repair response in inflamed intestine, thereby increasing the pathogenicity of the inflammatory response.

I had also previously observed that the barrier permeability of WT mice significantly decreased compared to COX2 TKO mice by 14 days of CCHF diet (see Chapter 3, Figure 1B). While some of this difference might be due to the development of intestinal inflammation the COX2 TKO mice,

permeability in WT mice alone significantly improved at day 14 compared to day 7. I thus considered the possibility that intestinal stem cells in the crypts of COX2 TKO mice were less responsive to CCHF challenge than those of WT mice. I injected i.p. 200 ug EdU/mouse into both COX2 TKO and WT mice on day 13 and determined EdU uptake in the crypts and villi of the ilea of these mice after sacrifice on day 14.(22) As the ilea of the COX2 TKO mice lacked the inflammation present in their ileo-ceco-colic junction, monitoring proliferative response in this compartment avoided any confounding due to intestinal inflammation itself. Compared to control COX2 TKO and WT mice on chow, WT crypts increased their incorporation of EdU in response to CCHF. By contrast, incorporation of EdU into the crypts and villi of COX2 TKO did not increase from the chow baseline (**Figure 10**). As only the intestinal stem cells (ISCs) at the base of the crypt undergo proliferation and thus incorporate EdU (with EdU signal working its way down villi only as CBCC progeny differentiate), this differential response to CCHF indicates that WT ISCs but not COX2 TKO ISCs increased their rate of proliferation in response to CCHF.

PGE2 has been shown to play a protective role in response to intestinal injury, exerting both pro-proliferative and anti-apoptotic effects on epithelial cells.(23) Consistent with these findings, I observed that PGE2 increases day 5 to day 7 crypt expansion in the intestinal organoid culture system (**Figure 11**).(24) Nonetheless, the role of COX2 in the intestinal epithelial response to injury remains somewhat unclear. COX2 is upregulated in colonic epithelium in response to DSS injury in a TLR4 and MyD88 dependent manner.(25) In turn, COX2 leads to the production of PGE2, which in this model enhances proliferation and inhibits apoptosis within the epithelium by signaling through EP4.(26) COX2 is upregulated in response to radiation damage, suggesting that COX2 plays a protective role against this injury as well.(27) Moreover, it has recently been reported that oxytocin is protective against DSS, radiation, and 5-FU injury in a COX2/PGE2 dependent manner.(28) However, other reports have argued that it is COX1 rather than COX2 is protective against radiation injury.(29, 30)

I made use of the intestinal organoid culture system to investigate the role of COX2 in the passage zero response of intestinal crypts to translocation and epithelial disruption. Within this system, crypts are first stripped from intestinal epithelium before being grown in 3D Matrigel cultures in the presence of R-spondin, Noggin, and EGF.(24) Translocated crypts can develop into either spheroids or enteroids, which differ both morphologically (**Figure 12**) and in their degree of differentiation. Enteroids contain ISCs, progenitors, and the full array of differentiated intestinal epithelial cells, whereas spheroids consist of more ISCs and progenitor cells and fewer differentiated cells.(31) I had myself observed a differential uptake of EdU by intestinal epithelial in COX2 TKO and WT mice in response to CCHF challenge (see Figure 10). I thus hypothesized that translocated crypts from COX2 TKO mice would exhibit impaired expansion compared to WT crypts in the organoid system. I originally intended to assess crypt size at day 5 as a measure of differential response.

Interestingly, while D5 WT organoids were significantly larger than COX2 KO organoids (data not shown), the most striking difference between cultures presented itself at the level of early spheroids. Approximately 20% of WT crypts passed through an early (day 1-2) transient spheroid phase prior to the emergence of almost 100% enteroids at day 5-7. By contrast, both COX2 inhibition and COX2 KO significantly suppressed this early transient spheroid response (**Figure 13**). I next sought to determine whether paracrine factors from WT structures could rescue the inhibition of early spheroids that I observed in COX2 KO cultures. I thus co-cultured both WT and COX2 KO crypts in contiguous but separate Matrigel capsules, and I determined the dose-dependent effect of WT crypts upon the early spheroid response of COX2 KO structures. I observed that WT crypts did indeed increase the number of early COX2 KO spheroids in a dose-dependent fashion (**Figure 14**), indicating that epithelial COX2-dependent paracrine factors were responsible for the early spheroid response. As a result, I next tested the effect of PGE2 on crypt cultures, and I observed that PGE2 increased both the penetrance and size of early (18 hour) spheroids in WT cultures. While PGE2 also increased the penetrance and size of early

spheroids in the COX2 KO cultures, the effect was not as pronounced (**Figure 15**). Last, in order to test my conjecture that the early spheroid response was associated with tissue disruption, I passaged day 7 WT enteroids after disrupting the enteroid structures with a wide (21 gauge) or fine gauge (27 gauge) needle. Not only did fine gauge disruption produce considerably more spheroids than wide gauge disruption (approx. 60% vs 20%), PGE2 dose-dependently increased the number of spheroid structures in the fine-gauge cultures (**Figure 16**). Taken together, this data supports the hypothesis that early transient spheroids are an epithelial COX2 and PGE2 dependent response of intestinal crypts to tissue disruption, as manifested in a 3D culture system.

There exist three separate questions that follow from these opening observations. First, what is the mechanism by which epithelial COX2 and PGE2 induce early spheroids? Second, what is the nature of the early spheroids? And third, to what extent do these in vitro responses recapitulate and thus illuminate in vivo responses to tissue damage? I have only partially addressed these questions, but I will present my remaining observations before detailing my future directions as regards COX2 and epithelial tissue repair.

I first sought to determine what receptor or receptors PGE2 signaled through in order to produce the early spheroid response. I combined PGE2 with individual antagonists to the PGE2 receptors EP1-4, and I observed whether any of these antagonists would block the PGE2-dependent induction of early spheres. While none of the EP1-3 antagonists blocked the inductive effect of PGE2 (data not shown), the EP4 antagonist completely inhibited the early spheroid response (**Figure 17**). I thus concluded that PGE2 signals through EP4 in this context. I have yet to determine the subsequent steps in this signaling process.

I next sought to determine the nature of the early spheroids. First, I considered their basic morphology. In contrast to enteroids, spheroids are swollen, thin-membranous, and fluid-filled structures, and their cores are empty of cells and debris. I thus entertained the hypothesis that this

swelling was the result of osmosis across an osmotic or ion gradient into what would have been intestinal lumen but now constitutes the spheroid core. The cAMP-activated cystic fibrosis transmembrane conductance regulator (CFTR) and calcium-activated chloride channels (CaCCs) are chloride channels that are expressed apically on enterocytes, and their activation can lead to the outflow of water and on occassion secretory diarrhea.(32) PGE2 can stimulate adenylate cyclase, thus raising intracellular cAMP levels. Moreover, PGE2 increased the size and apparent swelling of spheroids (see Figure 15). I thus considered the hypothesis that PGE2 increased the size of spheroids through cAMP-dependent activation of CFTR. I tested the effects both of a CFTR activator (2-Pyridin-4-yl-benzo[h]chromen-4-one) and of PGE2 in combination with a CFTR inhibitor (CFTR(inh)-172) on WT crypt cultures. While the CFTR inhibitor did not affect the capacity of PGE2 to induce early spheroids, the CFTR activator did produce spheroid-like structures (**Figure 18**). These results suggest that at least some of the spheroid phenotype might be the result of swelling due to the production of an osmotic gradient. If true, a corresponding in vivo response might be useful for crypts in the case of injury, potentially defending the epithelium and lamina propria against bacterial infection. For example, loss of CFTR osmoregulatory function can increase the chance of *Pseudomonas aeruginosa* infection in airway epithelia.(33) I intend next to determine whether PGE2/EP4 induce early spheres through activation of CaCC.

Independent of their morphology, it is a received view that the cells of spheroid structures are less differentiated and more stem-like than those of enteroid structures.(31) I thus sought to determine the effects of COX2 KO and PGE2 on various stem cell, reserve stem cell, and differentiation markers at 0 and 18 hrs. Across several experiments, I have observed the following patterns. First, expression of differentiation cell markers (*Muc2*, goblet cells; *Lyz*, Paneth cells; *Vil*, enterocytes) drops between 4 and 10 fold across the first 18 hrs of culture for both WT and COX2 KO, and the addition of PGE2 does not affect this drop (**Figure 19A**). Second, though expression of the reserve stem cell markers *Bmi1* and *Tert*

increases in both WT and COX2 KO cultures, this increase is several-fold higher in COX2 KO. Addition of PGE2 largely inhibits this increase in COX2 KO cultures without affecting expression of these markers in WT (**Figure 19B**). Third, addition of PGE2 increases expression of the ISC marker *Lgr5* several fold in WT compared to no-treatment control. *Lgr5* expression begins higher in COX2 KO compared to WT crypts, but PGE2 in fact lowers expression of *Lgr5* in COX2 KO compared to control (**Figure 19C**).

More interestingly, *Wnt3A* expression increases a hundred-fold across 18 hours in WT type, while PGE2 increases expression of *Wnt3A* several fold more. In COX2 KO by contrast, *Wnt3A* expression is increased neither at 18 hrs nor by addition of PGE2 (**Figure 19D**). However, PGE2 can signal through COX2 KO structures, as indicated by the effect of PGE2 on expression of *Hopx* and *Bmi1*, and by its capacity to produce early spheroids (see Figure 15). This suggests that the effect of PGE2 on *Wnt3A* expression is COX2 mediated, as PGE2 induces *Ptgs2* expression in WT but not COX2 KO. I thus added a stable analog of PGI2 (beraprost) to COX2 KO crypts and observed that beraprost unlike PGE2 increased expression of *Wnt3A* almost 100-fold. Wnt3A is required for maintenance of intestinal stem cells by way of signaling through the canonical Wnt pathway and beta-catenin.(34) This expression pattern correlates with the degree of early spheroids in WT cultures, suggesting that these early spheroids are oriented towards ISC maintenance. The fact that expression of *Wnt3A* in PGE2-treated WT and COX2 KO structures differs so greatly, even while PGE2 induces the production of spheroids in both cultures, indicates that morphologically similar spheroids may nonetheless be importantly different at the level of stem cell potential. Finally, the fact that the morphological effect of PGE2 comes apart from its effect on *Wnt3A* expression indicates that increased spheroid swelling and spheroid "stemness" constitute two distinct effects of PGE2.

Last, and unexpectedly, expression of the enteroendocrine marker chromogranin A (*ChgA*) increased by 300-fold at 18 hours in WT, and PGE2 increased the expression of this marker approximately 20-fold more. In COX2 KO, *ChgA* expression increased comparably through 18 HRs, but

PGE2 alone did not further increase its expression. However, as in the case of *Wnt3A*, beraprost increased *ChgA* expression comparable to the effect of PGE2 in WT (**Figure 19E**). *ChgA* and *Lgr5* are co-expressed in secretory progenitor cells that have shown the capacity to dedifferentiate back into actively dividing ISCs.(35) Additional studies have also identified enteroendocrine precursor cells marked in part by *ChgA* and *Bmi1* expression as capable of serving as a reserve population that can replenish the stem cell pool upon damage.(36) It is perhaps possible that PGE2 is increasing the population of this reserve pool in WT spheroids. However, while PGE2 increases the expression of *Bmi1* in WT, this change is nowhere comparable to that of the change in *ChgA* expression.

PGE2 induced WT spheroids while also increasing expression of *Lgr5* and *Wnt3A*, and at the same time markers for differentiated cells including goblet, Paneth, and enterocyte cells decreased. These observations are consistent with a picture of PGE2-induced WT spheroids as being more "stem-like" and less differentiated than time 0 crypts. Interestingly, I also observed that PGE2 increased the complexity of the late (day 5 to day 7) enteroids that replace the transient early spheroid structures (see Figure 11). Increased complexity or budding of an enteroid is the product of an increased number of actively dividing stem cell niches associated with that enteroid structure.(31) Release of quiescent or reserve stem cell populations to become actively dividing stem cell has been linked to release of PTEN inhibition of the PI3K/AKT/mTORC1 signaling pathway.(37) Moreover, PGE2 has been shown to activate PI3K/AKT by signaling through EP4.(38) I thus treated WT cultures with either PGE2 or PTEN inhibitor (VO-OHpic trihydrate) and determined their effect on complex budding of enteroids. I observed that both PGE2 and PTEN inhibition significantly and comparably increased the number of complex enteroids (**Figure 20**).

While rather incomplete, these in vitro studies suggest a model in which crypt translocation induces the expression of COX2 in crypts through some an unknown factor (see Figure 19). COX2 dependent PGE2 from crypt cells as well as from cells in the stem cell niche triggers the formation of

protective osmotic gradients while promoting the "stemness" of affected crypts, increasing expression of both *Lgr5* and *Wnt3A*. At the same time, the affected crypts lose differentiated cells while increasing the size of their reserve stem cell pool. Subsequent inactivation of PTEN, possibly through further PGE2/EP4 signaling, releases the "stem-like" cells of these pool from a more quiescent to an actively dividing state. These actively dividing stem cells repopulate crypts and drive subsequent production of fully differentiated epithelium (**Figure 21**). I will be testing this hypothesis in my upcoming work.

In order to link these in vitro observations back to the mouse, I am also asking whether COX2 and in particular myeloid COX2 play a role in the intestinal epithelial repair response to tissue injury in vivo. I have provided some data to suggest that both total COX2 and epithelial COX2 might mediate such a response. There is also evidence to suggest that macrophage COX2 plays a role in epithelial repair. In response to DSS injury, activated macrophages are recruited to the colonic crypt,(39) where they play an important role in bringing about the hyperproliferation of colonic stem cells.(39, 40) It has also been shown that macrophage COX2 appears to mediate this response, as COX2 MKO mice exhibit less colonic epithelial proliferation than WT controls in response to DSS injury.(41) I thus intend to investigate the role of COX2 TKO and MKO in the intestinal epithelial repair response in mouse models of intestinal injury.

While COX2 appears to mediate a proliferative response to CCHF, and while CCHF directly damages intestinal epithelium in the sense of decreasing barrier function, it is unclear that CCHF challenge alone--in the absence of intestinal inflammation—constitutes the basis of a true intestinal injury model. Received models of intestinal injury include 5-FU, abdominal irradiation, and DSS.(28) I am currently working with an abdominal irradiation injury model.(42) In a pilot study involving x-ray irradiation injury, I have determined that 16 Gy dose is sufficient to injure the intestinal epithelium of WT mice by day 5, while allowing these mice to recover by day 9 (data not shown). I thus intend to irradiate COX2 TKO, MKO, and WT mice with 16 Gy and assess stem cell proliferation and crypt health by

EdU uptake and histology at both D5 and D9 post-radiation. I hypothesize that in the absence of COX2, intestinal stem cells in the ileum will undergo less proliferation, while there will exist more crypt abscesses, blunted villi, and other histological evidence of exaggerated epithelial injury. If COX2 MKO mice exhibit a compromised injury repair response, I will proceed to investigate the role of variously activated primary macrophages on the response of translocated crypts in the in vitro organoid system.

§4: Protective mechanisms of 4F and trans-intestinal lipid transport

I identified two distinct novel therapeutic applications for the apoA-I mimetic peptides including 4F. First, I have here reported that 4F can modulate TICE (see Chapter 2), and I have shown that oral 4F therapy can both increase TICE (see Figure 6) and reduce total cholesterol in COX2 MKO mice fed CCHF diet (see Chapter 3, Figure 4E) . Moreover, my observations regarding the effect of 4F on TICE have been extended to apoA-I mimetics more generally. We have recently reported that Tg6F lowered TC and increased neutral sterol excretion in $LDLR^{-/-}$ mice fed a western diet.(16)

Elevated TC and dyslipidemia are risk factors for the development of CVD.(43) While the importance of TICE as a secondary excretion pathway for free cholesterol (FC) has been established in mice, it was only recently established that TICE plays an equally significant role in maintaining cholesterol homeostasis in humans.(4) Modulation of TICE is thus a promising therapeutic target for the treatment of CVD. LXR agonists were found to stimulate TICE up to six-fold in murine studies using different experimental methodologies.(1, 44) However, activation of LXRs concurrently promotes hepatic de novo lipogenesis, steatosis, and hypertriglyceridemia via direct activation of the sterol regulatory element-binding protein-1c (SREBP-1c) gene and fatty acid synthesis pathways.(45) Intestinal-specific LXR agonists have been developed that evade the unfavorable effects of general agonists on hepatic lipogenesis. Nonetheless, the development of LXR-targeted drugs has largely been

discontinued due to observations of marked increases in plasma apoB containing lipoproteins and/or a marked liver-steatotic response.(46) By contrast, 4F itself has a favorable toxicological profile and has advanced as far as phase 2 clinical trials.(47) Other apoA-I mimetic peptides appear to be likewise free of unfavorable side effects. 4F and other apoA-I mimetics may thus constitute an important new class of TICE-dependent modulators of TC. Of equal import, understanding the exact mechanism by which 4F increases TICE may reveal important new therapeutic targets within the space of TICE itself (see Figure 5).

Second, I have also shown that 4F is protective against IBD in both the COX2 CCHF and PAC IL10 mouse models. As I noted in my introduction to Chapter 3, IBD has high morbidity, but there currently exist few effective therapies for this disease. The identification of a new class of potential IBD therapy is thus of considerable significance as regards the treatment of this disease. Moving forward, our laboratory group will be continuing to investigate the potential of Tg6F as a treatment for IBD. Our aim is clinical trials. However, considerable work remains necessary in order to fully characterize the effectiveness of this class of therapy in animal models. First, are apoA-I mimetics only prophylactic against disease, or are they effective against disease that has already developed? In both of my mouse models, I began mimetic peptide therapy prior to the onset of disease. What is the effect of these therapies against existing disease? I thus plan to start mimetic peptide therapy part-way through the disease time course of both models, in order to determine if the drugs can either halt or reverse the progression of existing disease. Second, what is the full range of effectiveness of these drugs as IBD therapies? I showed that 4F is protective in two independent mouse models of IBD. However, I also showed that both models overlap in important ways. In particular, disease in both models appears to initiate when an environmental trigger increases barrier permeability and leads to the translocation of PAMP. Genetic alteration of COX2 and IL10 in turn effects loss of tolerance to these inflammatory triggers. In both models, I also showed that 4F appears to inhibit LPS-dependent activation of

macrophages, likely by interfering with LPS-dependent signaling itself. Is the therapeutic range of mimetic peptide therapy limited to mouse models of IBD that depend upon a dysregulated response to PAMP as a driving cause? It will be important to continue to test apoA-I mimetics in mouse models of IBD that differ in their underlying pathogenic mechanisms, at the same time that we continue to detail the exact protective mechanisms of this class of drugs.

Of importance, my combined investigation into the pathogenic mechanism of the COX2 CCHF model and into the protective mechanism of 4F has potentially identified a previously uncharacterized physiological pathway or pathways involved in the clearance of lipid inflammatory mediators from the circulation. The literature on trans-intestinal cholesterol efflux does not consider the possibility that lipid species other than cholesterol may also be subject to trans-intestinal transport. There are hints in the literature nonetheless that such transport might exist. ApoA-I can be produced in the small intestine,(48) and it has shown that apoA-I is released from the apical membrane of enterocytes into the SI lumen, where it continues to associate with the brush border membrane.(49) ApoA-I can accept both cholesterol and phospholipids from the ABC transporter ABCA1.(50) ABCG5/G8 is highly expressed on the apical surface of enterocytes, raising the possibility that not just cholesterol but also phospholipids as well are accepted by luminal apoA-I. In parallel, there also exists some evidence that lipid inflammatory mediators can themselves be transported from inside enterocytes into the intestinal lumen. The apical ABC transporter MDR2 has been shown to transport the pro-inflammatory eicosanoid hepoxilin A3 into the lumen, in order to produce a chemotactic gradient for the recruitment and transmigration of neutrophils.(51) However, no group has investigated whether trans-intestinal transport itself might also include these additional lipid species like phospholipids and eicosanoids.

In the experiment reported in Chapter 3, Figure 5C, I observed that tagged lipid inflammatory mediators were transported from serosal lipoproteins into the mucosal media ex vivo. To my knowledge, this is the first report suggesting the possibility of trans-intestinal lipid transport (TILT) for

lipid species other than cholesterol. I also observed that luminal 4F enhanced the trans-intestinal transport of these eicosanoids. Lipid pro-inflammatory mediators were elevated in the plasmas of diseased mice in both COX2 CCHF and PAC IL10 models (see 3.F2 and 3.F6). 4F protects against disease in both models while also rescuing the levels of these pro-inflammatory mediators (see 3.F4 and 3.F6). Together, these observations suggest that trans-intestinal transport of inflammatory mediators might play a protective physiological role against inflammation. At the least, they suggest the possibility that 4F clears pro-inflammatory mediators from plasma by targeting an already existing physiological clearance pathway.

Overall, my speculative model is as follows. LDL and circulating 4F transfer inflammatory mediators to HDL, and 4F-associated HDL is tagged for uptake by the enterocytes. In the absence of circulating 4F, pro-inflammatory mediators nonetheless continue to associate with lipoproteins, and as lipoproteins are taken up by enterocytes to deliver FC for TICE, so too are these inflammatory mediators internalized. 4F has high binding affinity for eicosanoids,(52) and it is possible that 4F associates with these mediators intracellularly. 4F is then transported out of the enterocytes into the lumen partially through abcb1, taking any associated inflammatory mediators with it. Alternatively, 4F acts as a lipid acceptor at apical ABC transporters, where it can accept not only cholesterol but also other lipid species as well. Once cleared into the lumen, 4F-constituted lipid micelles are then somehow potentiated for excretion or microbial metabolism. In parallel, lumen apoA-I might also be accepting both cholesterol and additional lipid species at ABC transporters, thereby constituting luminal lipoproteins that are again somehow blocked from reuptake and potentiated for excretion or breakdown (**Figure 22**).

Going forward, my aim is to employ the Ussing chamber system to first characterize the nature of the underlying TILT pathway. I will seek to determine the range of lipid species that can be transported in this manner—conducting experiments with heavy label versions of phospholipids, cholesterol esters, and additional inflammatory mediators. I will next work to characterize the nature of

the transport process. Is it passive or active, and transporter dependent or merely involving passive diffusion? If transporter dependent, I will then employ a range of transporter inhibitors and activators in order to try to identify the both the basolateral uptake and apical efflux transporters involved. Finally, are the TILT of other lipid species dependent upon TICE, somehow piggybacking not only on the basolateral uptake of lipoproteins but also the apical efflux of cholesterol itself?

Next, continuing with Ussing chambers, I hope to work out the manner in which 4F interacts with this underlying process, to increase the TILT of affected lipid species. Does 4F work as an intracellular chaperone, or as a apical-side acceptor? Can 4F increase the transport of other lipid species independently of cholesterol, or is the transport of these other species a secondary effect of 4F affecting TICE? Do luminal 4F and these lipid species constitute micelles or lipoprotein-like structures?

I will then work to try to establish the existence of TILT in vivo. I will conduct variants of the RCT experiments that I deployed in chapter 2, except that instead of using labelled cholesterol, I will track the transport of labeled and methylated lipid inflammatory mediators. Do these tagged stable mediators show up in intestinal tissue, and are they cleared into the intestinal lumen? And if so, does either luminal or circulating 4F increase this clearance? Lastly, what is the luminal fate of these mediators? Can they be detected in feces; are they metabolized by gut microbiota; or are they taken back up by enterocytes?

I also hope to do some work trying to establish the pathogenic and protective significance of elevated or rescued levels of plasma inflammatory mediators. I noted in my introduction to Chapter 2 that IBD is a risk factor for the development of CVD. We have moreover observed that IBD associates with elevated levels of plasma pro-inflammatory mediators. Do COX2 MKO mice on CCHF diet develop atherosclerosis, and do they do so in partial consequence of these elevated levels of plasma pro-inflammatory mediators? We have previously reported that COX2 MKO mice crossed into an $ApoE^{-/-}$ background do not develop atherosclerosis when fed a western diet.(53) However, the mice in this

model did not develop intestinal inflammation. As a result, any atherosclerosis that develops in COX2 MKO mice on CCHF diet will be more likely attributable to the development of intestinal inflammation itself. If COX2 MKO + CCHF mice do develop atherosclerosis, we will also have an excellent model for trying to figure out how changes in the intestine result in disease at distant loci. One obvious candidate hypothesis would be that changes in plasma inflammatory phenotype consequent to intestinal inflammation mediate the link between intestinal inflammation and the development of atherosclerosis.

Last, I have interest in trying to work out the role of intestinal apoA-I, in order to determine first whether 4F in its capacity to influence TILT is merely mimicking and amplifying a physiological role already performed by apoA-I; and second, whether intestinally-produced HDL varies in quality depending on the inflammatory status of the intestine. I would like to create mice whose intestinally produced apoA-I is somehow tagged fluorescently—perhaps by inserting a floxed fluorescent tag into the apoA-I gene, which is somehow turned on by e.g. flipping as a the result of Cre-recombinase activity. We could then cross the silent tagged apoA-I mouse with a Villin-cre mouse, to create intestinal-specific active tagged apoA-I. With this active tagged apoA-I, we would be able to fluorescently sort out intestinally produced HDL, in order to determine its phenotype across a range of alterations in the intestine, including intestinal inflammation. I could also track apoA-I inside the intestinal lumen, in order to try to determine whether intestinal apoA-I is e.g. constituting luminal lipoproteins, is accepting e.g. tagged lipid species from the circulation, and so on.

While the work of this thesis has ranged across what may seem to be a number of disparate subjects, it has nonetheless been united at its core by my overall aim of working back and forth between the pathogenic mechanisms of disease and protective mechanisms of therapy in order to better understand both. This approach came to some fruition in my work on the COX2 KO and CCHF model of IBD, for which I identified apoA-I mimetics as a promising class of potential therapies. At least as

important, however, my work identified types of changes in inflammatory mediator profile that were elevated by disease but which were rescued by 4F therapy. These observations raised important questions about the mechanistic importance of various tissue and plasma specific alterations in mediator profile—questions I hope to address, as detailed above. These observations also led in turn to my observations about TILT, whose underlying physiological nature and whose value as a therapeutic target I hope to determine in my work to come.

Materials and Methods

LXR agonist, WD, and trans-intestinal transport of 4F. The experiment of Figure 1 followed in accord with Methods in Chapter 2.(54) In brief, TG112 mice were pre-treated with the LXR agonist T0901317 for 7 days (25 mg/kg/day) or WD for 6 weeks. Then 25 mg/kg 14C-L-4F was injected via tail vein, and radioactivity in SI rinse was reported. Feces from the mice was collected directly from the distal colons of these mice, and neutral sterols in the feces were determined by GCMS.

Inhibition of ABCB1 and 4F secretory transport. The Ussing chamber experiment of Figure 2 followed in accord with the Methods in Chapter 2. In brief, D-4F was injected via tail vein into C57BL/6J mice. After 30 minutes, paired intestinal explants were mounted in Ussing chambers with and without 100 nM tariquidar in mucosal media (n = 6). Mucosal media was sampled at multiple time points, and concentration of D-4F was determined by LC-MS/MS.

Cholesterol efflux from macropahges. J774 macrophages were loaded with ^{3}H-cholesterol in accord with the Methods of Chapter 2. D-4F (10 and 50 ug/ml) was added to media, and after 1 hour cholesterol efflux was determined as a percent of starting cholesterol load by scintillation counting (n = 4/group).

Oral D-4F and RCT from lipoproteins. This experiment followed the methods as reported in Chapter 2, with modification. TG112 and WT mice were pre-treated with oral D-4F (500 ug/ml water) for 1 week and allowed to drink through the course of the experiment.

TLR activation of bone-marrow derived macrophages. Bone marrow derived macrophages were generated as previously described.(55) Macrophages were treated with activators of TLR2 (Pam3), 3 (PolyI:C), and 4 (LPS) as described previously.(19, 55) After 48 hours, lysates were collected and inflammatory mediator levels were determined by LC-MS/MS, as described in Chapter 3.

COX2 KO and CCHF survival study. COX2 TKO and MKO mice were fed CCHF for 16 days or 7-10 weeks, respectively. Survival was determined. For dead mice, cause of death was determined by pathological examination.

EdU incorporation. COX2 TKO and WT mice (n=5) were fed CCHF diet for 2 weeks. Additional mice were fed only chow. EdU (200 ug/ms) was injected i.p. into each mouse 24 hours prior to sacrifice. Histological sections were taken from the ilea of these mice, and EdU was labelled with a fluorescent tag as described.(22) Fluorescent intensity was determined for each mouse in three separate noncontiguous 5x fields and averaged.

Intestinal epithelial organoid cultures. Proximal small intestinal crypts were isolated and expanded in 3D Matrigel cultures as previously described.(24) In brief, crypts were stripped from intestinal epithelium by EDTA and manual disruption and then purified by fractionation and filtration. Crypts were added to Matrigel (approximately 100-200 crypts/culture) and grown in complete media supplemented with R-spondin, Noggin, and EGF. Crypts were isolated from either C57BL/6J of COX2 TKO ($COX2^{luc/luc}$) mice. For passage, day 7 enteroid structures in Matrigel were manually disrupted using a syringe with either a small gauge (27 gauge) or large gauge (21 gauge) needle. Disrupted enteroids were then re-cultured in Matrigel as for passage 0 crypts.

Treatment of organoid cultures. For those experiments involving treatment, cultures were treated with either vehicle control or the following compounds. For PG stimulation: 10 nM PGE2; 1 uM stable PGI2 analog beraprost.(56) For COX2 inhibition: 1 uM of the COX2 inhibitor NS398. For PGE2 receptor antagonism: EP1 antagonist (GW 848687X); EP2 antagonist (PF-04418948); EP3 antagonist (L-798106); EP4 antagonist (GW 627368X); dosing ranges as described.(57) For CFTR inhibition and activatin: CFTR inhibition (CFTR(inh)-172) ; CFTR activation (2-Pyridin-4-yl-benzo[h]chromen-4-one). For PTEN inhibition: 300 nM VO-OHpic trihydrate.(58)

Crypt culture gene expression. Crypts from both COX2 TKO and WT mice were seeded at 200 crypts/well and treated with either 10 nM PGE2 or 1 uM beraprost across 18 hrs. RNA was isolated from treated cultures together with untreated controls at 18 hrs, as well as from time 0 crypts. Gene expression was determined for the murine genes listed in Figure 19 and in §3 using Biorad SYBR green in accord with standard protocols.

1. van der Veen, J. N., T. H. van Dijk, C. L. Vrins, H. van Meer, R. Havinga, K. Bijsterveld, U. J. Tietge, A. K. Groen, and F. Kuipers. 2009. Activation of the liver X receptor stimulates trans-intestinal excretion of plasma cholesterol. *J Biol Chem* **284**: 19211-19219.

2. Repa, J. J., K. E. Berge, C. Pomajzl, J. A. Richardson, H. Hobbs, and D. J. Mangelsdorf. 2002. Regulation of ATP-binding cassette sterol transporters ABCG5 and ABCG8 by the liver X receptors alpha and beta. *The Journal of biological chemistry* **277**: 18793-18800.

3. Kimura, Y., S. Y. Morita, M. Matsuo, and K. Ueda. 2007. Mechanism of multidrug recognition by MDR1/ABCB1. *Cancer science* **98**: 1303-1310.

4. Jakulj, L., T. H. van Dijk, J. F. de Boer, R. S. Kootte, M. Schonewille, Y. Paalvast, T. Boer, V. W. Bloks, R. Boverhof, M. Nieuwdorp, U. H. Beuers, E. S. Stroes, and A. K. Groen. 2016. Transintestinal Cholesterol Transport Is Active in Mice and Humans and Controls Ezetimibe-Induced Fecal Neutral Sterol Excretion. *Cell metabolism* **24**: 783-794.

5. Le May, C., J. M. Berger, A. Lespine, B. Pillot, X. Prieur, E. Letessier, M. M. Hussain, X. Collet, B. Cariou, and P. Costet. 2013. Transintestinal Cholesterol Excretion Is an Active Metabolic Process Modulated by PCSK9 and Statin Involving ABCB1. *Arteriosclerosis, Thrombosis, and Vascular Biology* **33**: 1484-1493.

6. Amin, M. L. 2013. P-glycoprotein Inhibition for Optimal Drug Delivery. *Drug Target Insights* **7**: 27-34.

7. Shugarts, S., and L. Z. Benet. 2009. The Role of Transporters in the Pharmacokinetics of Orally Administered Drugs. *Pharmaceutical Research* **26**: 2039-2054.

8. Troost, J., N. Albermann, W. Emil Haefeli, and J. Weiss. 2004. Cholesterol modulates P-glycoprotein activity in human peripheral blood mononuclear cells. *Biochemical and biophysical research communications* **316**: 705-711.

9. Troost, J., H. Lindenmaier, W. E. Haefeli, and J. Weiss. 2004. Modulation of cellular cholesterol alters P-glycoprotein activity in multidrug-resistant cells. *Molecular pharmacology* **66**: 1332-1339.

10. Weidner, L. D., K. L. Fung, P. Kannan, J. K. Moen, J. S. Kumar, J. Mulder, R. B. Innis, M. M. Gottesman, and M. D. Hall. 2016. Tariquidar Is an Inhibitor and Not a Substrate of Human and Mouse P-glycoprotein. *Drug Metabolism and Disposition* **44**: 275-282.

11. Vrins, C. L. J., R. Ottenhoff, K. van den Oever, D. R. de Waart, J. K. Kruyt, Y. Zhao, T. J. C. van Berkel, L. M. Havekes, J. M. Aerts, M. van Eck, P. C. N. Rensen, and A. K. Groen. 2012. Trans-intestinal cholesterol efflux is not mediated through high density lipoprotein. *Journal of Lipid Research* **53**: 2017-2023.

12. Mottino, A. D., T. Hoffman, L. Jennes, and M. Vore. 2000. Expression and localization of multidrug resistant protein mrp2 in rat small intestine. *The Journal of pharmacology and experimental therapeutics* **293**: 717-723.

13. Navab, M., S. T. Reddy, G. M. Anantharamaiah, S. Imaizumi, G. Hough, S. Hama, and A. M. Fogelman. 2011. Intestine may be a major site of action for the apoA-I mimetic peptide 4F whether administered subcutaneously or orally. *J Lipid Res* **52**: 1200-1210.

14. Adibi, S. A. 1997. The oligopeptide transporter (Pept-1) in human intestine: biology and function. *Gastroenterology* **113**: 332-340.

15. Ziv, E., and M. Bendayan. 2000. Intestinal absorption of peptides through the enterocytes. *Microscopy research and technique* **49**: 346-352.

16. Mukherjee, P., G. Hough, A. Chattopadhyay, M. Navab, H. R. Fogelman, D. Meriwether, K. Williams, S. Bensinger, T. Moller, K. F. Faull, A. J. Lusis, M. L. Iruela-Arispe, K. I. Bostrom, P. Tontonoz, S. T. Reddy, and A. M. Fogelman. 2017. Transgenic tomatoes expressing the 6F peptide and ezetimibe prevent diet-induced increases of IFN-β and cholesterol 25-hydroxylase in jejunum. *Journal of Lipid Research* **58**: 1636-1647.

17. Norris, P. C., D. Gosselin, D. Reichart, C. K. Glass, and E. A. Dennis. 2014. Phospholipase A2 regulates eicosanoid class switching during inflammasome activation. *Proc Natl Acad Sci U S A* **111**: 12746-12751.

18. Groeger, A. L., C. Cipollina, M. P. Cole, S. R. Woodcock, G. Bonacci, T. K. Rudolph, V. Rudolph, B. A. Freeman, and F. J. Schopfer. 2010. Cyclooxygenase-2 generates anti-inflammatory mediators from omega-3 fatty acids. *Nature Chemical Biology* **6**: 433.

19. Oishi, Y., N. J. Spann, V. M. Link, E. D. Muse, T. Strid, C. Edillor, M. J. Kolar, T. Matsuzaka, S. Hayakawa, J. Tao, M. U. Kaikkonen, A. F. Carlin, M. T. Lam, I. Manabe, H. Shimano, A. Saghatelian, and C. K. Glass. 2017. SREBP1 contributes to resolution of pro-inflammatory TLR4 signaling by reprogramming fatty acid metabolism. *Cell metabolism* **25**: 412-427.

20. Fredman, G., J. Hellmann, J. D. Proto, G. Kuriakose, R. A. Colas, B. Dorweiler, E. S. Connolly, R. Solomon, D. M. Jones, E. J. Heyer, M. Spite, and I. Tabas. 2016. An imbalance between specialized pro-resolving lipid mediators and pro-inflammatory leukotrienes promotes instability of atherosclerotic plaques. *Nat Commun* **7**: 12859.

21. Watanabe, J., J. A. Lin, A. J. Narasimha, A. Shahbazian, T. O. Ishikawa, M. G. Martin, H. R. Herschman, and S. T. Reddy. 2010. Novel anti-inflammatory functions for endothelial and myeloid cyclooxygenase-2 in a new mouse model of Crohn's disease. *Am J Physiol Gastrointest Liver Physiol* **298**: G842-850.

22. Salic, A., and T. J. Mitchison. 2008. A chemical method for fast and sensitive detection of DNA synthesis in vivo. *Proceedings of the National Academy of Sciences* **105**: 2415-2420.

23. Stenson, W. F. 2007. Prostaglandins and epithelial response to injury. *Current Opinion in Gastroenterology* **23**: 107-110.

24. Lei, N. Y., Z. Jabaji, J. Wang, V. S. Joshi, G. J. Brinkley, H. Khalil, F. Wang, A. Jaroszewicz, M. Pellegrini, L. Li, M. Lewis, M. Stelzner, J. C. Dunn, and M. G. Martin. 2014. Intestinal subepithelial myofibroblasts support the growth of intestinal epithelial stem cells. *PLoS One* **9**: e84651.

25. Fukata, M., A. Chen, A. Klepper, S. Krishnareddy, A. S. Vamadevan, L. S. Thomas, R. Xu, H. Inoue, M. Arditi, A. J. Dannenberg, and M. T. Abreu. 2006. Cox-2 is regulated by Toll-like receptor-4 (TLR4) signaling: Role in proliferation and apoptosis in the intestine. *Gastroenterology* **131**: 862-877.

26. Jiang, G. L., A. Nieves, W. B. Im, D. W. Old, D. T. Dinh, and L. Wheeler. 2007. The prevention of colitis by E Prostanoid receptor 4 agonist through enhancement of epithelium survival and regeneration. *J Pharmacol Exp Ther* **320**: 22-28.

27. Keskek, M., E. Gocmen, M. Kilic, S. Gencturk, B. Can, M. Cengiz, R. M. Okten, and M. Koc. 2006. Increased Expression of Cyclooxygenase-2 (COX-2) in Radiation-Induced Small Bowel Injury in Rats. *Journal of Surgical Research* **135**: 76-84.

28. Chen, D., J. Zhao, H. Wang, N. An, Y. Zhou, J. Fan, J. Luo, W. Su, C. Liu, and J. Li. 2015. Oxytocin evokes a pulsatile PGE2 release from ileum mucosa and is required for repair of intestinal epithelium after injury. *Scientific Reports* **5**: 11731.

29. Cohn, S. M., S. Schloemann, T. Tessner, K. Seibert, and W. F. Stenson. 1997. Crypt stem cell survival in the mouse intestinal epithelium is regulated by prostaglandins synthesized through cyclooxygenase-1. *The Journal of clinical investigation* **99**: 1367-1379.

30. Houchen, C. W., W. F. Stenson, and S. M. Cohn. 2000. Disruption of cyclooxygenase-1 gene results in an impaired response to radiation injury. *American journal of physiology. Gastrointestinal and liver physiology* **279**: G858-865.

31. Hong, S. N., J. C. Y. Dunn, M. Stelzner, and M. G. Martín. 2017. Concise Review: The Potential Use of Intestinal Stem Cells to Treat Patients with Intestinal Failure. *STEM CELLS Translational Medicine* **6**: 666-676.

32. Thiagarajah, J. R., and A. S. Verkman. 2013. Chloride Channel-Targeted Therapy for Secretory Diarrheas. *Current opinion in pharmacology* **13**: 888-894.

33. Jolly, A. L., D. Takawira, O. O. Oke, S. A. Whiteside, S. W. Chang, E. R. Wen, K. Quach, D. J. Evans, and S. M. Fleiszig. 2015. Pseudomonas aeruginosa-induced bleb-niche formation in epithelial cells is independent of actinomyosin contraction and enhanced by loss of cystic fibrosis transmembrane-conductance regulator osmoregulatory function. *mBio* **6**: e02533.

34. Krausova, M., and V. Korinek. 2014. Wnt signaling in adult intestinal stem cells and cancer. *Cellular Signalling* **26**: 570-579.

35. Tetteh, P. W., H. F. Farin, and H. Clevers. 2015. Plasticity within stem cell hierarchies in mammalian epithelia. *Trends in cell biology* **25**: 100-108.

36. Jadhav, U., M. Saxena, N. K. O'Neill, A. Saadatpour, G. C. Yuan, Z. Herbert, K. Murata, and R. A. Shivdasani. 2017. Dynamic Reorganization of Chromatin Accessibility Signatures during Dedifferentiation of Secretory Precursors into Lgr5+ Intestinal Stem Cells. *Cell stem cell* **21**: 65-77.e65.

37. Richmond, C. A., M. S. Shah, L. T. Deary, D. C. Trotier, H. Thomas, D. M. Ambruzs, L. Jiang, B. B. Whiles, H. D. Rickner, R. K. Montgomery, A. Tovaglieri, D. L. Carlone, and D. T. Breault. 2015. Dormant Intestinal Stem Cells Are Regulated by PTEN and Nutritional Status. *Cell reports* **13**: 2403-2411.

38. Fujino, H., K. A. West, and J. W. Regan. 2002. Phosphorylation of Glycogen Synthase Kinase-3 and Stimulation of T-cell Factor Signaling following Activation of EP2 and EP4 Prostanoid Receptors by Prostaglandin E2. *Journal of Biological Chemistry* **277**: 2614-2619.

39. Pull, S. L., J. M. Doherty, J. C. Mills, J. I. Gordon, and T. S. Stappenbeck. 2005. Activated macrophages are an adaptive element of the colonic epithelial progenitor niche necessary for regenerative responses to injury. *Proc Natl Acad Sci U S A* **102**: 99-104.

40. Fukata, M., Y. Hernandez, D. Conduah, J. Cohen, A. Chen, K. Breglio, T. Goo, D. Hsu, R. Xu, and M. T. Abreu. 2009. Innate immune signaling by Toll-like receptor-4 (TLR4) shapes the inflammatory microenvironment in colitis-associated tumors. *Inflamm Bowel Dis* **15**: 997-1006.

41. Ishikawa, T. O., M. Oshima, and H. R. Herschman. 2011. Cox-2 deletion in myeloid and endothelial cells, but not in epithelial cells, exacerbates murine colitis. *Carcinogenesis* **32**: 417-426.

42. Saha, S., P. Bhanja, R. Kabarriti, L. Liu, A. A. Alfieri, and C. Guha. 2011. Bone Marrow Stromal Cell Transplantation Mitigates Radiation-Induced Gastrointestinal Syndrome in Mice. *PLOS ONE* **6**: e24072.

43. Nelson, R. H. 2013. Hyperlipidemia as a Risk Factor for Cardiovascular Disease. *Primary care* **40**: 195-211.

44. Kruit, J. K., T. Plosch, R. Havinga, R. Boverhof, P. H. Groot, A. K. Groen, and F. Kuipers. 2005. Increased fecal neutral sterol loss upon liver X receptor activation is independent of biliary sterol secretion in mice. *Gastroenterology* **128**: 147-156.

45. Bonamassa, B., and A. Moschetta. 2013. Atherosclerosis: lessons from LXR and the intestine. *Trends Endocrinol Metab* **24**: 120-128.

46. Jakulj, L., J. Besseling, E. S. Stroes, and A. K. Groen. 2013. Intestinal cholesterol secretion: future clinical implications. *Neth J Med* **71**: 459-465.

47. Watson, C. E., N. Weissbach, L. Kjems, S. Ayalasomayajula, Y. Zhang, I. Chang, M. Navab, S. Hama, G. Hough, S. T. Reddy, D. Soffer, D. J. Rader, A. M. Fogelman, and A. Schecter. 2011. Treatment of patients with cardiovascular disease with L-4F, an apo-A1 mimetic, did not improve select biomarkers of HDL function. *J Lipid Res* **52**: 361-373.

48. Davidson, N. O., and R. M. Glickman. 1985. Apolipoprotein A-I synthesis in rat small intestine: regulation by dietary triglyceride and biliary lipid. *J Lipid Res* **26**: 368-379.

49. Danielsen, E. M., G. H. Hansen, K. Rasmussen, L.-L. Niels-Christiansen, and F. Frenzel. 2012. Apolipoprotein A-1 (apoA-1) deposition in, and release from, the enterocyte brush border: A possible

role in transintestinal cholesterol efflux (TICE)? *Biochimica et Biophysica Acta (BBA) - Biomembranes* **1818**: 530-536.

50. Oram, J. F., R. M. Lawn, M. R. Garvin, and D. P. Wade. 2000. ABCA1 Is the cAMP-inducible Apolipoprotein Receptor That Mediates Cholesterol Secretion from Macrophages. *Journal of Biological Chemistry* **275**: 34508-34511.

51. Pazos, M., D. Siccardi, K. L. Mumy, J. D. Bien, S. Louie, H. N. Shi, K. Gronert, R. J. Mrsny, and B. A. McCormick. 2008. Multi-Drug Resistance Transporter 2 Regulates Mucosal Inflammation by Facilitating the Synthesis of Hepoxilin A(3). *Journal of immunology (Baltimore, Md. : 1950)* **181**: 8044-8052.

52. Van Lenten, B. J., A. C. Wagner, C. L. Jung, P. Ruchala, A. J. Waring, R. I. Lehrer, A. D. Watson, S. Hama, M. Navab, G. M. Anantharamaiah, and A. M. Fogelman. 2008. Anti-inflammatory apoA-I-mimetic peptides bind oxidized lipids with much higher affinity than human apoA-I. *J Lipid Res* **49**: 2302-2311.

53. Narasimha, A. J., J. Watanabe, T. O. Ishikawa, S. J. Priceman, L. Wu, H. R. Herschman, and S. T. Reddy. 2010. Absence of myeloid COX-2 attenuates acute inflammation but does not influence development of atherosclerosis in apolipoprotein E null mice. *Arterioscler Thromb Vasc Biol* **30**: 260-268.

54. Meriwether, D., D. Sulaiman, A. Wagner, V. Grijalva, I. Kaji, K. J. Williams, L. Yu, S. Fogelman, C. Volpe, S. J. Bensinger, G. M. Anantharamaiah, I. Shechter, A. M. Fogelman, and S. T. Reddy. 2016. Transintestinal transport of the anti-inflammatory drug 4F and the modulation of transintestinal cholesterol efflux. *J Lipid Res* **57**: 1175-1193.

55. York, A. G., K. J. Williams, J. P. Argus, Q. D. Zhou, G. Brar, L. Vergnes, E. E. Gray, A. Zhen, N. C. Wu, D. H. Yamada, C. R. Cunningham, E. J. Tarling, M. Q. Wilks, D. Casero, D. H. Gray, A. K. Yu, E. S. Wang, D. G. Brooks, R. Sun, S. G. Kitchen, T. T. Wu, K. Reue, D. B. Stetson, and S. J. Bensinger. 2015. Limiting Cholesterol Biosynthetic Flux Spontaneously Engages Type I IFN Signaling. *Cell* **163**: 1716-1729.

56. Kim, J., C. S. Park, C. H. Park, D. I. Jeoung, Y. M. Kim, and J. Choe. 2011. Beraprost enhances the APC function of B cells by upregulating CD86 expression levels. *J Immunol* **186**: 3866-3873.

57. Maher, S. A., M. A. Birrell, and M. G. Belvisi. 2009. Prostaglandin E2 mediates cough via the EP3 receptor: implications for future disease therapy. *Am J Respir Crit Care Med* **180**: 923-928.

58. Mak, L. H., R. Vilar, and R. Woscholski. 2010. Characterisation of the PTEN inhibitor VO-OHpic. *Journal of Chemical Biology* **3**: 157-163.

Figure Legends

Figure 4-1 LXR agonist treatment fails to increase the trans-intestinal transport of L-4F. TG112 mice were pre-treated with LXR agonist for 7 days or western diet (WD) for 6 weeks. Mice were injected via tail vein with ^{14}C-L-4F, and after 1 hr radioactiivty was determined in SI lumen wash. While western diet significantly increased the trans-intestinal transport of L-4F in both male and female mice (*, $p < 0.01$), LXR agonist pre-treatment did not.

Figure 4-2 Inhibition of ABCB1 suppresses the secretory transport of 4F from intestinal explants. D-4F was injected via tail vein into C57BL/6J mice. After 30 minutes, paired intestinal explants were mounted in Ussing chambers with and without the apical transporter ABCB1 inhibitor tariquidar (TQR). Mucosal media was sampled at multiple time points and concentration of D-4F was determined by LC-MS/MS. TQR significantly inhibited 4F transport into the mucosal media at all time points from 20 minutes on (*, $p < 0.001$).

Figure 4-3 Model of uptake and transport of 4F by enterocytes. This model represents the working hypothesis for the uptake and transport of 4F by enterocytes (for detailed description, see §1). In brief, 4F associates with lipoproteins in circulation and is taken up by enterocytes through basolateral transporters. 4F is then transported into the intestinal lumen in conjunction with free cholesterol (FC) through the ABC transporter ABCB1. Once in the lumen, 4F can be taken up again into enterocytes.

Figure 4-4 4F increases cholesterol efflux from macrophages. J774 macrophages were loaded with ^{3}H-cholesterol. D-4F was added to media, and after 1 hour cholesterol efflux was determined as a percent

of starting cholesterol load by scintillation counting. D-4F dose-dependently increased cholesterol efflux (*, $p < 0.001$; **, compared to control, $p < 0.001$; ***, compared to 10 ug/ml 4F, $p < 0.001$).

Figure 4-5 Model of the modulation of trans-intestinal cholesterol efflux by 4F. This model represents my working hypotheses for mechanism by which 4F increases TICE (for detailed description, see §1). In brief, 4F associates with HDL in circulation, and 4F-associated HDL is taken up into enterocyte through basolateral transporters (I). Additional lipoproteins also deliver free cholesterol (FC) to enterocytes. 4F can be co-transported with cholesterol through ABCB1, thereby increasing cholesterol efflux (II). Alternatively, 4F that has already entered the lumen can accept FC at the sterol transporters ABCG5/G8 (III).

Figure 4-6 Oral D-4F increases RCT from circulating lipoproteins via the TICE pathway. WT and TG112 were pre-treated with oral D-4F (500 ug/ml drinking water) for 1 week and allowed to drink through the experiment. HDL and LDL were loaded with ^{3}H-cholesterol and introduced via tail vein into the mice. After 1 hour, SI lumen rinse was collected. **A**: Bile acids were separated from cholesterol and radioactivity was determined in each fraction. Cholesterol levels did not differ between TG112 and WT mice, indicating that TICE was active in TG112 mice. **B**: The effect of D-4F on cholesterol transport into the intestinal lumen was determined by scintillation counting of the cholesterol fractions from each rinse. D-4F significantly increased cholesterol efflux in both WT and TG112 mice (*, $p < 0.01$). The result in TG112 mice indicates that oral D-4F can increase RCT through the TICE pathway.

Figure 4-7 Model of the initiation of intestinal inflammation in COX2 MKO mice by CCHF challenge. This model represents my hypothesis regarding the manner in which CCHF and COX2 MKO combine to initiate chronic intestinal inflammation (for detailed description, see §2). In brief, CCHF increases barrier

permeability and increases the translocation of PAMP into the lamina propria. PAMP signaling through TLR/MyD88 trigger induction of NFkB pro-inflammatory target genes including *IL1β and TNFα* as well as *COX2*. COX2 and its products act as negative regulators of NFkB. In the absence of COX2, levels of cytokine pro-inflammatory mediators are elevated. In turn, these cytokines can trigger additional TLR/MyD88/NFkB signaling in COX2 MKO macrophages, leading to further dysregulated amplification of the pro-inflammatory signal.

Figure 4-8 TLR activation increases production of pro-resolving mediator pathway marker 17HDHA in macrophages. Bone marrow derived macrophages were treated with PAM3 (TLR2 agonist), PolyIC (PIC, TLR3 agonist), or LPS. After 48 hours, lysates were collected and levels of pro-resolving mediators were determined by LC-MS/MS. Compared to no-treatment (NT), all three TLR activators significantly induced production of 17HDHA, a DHA-derived pro-resolving mediator pathway marker (*, $p < 0.05$).

Figure 4-9 CCHF challenge impairs survival of COX2 KO mice. COX2 KO mice were challenged with CCHF diet and survival was determined. A: COX2 TKO mice were fed CCHF. By 16 days, 50% of COX2 KO but no WT mice had died of burst ceca. B: COX2 MKO mice were fed CCHF for either 7 or 10 weeks. While COX2 MKO survived longer than COX2 TKO mice on CCHF diet, after 10 weeks 4 of 7 mice had died of burst ceca.

Figure 4-10 COX2 TKO inhibits intestinal stem cell proliferation in response to CCHF challenge. COX2 TKO and WT mice were fed CCHF diet for 2 weeks (n = 5). EdU was injected i.p. into the mice 24 hours prior to sacrifice (200 ug/mouse). Histological sections of ilea were prepared, and EdU uptake into intestinal epithelium was determined by fluorescent microscopy. While both COX2 TKO and WT mice

exhibited comparable uptake on chow, COX2 TKO significantly inhibited uptake in response to CCHF challenge (*, $p < 0.01$).

Figure 4-11 PGE2 increases both the size and complexity of day 5 enteroids. Crypts were isolated from C57BL/6J mice and grown in 3D Matrigel cultures. The cultures were treated with either vehicle or 10 nM PGE2 for 5 days. Enteroid structures were assessed for both size and budding complexity (representative images).

Figure 4-12 Examples of structures observed in organoid cultures. Upon isolation, crypts appear as small cigar shaped structures (crypts). Exogenous PGE2 (10 nM) pushes crypts through an early spheroid stage (early spheroids at 18 hours). After 5 days, PGE2-treated crypts develop a complex structure marked by multiple buds, with each bud forming from crypts that have newly formed within the overall enteroid structure (complex spheroids).

Figure 4-13 Loss of COX2 activity inhibits the formation of early spheroids. Crypts were isolated from either C57BL/6J or COX2 TKO ($COX2^{luc/luc}$) mice. Some crypt cultures from BL6 mice were treated with the COX2 inhibitor NS398. The number of early spheroids was determined after 36 hours (n=5). In both cases absence of COX2 activity significantly inhibited the formation of early spheroids (*, $p < 0.001$).

Figure 4-14 Co-culture with WT crypts rescues the COX2 KO dependent inhibition of early spheroids. Crypts from COX2 TKO mice were co-cultured with increasing number of crypts from C57BL/6J mice (n = 4). Compared to the production of early spheroids in WT cultures (see Figure 13), co-culture with WT crypts dose-dependently rescued the inhibitory effect of COX2 KO on the production of early spheroids (*, compared to 0 WT co-culture, $p < 0.001$; **, compared to 100 WT co-culture, $p < 0.001$).

Figure 4-15 COX2 and PGE2 increase the number of early spheroids in both COX2 TKO and WT crypt cultures. Organoid cultures from WT and COX2 KO mice were treated with PGE2 (10 nM), and the number of early spheroids at 18 hrs was determined. COX2 in creased the number of early spheroids (*, WT v COX2 KO; $p < 0.01$). While addition of exogenous PGE2 increased the number of early spheroids in both WT and KO cultures (**, compared to no-treatment control; $p < 0.01$), the effect was more pronounced in WT than KO (***, $p < 0.01$).

Figure 4-16 Early spheroids are produced in response to tissue disruption, while PGE2 enhances this response. Mature enteroids from WT cultures were mechanically disrupted with wide or narrow gauge needle. Narrow gauge produced greater tissue disruption and considerably more penetrance of early spheroids (representative images). Exogenous PGE2 enhanced the production of early spheroids, with $EC_{max} = 1.5$ nM.

Figure 4-17 PGE2 signals through EP4 to produce early spheroids. Organoid cultures from WT mice were treated with PGE2 (2.5 nM) in combination with antagonists to the the PGE2 receptors EP1-4 across a range of doses. While none of the EP1-3 antagonists affected the induction of early spheroids by PG2, the EP4 antagonist completely abrogated this response (representative image).

Figure 4-18 While CFTR activation produces sphere-like structures, CFTR inhibition did not block the induction of early spheroids by PGE2. Organoid cultures from WT mice were treated either with a CFTR activator (2-Pyridin-4-yl-benzo[h]chromen-4-one) or with PGE2 in combination with a CFTR inhibitor (CFTR(inh)-172) in combination with PGE2 (2.5 nM). CFTR activation dose-dependently increased

structure swelling (representative image), while CFTR inhibition even at high dose did not block the induction of 24 hr spheroids by PGE2.

Figure 4-19 Early spheroids lose expression of differentiation markers, while COX2 and PGE2 enhance expression of stem cell associated markers Lgr5 and especially Wnt3A. WT and COX2 KO crypt cultures were treated with either PGE2 or a stable analog of PGI2. Expressions of various stem cell, reserve stem cell, and differentiation markers were determined by qPCR for both time 0 crypts and 18 hr cultures. A: Expression of differentiation cell markers (*Muc2*, goblet cells; *Lyz*, Paneth cells; *Vil*, enterocytes) drops between 4 and 10 fold across 18 hours of culture in a COX2 independent manner. B: The increase of expression of reserve stem cell markers *Bmi1* and *Tert* is several-fold greater in KO than in WT, while PGE2 rescues this difference. C: PGE2 increases the stem-cell marker *Lgr5* several fold more in WT than KO compared to baseline. D: PGE2 increases *Wnt3A* expression several hundred fold in WT compared to time zero, while also increasing expression of *Ptgs2*. By contrast, *Wnt3A* expression remains low in KO and unaffected by PGE2, while PGI2 increases expression comparable to WT at 18 hrs. E: Expression of *ChgA*, an enteroendocrine and potential reserve stem cell marker, is dramatically elevated in WT cultures, with PGE2 further enhancing this change. KO alone exhibit no increase in *ChgA* over time, with only PGI2 but not PGE2 increasing expression by 18 hrs. (n = 4)

Figure 4-20 Both PTEN inhibition and PGE2 increase the number of complex enteroid. Crypts were isolated from WT mice and cultured with either PGE2 (10 nM) or PTEN inhibitor for 5 days. The number of complex enteroids was determined, as those enteroids with 2+ budding structures. Both PGE2 and PTEN inhibition significantly increased the number of complex enteroids compared to vehicle control ($p < 0.001$). (n=5)

Figure 4-21 Model of role of COX2 and PGE2 in expansion of crypts through early spheroids into complex enteroids. This model represents my hypothesis regarding the manener in which both COX2 and PGE2 mediate the development of intestinal crypts into early spheroids and then complex enteroids in culture (for detailed description, see §3). In brief, crypt translocation induces some damage signal(s) X, which induces COX2 and PGE2. PGE2 in turn signals through EP4, producing both crypt swelling. The crypts lose differentiation marks as PGE2/EP4 increases expression of Lgr5 and Wnt3A. Subsequent release of PTEN blockadge of PI3K/AKT, possibly through PGE2/EP4, activates stem cells and generates new crypts in later enteroids.

Figure 4-1

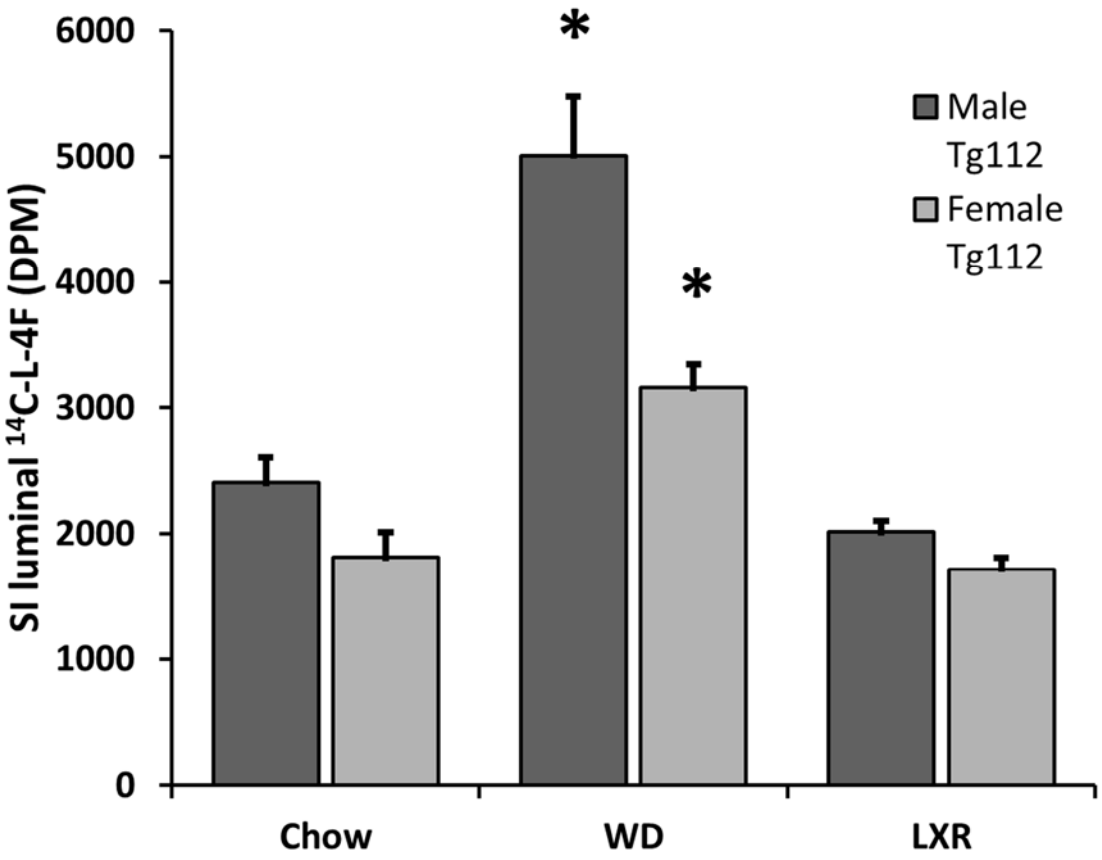
6000
5000
4000
3000
2000
1000
0
SI luminal ^{14}C-L-4F (DPM)
*
*
Male Tg112
Female Tg112
Chow
WD
LXR

Figure 4-2

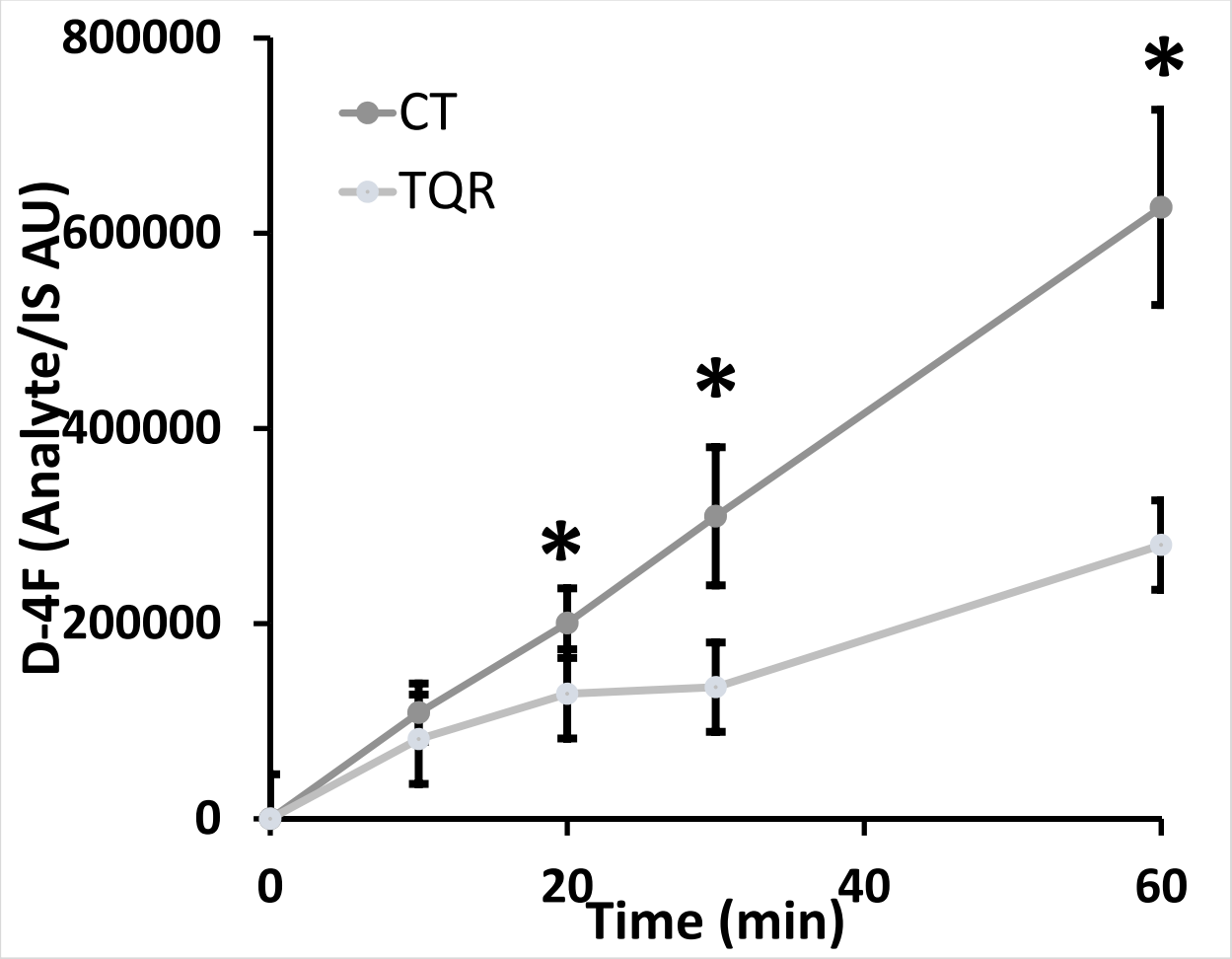
800000
600000
400000
200000
0
D-4F (Analyte/IS AU)
CT
TQR
*
*
*
0
20
40
60
Time (min)

Figure 4-3

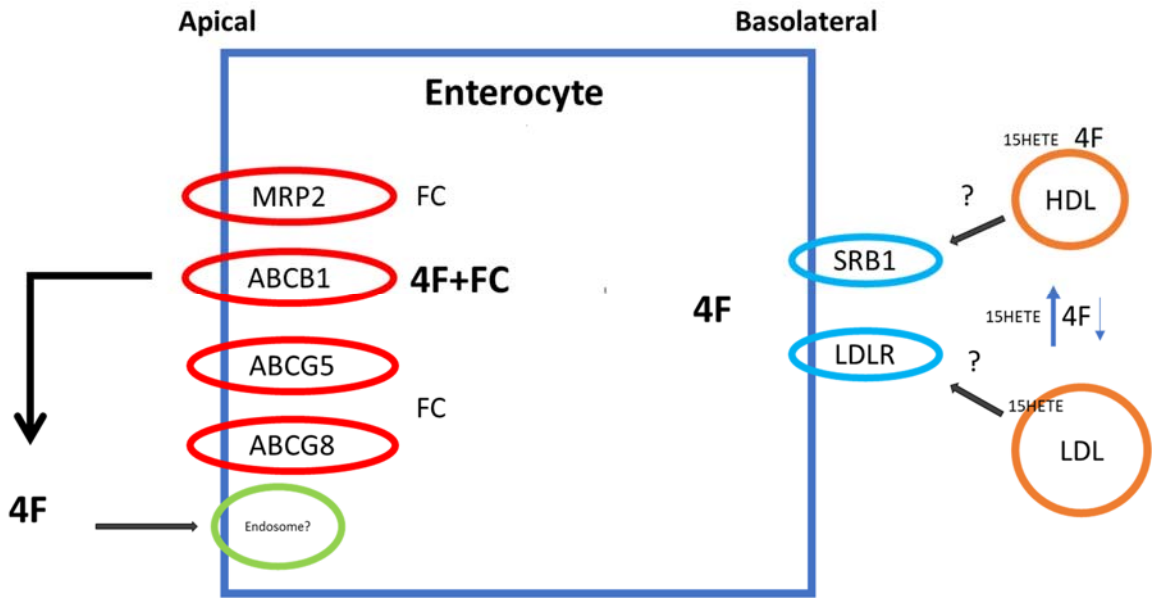
Apical
Basolateral
Enterocyte
MRP2
FC
ABCB1
4F+FC
ABCG5
FC
ABCG8
4F
Endosome?
4F
SRB1
LDLR
15HETE
4F
?
HDL
15HETE
4F
?
15HETE
LDL

Figure 4-4

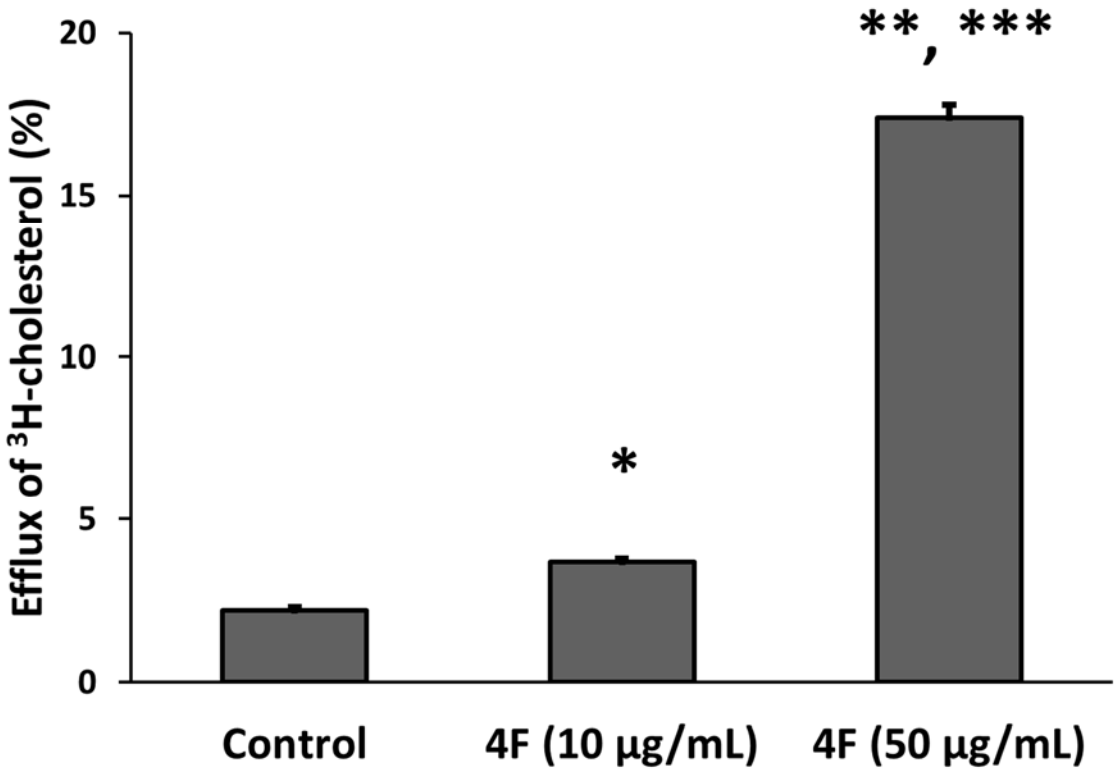
Efflux of ^{3}H-cholesterol (%)
20
15
10
5
0
, *
*
Control
4F (10 µg/mL)
4F (50 µg/mL)

Figure 4-5

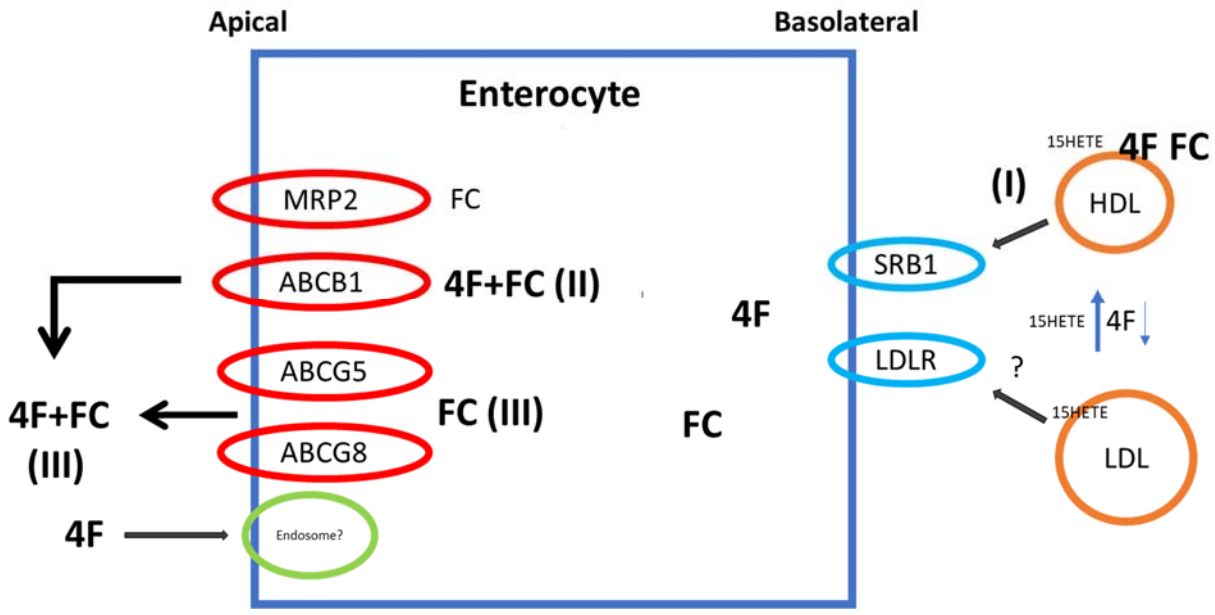
Apical
Basolateral
Enterocyte
MRP2
FC
ABCB1
4F+FC (II)
ABCG5
FC (III)
ABCG8
4F+FC
(III)
4F
Endosome?
4F
FC
SRB1
LDLR
15HETE
4F FC
(I)
HDL
15HETE
4F
?
15HETE
LDL

Figure 4-6

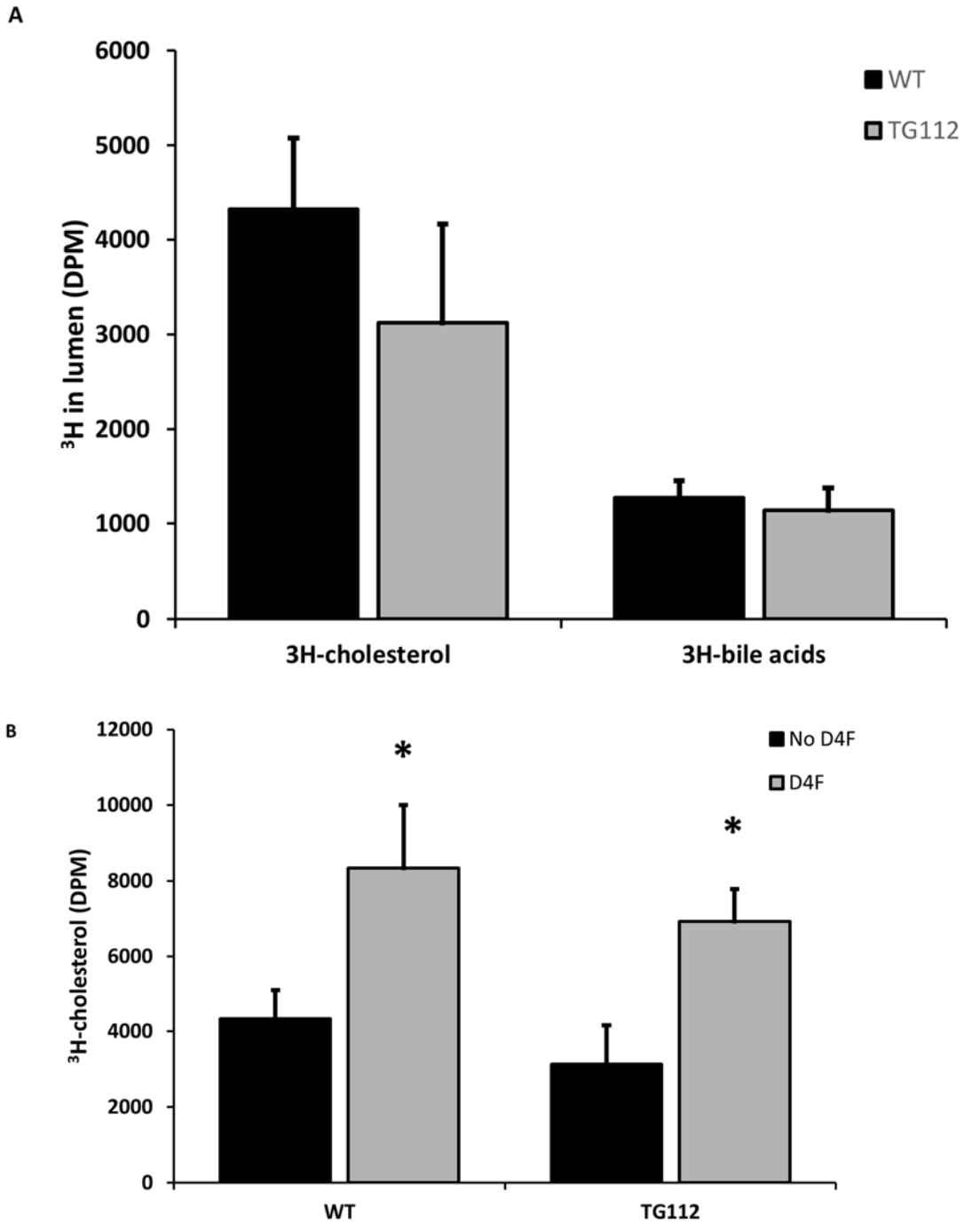
A
6000
5000
4000
3000
2000
1000
0
^{3}H in lumen (DPM)
WT
TG112
3H-cholesterol
3H-bile acids
B
12000
10000
8000
6000
4000
2000
0
^{3}H-cholesterol (DPM)
No D4F
D4F
*
*
WT
TG112

Figure 4-7

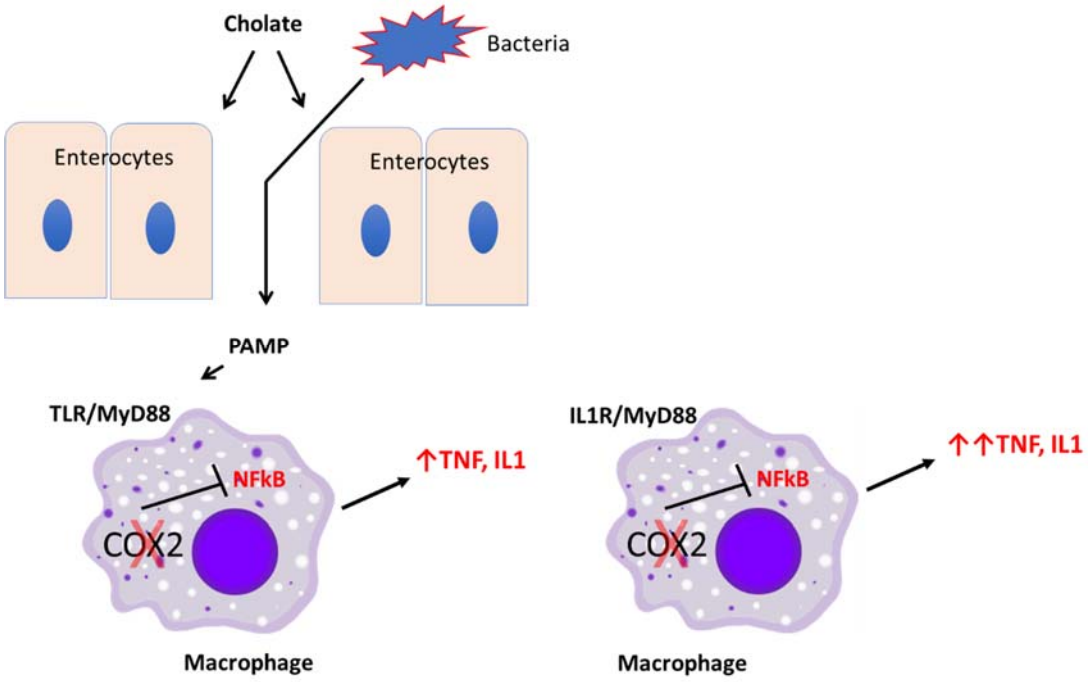
Cholate
Bacteria
Enterocytes
Enterocytes
PAMP
TLR/MyD88
NFkB
COX2
↑TNF, IL1
Macrophage
IL1R/MyD88
NFkB
COX2
↑↑TNF, IL1
Macrophage

Figure 4-8

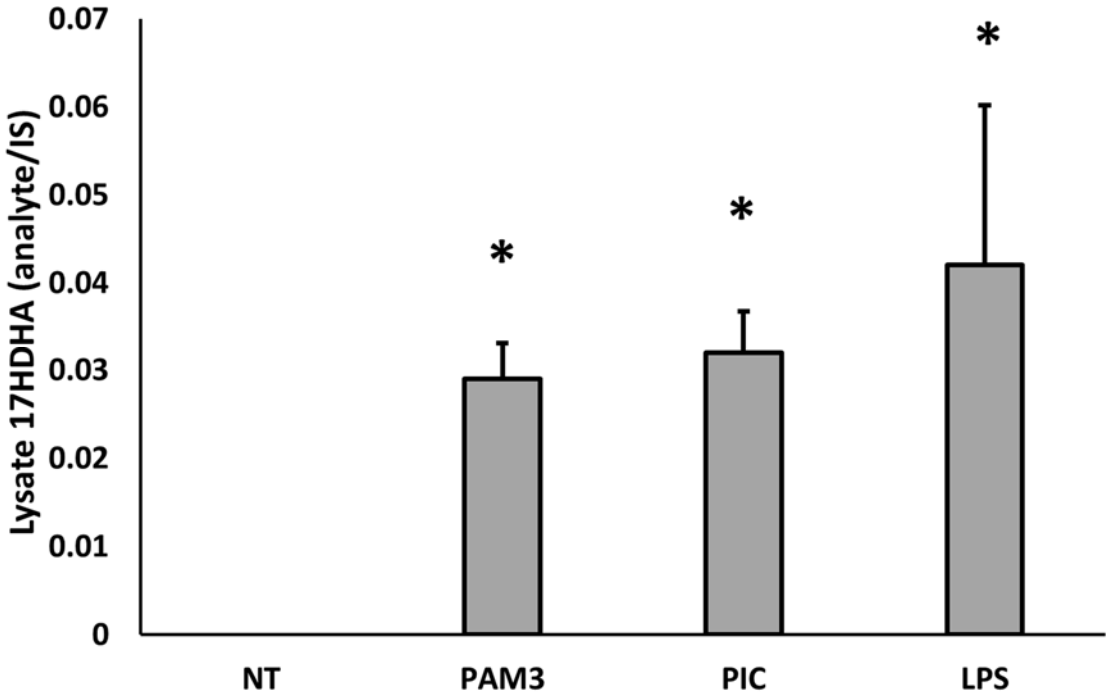
0.07
0.06
0.05
0.04
0.03
0.02
0.01
0
Lysate 17HDHA (analyte/IS)
*
*
*
NT
PAM3
PIC
LPS

Figure 4-9

A.

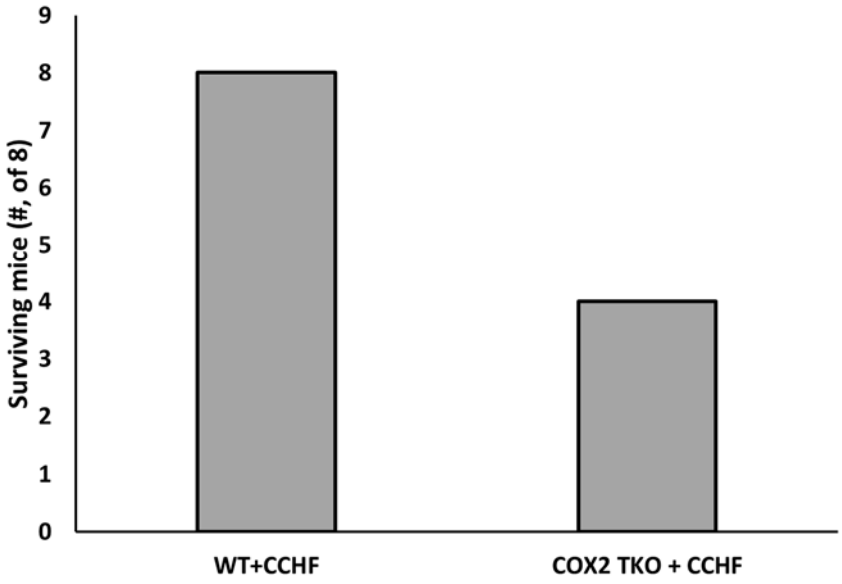
Surviving mice (#, of 8)
9
8
7
6
5
4
3
2
1
0
WT+CCHF
COX2 TKO + CCHF

B.

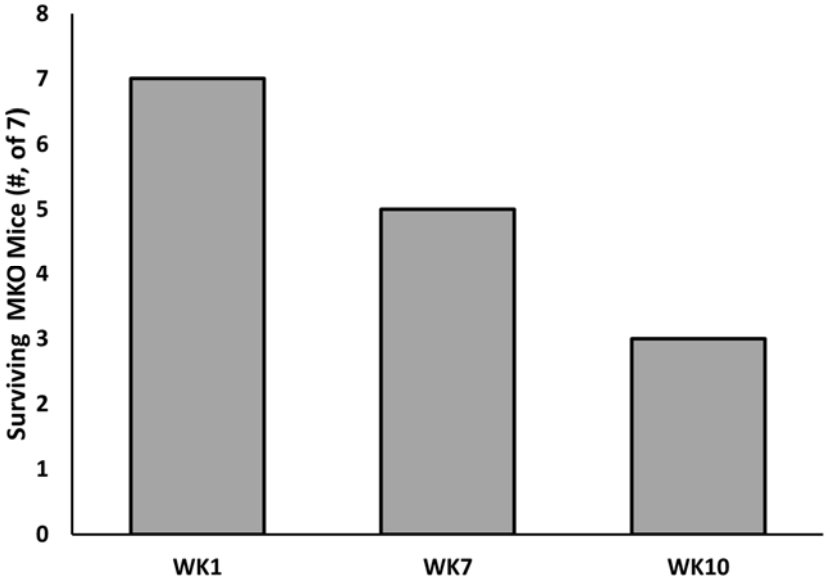
Surviving MKO Mice (#, of 7)
8
7
6
5
4
3
2
1
0
WK1
WK7
WK10

Figure 4-10

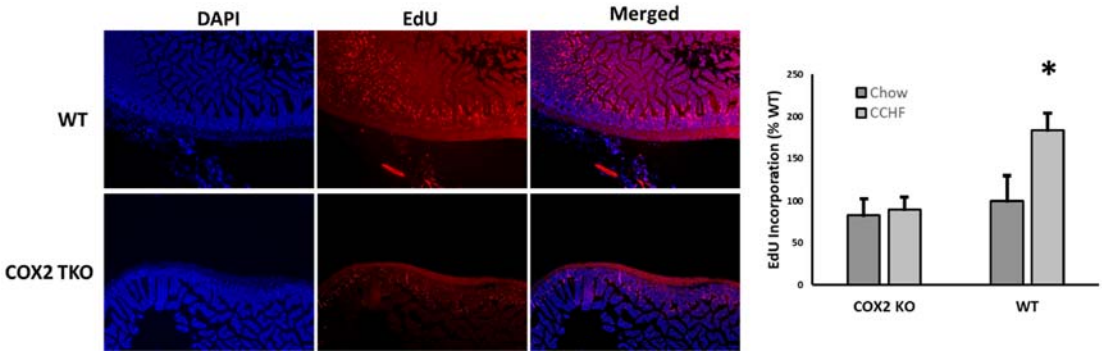
DAPI
EdU
Merged
WT
COX2 TKO
EdU Incorporation (% WT)
250
200
150
100
50
0
Chow
CCHF
*
COX2 KO
WT

Figure 4-11

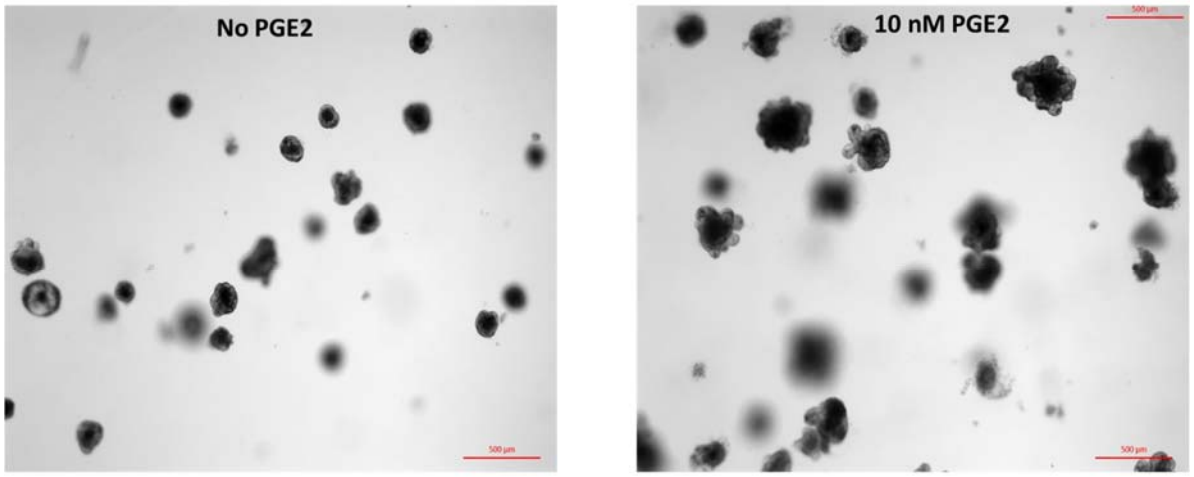

C57BL/6J intestinal crypts

Figure 4-12

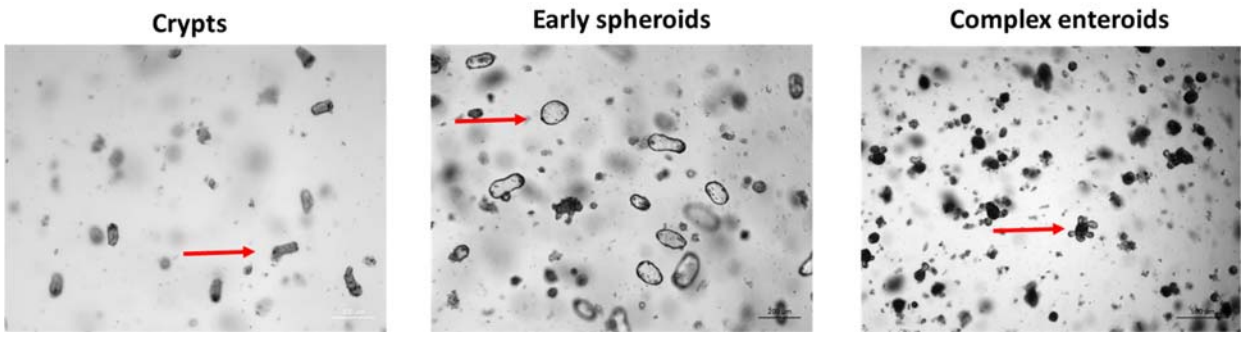

Figure 4-13

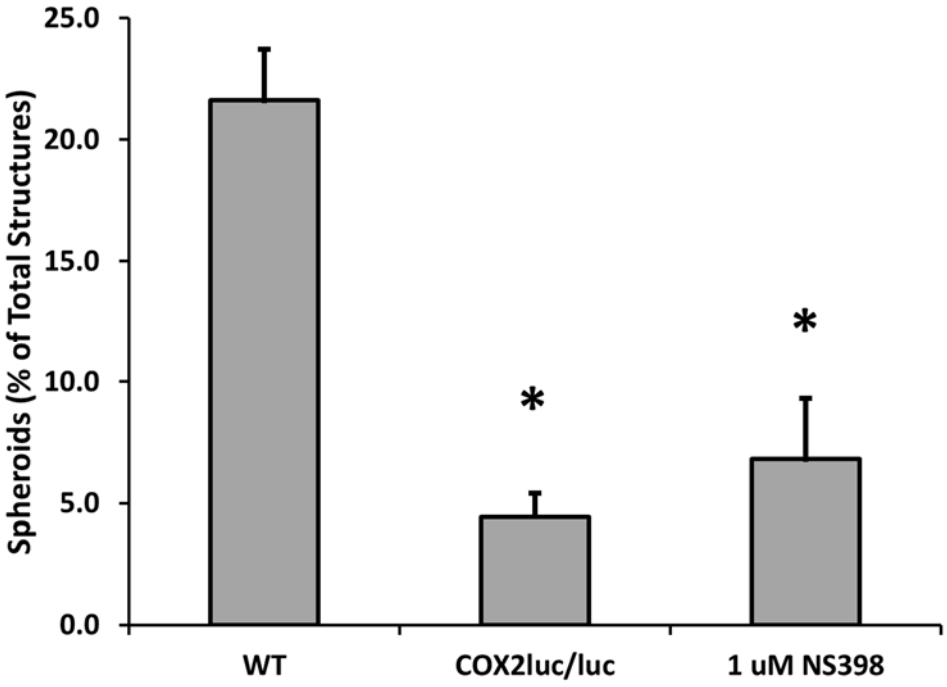
25.0
20.0
15.0
10.0
5.0
0.0
Spheroids (% of Total Structures)
*
*
WT
COX2luc/luc
1 uM NS398

Figure 4-14

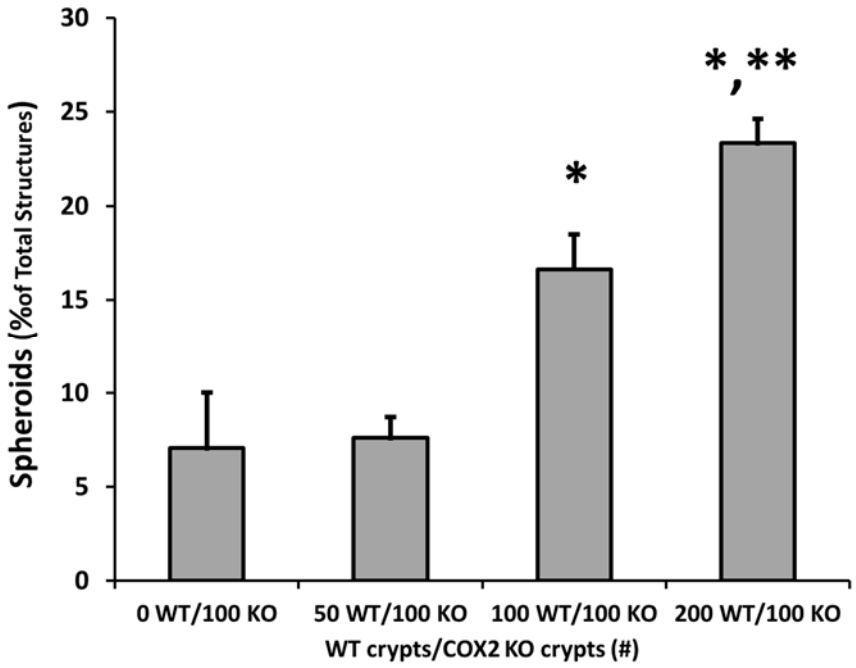
30
25
20
15
10
5
0
Spheroids (%of Total Structures)
*
*,**
0 WT/100 KO
50 WT/100 KO
100 WT/100 KO
200 WT/100 KO
WT crypts/COX2 KO crypts (#)

Figure 4-15

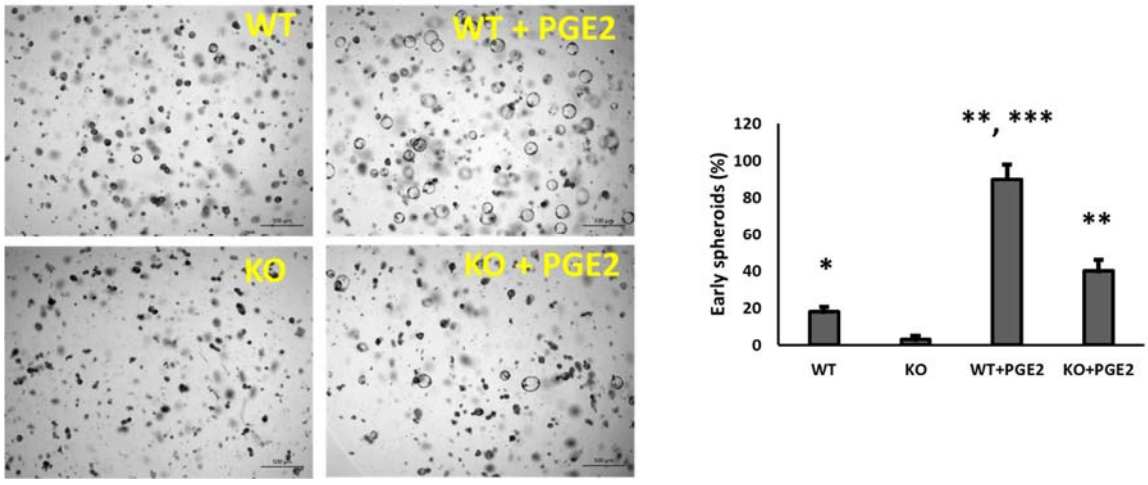
WT
WT + PGE2
KO
KO + PGE2
Early spheroids (%)
120
100
80
60
40
20
0
*
, *
**
WT
KO
WT+PGE2
KO+PGE2

Figure 4-16

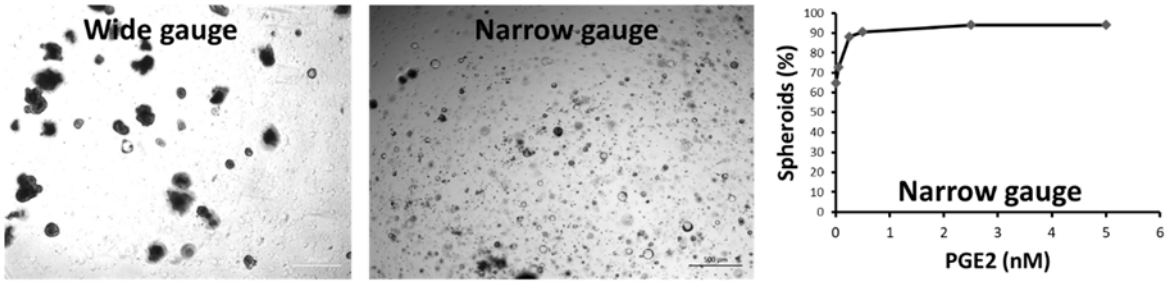

Figure 4-17

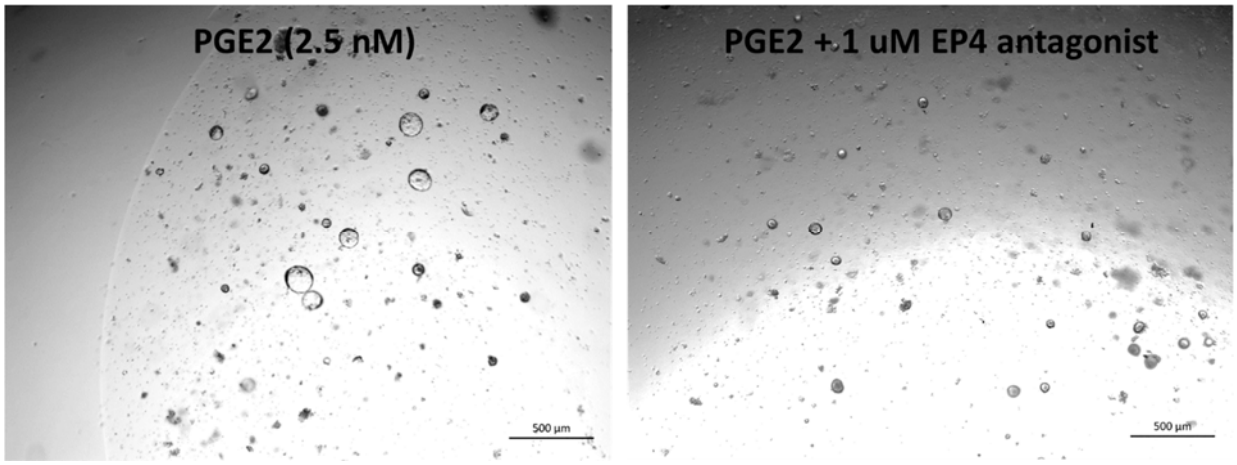

Figure 4-18

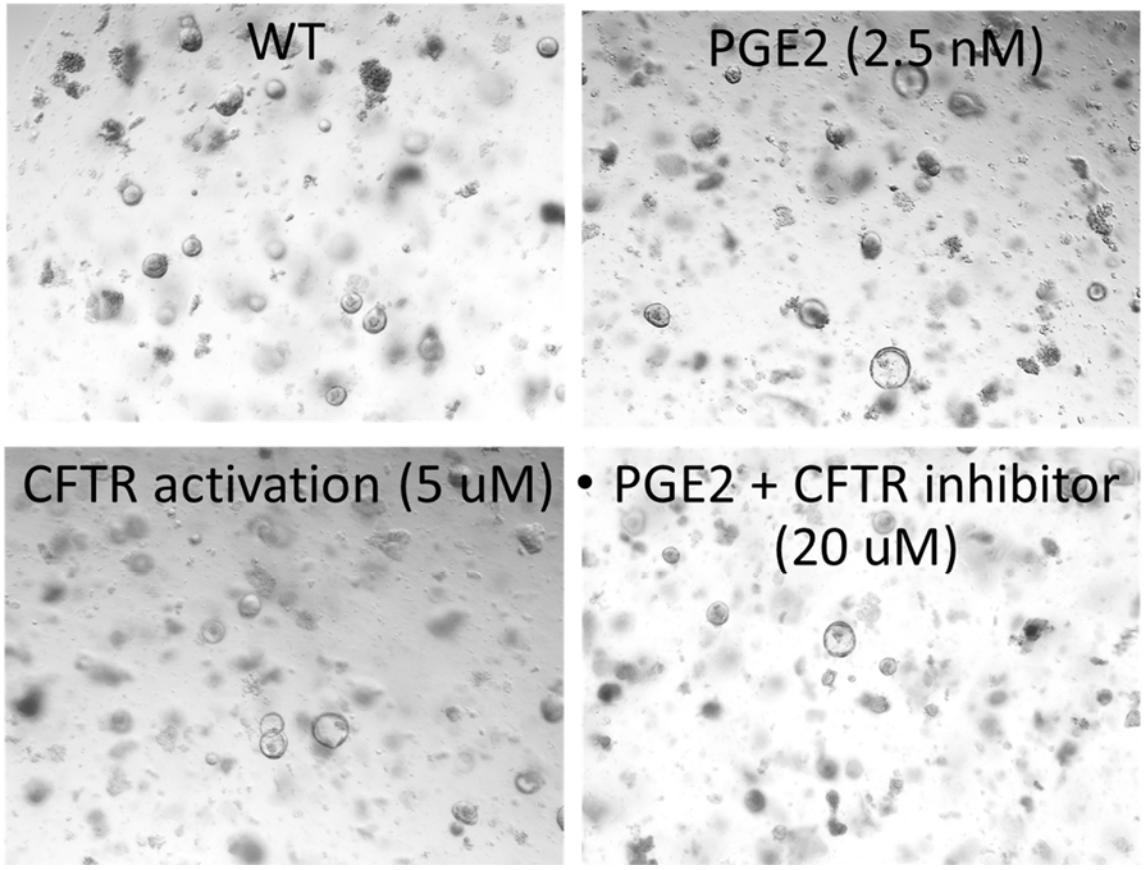

Figure 4-19

19A

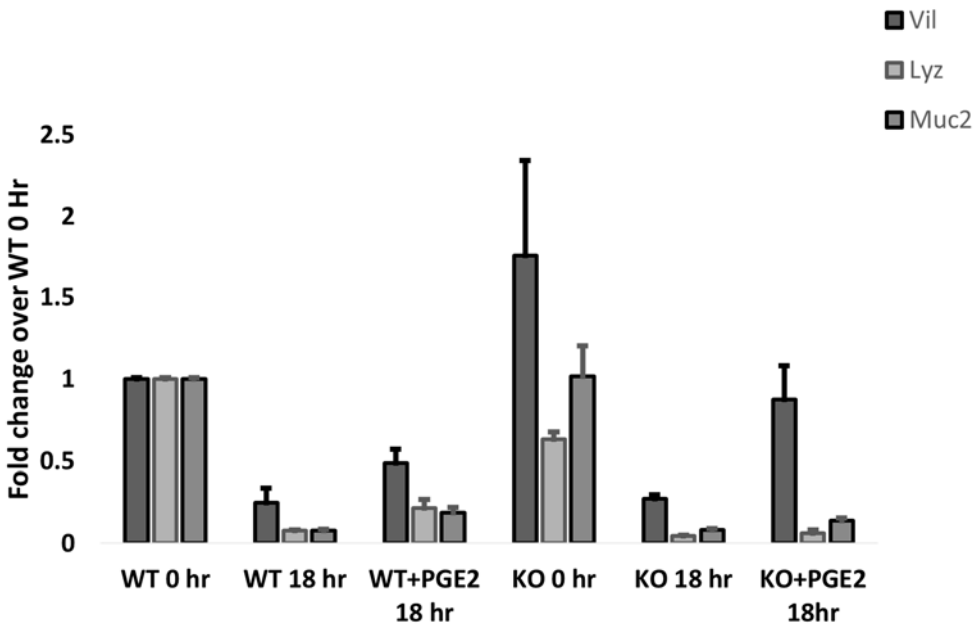

19B

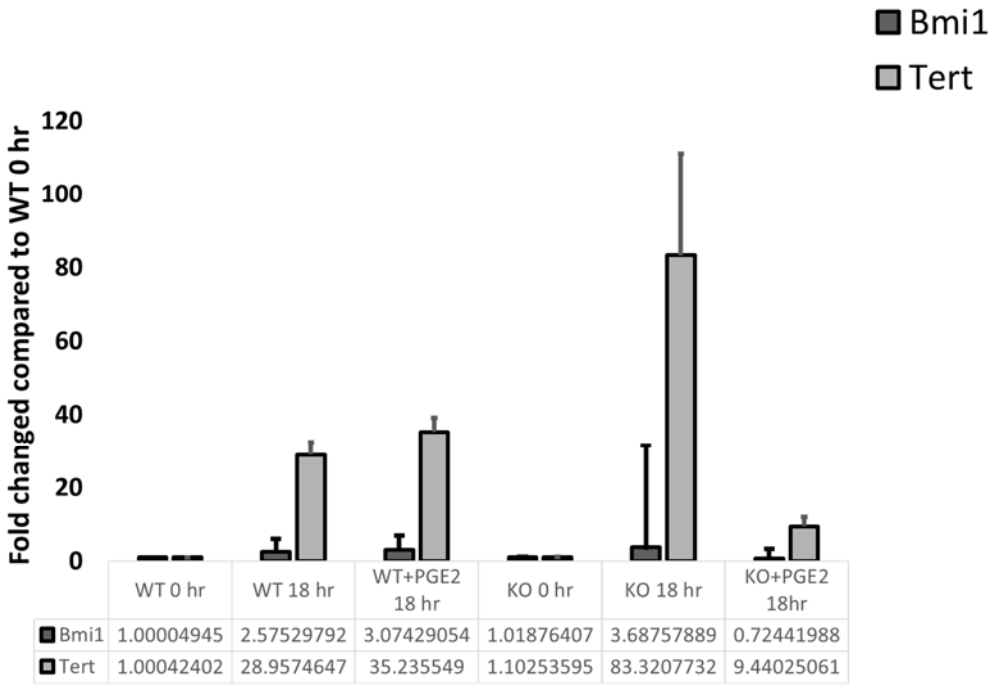

	WT 0 hr	WT 18 hr	WT+PGE2 18 hr	KO 0 hr	KO 18 hr	KO+PGE2 18hr
Bmi1	1.00004945	2.57529792	3.07429054	1.01876407	3.68757889	0.72441988
Tert	1.00042402	28.9574647	35.235549	1.10253595	83.3207732	9.44025061

19C

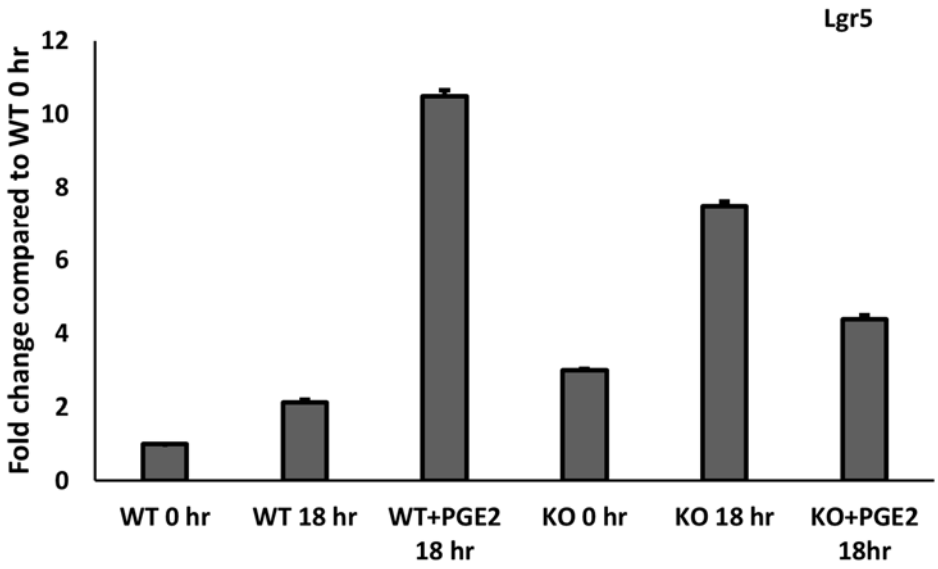
Lgr5
Fold change compared to WT 0 hr
0
2
4
6
8
10
12
WT 0 hr
WT 18 hr
WT+PGE2 18 hr
KO 0 hr
KO 18 hr
KO+PGE2 18hr

19D

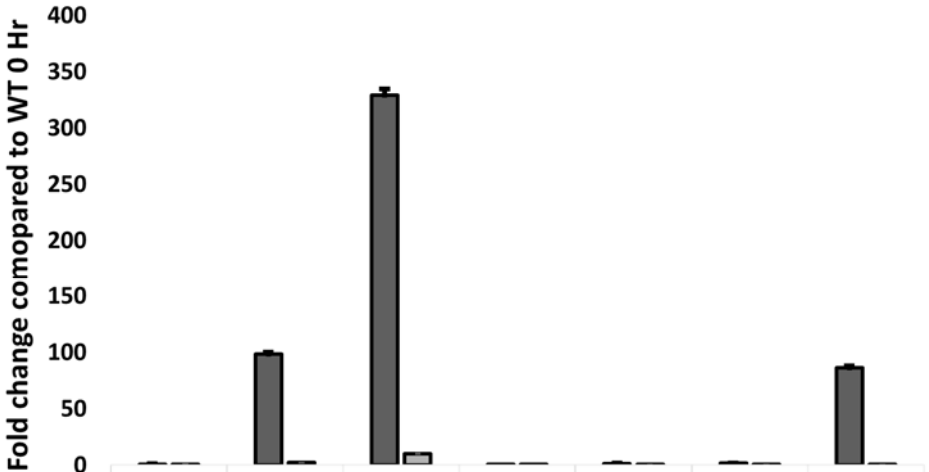

	WT 0 hr	WT 18 hr	WT+PGE 2 18 hr	KO 0 hr	KO 18 hr	KO+PGE 2 18hr	KO+PGI2 18 hr
Wnt3A	1.000675	98.57132	329.3479	0.353238	1.467522	1.575178	86.24134
Ptgs2	1.0009	2.183542	10.07029	0.166885	0.509992	0.576248	0.566391

19E

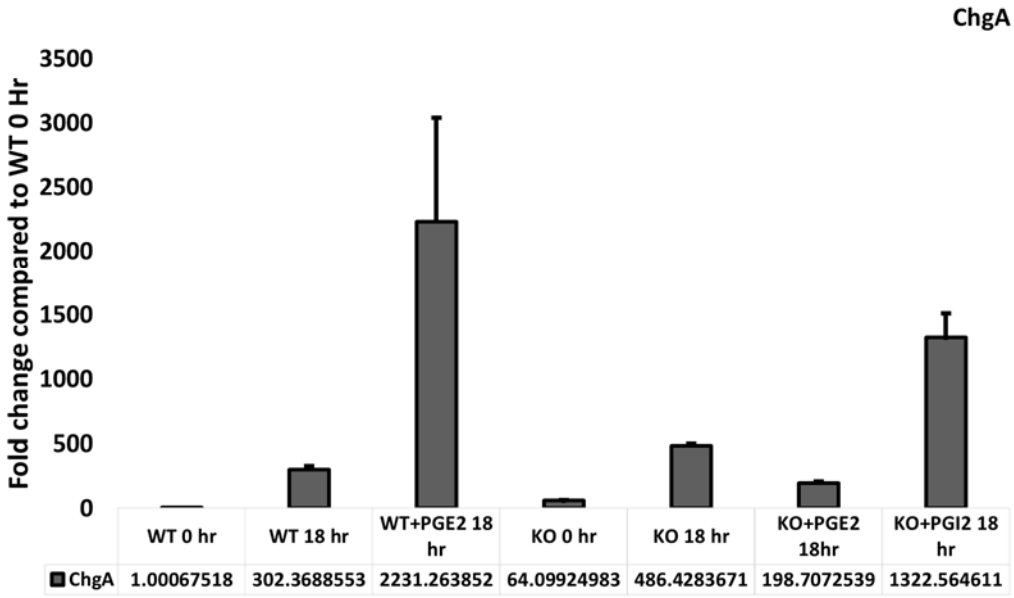
ChgA
Fold change compared to WT 0 Hr
3500
3000
2500
2000
1500
1000
500
0
WT 0 hr
WT 18 hr
WT+PGE2 18 hr
KO 0 hr
KO 18 hr
KO+PGE2 18hr
KO+PGI2 18 hr
ChgA
1.00067518
302.3688553
2231.263852
64.09924983
486.4283671
198.7072539
1322.564611

Figure 4-20

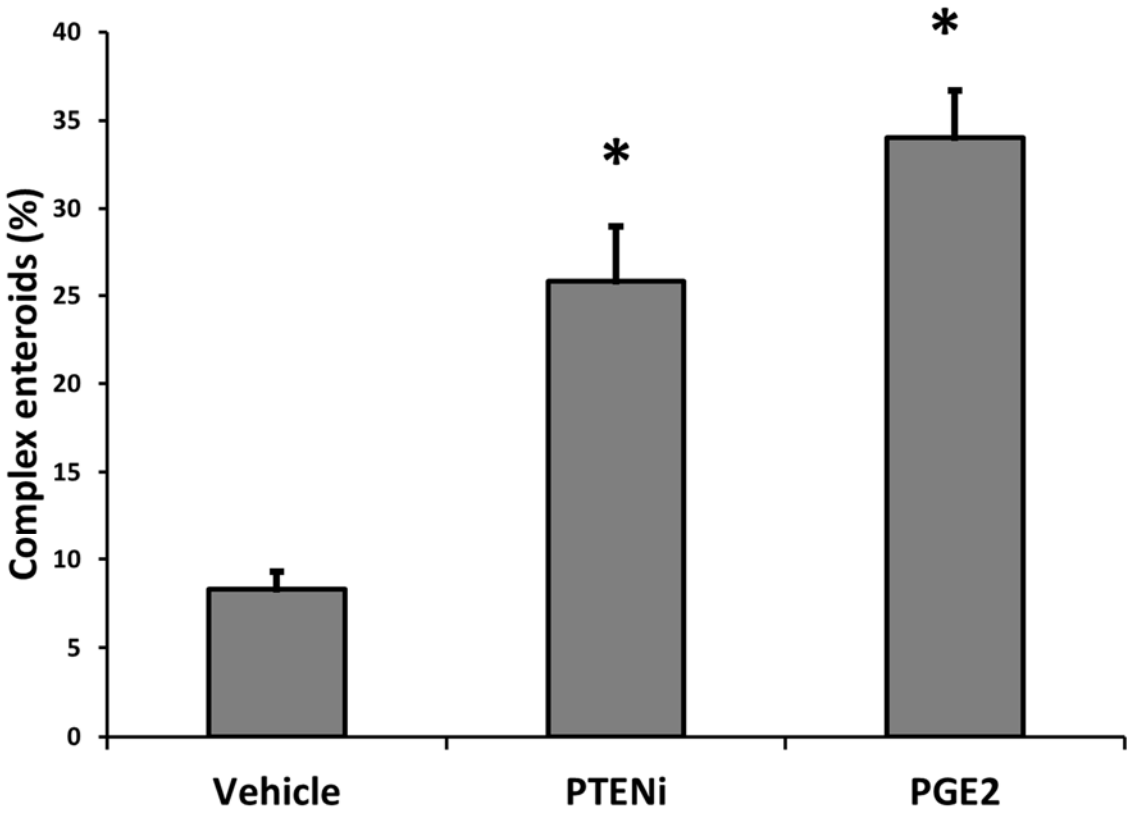

Figure 4-21

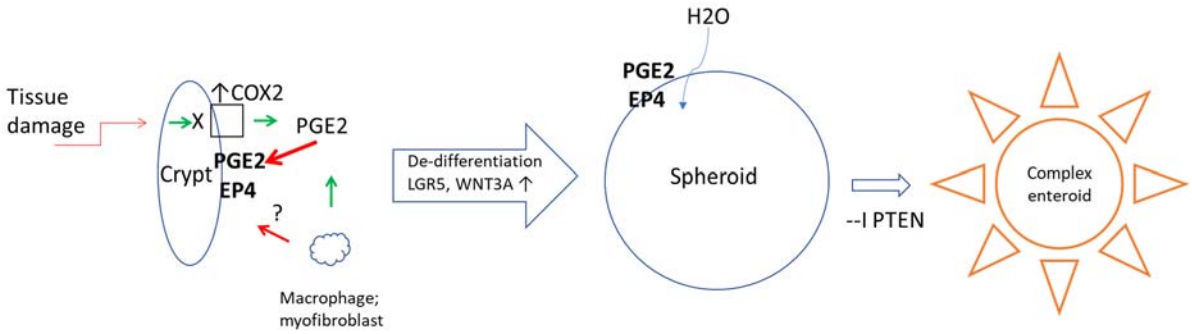
Tissue
damage
↑COX2
X
PGE2
PGE2
EP4
Crypt
?
Macrophage;
myofibroblast
De-differentiation
LGR5, WNT3A ↑
H2O
PGE2
EP4
Spheroid
--I PTEN
Complex
enteroid

Appendix: Enhancement by LDL of Transfer of L-4F and Oxidized Lipids to HDL in C57BL/6J Mice and Human Plasma

Abstract

The apoA-I mimetic peptide L-4F has shown potential for the treatment of a variety of diseases. Here we demonstrate that LDL promotes association between L-4F and HDL. A 2-3 fold greater association of L-4F with human HDL was observed in the presence of human LDL as compared with HDL by itself. This association further increased when LDL was supplemented with the oxidized lipid 15HETE. Additionally, L-4F significantly ($p = 0.02$) promoted the transfer of 15HETE from LDL to HDL. The transfer of L-4F from LDL to HDL was demonstrated both *in-vitro* and in C57BL/6J mice. L-4F, injected into C57BL/6J mice, associated rapidly with HDL and was then cleared quickly from the circulation. Similarly, human HDL, preloaded with L-4F and injected into C57BL/6J mice was cleared quickly with $T_{1/2} = 23.6$ min. This was accompanied by a decline in human apoA-I with little or no effect on the mouse apoA-I. Based on these results, we propose that i) LDL promotes the association of L-4F with HDL and ii) in the presence of L-4F oxidized lipids in LDL are rapidly transferred to HDL allowing these oxidized lipids to be acted upon by HDL-associated enzymes and/or cleared from the circulation.

Supplementary key words: atherosclerosis ● apolipoprotein A-I ● apolipoprotein A-I mimetic peptides ● lipoproteins ● HDL ● LDL

Introduction

One class of apolipoprotein A-I mimetic peptides are 18 amino acids in length. The progenitor was originally designed as a tool for investigating the functional properties of apoA-I (1, 2). The 243 amino acids of apoA-I form a class A amphipathic helix—an α-helix with opposing polar and non-polar faces, with the positively charged amino acids of the polar face being found at the polar/non-polar interface and with the negatively charged amino acids of this same face being found in its center (3, 4). ApoA-I mimetics do not share sequence homology with apoA-I, but each possesses the same class A amphipathic helical structure (5). The mimetics differ with respect to the number of phenylalanines present on the non-polar face of the amphipathic helix, ranging from the two phenylalanines of the original 18A (since named *2F*) up to seven phenylalanines (so-called *7F*) (6). Because of their common class A helical structure, all six mimetics in this group reproduce the basic lipid associating properties of apoA-I (1, 6).

ApoA-I has been shown to possess both anti-atherogenic (7-9) and anti-inflammatory properties (10-12). The apoA-I mimetics, however, differ with respect to their biological activity. 2F, for example, was not able to inhibit atherosclerosis when administered to atherosclerosis-sensitive mice (6). By contrast, 5F significantly reduced diet-induced atherosclerosis in C57BL/6J mice fed an atherogenic diet (13). The peptides were thus screened for their ability to inhibit LDL-induced monocyte chemotaxis in a co-culture of human aortic wall cells (6). The performance of the peptides within this model turned out to be an important predictor of their ability to inhibit atherosclerosis in mouse models (14). While 4F, 5F, and 6F all inhibited monocyte chemotaxis, 4F was singled out for follow up testing on the basis of its greater solubility (5).

4F has the structure Ac-D-W-F-K-A-F-Y-D-K-V-A-E-K-F-K-E-A-F-NH_2. There are four phenylalanines on the hydrophobic face of the amphipathic helix. The peptide is capped at the N and C terminals with acetyl and NH_2 groups, respectively. These caps stabilize the α-helix of 4F and thereby increase its lipid binding capacity (15). 4F synthesized from L amino acids (L-4F) and from D amino acids (D-4F) have both been used in biological studies. D-4F and L-4F were shown to have the same *in vitro* and *in vivo* properties, indicating that stereo-specificity is not essential to the activity of the peptide (16, 17).

In mouse models of atherosclerosis, 4F significantly reduced atherosclerotic lesions while improving the anti-inflammatory properties of HDL (18). 4F has also been reported to show promise in the treatment of other inflammatory disorders in preclinical studies (14, 19-21) including diabetes (22, 23), arthritis (22), hyperlipidemia-induced renal inflammation(23), influenza A pneumonia (24), vascular dementia (25), Alzheimer's disease (26) and ovarian cancer (27). As discussed in detail (28), two recent studies in humans gave conflicting results regarding the ability of the peptide to alter HDL inflammatory properties. Based on new mouse studies, the most likely explanation for the discrepancy is that the negative study employed doses that were significantly lower than the positive study (28).

At least two mechanisms of action have been proposed to explain the effects of 4F, particularly on atherosclerosis (16). First, it has been shown that 4F can cause the remodeling of HDL and the formation of pre-β HDL enriched in both apoA-I and paraoxonase activity (29, 30). This transformation lowers lipoprotein hydroperoxide levels; HDL becomes anti-inflammatory; and HDL-mediated cholesterol efflux and reverse cholesterol transport from macrophages are stimulated (29). Reverse cholesterol transport through pre-β HDL is considered athero-protective (31). It has thus been

hypothesized that it is through the remodeling of HDL and the stimulation of reverse cholesterol transport that 4F was able to reduce lesions in mouse models of atherosclerosis (29). In objection to this mechanism, it has been pointed out that the physiological concentration of 4F necessary for HDL remodeling is higher than the minimum that has been shown necessary for atheroprotection (16).

In a second hypothesis, 4F was proposed to be involved in the sequestration and removal of oxidized lipids. It has been shown that 4F binds oxidized phospholipids and oxidized fatty acids with a high affinity, which is several orders of magnitude greater than apoA-I (32). Since oxidized lipids play central roles in both atherosclerosis (33) and other inflammatory disorders (34-36) including cancer (37, 38) the sequestration and removal of oxidized lipids by 4F has been put forward as the basis of a general mechanism of action regarding its various positive effects (20).

Consistent with this second hypothesis, administration of 4F to diabetic apoE null mice has been shown to significantly reduce atherosclerotic lesions while also decreasing hepatic concentrations of 15HETE, 12HETE, and 13HODE (39). It has also been shown that L-4F injected into apoE null mice resulted in a significant reduction in plasma levels of oxidized fatty acids including 15HETE and 13HODE, while at the same time lowering the HDL inflammatory index (HII) (40). However, the mechanism by which 4F causes the clearance of oxidized lipids remains unknown.

Both proposed mechanisms may involve the interaction between 4F and HDL. Thus, one purpose of our investigation was to use ^{14}C-labeled L-4F to investigate the *in vivo* interaction between 4F and HDL. This aspect of our study received added importance due to a recent report questioning this relationship (41). We report here that L-4F associates immediately and preferentially with HDL upon its

introduction into the circulation of C57BL/6J mice, and that this complex of HDL and L-4F is cleared quickly.

In the course of this and other lipoprotein association studies, we observed for the first time that LDL plays an important role in the relationship between L-4F and HDL. Not only does LDL appear to direct L-4F to HDL, it also amplifies the association between HDL and L-4F by several-fold. In the process, L-4F transfers oxidized lipids from LDL onto HDL. Thus, our results suggest a possible model by which oxidized lipids are cleared from the system by L-4F. L-4F transfers oxidized lipids into HDL, at least in part from LDL, and this complex of HDL and L-4F and oxidized lipids is then cleared from the circulation.

Materials and Methods

ApoA-I Mimetic Peptide L-4F. The amino acid sequence of 4F is Ac-DWFKAFYDKVAEKFKEAF-NH_2. L-4F was synthesized from L-amino acids by the solid phase peptide synthesis method previously described (42, 43) with the modification that rink amide resin instead of Wang resin was used. During the peptide chain elongation the ε-amino groups of the lysines were protected by t-Butyloxycarbonyl (t-BOC). The final step for the cleavage of the peptide from the resin along with the cleavage of tBOC protecting groups was accomplished using trifluoroacetic acid with suitable scavengers. Under these conditions the N-terminal acetyl group is stable whereas all of the other t-butanol protecting groups are cleaved. For synthesizing ^{14}C-peptide, ^{14}C-acetic anhydride was used instead of acetic anhydride as previously described (44). Peptide purity was ascertained by mass spectral analysis and analytical HPLC. Both L-4F and ^{14}C-L-4F were synthesized in the laboratory of G.M. Anantharamaiah of the University of Alabama at Birmingham.

Human plasma. Healthy human donor subjects were recruited after written consent approved by the University of California at Los Angeles (UCLA) Institutional Review Board. Fasting blood was collected in heparinized tubes (Becton Dickinson) and the plasma was separated by centrifugation.

Mice and mouse plasma. Both wild-type C57BL/6J mice and apoE null mice on a C57BL/6J background were obtained from the breeding colony of the Department of Laboratory and Animal Medicine at the David Geffen School of Medicine at UCLA after having been originally purchased from Jackson Laboratories. The mice were maintained on a chow diet (Ralston Purina). To obtain blood for assays, the mice were subjected after overnight fast to either local or terminal bleeds in which either 75 or 250 µl of blood was removed from the retro-orbital sinus. The mice were under mild isoflourane anesthesia, and

the blood was collected into heparinized capillary tubes and chilled plasma separator tubes (Becton-Dickson). Plasma was preserved in 10% sucrose. All experiments were performed using protocols approved by the Animal Research Committee at UCLA and in conformity with the Public Health Service Policy on Humane Care and Use of Laboratory Animals.

Isolation of lipoproteins. Human LDL and HDL were isolated by density centrifugation and were obtained from the Atherosclerosis Research Unit Core facility. LDL was isolated between densities of 1.019 - 1.063 g/ml and HDL between densities of 1.063 - 1.21 g/ml. After isolation the lipoproteins were dialyzed to remove the added salts (45).

FPLC separation and purification of plasma and lipoprotein mixtures. Plasma and isolated lipoprotein mixtures were fractionated by gel permeation fast protein liquid chromatography (FPLC). The system consisted of dual Superose 6 columns in series (Amersham Biosciences) driven by a Beckman Coulter SystemGold 126NM Solvent Module though a 168NM Detector; controlled by Beckman's 32 Karat 7.0 software; and collected by a Foxy 200 (Teledyne Isco). The column was eluted with a solution of 0.9% (w/v) NaCl, 0.03% (w/v) NaN_3, pH 8.2 at a rate of 0.500 ml/min and fractions were collected. \

Determination of cholesterol, radioactivity, and protein. Cholesterol was determined using a commercially available kit (Thermo Scientific, 2011). Radioactivity was determined as DPM by scintillation counting either 0.250 or 0.500 ml of each fraction in 10.0 ml BioSafe II scintillation fluid (RPI Corporation) on a Packard Tri-Carb Model A900TR using QuantaSmart software. Protein concentration of isolated lipoproteins was determined by the Lowry method with Peterson's modification using a commercially available kit (Sigma-Aldrich, TP0300).

Incubation of ^{14}C-L-4F with human and mouse plasma. Human plasma, C57BL/6J plasma, and apoE -/- plasma samples were incubated separately with ^{14}C-L-4F (200 µl plasma; 50 µg ^{14}C-L-4F with specific

activity of 0.25 to 1.0 μCi) for 1 hour at 37°C after light vortexing. Subsequently, the mixes were separated using FPLC, and cholesterol and radioactivity were determined for the fractions.

Lipid supplementation of LDL: 5HETE, 15HETE. Human LDL was supplemented separately with 5S-hydroxy-6E, 8Z, 11Z, 14Z-eicosatetraenoic acid (5HETE) and with 15S-hydroxy-5Z, 8Z, 11Z, 13E-eicosatetraenoic acid (15HETE). Both lipids were from Cayman Chemical (34230, 34720) and were supplied as 0.1 μg/μl solutions in ethanol. Lipid (0.5 μg/1.0 mg protein of LDL) was injected directly into the LDL, which had been brought up to 100 μl in PBS. The lipid was injected all at once from above the surface of the LDL and the resultant solution was pipetted up and down followed by gentle vortexing. The mixes were washed using a 100 kDa cut-off filter (Millipore, UFC810024) to remove any unassociated lipids.

Incubation of ^{14}C-L-4F with isolated human lipoproteins. Isolated human lipoproteins (1.0 mg protein each of HDL, LDL, LDL-5HETE, and LDL-15HETE) were separately mixed with ^{14}C-L-4F **(**50 μg and 0.5 μCi) and brought up to 300 μl in PBS. Each mix was lightly vortexed and incubated at 37° C for one hour before being fractionated using FPLC. Radioactivity and cholesterol were determined for the fractions. In additional experiments, ^{14}C-L-4F (50 μg and 0.5 μCi) was combined with both HDL and LDL or LDL-15HETE (1.0 mg protein each). After light vortexing, the mixes were incubated for either 5 minutes or 1 hour at 37°C before being fractionated using FPLC and assayed as described above.

Loading of human LDL and HDL with ^{14}C-L-4F. Human LDL (2.0 mg protein) was mixed with 100 μg and 1.5 μCi ^{14}C-L-4F and incubated at 37°C for one hour. In order to remove un-associated ^{14}C-L-4F, the mix was fractionated using FPLC after spin filtering. Cholesterol and radioactivity were determined in order to ensure that ^{14}C-L-4F had associated with LDL. The LDL fractions were pooled and subsequently concentrated using a 100kDa cut-off filter (Millipore, UFC810024). Radioactivity per cholesterol was determined before and after concentration to ensure the integrity and adequate recovery of LDL-^{14}C-L-

4F. Alternatively, human HDL (1.0 mg protein/sample) was loaded with ^{14}C-L-4F (ranging from 5.0 to 200 μg) by mixing and a brief incubation at 37°C.

Incubation of hLDL-^{14}C-L-4F and mouse and human plasma. Human LDL was loaded with ^{14}C-L-4F as described above. Human plasma (200 μl) or C57BL/6J plasma (120 μl) were mixed with concentrated hLDL-^{14}C-L-4F (125 μl of a 250 μl concentrate, see above). The mixes were incubated at 37°C for 1 hour before being fractionated using FPLC. Cholesterol and radioactivity were determined for the fractions.

Lipid supplementation of LDL with 15HETE-d_8. LDL was supplemented with 30.0 μg 15S-hydroxy-5Z,8Z, 11Z,13E-eicosatetraenoic-5,6,8,9,11,12,14,15-d8 acid (15HETE-d_8) (Cayman, 334720). The solvent was evaporated under argon in a 10 ml glass test tube, and the lipid was brought up directly in human LDL (4.0 mg protein, 290 μl) by five minutes of gentle swirling and vortexing. The LDL was then purified by washing three times using a 100kDa cut-off filter. Cholesterol and protein were then determined for the concentrate.

Transfer of 15HETE-d_8 from LDL to HDL. The experiment was carried out as follows: first, LDL was supplemented with 15HETE-d_8 as above (referred to as "L only"). Then, a portion was incubated with purified human HDL in the absence (L+H) or the presence of L-4F (L+H+4F). For this, 0.5 mg LDL protein, 0.5 mg LDL protein and 0.5 mg HDL protein, and, the latter together with 25 μg L-4F, were brought up to a total volume of 150 μl in PBS. The three preparations were then incubated at 37° C for 1 hour. 125 μl of each sample was then separated using FPLC as described. The isolated lipoprotein fractions from the various experimental groups were pooled, the lipids were extracted, and the extracts were analyzed by LC/MS/MS.

Lipid extraction and sample preparation for LC-ESI-MS/MS analysis. Lipoproteins were separated using FPLC; fractions for each individual lipoprotein were pooled in accord with the distributions of

cholesterol; and the volumes of the pooled samples were recorded. 12HETE-d_8 (Cayman, 334570) was added to each pooled sample as an internal standard (100 µL of 100 ng 12HETE- d_8/ml methanol). The pH of the samples was adjusted to ~ pH 3.0 using formic acid. Oasis HLB 3 cc (60mg) solid-phase extraction cartridges (Waters, 186001880) on a vacuum manifold were equilibrated with 2 ml methanol followed by 2 ml water. The samples were slowly loaded on the cartridges under vacuum. After the samples had completely flowed through at approximately 0.5 ml/min, the cartridges were washed with 2ml 5% methanol in water. Lipids were then eluted from the cartridges with 2 ml methanol. The eluates were evaporated to dryness under argon at 37° C. Each dried lipid extract was then re-suspended in 100 µl of methanol using gentle vortexing. The samples were transferred to autosampler vials (Fisher scientific, 03-396-74) for LC/MS/MS analysis.

LC/MS/MS analysis. LC/MS/MS was performed using a 4000 QTRAP quadruple mass spectrometer (Applied Biosystems) equipped with electrospray ionization source. The HPLC system utilized an Agilent 1200 series LC pump equipped with a thermostatted autosampler (Agilent Technologies). Chromatography was performed using a Luna C-18(2) column (3 µm particle, 150 × 3.0mm; Phenomenex) with a security guard cartridge (C-18; Phenomenex) at 40^{o}C. Mobile phase A consisted of 0.1% formic acid in water, and mobile phase B consisted of 0.1% formic acid in acetonitrile. The auotosampler was set at 4^{o}C. The injection volume was 10 µl, and the flow rate was controlled at 0.4mL/min. The gradient program was as follows: 0-2min, 50% B; 2-3min, linear gradient from 50% to 60% B; 3-15min, linear gradient from 60-65% B; 15-17min, 65% B; 17-19min, linear gradient from 65-100% B; 19-21min 100% B; 21-23min, linear gradient from 100% to 50% B; 23-27min, 50% B. The data acquisitions and instrument control were accomplished using Analyst 1.4.2 software (Applied Biosystems). Detection was accomplished by using the multiple reaction monitoring (MRM) mode with negative ion detection; the parameter settings used were: ion spray voltage=-4500 V; curtain gas=20

(nitrogen); ion source gas 1=50; ion source gas 2 =30; ion source gas 2 temperature=550°C. Collision energy, declustering potential and collision cell exit potential were optimized for each compound to obtain optimum sensitivity. The transitions monitored were mass-to-charge ratio (m/z): m/z 327.1→226.1 for 15HETE-d_8; and 327.1→184.0 for 12HETE-d_8.

Binding Studies. Binding studies were performed by SPR on a BIAcore 3000 system (BiaCore AB) as previously described(32). In short, L-4F was immobilized on a BIAcore CM5 sensor chip activated per the manufacturer's protocol. Human LDL and HDL that had been isolated by ultracentrifugation was further purified using FPLC. FPLC was also used to isolate HDL from the plasma of a male C57Bl/6J mouse. The FPLC fractions were pooled and the protein concentrations of the lipoproteins were first determined. Molarity was subsequently calculated by assuming an average MW for HDL of 360 kD and for LDL of 2500 kD, while also supposing that protein makes up 40% of the mass of HDL and 22.5% of the mass of LDL(46). Further solutions of these analytes were then prepared in buffer containing 10 mM HEPES, pH 7.4, 150 mM NaCl, 3 mM EDTA, 0.005% (v/v) surfactant P20. Binding was measured by observing the change in the SPR angle as 30 µL of analyte in various concentrations flowed over the sample for 3 min at 10 µL/min. Equilibrium affinity constant (K_D) values were calculated from assays performed with five different analyte concentrations that gave binding responses of 50 to 300 resonance units (RUs). The calculations were done with BIAcore's BIAevaluation software, version 4.1, assuming a molar ratio of 1:1 analyte:peptide binding.

Injection of mice and collection of plasma. C57BL/6J mice were fasted overnight. Samples of ^{14}C-L-4F alone, hHDL/hHDL-^{14}C-L-4F, or hLDL-^{14}C-L-4F were introduced directly into the circulation of these mice via their tail veins using a 29 gauge insulin needle and syringe (Becton Dickinson, 329424). In the case of ^{14}C-L-4F alone (600 µg and 0.5 µCi brought up to 150 µl in 1x PBS), the peptide was introduced into each of 5 female 12 week old mice. In the case of hHDL/hHDL-^{14}C-L-4F, each of 6 female 12 week old mice

was injected with hHDL (1.0 mg protein) that had been loaded with 0 to 200 µg ^{14}C-L-4F and brought up to 150 µl in 1x PBS, in the manner described above. In the case of hLDL-^{14}C-L-4F, three male 10 week old mice were injected with hLDL-^{14}C-L-4F concentrate (0.10 µCi, 1.2 mg protein LDL, 70 µl total volume). Blood was drawn at various times after injection (^{14}C-L-4F, from 3 min to 30 min; hHDL/hHDL-^{14}C-L-4F, from 0 min to 120 min; and hLDL-^{14}C-L-4F, from 3 min to 60 min). During each bleed, approximately 100 µl of blood was drawn from the retro-orbital sinus under mild isoflourane anesthesia, as above. The plasma samples were separated and preserved, as above. The plasma samples were then either assayed directly or fractionated before further assays were performed.

Western blotting and quantification. Samples were first separated by gel electrophoresis under reduced and denaturing conditions on 10% NuPAGE Novex bis-tris gels (Invitrogen) using MOPS SDS running buffer (Invitogen). Gels were transferred to PVDF membrane (Millipore, IPVH00010) and some probed 1:100 with rabbit, human-and-mouse-specific anti-apoA-I antibody (Abcam, ab33470) and 1:5000 with HRP-conjugated anti-rabbit IgG (Amersham, NA934). Others were probed 1:10,000 with rabbit, anti human-specific anti-apo-AI (Abcam ab52945), or 1:20,000 with rabbit antimouse specific anti apoA1 (Abcam ab20355). For loading control the blots were probed 1:1500 with mouse, mouse-and-human-specific anti-albumin (Santa Cruz, sc58588) followed 1:5000 with HRP-conjugated anti-rabbit IgG or 1:5000 with anti-mouse IgG (Amersham, NXA931) . Blots were detected fluorescently on a Typhoon 9400 fluorescent scanner (GE Healthcare) using ECL Plus western blotting detection reagent (Amersham, RPN2106). In order to quantify the amount of apoA-I present in each sample, the scan of each blot was subjected to analysis using ImageQuant 5.0 software (Molecular Dynamics).

Statistical Analyses. Statistical analyses were performed by unpaired two-tail t-test.

Results

When ^{14}C-L-4F was incubated with fasted human plasma it associated almost completely with the HDL fraction as determined by FPLC fractionation (Fig. 1a). On occasion, when a low level of VLDL was present in some of the donors' plasma, ^{14}C-L-4F was detected in this fraction as well (data not shown). However, repeatedly, the LDL fraction of the human plasma (fractions 18 – 26) contained little to no radioactivity under these conditions.

Similar results were obtained for the association of ^{14}C-L-4F with C57BL/6J mouse plasma lipoproteins. Here too, the L-4F radioactivity was associated almost completely with the HDL fraction of fasting C57BL/6J mice (Fig. 1b). In contrast, when ^{14}C-L-4F was incubated with the plasma of fasting apoE-null mice, very little L-4F is associated with the HDL fraction. Rather, L-4F was detected in earlier fractions together with the distribution of cholesterol.

When incubated with ultracentrifuge-purified human HDL, ^{14}C-L-4F was associated with the HDL fraction off the FPLC. However, unlike in full human plasma, when ultracentrifuge-purified LDL alone was incubated with ^{14}C-L-4F, in the absence of other lipoproteins the radioactivity was associated with the LDL (Fig. 2b). This association of L-4F with isolated LDL can be enhanced when the LDL is preloaded with the oxidized lipids 15HETE. This enhanced association is dose-dependent and a calculated 2.07 – fold significant increase in radioactivity associated with LDL was observed when 5.0 μg 15HETE was preloaded into the purified human LDL ($p < 0.001$, $n=3$) (Fig. 2b). Similar results were observed for 5HETE-loaded LDL (data not shown).

In an attempt to study partially reconstituted human plasma, the purified HDL and LDL were incubated with ^{14}C-L-4F both separately and together (Fig 3a). As observed before, each of the isolated lipoproteins associated with ^{14}C-L-4F, with the HDL efficiency for the association exceeding by 8-fold that of the purified LDL alone on a per cholesterol basis. However, a highly synergistic effect in the binding of ^{14}C-L-4F to the HDL was observed when LDL was present. While there was a 60% decrease in the binding of ^{14}C-L-4F to the LDL (a loss of 7350 counts), a most-pronounced 2.5-fold increase in its binding to HDL is shown (a gain of 36307 counts). The association of ^{14}C-L-4F with the HDL component of the mix was virtually complete in 5 min (data not shown) as compared with 60 min. A comparable low level of ^{14}C-L-4F with the LDL was also observed for the two time periods. This result was not plasma donor-specific and was reproducible with three different donor pairs of HDL and LDL preparations. The ability of L-4F to be transferred from human LDL to mouse HDL in full C57BL/6J plasma is demonstrated in Figure 3b. When ^{14}C-L-4F-pre-loaded human LDL isolated by FPLC (from Fig. 2b) was mixed with C57BL/6J mouse plasma, a distinct transfer of the L-4F to the HDL fraction was observed. This transfer was incomplete under the *in vitro* experimental conditions and when compared to the transfer of ^{14}C-L-4F from the same pre-loaded LDL to the mouse HDL upon introduction to the mouse circulation (see below). Similar transfer to the HDL fraction in isolated human plasma was observed (data not shown).

15HETE increased the binding of ^{14}C-L-4F to isolated LDL as demonstrated in Figure 2b. One might expect, therefore, that a pre-loading of LDL with 15HETE would result in a decrease in association between L-4F and HDL when all three are co-incubated, as the 4F would adhere to the LDL. Instead, a 50% increase in the association of ^{14}C-L-4F with HDL was observed for a mixture of HDL with 15HETE-preloaded LDL as compared with LDL by itself. Under the incubation conditions there was no observed net transfer of free or esterified cholesterol between the two purified lipoproteins (Fig. 4b). However, we have obtained evidence that the presence of L-4F can initiate the transfer of oxidized lipids present

in LDL to the HDL fraction. Figure 5 depicts the effect of L-4F on the transfer of deuterated 15HETE-d from pre-loaded LDL to HDL as determined by LC/MS/MS analysis. Only a residual transfer of this oxidized lipid to the HDL was observed in the absence of L-4F. However a 35-fold increase was observed when L-4F was added to the mix (Fig. 5).

The association of ^{14}C-L-4F with lipoproteins was also studied in the circulation by introducing the radioactive peptide or a lipoprotein pre-loaded with it by tail vein injection into C57BL/6J mice. Fractionation of plasma obtained immediately post tail vein injection with ^{14}C-L-4F showed association with a fraction containing cholesterol and the protein apoA-I. This fraction is eluted off the FPLC column with retention expected for HDL (Fig 6a). The amount of L-4F radioactivity associated with this fraction rapidly declined in time with each subsequent bleed from the same mouse (Fig. 6b). After 30 min, it accounted for only 30% of the amount observed three minutes after injection. The radioactive material associated with the HDL fraction was identified as intact L-4F by LC/MS/MS. There was a time-dependent increase of the later eluting fractions containing radioactive substance at fractions 41 to 44. However, no intact ^{14}C-L-4F was present in these fractions as determined by LC/MS/MS. The identity of this material(s) is presently unknown, but it appears to be an aggregation of degraded/processed substance(s). The results of this independent experiment confirm and extend our previously published data (19).

Clearance data that was combined from five separate mice exhibited the same pattern of clearance over time (Fig. 6c). By seven minutes, there was already a significant 15% reduction ($p < .01$) in ^{14}C-L-4F associated with the HDL-containing fractions of the plasma. Further significant reductions of 28% ($p < .01$) and 50% ($p < .001$) were observed by 10 and 15 minutes, respectively. Finally, by 30 min, there was a decline in 80% of the ^{14}C-L-4F radioactivity ($p < .001$).

Clearance of radioactivity and human apoA-I from ^{14}C-L-4F-preloaded human HDL was measured by injecting four fasting C57BL/6J female mice with this substance and comparing to two mice injected with the same human HDL lacking L-4F (Fig. 7). In this study, samples of human HDL (1.0 mg protein) were pre-loaded with increasing amounts of ^{14}C-L-4F, ranging from 0 μg up to 200 μg. Blood was drawn and plasma isolated immediately post-injection (time 0), and at 30, 60, and 120 minutes. Time-dependent clearance of radioactivity from the circulation was observed for each of the mice. The average $T_{1/2}$ clearance value for all concentrations of ^{14}C-L-4F is calculated to be 23.6 min (stdv = 5.0 min) (Fig 7a). In addition, using monospecific antibodies, time-dependent decline in the amounts of human and mouse apoA-I were determined in these plasma samples by Western blot analyses. ^{14}C-L-4F concentration-dependent rate of decline was observed for the human apoA-I at all amounts of ^{14}C-L-4F (Fig. 7b) whereas lack of such decline was observed for the mouse apoA-I for 120 min in up to 100 μg ^{14}C-L-4F (Fig. 7c). A 12% decline in mouse apoA-I was observed for 200 μg ^{14}C-L-4F after 2 hr as compared to about 85% decline in human apoA-I in the same plasma. No decline in either human or mouse apoA-I was detected in the plasma of mice injected with human HDL lacking L-4F. At 120 min a decrease of about 20% total HDL cholesterol is observed (Fig. 7d). This decrease in HDL cholesterol is dependent on the presence of L-4F and cannot be observed in its absence.

The transfer of ^{14}C-L-4F from pre-loaded human LDL (from Fig. 2b) to plasma lipoproteins and its clearance from the circulation was studied by injecting fasting female C57BL/6J mice (Fig. 8). Unlike in the *in-vitro* experiment (Fig. 3b), here by 3 minutes post-injection, the majority of radioactivity present in the plasma was associated with the HDL-containing fractions of the plasma and only 14% of the counts were detected on the LDL fraction. These counts were altogether cleared from the LDL fraction by 10 minutes. Time dependent clearance of radioactivity was observed in the HDL fraction as well. At

60 min, only 15% of the radioactivity remained in the HDL compared to the 3 min time collection (Fig 8a). Since no substantial parallel decrease in the LDL cholesterol was observe (Fig 8b), it indicates that L-4F was transferred from LDL to HDL in the circulation, both quickly and completely to the limits of detection.

The affinity of the individual isolated lipoproteins to L-4F was evaluated by a determination of their dissociation constants (K_D) to immobilized L-4F onto a sensor chip in a BIAcore 3000 system. The binding was determined by a surface plasmon resonance (SPR) using multiple concentrations of the lipoproteins. These results are depicted in Figure 9 and show that L-4F binds to HDL with significantly greater affinity than to LDL. The affinities between L-4F and human and mouse HDL were not significantly different, with $K_D = 3.36 \times 10^{-8}$ and 1.03×10^{-8} M, respectively. By contrast, the affinity between L-4F and human LDL was significantly less than the affinity between L-4F and either human or mouse HDL, with $K_D = 1.17 \times 10^{-6}$ M (**, *: p= 0.001, n=5).

Discussion

Our *in-vitro* studies indicate that L-4F associates with the HDL fraction of human and C57BL/6J plasma (Figs 1a and 1b). Similarly, L-4F associated with isolated human HDL (Fig 2a) as was reported by others. (13, 29, 47) What is interesting to note is the variable association between LDL and L-4F under different conditions. When HDL was present, as in full human plasma, L-4F associated little to none with the LDL fraction of the plasma, even when LDL exceeded HDL by approximately two-fold on a cholesterol basis (see Figure 1a). However, if no other lipoprotein is present, L-4F will associate with purified human LDL (see Figure 2b). Likewise, if HDL is markedly decreased, as is the case in apoE-/- mouse plasma, the association profile of L-4F with the FPLC fractions of the plasma mirrors the profile of cholesterol across those same fractions (see Figure 1b).

L-4F displays greater relative affinity for purified HDL than for purified LDL when the binding is compared on a per cholesterol basis of the lipoproteins. A 12-fold greater relative affinity of L-4F is shown for isolated human HDL than for isolated human LDL (Figs 3a and 3b). Even when LDL is supplemented with oxidized lipids, which are reported to bind 4F with high affinity (32), L-4F still exhibits an almost 9-fold greater relative affinity for an un-supplemented HDL than for 15HETE-supplemented LDL. This difference in relative affinity to the two isolated lipoproteins cannot, by itself, fully account for the lack of association between LDL and L-4F observed in plasma. Based on the differing affinities, it would be anticipated that a partition of radioactivity would be observed between LDL and HDL when ^{14}C-L-4F was applied to full plasma. However, in most experiments, as the one depicted in Figure 1a, the L-4F radioactivity was associated with HDL with no detectable radioactivity in the LDL fraction. A more quantitative determination of the affinities of the various lipoproteins to L-4F is the determination of the individual K_Ds. (Fig. 9). In agreement with the data presented in Figure 3, L-

4F binds with about two orders of magnitude higher affinity (lower K_D) to both mouse and human HDL as compared with the affinity to human LDL. This, by itself, can explain the high association of ^{14}C-L-4F to HDL when introduced to human plasma or injected to mouse.

To further elucidate the binding of L-4F with HDL and LDL we studied the interaction of L-4F with lipoproteins in partially reconstituted human plasma that consisted of only HDL and LDL. As noted above, L-4F will bind with isolated HDL or LDL. Interestingly, when L-4F was co-incubated with both HDL and LDL, the association between L-4F and LDL decreased by at least 60% whereas, the association between L-4F and HDL increased 2-3 fold (Fig 3a). This cannot be the consequence of a competition for the L-4F between HDL over LDL since in the absence of LDL the binding of the L-4F to the HDL is several fold lower compared to the same binding in the presence of LDL under the same experimental conditions. Therefore there was a true synergistic binding of L-4F to HDL in the presence of LDL.

The increase in the binding of L-4F to HDL in the presence of LDL can be partially explained by a transfer of L-4F from LDL to HDL. This possibility was investigated by the use of purified isolated LDL pre-loaded with ^{14}C-L-4F (Figure 2b) or in incubation with mouse plasma (Fig 3b). As shown in Fig 3b 50.7% of the L-4F was found in the HDL fraction of the mouse plasma, clearly indicating a possible transfer of L-4F between these lipoproteins. This process of transfer of L-4F from preloaded LDL to HDL was by far more efficient in vivo (see below).

LDL and HDL can exchange lipids. In the circulation, this transfer is often effected by mediating proteins such as lipid transfer protein (LTP) (48), lipid transfer inhibitor protein (LTIP) (48), and cholesterol ester transfer protein (CETP) (49). CETP is often bound to HDL (50, 51). However, there is evidence that lipid transfer can occur even in the absence of transfer proteins (48). Moreover, it has

been shown that L-4F binds some oxidized lipids with very high affinity (32). It is, therefore, reasonable to assume that the transfer of some lipids, which are complexed to L-4F, from LDL into HDL, is involved in the enhanced uptake of L-4F by HDL. In this proposed mechanism, L-4F associates with both lipoproteins, in part, by binding with the oxidized lipids. The L-4F-lipid complex would then be transferred from LDL to HDL efficiently, explaining the loss of L-4F from LDL and the gain by HDL. In addition, it is possible that when HDL takes up these lipids it increases the uptake of free L-4F from the mix explaining the synergistic increase in the binding of L-4F to HDL in the presence of LDL. The FPLC profile of HDL does not reflect the heterogenous nature of HDL. In Figure 6a there is a small tail of peptide that does not completely coincide with apoA-I and cholesterol. Thus, the studies in Figure 6a do not by themselves prove that the peptide is physically associated with HDL. However, these data together with the data in Figure 7 which demonstrate that L-4F enhances the clearance of human apoA-I from the circulation make it highly likely that most of the peptide is physically associated with HDL. Nonetheless, future studies will be required to completely prove this point. Future studies will also be needed to determine whether a particular component of HDL is responsible for L-4F association with HDL or whether the radius of the curvature of the lipoprotein and the available surface provide a favorable environment for the peptide.

If such a mechanism, in which an oxidized lipid-L-4F adduct is transferred as a complex from LDL to HDL exists, it implies that addition of L-4F, or oxidized lipid, to LDL should enhance the transfer of oxidized lipid or L-4F, respectively, to HDL. These two complementing experiments are demonstrated in Figures 4 and 5. In the first experiment, HDL exhibited an approximately 2-fold increase in its association with L-4F when incubated in the presence of LDL as compared to the uptake of L-4F by HDL alone. However, when an LDL, pre-loaded with 15HETE, was used instead, a 3-fold increase in the association of L-4F with HDL was observed (Fig 4a). If the added 15HETE had remained on LDL particles,

we might have expected an increase in the amount of L-4F associated with the LDL fraction compared to unsupplemented LDL, as demonstrated before (Fig 2b). However, in the presence of HDL no such increase was observed and, instead, an increase in radioactivity was demonstrated strictly for HDL. This result strongly suggests that the oxidized lipid is transferred to HDL, most likely as a complex with L-4F.

The oxidized lipid transfer hypothesis is further supported by the experiments represented in Figure 5. In these studies the LDL was preloaded with deuterated 15HETE, and the transfer to HDL was determined by LC/MS/MS. In the absence of L-4F only residual amounts of 15HETE-d_8 appeared in the HDL fraction (Fig 5). In contrast, L-4F triggered a significant transfer of 15HETE-d_8 from LDL to the HDL fraction during the co-incubation. This *in-vitro* study strongly suggest that the transfer of L-4F from LDL to HDL is essential for the transport of the oxidized lipids, which would not occur spontaneously in its absence. These observations also explain the synergistic increase in the binding of L-4F to HDL in the presence of LDL. LDL serves as a potential source of oxidized lipids, for which HDL serves as the sink in the presence of L-4F.

Our *in vivo* studies establish that L-4F associates primarily with HDL in the circulation of fasting mice. As noted above, these *in vivo* association data, using ^{14}C-labeled L-4F, counter the central result from which Wool et. al., employing biotinylated 4F, concluded that 4F does not associate with HDL *in vivo* (41). By contrast, ^{14}C-L-4F in a comparable experiment eluted with almost complete overlap with the cholesterol and apoA-I peaks (see Figure 6a). This exact overlap of peaks strongly suggest that ^{14}C-L-4F associates with the HDL fraction of the plasma and thus with HDL *in vivo*. The same studies also indicate that the complexes of L-4F and HDL are cleared quickly from the circulation. Direct injection of L-4F resulted in a time-dependent decline in the amount of L-4F associating with the HDL fraction of the plasma (see Figure 6b). The radioactive signal associated with the HDL fraction was validated as ^{14}C-L-4F

by LC/MS/MS (data not shown). The time-decrease in L-4F in the HDL fraction was associated with an appearance of lower size radioactively eluting material (Fig 6b, Fractions 41-45) which did not consist of ^{14}C-L-4F as determined by LC/MS/MS. Although detailed analysis to elucidate the structure(s) of the radioactive materials in these fractions was not done it is assumed that they represent degradation products of the ^{14}C-L-4F. In this experiment the calculated $T_{1/2}$ for the decline is 16 min, indicating a quick removal of the ^{14}C-L-4F from the circulation (Fig 6c). Comparable results were obtained when a complex consisting of human HDL that had been pre-loaded with L-4F was injected directly into the circulation of C57BL/6J mice. Here again, the ^{14}C-L-4F was cleared quickly from the circulation (Fig 7a). The average $T_{1/2}$ for the decline in Fig 7a was calculated to be 23.6 min, which is somewhat longer than the clearance time of the ^{14}C-L-4F from the mHDL complex. Watson et al. (52) reported that the $T_{1/2}$ for L-4F in humans was ~1.5 hours after intravenous administration and was ~2.5 – 3.0 hours after subcutaneous administration. We do not know if the difference between the values reported here ($T_{1/2}$ < 30 min) is due to the difference between mice and humans or is because we relied on measurements of radioactivity for our determination of $T_{1/2}$ and Watson et al. (52) relied on mass measurements using LC-MS/MS. The time dependent decline of ^{14}C-L-4F from the plasma of these mice was associated with a time dependent decline in human apoA-I, strongly indicating a relationship between the presence of L-4F and the clearance of the human HDL . The importance of L-4F in this clearance is indicated by the lack of decline in human apoA-I from native human HDL devoid of L-4F (Fig 7b). We cannot rule out a deacylation of ^{14}C-L-4F in the HDL as a mechanism that may explain the difference in the rate of clearance of ^{14}C-L-4F radioactivity and human apoA-I. The differential effect of the injected ^{14}C-L-4F-hHDL complex on the clearance of human apoA-I as compared to mouse apoA-I, strongly indicate a selective clearance of the L-4F bound HDL. The 12% decline in the mouse apoA-I at the highest ^{14}C-L-4F level of 200 μg after 120 min may represent an overflow of the high amount of L-4F from the hHDL to the mHDL. Whatever the explanation, this represents only a small fraction of cleared mHDL compared

to the 85% decrease in hHDL in the same fraction. The injected one mg of human HDL by protein would about double the plasma HDL-cholesterol in the mouse. If 40% of the human apoA-I were cleared by 120 minutes one should expect a decline of about 20% HDL cholesterol (assuming no significant replenishment from other body cholesterol pools in this time period). Indeed, such decline in cholesterol is observed whereas no decline in plasma cholesterol was seen in the absence of added ^{14}C-L-4F (Fig 7d).

The essential identity in affinities (K_Ds) of the mouse and the human HDL to L-4F (Fig 9) does not mean that in the period of time the L-4F-loaded hHDL is in the circulation, the L-4F should equilibrate equally between the two. In fact, the data indicate that the loaded hHDL is cleared from the circulation before significant transfer of L-4F to the mHDL can take place (Fig 7). This is one more example in which the affinity (which is a thermodynamic parameter) may not predict a short-term equilibration (which is a kinetic parameter). In short, the hHDL-L-4F complex is cleared from the circulation much faster than any possible transfer of the L-4F from the hHDL to the mHDL can take place. This phenomenon allowed us to determine that only L-4F-tagged HDL is targeted for clearance as compared to native HDL.

The efficiency of the transfer of ^{14}C-L-4F from human LDL to mouse HDL was observed to be much higher in the mouse circulation compared to an *in-vitro* transfer in isolated mouse plasma (compare Figs 3b and 8). By 3 min post injection, over 85% of all detectable counts had transferred to the HDL fraction, and by 10 min no radioactivity could be detected in the LDL fraction. ^{14}C-L-4F associated with HDL was cleared quickly from the circulation with a decline of 85% being observed between 3 and 60 min. Here again, we cannot exclude deacylation and rapid loss of the radiolabel in vivo compared to in vitro as the explanation for the seemingly different results of Fig 3b and Fig 8.

Recently Navab et al. reported that dose rather than the plasma level of 4F is predictive of its efficacy (28). Oral administration of D4F (≥ 4.5 mg/kg) to apoE null mice significantly improved biomarkers of atherosclerosis, even though plasma levels of peptide did not exceed 20 ng/ml. By contrast, SQ injection of 4F failed to improve biomarkers even when plasma levels over 700 ng/ml were achieved (SQ dose of 0.45 mg/kg). SQ injections were effective at doses similar to the doses effective orally i.e ≥ 4.5 mg/kg. Although less likely, the results by Navab et al. suggest that the effects of 4F on plasma lipoproteins may not be a major mechanism of 4F peptides. A currently accepted mechanism of action of 4F peptides is their ability to bind and remove oxidized lipids (40) from the circulation and tissue (39). Our studies support this mechanism for the circulation. Future studies will determine whether the effects of 4F on the intestine, which was proposed to be their major site of action by Navab et al., also involves the removal of oxidized lipids *via* lipoproteins similar to those in the circulation. It should be noted that intestine is the second major site of lipoprotein synthesis (~30%) (53-55).

We report here that L-4F associates with HDL in both human plasma and in the circulation of C57BL/6J mice. Both observations are consistent with prior reports (13, 29, 47), and with a previous report from our laboratory (19). However, Wool et al. have recently argued against the conclusion that 4F associates with HDL *in vivo* (41). In studies by Wool et al. direct injection of biotinylated 4F (b4F) into the circulation of C57BL/6J mice resulted in two peaks of b4F associated with plasma fractions, neither of which directly overlapped the peak of HDL, as determined by apoA-I and cholesterol. Based on this observation and their assumption that the effect of the biotin moiety on the physical properties of 4F is negligible, they concluded that 4F itself does not associate with HDL in vivo. Our *in vivo* association data, using ^{14}C labeled L-4F, counter the central conclusion of Wool et al. that 4F does not associate with HDL *in vivo*. Biotinylated 4F introduced into the circulation of C57BL/6J mice was found by FPLC to elute

several fractions behind the peaks of cholesterol and apoA-I that associate with HDL. By contrast, ^{14}C-L-4F in a comparable experiment eluted with almost complete overlap with the cholesterol and apoA-I peaks (Figure 6a). This exact overlap of peaks strongly suggests that ^{14}C-L-4F associates with the HDL fraction of the plasma and, thus, with HDL *in vivo*. The discrepancy in our observations could be due to the chemical modification of the L-4F by biotinylation. Biotinylation of L-4F alters its mass by approximately 10% (addition of 241 daltons). While the addition of biotin to the N-terminal of L-4F may not affect the ability of immobilized b4F to bind both native and oxidized PAPC in *vitro* (32), comparison to our studies is difficult since we demonstrate binding of L-4F to intact lipoproteins in the circulation. It is possible that the addition of the comparatively large moiety affects the interaction, within the circulation, between L-4F and lipoproteins. It is entirely possible that other chemical modifications of L-4F for the purpose of detection (e.g. ^{125}I-tyrosine modification) may alter the amphipathicity of the 4F alpha helix as well and result in similar change in binding properties to lipoproteins. Hence, the choice in the use of ^{14}C-L-4F in our present study.

In summary, the results of the studies reported here suggest that i) LDL promotes the association of L-4F with HDL and ii) in the presence of L-4F oxidized lipids in LDL are rapidly transferred to HDL allowing these oxidized lipids to be acted upon by the enzymes in HDL and/or cleared from the circulation.

1. Anantharamaiah Gm Fau - Jones, J. L., C. G. Jones Jl Fau - Brouillette, C. F. Brouillette Cg Fau - Schmidt, B. H. Schmidt Cf Fau - Chung, T. A. Chung Bh Fau - Hughes, A. S. Hughes Ta Fau - Bhown, J. P. Bhown As Fau - Segrest, and S. JP. 1985. - Studies of synthetic peptide analogs of the amphipathic helix. Structure of complexes with dimyristoyl phosphatidylcholine. *J Biol Chem* **260**: 10248-10255.

2. GM, A. 1986. - Synthetic peptide analogs of apolipoproteins. *Methods Enzymol* **128**: 627-647.

3. Segrest Jp Fau - Jackson, R. L., J. D. Jackson Rl Fau - Morrisett, A. M. Morrisett Jd Fau - Gotto, Jr., and J. Gotto AM. 1974. - A molecular theory of lipid-protein interactions in the plasma lipoproteins. *FEBS Lett* **38**: 247-258.

4. Segrest Jp Fau - Jones, M. K., H. Jones Mk Fau - De Loof, C. G. De Loof H Fau - Brouillette, Y. V. Brouillette Cg Fau - Venkatachalapathi, G. M. Venkatachalapathi Yv Fau - Anantharamaiah, and A. GM. 1992. - The amphipathic helix in the exchangeable apolipoproteins: a review of secondary structure and function. *J Lipid Res* **33**: 141-166.

5. Anantharamaiah Gm Fau - Mishra, V. K., D. W. Mishra Vk Fau - Garber, G. Garber Dw Fau - Datta, S. P. Datta G Fau - Handattu, M. N. Handattu Sp Fau - Palgunachari, M. Palgunachari Mn Fau - Chaddha, M. Chaddha M Fau - Navab, S. T. Navab M Fau - Reddy, J. P. Reddy St Fau - Segrest, A. M. Segrest Jp Fau - Fogelman, and F. AM. 2007. - Structural requirements for antioxidative and anti-inflammatory properties of apolipoprotein A-I mimetic peptides. *J Lipid Res* **48**: 1915-1923.

6. Datta G Fau - Chaddha, M., S. Chaddha M Fau - Hama, M. Hama S Fau - Navab, A. M. Navab M Fau - Fogelman, D. W. Fogelman Am Fau - Garber, V. K. Garber Dw Fau - Mishra, R. M. Mishra Vk Fau - Epand, R. F. Epand Rm Fau - Epand, S. Epand Rf Fau - Lund-Katz, M. C. Lund-Katz S Fau - Phillips, J. P. Phillips Mc Fau - Segrest, G. M. Segrest Jp Fau - Anantharamaiah, and A. GM. 2001. - Effects of increasing hydrophobicity on the physical-chemical and biological properties of a class A amphipathic helical peptide. *J Lipid Res* **42**: 1096-1104.

7. Plump As Fau - Scott, C. J., J. L. Scott Cj Fau - Breslow, and B. JL. 1994. - Human apolipoprotein A-I gene expression increases high density lipoprotein and suppresses atherosclerosis in the apolipoprotein E-deficient mouse. *Proc Natl Acad Sci U S A* **91**: 9607-9611.

8. Chiesa G Fau - Sirtori, C. R., and S. CR. 2002. - Use of recombinant apolipoproteins in vascular diseases: the case of apoA-I. *Curr Opin Investig Drugs* **3**: 420-426.

9. Nissen Se Fau - Tsunoda, T., E. M. Tsunoda T Fau - Tuzcu, P. Tuzcu Em Fau - Schoenhagen, C. J. Schoenhagen P Fau - Cooper, M. Cooper Cj Fau - Yasin, G. M. Yasin M Fau - Eaton, M. A. Eaton Gm Fau - Lauer, W. S. Lauer Ma Fau - Sheldon, C. L. Sheldon Ws Fau - Grines, S. Grines Cl Fau - Halpern, T. Halpern S Fau - Crowe, J. C. Crowe T Fau - Blankenship, R. Blankenship Jc Fau - Kerensky, and K. R. 2003. - Effect of recombinant ApoA-I Milano on coronary atherosclerosis in patients with acute coronary syndromes: a randomized controlled trial. *Jama* **290**: 2292-2300.

10. Barter Pj Fau - Nicholls, S., K.-A. Nicholls S Fau - Rye, G. M. Rye Ka Fau - Anantharamaiah, M. Anantharamaiah Gm Fau - Navab, A. M. Navab M Fau - Fogelman, and F. AM. 2004. - Antiinflammatory properties of HDL. *Circ Res* **95**: 764-772.

11. Navab M Fau - Hama, S. Y., C. J. Hama Sy Fau - Cooke, G. M. Cooke Cj Fau - Anantharamaiah, M. Anantharamaiah Gm Fau - Chaddha, L. Chaddha M Fau - Jin, G. Jin L Fau - Subbanagounder, K. F. Subbanagounder G Fau - Faull, S. T. Faull Kf Fau - Reddy, N. E. Reddy St Fau - Miller, A. M. Miller Ne Fau - Fogelman, and F. AM. 2000. - Normal high density lipoprotein inhibits three steps in the formation of mildly oxidized low density lipoprotein: step 1. *J Lipid Res* **41**: 1481-1494.

12. Navab M Fau - Hama, S. Y., G. M. Hama Sy Fau - Anantharamaiah, K. Anantharamaiah Gm Fau - Hassan, G. P. Hassan K Fau - Hough, A. D. Hough Gp Fau - Watson, S. T. Watson Ad Fau - Reddy, A. Reddy St Fau - Sevanian, G. C. Sevanian A Fau - Fonarow, A. M. Fonarow Gc Fau - Fogelman, and F. AM. 2000. - Normal high density lipoprotein inhibits three steps in the formation of mildly oxidized low density lipoprotein: steps 2 and 3. *J Lipid Res* **41**: 1495-1508.

13. Garber Dw Fau - Datta, G., M. Datta G Fau - Chaddha, M. N. Chaddha M Fau - Palgunachari, S. Y. Palgunachari Mn Fau - Hama, M. Hama Sy Fau - Navab, A. M. Navab M Fau - Fogelman, J. P. Fogelman Am Fau - Segrest, G. M. Segrest Jp Fau - Anantharamaiah, and A. GM. 2001. - A new synthetic class A amphipathic peptide analogue protects mice from diet-induced atherosclerosis. *J Lipid Res* **42**: 545-552.

14. Navab M Fau - Anantharamaiah, G. M., S. T. Anantharamaiah Gm Fau - Reddy, S. Reddy St Fau - Hama, G. Hama S Fau - Hough, V. R. Hough G Fau - Grijalva, N. Grijalva Vr Fau - Yu, B. J. Yu N Fau - Ansell, G. Ansell Bj Fau - Datta, D. W. Datta G Fau - Garber, A. M. Garber Dw Fau - Fogelman, and F. AM. 2005. - Apolipoprotein A-I mimetic peptides. *Arterioscler Thromb Vasc Biol* **25**: 1325-1331.

15. Venkatachalapathi Yv Fau - Phillips, M. C., R. M. Phillips Mc Fau - Epand, R. F. Epand Rm Fau - Epand, E. M. Epand Rf Fau - Tytler, J. P. Tytler Em Fau - Segrest, G. M. Segrest Jp Fau - Anantharamaiah, and A. GM. 1993. - Effect of end group blockage on the properties of a class A amphipathic helical peptide. *Proteins* **15**: 349-359.

16. Getz Gs Fau - Wool, G. D., C. A. Wool Gd Fau - Reardon, and R. CA. 2009. - Apoprotein A-I mimetic peptides and their potential anti-atherogenic mechanisms of action. *Curr Opin Lipidol* **20**: 171-175.

17. Van Lenten, B. J., A. C. Wagner, M. Navab, G. M. Anantharamaiah, S. Hama, S. T. Reddy, and A. M. Fogelman. 2007. Lipoprotein inflammatory properties and serum amyloid A levels but not cholesterol levels predict lesion area in cholesterol-fed rabbits. *J Lipid Res* **48**: 2344-2353.

18. Navab, M., G. M. Anantharamaiah, S. Hama, D. W. Garber, M. Chaddha, G. Hough, R. Lallone, and A. M. Fogelman. 2002. Oral administration of an Apo A-I mimetic Peptide synthesized from D-amino acids dramatically reduces atherosclerosis in mice independent of plasma cholesterol. *Circulation* **105**: 290-292.

19. Navab M Fau - Shechter, I., G. M. Shechter I Fau - Anantharamaiah, S. T. Anantharamaiah Gm Fau - Reddy, B. J. Reddy St Fau - Van Lenten, A. M. Van Lenten Bj Fau - Fogelman, and F. AM. 2010. - Structure and function of HDL mimetics. *Arterioscler Thromb Vasc Biol* **30**: 164-168.

20. Van Lenten, B. J., A. C. Wagner, G. M. Anantharamaiah, M. Navab, S. T. Reddy, G. M. Buga, and A. M. Fogelman. 2009. Apolipoprotein A-I mimetic peptides. *Curr Atheroscler Rep* **11**: 52-57.

21. Navab, M., G. M. Anantharamaiah, and A. M. Fogelman. 2008. The effect of apolipoprotein mimetic peptides in inflammatory disorders other than atherosclerosis. *Trends Cardiovasc Med* **18**: 61-66.

22. Charles-Schoeman, C., M. L. Banquerigo, S. Hama, M. Navab, G. S. Park, B. J. Van Lenten, A. C. Wagner, A. M. Fogelman, and E. Brahn. 2008. Treatment with an apolipoprotein A-1 mimetic peptide in combination with pravastatin inhibits collagen-induced arthritis. *Clin Immunol* **127**: 234-244.

23. Buga, G. M., J. S. Frank, G. A. Mottino, A. Hakhamian, A. Narasimha, A. D. Watson, B. Yekta, M. Navab, S. T. Reddy, G. M. Anantharamaiah, and A. M. Fogelman. 2008. D-4F reduces EO6 immunoreactivity, SREBP-1c mRNA levels, and renal inflammation in LDL receptor-null mice fed a Western diet. *J Lipid Res* **49**: 192-205.

24. Van Lenten, B. J., A. C. Wagner, G. M. Anantharamaiah, D. W. Garber, M. C. Fishbein, L. Adhikary, D. P. Nayak, S. Hama, M. Navab, and A. M. Fogelman. 2002. Influenza infection promotes macrophage traffic into arteries of mice that is prevented by D-4F, an apolipoprotein A-I mimetic peptide. *Circulation* **106**: 1127-1132.

25. Buga, G. M., J. S. Frank, G. A. Mottino, M. Hendizadeh, A. Hakhamian, J. H. Tillisch, S. T. Reddy, M. Navab, G. M. Anantharamaiah, L. J. Ignarro, and A. M. Fogelman. 2006. D-4F decreases brain arteriole inflammation and improves cognitive performance in LDL receptor-null mice on a Western diet. *J Lipid Res* **47**: 2148-2160.

26. Handattu, S. P., D. W. Garber, C. E. Monroe, T. van Groen, I. Kadish, G. Nayyar, D. Cao, M. N. Palgunachari, L. Li, and G. M. Anantharamaiah. 2009. Oral apolipoprotein A-I mimetic peptide improves cognitive function and reduces amyloid burden in a mouse model of Alzheimer's disease. *Neurobiol Dis* **34**: 525-534.

27. Su, F., K. R. Kozak, S. Imaizumi, F. Gao, M. W. Amneus, V. Grijalva, C. Ng, A. Wagner, G. Hough, G. Farias-Eisner, G. M. Anantharamaiah, B. J. Van Lenten, M. Navab, A. M. Fogelman, S. T. Reddy, and R. Farias-Eisner. 2010. Apolipoprotein A-I (apoA-I) and apoA-I mimetic peptides inhibit tumor development in a mouse model of ovarian cancer. *Proc Natl Acad Sci U S A* **107**: 19997-20002.

28. Navab, M., S. T. Reddy, G. M. Anantharamaiah, S. Imaizumi, G. Hough, S. Hama, and A. M. Fogelman. 2011. The intestine maybe a major site of action for the ApoA-I mimetic peptide 4F whether the peptide is administered subcutaneously or orally. *J Lipid Res*.

29. Navab M Fau - Anantharamaiah, G. M., S. T. Anantharamaiah Gm Fau - Reddy, S. Reddy St Fau - Hama, G. Hama S Fau - Hough, V. R. Hough G Fau - Grijalva, A. C. Grijalva Vr Fau - Wagner, J. S. Wagner Ac Fau - Frank, G. Frank Js Fau - Datta, D. Datta G Fau - Garber, A. M. Garber D Fau - Fogelman, and F. AM. 2004. - Oral D-4F causes formation of pre-beta high-density lipoprotein and improves high-density lipoprotein-mediated cholesterol efflux and reverse cholesterol transport from macrophages in apolipoprotein E-null mice. *Circulation* **109**: 3215-3220.

30. Troutt, J. S., W. E. Alborn, M. K. Mosior, J. Dai, A. T. Murphy, T. P. Beyer, Y. Zhang, G. Cao, and R. J. Konrad. 2008. An apolipoprotein A-I mimetic dose-dependently increases the formation of prebeta1 HDL in human plasma. *J Lipid Res* **49**: 581-587.

31. Fielding Cj Fau - Fielding, P. E., and F. PE. 2001. - Cellular cholesterol efflux. *Biochim Biophys Acta* **31**: 175-189.

32. Van Lenten Bj Fau - Wagner, A. C., C.-L. Wagner Ac Fau - Jung, P. Jung Cl Fau - Ruchala, A. J. Ruchala P Fau - Waring, R. I. Waring Aj Fau - Lehrer, A. D. Lehrer Ri Fau - Watson, S. Watson Ad Fau -

Hama, M. Hama S Fau - Navab, G. M. Navab M Fau - Anantharamaiah, A. M. Anantharamaiah Gm Fau - Fogelman, and F. AM. 2008. - Anti-inflammatory apoA-I-mimetic peptides bind oxidized lipids with much higher affinity than human apoA-I. *J Lipid Res* **49**: 2302-2311.

33. Berliner Ja Fau - Watson, A. D., and W. AD. 2005. - A role for oxidized phospholipids in atherosclerosis. *N Engl J Med* **353**: 9-11.

34. Natarajan, R., and J. L. Nadler. 2004. Lipid inflammatory mediators in diabetic vascular disease. *Arterioscler Thromb Vasc Biol* **24**: 1542-1548.

35. Epand Rf Fau - Mishra, V. K., M. N. Mishra Vk Fau - Palgunachari, G. M. Palgunachari Mn Fau - Anantharamaiah, R. M. Anantharamaiah Gm Fau - Epand, and E. RM. 2009. - Anti-inflammatory peptides grab on to the whiskers of atherogenic oxidized lipids. *Biochim Biophys Acta* **9**: 25.

36. Leitinger, N. 2008. The role of phospholipid oxidation products in inflammatory and autoimmune diseases: evidence from animal models and in humans. *Subcell Biochem* **49**: 325-350.

37. Ferguson, L. R. 2010. Chronic inflammation and mutagenesis. *Mutat Res* **690**: 3-11.

38. Moreno, J. J. 2009. New aspects of the role of hydroxyeicosatetraenoic acids in cell growth and cancer development. *Biochem Pharmacol* **77**: 1-10.

39. Morgantini C Fau - Imaizumi, S., V. Imaizumi S Fau - Grijalva, M. Grijalva V Fau - Navab, A. M. Navab M Fau - Fogelman, S. T. Fogelman Am Fau - Reddy, and R. ST. 2010. - Apolipoprotein A-I mimetic peptides prevent atherosclerosis development and reduce plaque inflammation in a murine model of diabetes. *Diabetes* **59**: 3223-3228.

40. Imaizumi S Fau - Grijalva, V., M. Grijalva V Fau - Navab, B. J. Navab M Fau - Van Lenten, A. C. Van Lenten Bj Fau - Wagner, G. M. Wagner Ac Fau - Anantharamiah, A. M. Anantharamiah Gm Fau - Fogelman, S. T. Fogelman Am Fau - Reddy, and R. ST. 2010. - L-4F differentially alters plasma levels of oxidized fatty acids resulting in more anti-inflammatory HDL in mice. *Drug Metab Lett* **4**: 139-148.

41. Wool Gd Fau - Vaisar, T., C. A. Vaisar T Fau - Reardon, G. S. Reardon Ca Fau - Getz, and G. GS. 2009. - An apoA-I mimetic peptide containing a proline residue has greater in vivo HDL binding and anti-inflammatory ability than the 4F peptide. *J Lipid Res* **50**: 1889-1900.

42. Jones Mk Fau - Anantharamaiah, G. M., J. P. Anantharamaiah Gm Fau - Segrest, and S. JP. 1992. - Computer programs to identify and classify amphipathic alpha helical domains. *J Lipid Res* **33**: 287-296.

43. Palgunachari, M. N., V. K. Mishra, S. Lund-Katz, M. C. Phillips, S. O. Adeyeye, S. Alluri, G. M. Anantharamaiah, and J. P. Segrest. 1996. Only the two end helixes of eight tandem amphipathic helical domains of human apo A-I have significant lipid affinity. Implications for HDL assembly. *Arterioscler Thromb Vasc Biol* **16**: 328-338.

44. Handattu Sp Fau - Garber, D. W., D. C. Garber Dw Fau - Horn, D. W. Horn Dc Fau - Hughes, B. Hughes Dw Fau - Berno, A. D. Berno B Fau - Bain, V. K. Bain Ad Fau - Mishra, M. N. Mishra Vk Fau - Palgunachari, G. Palgunachari Mn Fau - Datta, G. M. Datta G Fau - Anantharamaiah, R. M. Anantharamaiah Gm Fau - Epand, and E. RM. 2007. - ApoA-I mimetic peptides with differing ability to inhibit atherosclerosis also exhibit differences in their interactions with membrane bilayers. *J Biol Chem* **282**: 1980-1988.

45. Havel Rj Fau - Eder, H. A., J. H. Eder Ha Fau - Bragdon, and B. Jh. 1955. - The distribution and chemical composition of ultracentrifugally separated lipoproteins in human serum. *J Clin Invest* **34**: 1345-1353.

46. Eisenberg, S. 1991. Plasma Lipoproteins: Structure, Composition, Classification, and Metabolism. *In* Primary hyperlipoproteinemias. G. Steiner and E. Shafrir, editors. McGraw-Hill, Health Professions Division. pp. 23-41.

47. Garber Dw Fau - Venkatachalapathi, Y. V., K. B. Venkatachalapathi Yv Fau - Gupta, J. Gupta Kb Fau - Ibdah, M. C. Ibdah J Fau - Phillips, J. B. Phillips Mc Fau - Hazelrig, J. P. Hazelrig Jb Fau - Segrest, G. M. Segrest Jp Fau - Anantharamaiah, and A. GM. 1992. - Turnover of synthetic class A amphipathic

peptide analogues of exchangeable apolipoproteins in rats. Correlation with physical properties. *Arterioscler Thromb* **12**: 886-894.

48. Morton Re Fau - Greene, D. J., and G. DJ. 1994. - Regulation of lipid transfer between lipoproteins by an endogenous plasma protein: selective inhibition among lipoprotein classes. *J Lipid Res* **35**: 836-847.

49. Christison Jk Fau - Rye, K. A., R. Rye Ka Fau - Stocker, and S. R. 1995. - Exchange of oxidized cholesteryl linoleate between LDL and HDL mediated by cholesteryl ester transfer protein. *J Lipid Res* **36**: 2017-2026.

50. Asztalos Bf Fau - Horvath, K. V., K. Horvath Kv Fau - Kajinami, C. Kajinami K Fau - Nartsupha, C. E. Nartsupha C Fau - Cox, M. Cox Ce Fau - Batista, E. J. Batista M Fau - Schaefer, A. Schaefer Ej Fau - Inazu, H. Inazu A Fau - Mabuchi, and M. H. 2004. - Apolipoprotein composition of HDL in cholesteryl ester transfer protein deficiency. *J Lipid Res* **45**: 448-455.

51. Tall, A. 1995. - Plasma lipid transfer proteins. *Annu Rev Biochem* **64**: 235-257.

52. Watson, C. E., N. Weissbach, L. Kjems, S. Ayalasomayajula, Y. Zhang, I. Chang, M. Navab, S. Hama, G. Hough, S. T. Reddy, D. Soffer, D. J. Rader, A. M. Fogelman, and A. Schecter. 2011. Treatment of patients with cardiovascular disease with L-4F, an apo-A1 mimetic, did not improve select biomarkers of HDL function. *J Lipid Res* **52**: 361-373.

53. Windmueller, H. G., and A. L. Wu. 1981. Biosynthesis of plasma apolipoproteins by rat small intestine without dietary or biliary fat. *J Biol Chem* **256**: 3012-3016.

54. Brunham, L. R., J. K. Kruit, J. Iqbal, C. Fievet, J. M. Timmins, T. D. Pape, B. A. Coburn, N. Bissada, B. Staels, A. K. Groen, M. M. Hussain, J. S. Parks, F. Kuipers, and M. R. Hayden. 2006. Intestinal ABCA1 directly contributes to HDL biogenesis in vivo. *J Clin Invest* **116**: 1052-1062.

55. Bisgaier, C. L., and R. M. Glickman. 1983. Intestinal synthesis, secretion, and transport of lipoproteins. *Annu Rev Physiol* **45**: 625-636.

Figure Legends

Figure A-1. **L-4F association with lipoproteins in human plasma and in C57BL/6J and apoE -/- mouse plasma.** ^{14}C-L-4F (50.0 µg with 0.25 µCi) was incubated with 200 µl human plasma for 1 hour at 37° C. The mix was separated using FPLC, and radioactivity (**-●-)** and cholesterol (**-**○**-)** were determined for the fractions (*Figure 1a*). ^{14}C-L-4F (50 µg with 1.0 µCi) was also incubated with 200 µl of either wild-type C57BL/6J or apoE -/- plasma for 1 hour at 37° C. The mixes were fractionated using FPLC, and radioactivity (**-■-**: apoE-/-;**-▲-:** BL6) and cholesterol (**-**□**-**: apoE-/-; **-Δ-**: BL6) were determined for the fractions (*Figure 1b*). The figure depicts almost complete association with HDL in human and C57BL/6J plasma and preferential association with apoB-containing lipoproteins in plasma of the apoE -/- mouse (the figure is a representative of four different experiments).

Figure A-2. **L-4F associates with isolated human HDL and LDL. 15HETE supplementation of LDL increases the association between L-4F and LDL.** Human HDL and LDL were isolated from plasma by ultracentrifugation. 1.0 mg of HDL protein (*Figure 2a*) was incubated for 1 hour with ^{14}C-L-4F (50 µg; 0.5 µCi), and radioactivity (**-■-**)and cholesterol (**-**○**-**) were determined for the isolated fractions.

15HETE enhances the association between L-4F and human LDL. In a parallel experiment, samples of 1.0 mg protein of human LDL were supplemented with 0 to 5.0 µg 15HETE. The lipoprotein preparations were then incubated with ^{14}C-L-4F (50 µg; 0.25 µCi), isolated on FPLC and the FPLC fractions were assayed for both radioactivity (**-◆-**: LDL only **; -▲-**: LDL + 0.5 µg 15HETE; **-■-**: LDL + 1.0 µg 15HETE; **-●-**: LDL + 5.0 µg 15HETE) and cholesterol (**-◊-:** LDL only). A dose-dependent increase in association between L-4F and LDL was observed, with calculated total counts in the various LDL fractions of 3975, 4653, 5661

and 8258 DPM accordingly. A significant 2.07 fold increase was observed between the association of ^{14}C-L-4F with 5.0 μg 15HETE supplemented and with 15HETE unsupplemented LDL ($p < 0.001$, n=3).

Figure A-3. **hLDL enhances the association between L-4F and hHDL; and L-4F, preloaded into hLDL, transfers to mHDL in C57BL/6J plasma.** Isolated human LDL and HDL were co-incubated with ^{14}C-L-4F, and the association pattern of L-4F in the co-incubation was compared to that in individual LDL and HDL controls by FPLC fractionations. 2.0 mg LDL protein was combined with 2.0 mg HDL protein and with ^{14}C-L-4F (100 μg; 1.0 μCi). Half was incubated for at 37° for 1 hour before fractionation on the FPLC, while the other half was fractionated after 5 minutes. In parallel, 1.0 mg LDL protein or 1.0 mg HDL protein was separately incubated with ^{14}C-L-4F for 1 hour before FPLC fractionation. Radioactivity (**-◆-**: LDL only; **-■-**: HDL only; **-●-**: LDL+HDL 60 min) and cholesterol (-○-: LDL+HDL 60 min) were determined for the isolated fractions (Fig. 3a). Radioactivity and cholesterol for the 5 min sample were very similar to those of the 60 min sample (data not shown). In a separate experiment, human LDL was first pre-loaded with ^{14}C-L-4F by incubating 2.0 mg LDL protein with 100 μg (1.0 μCi) ^{14}C-L-4F before processing by FPLC to remove unbound peptide. The LDL fractions were pooled and concentrated, and the LDL-^{14}C-L-4F concentrate was incubated for 1 hour with isolated C57BL/6J plasma. The reaction mixture was fractionated by FPLC, and radioactivity (**-●-**) and cholesterol (-○-) were determined for the individual fractions (Fig. 3b). This result was not plasma donor-specific and was reproducible with three different donor pairs of HDL and LDL preparations as well as using isolated plasma from a different mouse.

Figure A-4. **Loading of LDL with 15HETE enhances the association between L-4F and HDL compared to unsupplemented LDL.** 1.0 mg LDL protein supplemented with 0.5 μg 15HETE (See Materials and Methods Section) was added to 1.0 mg HDL protein and incubated with ^{14}C-L-4F (50 μg with 0.5 μCi) for

1 hour at 37°. The mixture was then analyzed by FPLC and radioactivity was determined for the isolated fractions. HDL by itself or a combination of LDL and HDL controls were treated in the same manner (**-◆-** : HDL; **-■-**: HDL+LDL; **-▲-**: HDL+ (LDL+15HETE)). An increase of 1.9-fold and 2.9-fold in the uptake of L-4F by HDL was observed in the presence of LDL and the presence of 15HETE supplemented LDL, respectively (a representative of two separate experiments is depicted in Fig. 4a). In a separate experiment, HDL, LDL, or a mixture of both were incubated as above, isolated on FPLC; and total cholesterol was determined for the isolated fractions (**-○-**: LDL; **-◊-**: HDL; **-□-**: HDL+LDL). No significant net transfer of total cholesterol between the lipoproteins was observed (Fig. 4b) (Both Figs. 3a and 3b are representatives of three different experiments).

Figure A-5. **L-4F enhances the transfer of 15HETE from LDL onto HDL.** Human LDL was supplemented with 7.5 μg deuterated 15HETE (15HETE-d_8) per mg of LDL protein. 0.5 mg of HDL protein and 0.5 mg of the 15HETE-d_8 supplemented LDL protein were then incubated at 37°C for 1.0hr with or without L-4F. The mixes were fractionated on the FPLC. The isolated lipoprotein fractions were pooled, and lipids were extracted from those pooled fractions. Supplemented LDL alone was treated similarly. The extracts were analyzed using LC/MS/MS. The figure shows the amount of 15HETE-d_8 present in the isolated lipoproteins as a percentage of the amount originally present in the LDL. A 35-fold increase in the transferred 15HETE-d_8 is observed in the presence of L-4F ($p = 0.02$). n=3.

Figure A-6. **L-4F injected into the circulation of C57BL/6J mice associates rapidly and primarily with the HDL fraction of the plasma and then is cleared quickly from the circulation.** ^{14}C-L-4F (600 μg ; 0.5 μCi) was injected directly into the circulation of each of five female C57BL/6J mice. Blood was collected at various time points, and the plasma was fractionated using FPLC. Radioactivity (**-●-**), cholesterol (**-□-**),

and apoA-I (**-▲-**) were determined for the individual FPLC fractions of the 3 min bleed of a representative mouse (Fig. 6a). Radioactivity (**-◆-**: 3 min; **-■-**: 7 min; **-▲-**: 15 min; **-●-**: 30 min) was determined for the FPLC fractions from all time point bleeds of that same representative mouse (Fig. 6b). Radioactivity (**-●-)** in the FPLC fractions of five mice at all time points was determined. The average amount of radioactivity in the HDL fraction for each time point for the different mice is expressed as a percent of the 3 min value for each mouse. (Fig. 6c). A time-dependent decline in radioactivity is observed. Significant reductions are observed between 3 minutes and all other time points (*****: $p < 0.01$; ****:** $p < 0.001$). Further significant reductions were observed between 7 and 15 min ($p < 0.01$) and 7 and 30 min ($p < 0.001$); and between 10 and 30 min ($p < 0.01$)(n=5).

Figure A-7. **Radioactivity and apoA-I from ^{14}C-L-4F loaded human HDL, injected via tail vein into C57Bl/6J mice, are cleared quickly from the circulation.** Increasing amounts of ^{14}C-L-4F (0 ug to 200 µg) were loaded into samples of human HDL (1.0 mg protein). Each of the samples was then tail vein - injected into separate male C57Bl/6J mice. Blood was collected from each mouse immediately after injection (0 min) and then at 30, 60, and 120 min post injection. Radioactivity in plasma aliquots was determined for each collected sample (**-x-**: 0 µg ^{14}C-L-4F; **-□-**: 5.0 µg ^{14}C-L-4F; **-Δ-**: 50 µg ^{14}C-L-4F; **-○-**: 100 µg ^{14}C-L-4F; **-◊-**: 200 µg ^{14}C-L-4F). A time-dependent decline of radioactivity in the plasma is shown for each of the injected L-4F concentrations with average $T_{1/2}$ = 23.6 min (STDV = 5.0 min) (Fig. 7a). Plasma samples were also analyzed by Western blots for human-specific apoA-I using mouse albumin as a loading control. The amount of human apoA-I present in each sample is expressed as a percent of the amount at time=0 for that mouse or, in the case of 0 µg ^{14}C-L-4F, for those two mice (**-x-**: 0 µg ^{14}C-L-4F; **-■-**: 5.0 µg ^{14}C-L-4F; **-▲-**: 50 µg ^{14}C-L-4F; **-●-**: 100 µg ^{14}C-L-4F; **-◆-**: 200 µg ^{14}C-L-4F). Time-dependent decrease in human apoA-I is shown for the HDL samples loaded with L-4F. The most significant decrease in human apoA-I is shown for the 120 min, the longest bleed time, for all ^{14}C-L-4F loaded samples.

Western blots show human apoA-I across all four bleed times for both the mouse injected with human HDL loaded with 100 μg ^{14}C-L-4F and for a control injection with no ^{14}C-L-4F (Fig. 7b). The same plasma bleeds were probed for mouse-specific apoA-I. The amount of mouse apoA-I present in each sample is expressed as a percent of the amount at time=0 (**-x-**: 0 μg ^{14}C-L-4F; **-■-**: 5.0 μg ^{14}C-L-4F; **-▲-**: 50 μg ^{14}C-L-4F; **-●-**: 100 μg ^{14}C-L-4F; **-◆-**: 200 μg ^{14}C-L-4F) (Fig. 7c). Unlike human apoA-I, mouse A-I showed little to no decline across time in ^{14}C-L-4Famounts of up to 100 μg and only 12% decline is observed at 200 μg 14C-L-4F. Western blots show mouse apoA-I across all four bleed times for both the mouse injected with human HDL loaded with 100 μg ^{14}C-L-4F and for a control mouse injected with human HDL without supplementation with ^{14}C-L-4F. Lastly, total HDL cholesterol in these same plasma samples was determined (**-x-**: 0 μg ^{14}C-L-4F; **-□-**: 5.0 μg ^{14}C-L-4F; **-Δ-**: 50 μg ^{14}C-L-4F; **-○-**: 100 μg ^{14}C-L-4F; **-◊-**: 200 μg ^{14}C-L-4F) (Figure 7d). HDL cholesterol showed a time-dependent decline consistent with the decline in human apoA-I (The figure is a representative of two separate experiments).

Figure A-8. **^{14}C-L-4F transfers rapidly from pre-loaded human LDL to mouse HDL in the circulation of C57BL/6J mice and is then quickly cleared.** Human LDL was loaded with ^{14}C-L-4F, and the complex was purified by FPLC fractionation (see Fig 2b) and concentrated. Approximately 1.25 mg protein of the ^{14}C-L-4F -LDL (0.10 μCi) concentrate was then injected directly into the circulation of each of three male C57BL/6J mice. Blood was drawn at 3, 10, and 60 min post injection. Plasma samples were fractionated by FPLC, and radioactivity and cholesterol were determined for all three mice. Radioactivity in the various FPLC fractions is shown for the three bleed times of a representative mouse (**-◆-**: 3 min; **-■-**: 10 min; **-▲-**: 60 min). Over 85% of detectable counts were already transferred to the HDL fraction of the plasma by 3 minutes. No counts were detected within the LDL fraction by 10 minutes. At 60 minutes the radioactivity associated with the HDL fraction had decreased by over 85% compared to the 3 min

bleed time (Fig. 8a) The cholesterol values associated with this same mouse (**-◊-**: 3 min; **-□-**: 10 min; **-Δ-**: 60 min) indicate a minimal decline in LDL cholesterol across 60 minutes (Fig. 8b) (The figure is a representative of three separate experiments).

Figure A-9. **L-4F binds to HDL with significantly greater affinity than to LDL.** A binding study was performed by surface plasmon resonance (SPR) on a BIAcore 3000 system. L-4F was immobilized on a sensor chip. Analyte solutions of isolated human and mouse lipoproteins were then passed over the chip, and binding was measured by observing the change in SPR angle. Equilibrium affinity constant (K_D) values were calculated from assays performed with five different analyte concentrations. The affinities between L-4F and human and mouse HDL were not significantly different, with $K_D = 3.36 \times 10^{-8}$ and 1.03×10^{-8} M, respectively. By contrast, the affinity between L-4F and human LDL was significantly less than the affinity between L-4F and either human or mouse HDL, with $K_D = 1.17 \times 10^{-6}$ M (**, *: p= 0.001, n=5).

Figure A-1

1a

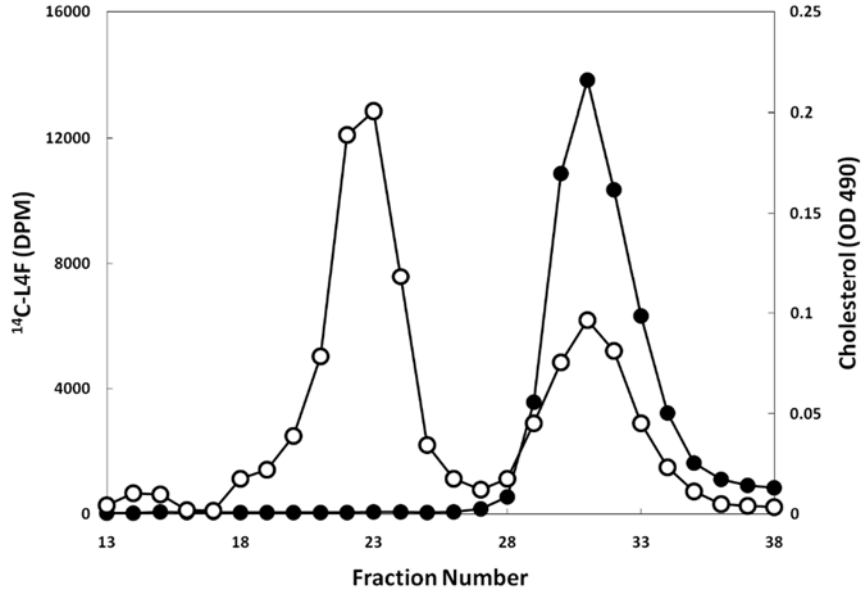

1b

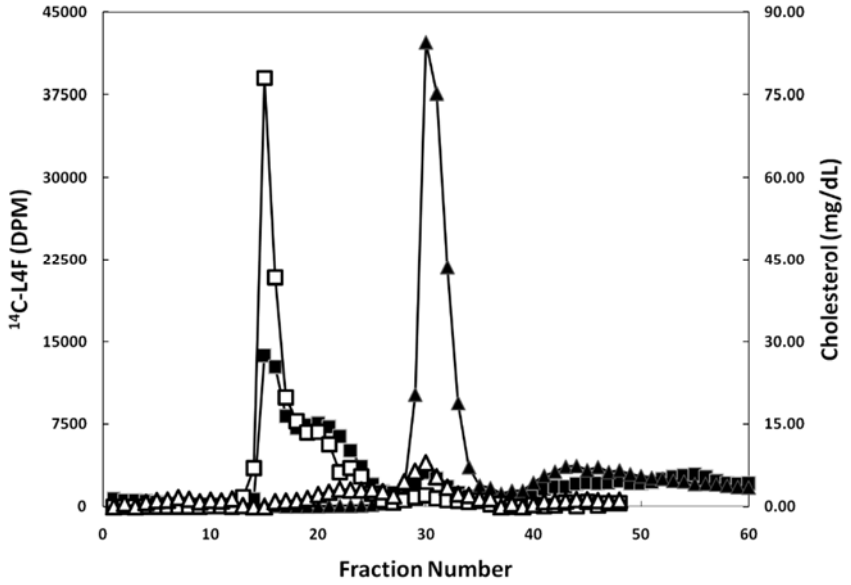

Figure A-2

2a

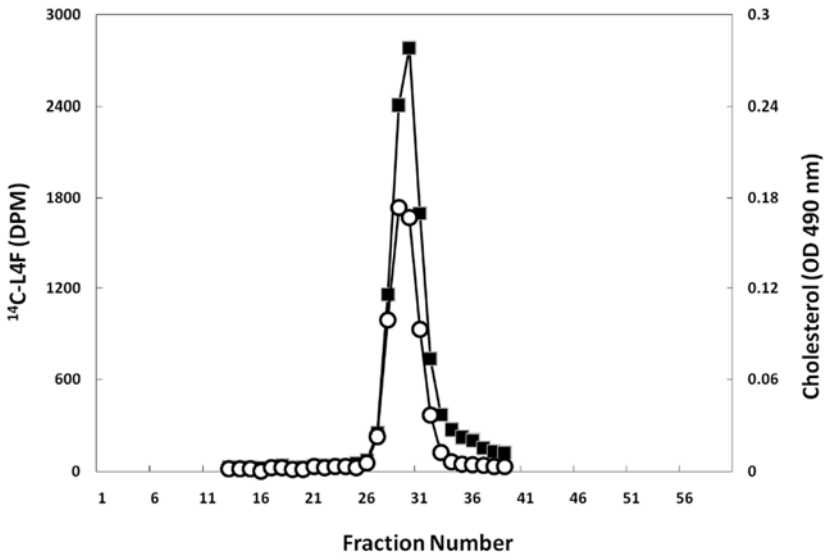

2b

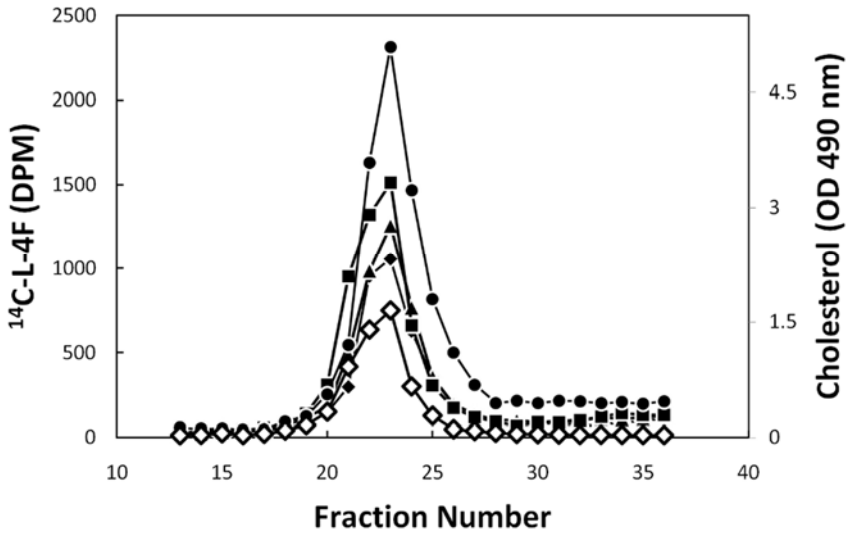
2500
2000
1500
1000
500
0
^{14}C-L-4F (DPM)
4.5
3
1.5
0
Cholesterol (OD 490 nm)
10
15
20
25
30
35
40
Fraction Number

Figure A-3

3a

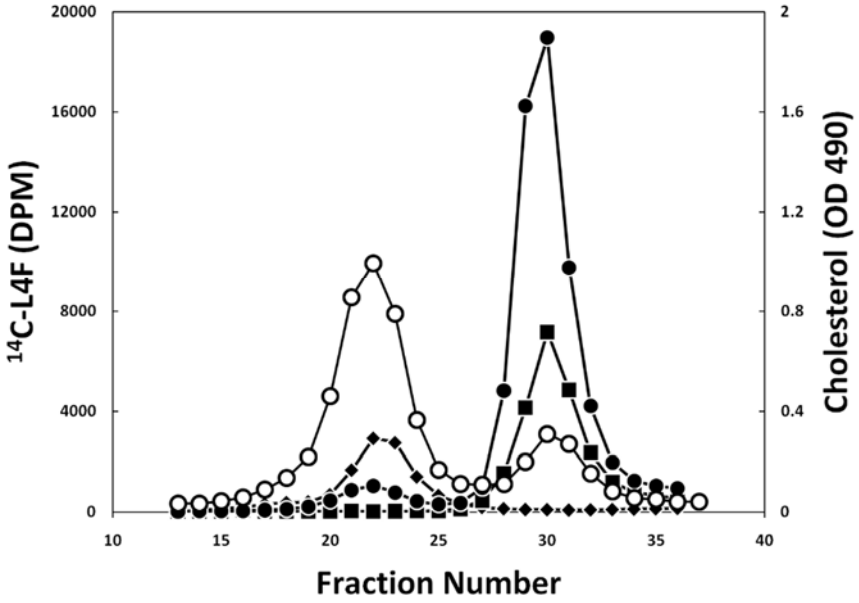
20000
16000
12000
8000
4000
0
2
1.6
1.2
0.8
0.4
0
10
15
20
25
30
35
40
^{14}C-L4F (DPM)
Cholesterol (OD 490)
Fraction Number

3b

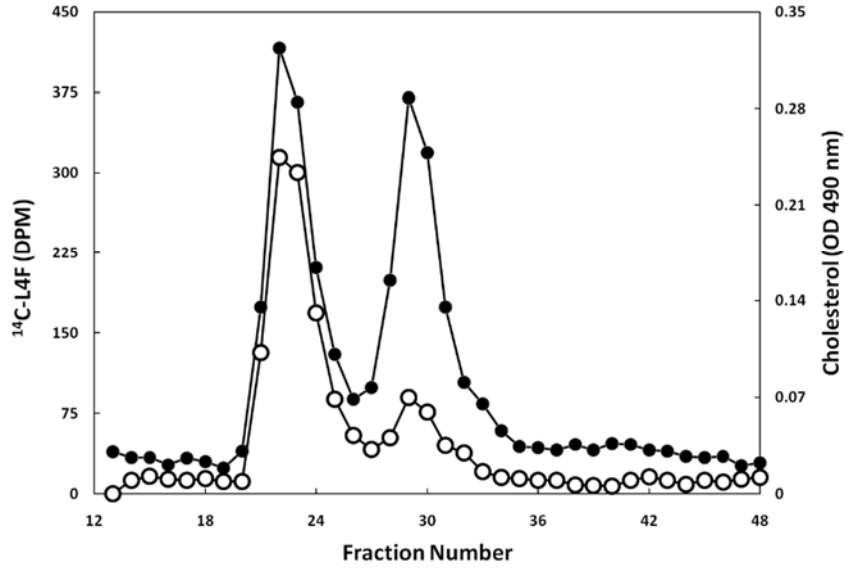
450
375
300
225
150
75
0
0.35
0.28
0.21
0.14
0.07
0
12
18
24
30
36
42
48
^{14}C-L4F (DPM)
Cholesterol (OD 490 nm)
Fraction Number

Figure A-4

4a

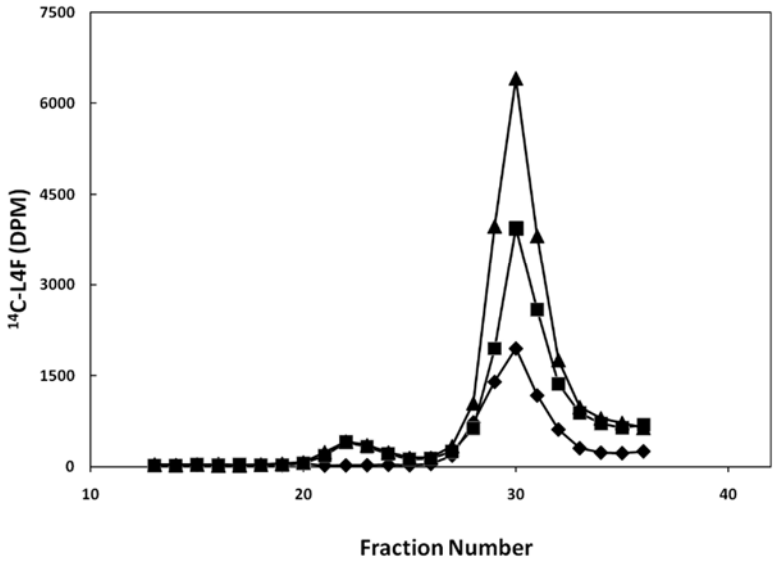

4b

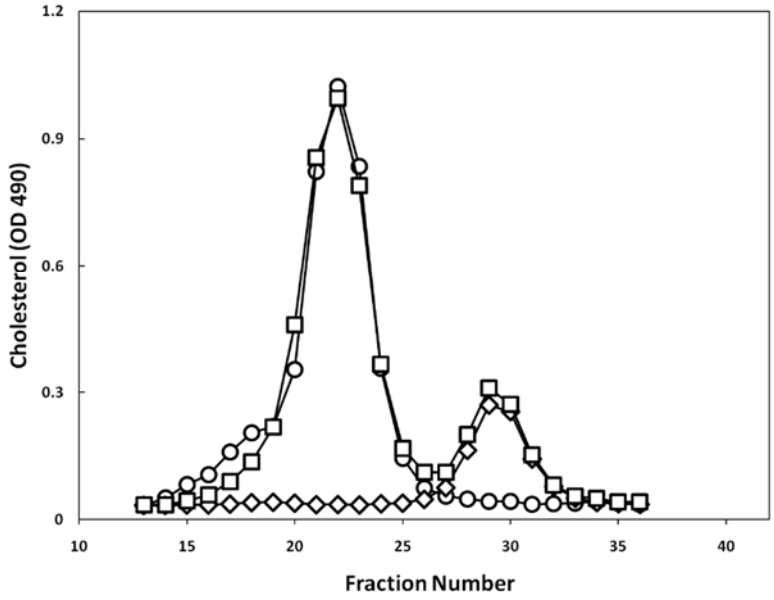
1.2
0.9
0.6
0.3
0
Cholesterol (OD 490)
10
15
20
25
30
35
40
Fraction Number

Figure A-5

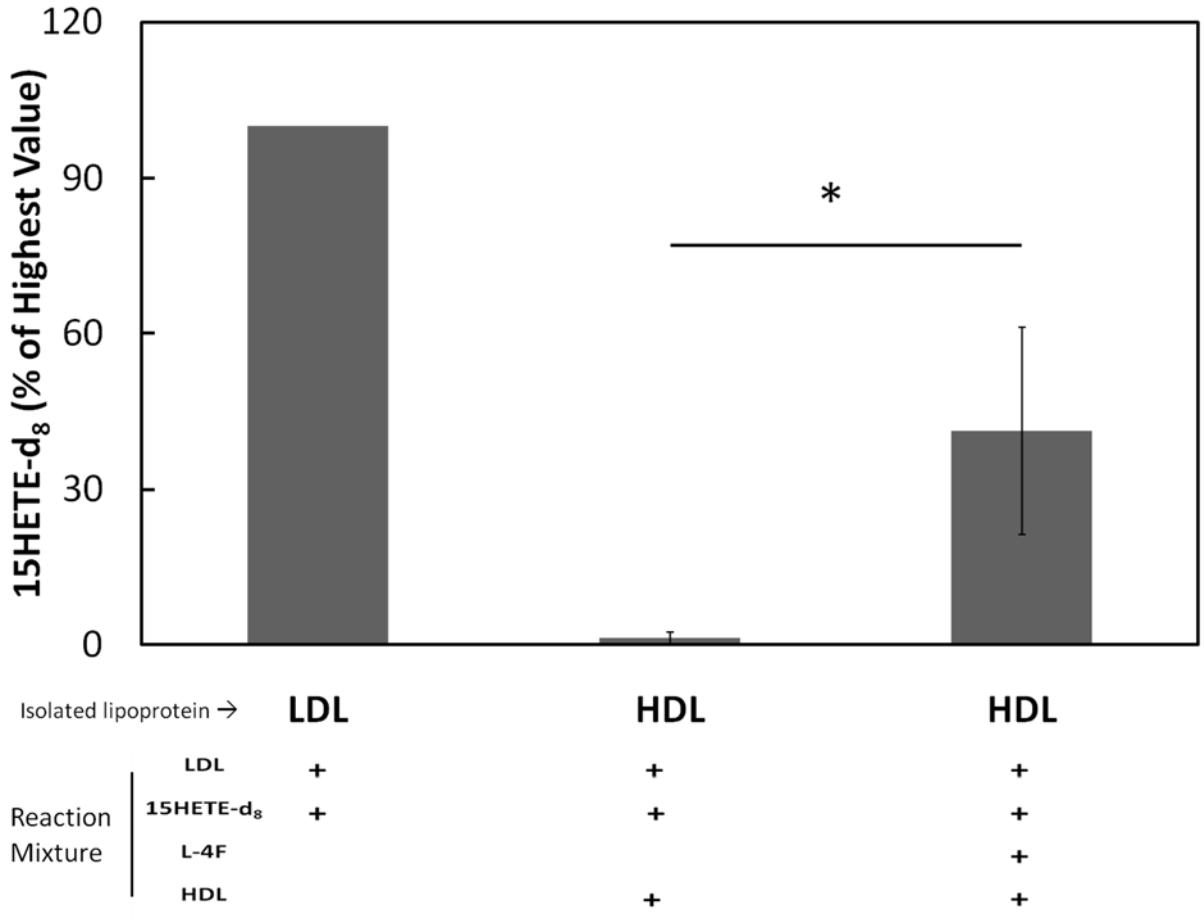
120
90
60
30
0
15HETE-d8 (% of Highest Value)
*
Isolated lipoprotein →
LDL
HDL
HDL
Reaction Mixture
LDL
15HETE-d8
L-4F
HDL
+
+
+
+
+
+
+
+
+

Figure A-6

6a

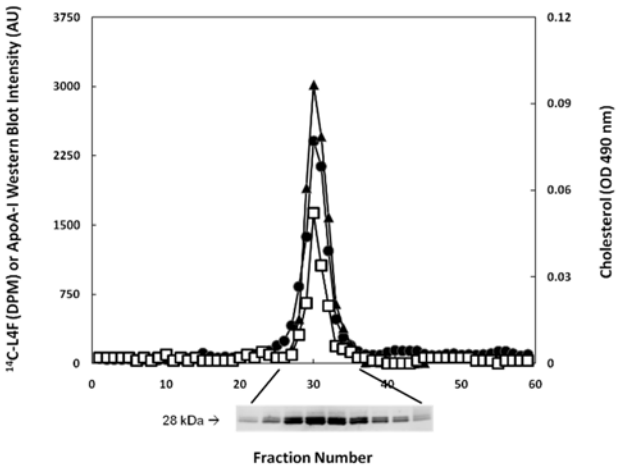

6b

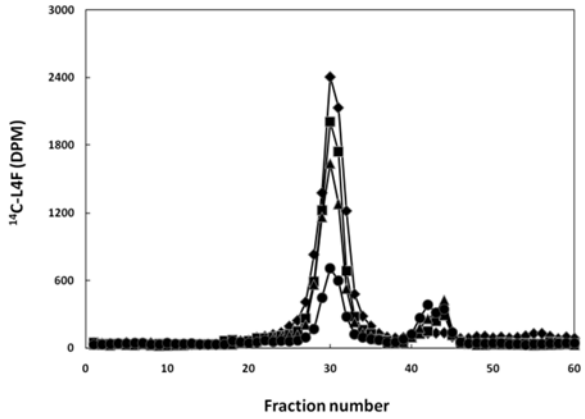

6c

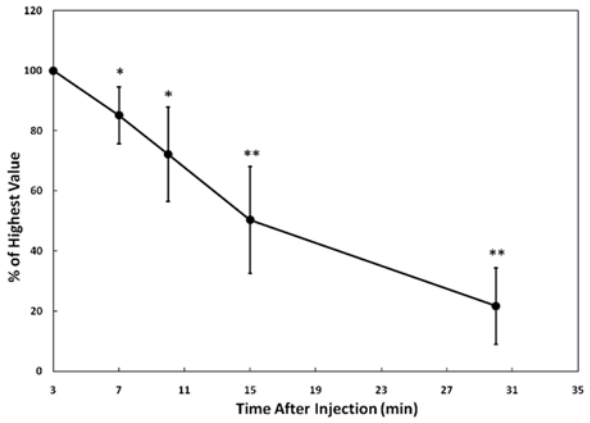
120
100
80
60
40
20
0
% of Highest Value
*
*
**
**
3
7
11
15
19
23
27
31
35
Time After Injection (min)

Figure A-7

7a

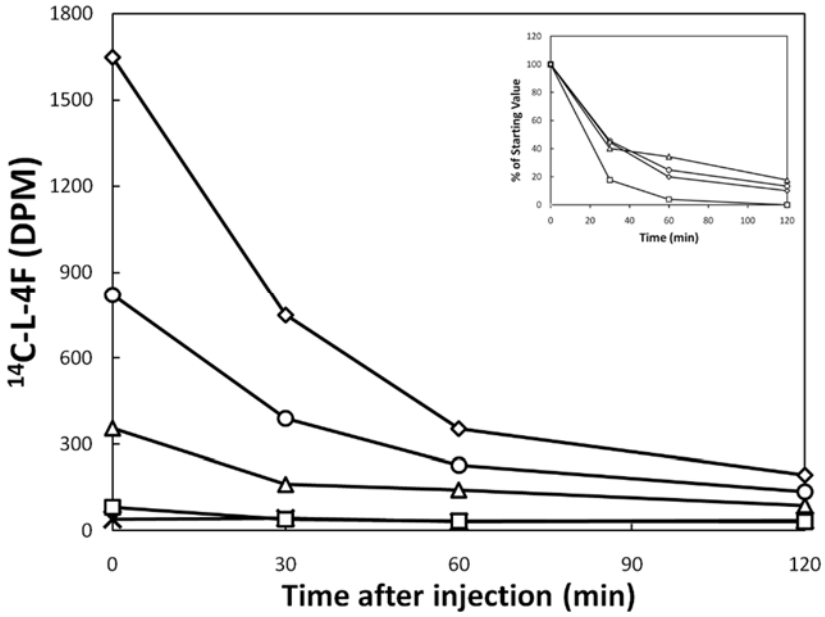

7b

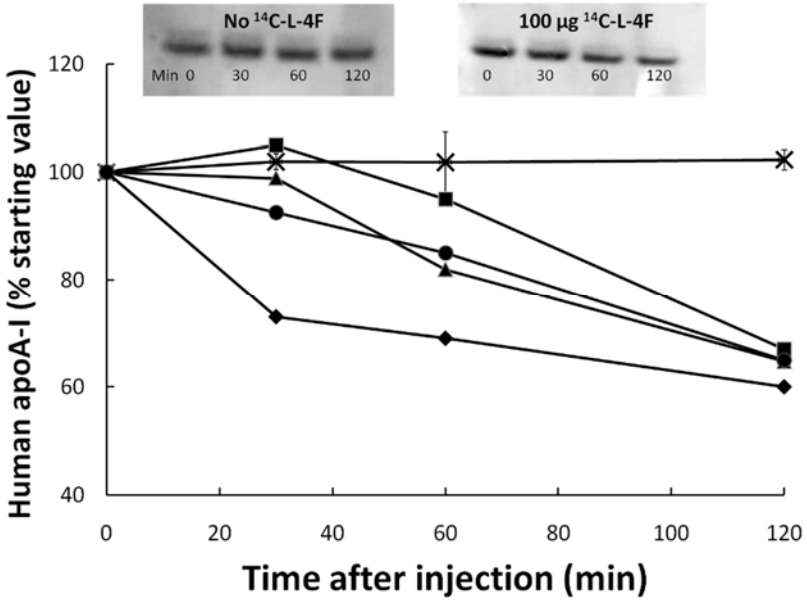

Figure 7 (continued)

7c

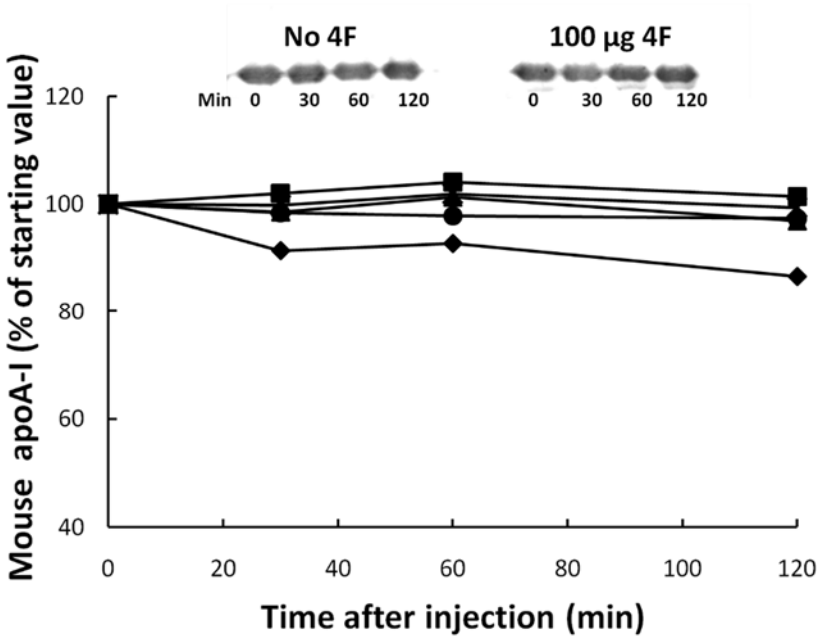

7d

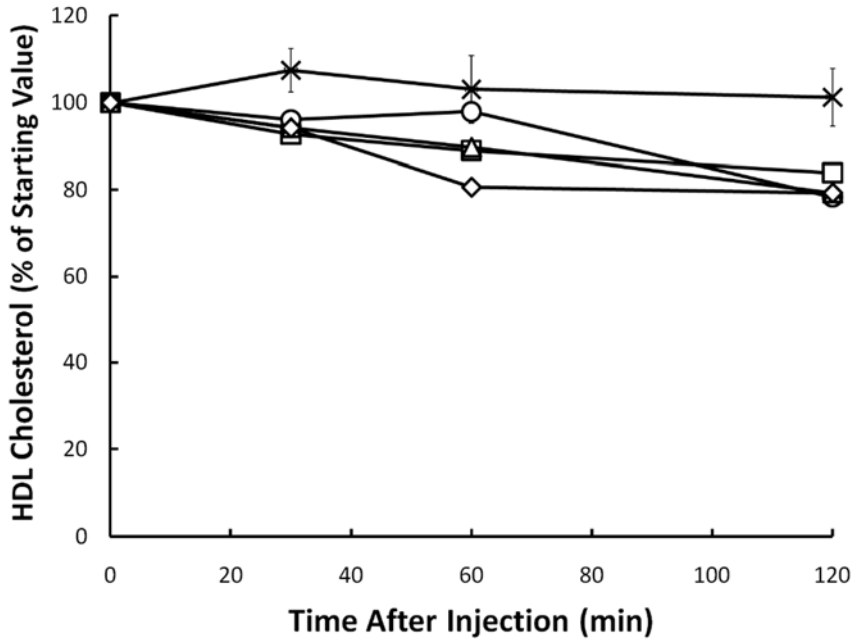

Figure A-8

8a

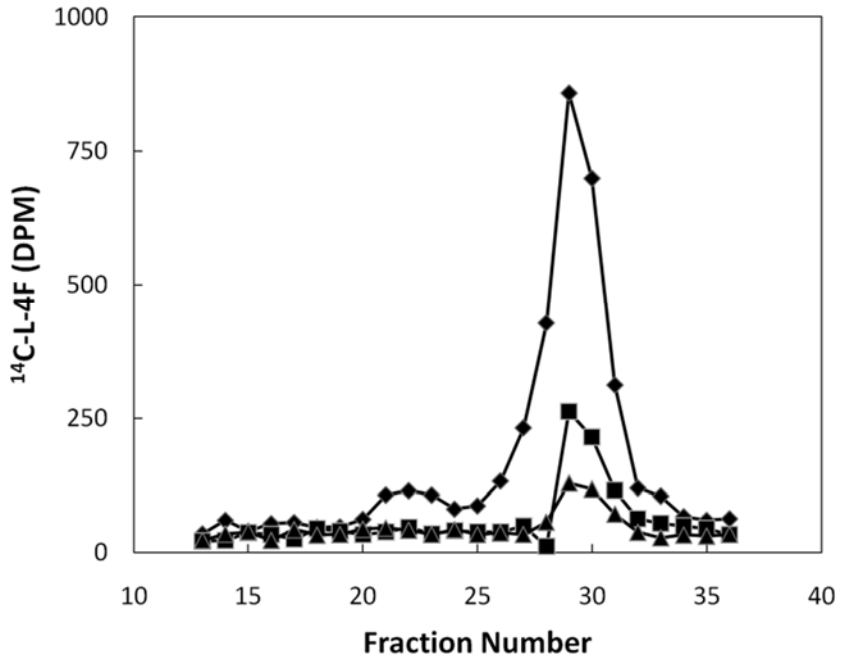
1000
750
500
250
0
^{14}C-L-4F (DPM)
10
15
20
25
30
35
40
Fraction Number

8b

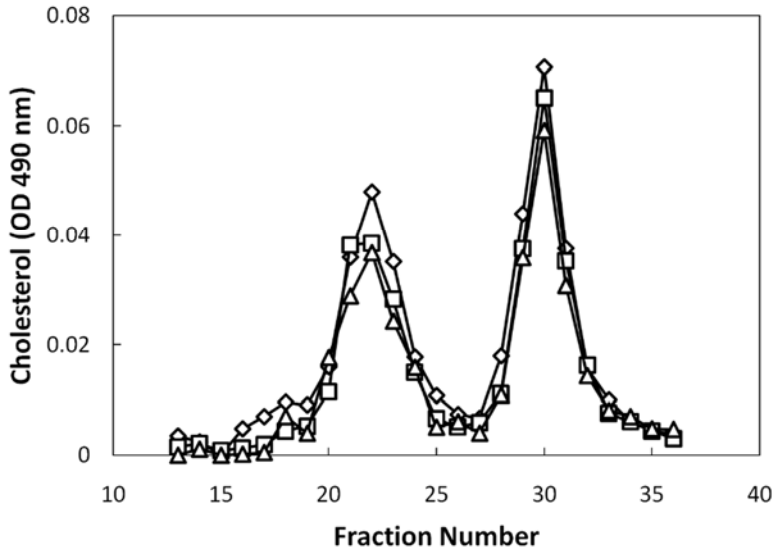
0.08
0.06
0.04
0.02
0
Cholesterol (OD 490 nm)
10
15
20
25
30
35
40
Fraction Number

Figure A-9

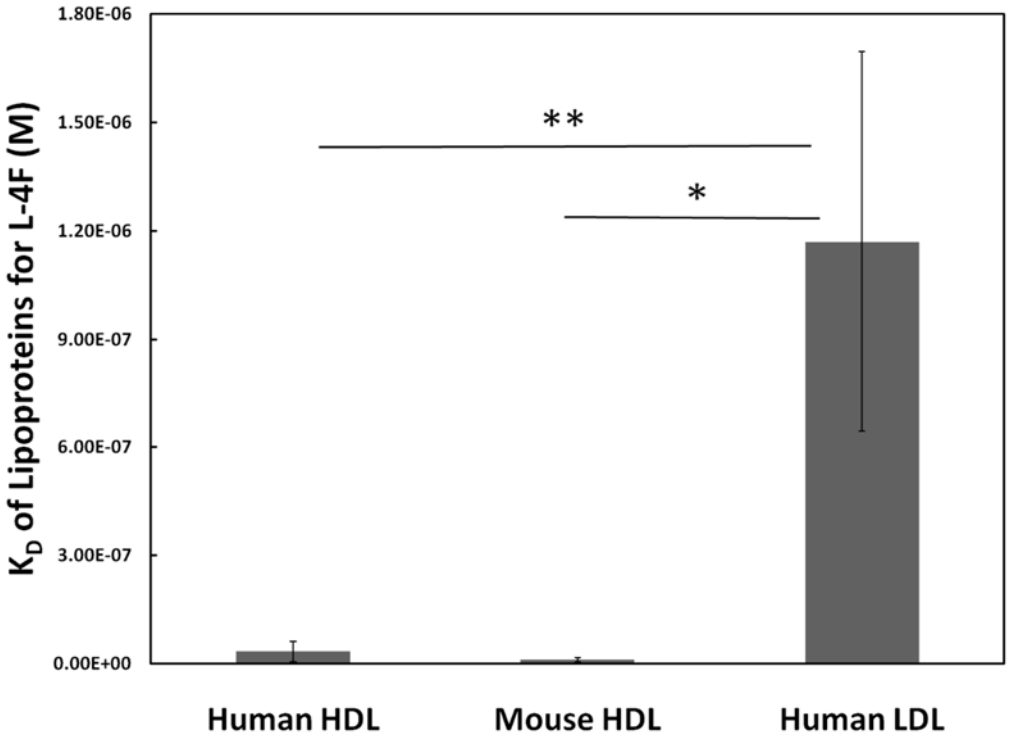
1.80E-06
1.50E-06
1.20E-06
9.00E-07
6.00E-07
3.00E-07
0.00E+00
K_D of Lipoproteins for L-4F (M)
**
*
Human HDL
Mouse HDL
Human LDL